SELF-ASSEMBLY OF BORON CLUSTER COMPOUNDS AND THEIR COASSEMBLY WITH POLYMERS

SAMOSKLÁDÁNÍ SLOUČENIN OBSAHUJÍCÍCH BOROVÉ KLASTRY A JEJICH SPOLUSKLÁDÁNÍ S POLYMERY

A dissertation presented

by

Vladimír Ďorďovič

to

Department of Physical and Macromolecular Chemistry

in partial fulfillment of the requirements for the degree of
Doctor of Philosophy in the subject of Physical Chemistry

CHARLES UNIVERSITY
Faculty of Science

Supervisor: RNDr. Pavel Matějíček, Ph.D.
Advisor: Ing. Mariusz Uchman, PhD.

Prague 2017

Abstract

This thesis focuses on the self-assembly of the boron cluster compounds and the coassembly of metallacaborane cobalt bis(dicarbollide), COSAN, with hydrophilic polymers. The research was motivated by the discovery of HIV inhibition by COSAN and its conjugates. Therefore, we decided to study in detail the behavior of boron cluster compounds in water. We demonstrated the amphiphilic character of several boranes and carboranes by the study of surface tension and self-assembly despite the absence of classical amphiphilic topology. The behavior of COSAN showed similarities with classical surfactants, such as SDS, whereas the behavior of smaller clusters with high charge density reminded of hydrotropes or chaotropes. Furthermore, we searched for the most suitable carriers of COSAN for drug delivery. Based on the earlier findings that COSAN interacts with both poly(ethylene oxide), PEO, and poly(2-oxazoline), POX, we prepared nanoparticles by mixing COSAN with block copolymers of various types of POX. Comparing linear and star-like block copolymers, we showed that the polymer architecture has a crucial role in the morphology of nanoparticles. In addition, we proved different selectivity of alkaline cations towards PEO and POX, resulting in the different structures of nanoparticles depending on the present cations. Cation selectivity was also achieved by the synthesized COSAN conjugates, dumbbells, in which two COSAN anions were connected by an oligo(ethylene oxide) linker. Finally, we extended the studies of polymeric COSAN carriers by thermoresponsive block copolymer of POX. Its interaction with COSAN led to the nanoparticles which structure showed dependence on the temperature. The presented results have a potential for tailored nano-carriers in drug delivery and other applications. For the characterization of all the studied assemblies we used light and X-ray scattering, ^{1}H and DOSY NMR spectroscopy, transmission electron microscopy, surface tension, calorimetry, and conductometry.

Prohlášení

Prohlašuji, že jsem disertační práci zpracoval samostatně a že jsem uvedl všechny použité informační zdroje a literaturu. Tato práce ani její podstatná část nebyla předložena k získání jiného nebo stejného akademického titulu.

Prague, 13. 4. 2016

.....

Podpis

Contents

Acknowledgements

I would like to thank all the people who contributed to this thesis: Pavel Matějíček, my supervisor, for the excellent guidance and the motivation for science. Mariusz Uchman, my advisor, for the great opportunities to grow. All my colleages for the help, especially Miroslav Štěpánek, Jana Vojtová, David Vrbata, and Roberto Fernandez Alvarez. Special thanks go to Mariana, my wife, who has made my work and life more effective, and my parents for their support.

List of abbreviations

2c–2e	Two-center, two-electron
3c–2e	Three-center, two-electron
AFM	Atomic force microscopy
BNCT	Boron neutron capture therapy
BSH	Sodium mercaptododecaborate
CAC	Critical aggregation concentration
CMC	Critical micelle concentration
COP	Conducting organic polymer
COSAN	Cobalt sandwich
COX	Cyclooxygenase
Cryo-TEM	Cryogenic transmission electron microscopy
DHB	Dihydrogen bond
DLS	Dynamic light scattering
DNA	Deoxyribonucleic acid
DOSY	Diffusion-ordered spectroscopy
ESI-MS	Electrospray ionization mass spectroscopy
GPC	Gel permeation chromatography
HIV	Human immunodeficiency virus
HLB	Hydrophile-lipophile balance
HPLC	High-performance liquid chromatography
IR	Infra-red
ITC	Isothermal titration calorimetry
IUPAC	International Union of Pure and Applied Chemistry
LCST	Lower critical solution temperature
LS	Light scattering
MALDI-TOF	Matrix-assisted laser desorption/ionization – time of flight
MS	Mass spectrometry
NMR	Nuclear magnetic resonance
ORTEP	Oak ridge thermal ellipsoid plot
P2VP	Poly(2-vinylpyridine)
P4VP	Poly(4-vinylpyridine)
PAT	Profile analysis tensiometry
PEG	Poly(ethylene glycol)
PEO	Poly(ethylene oxide)
PEtOx	Poly(2-ethyl-2-oxazoline)
PMA	Poly(methyl acrylate)
PMeOx	poly(2-methyl-2-oxazoline)
PNIPAM	poly(N-isopropylacrylamide)

POX	Poly(2-oxazoline)
PPrOx	Poly(2-*n*-propyl 2-oxazoline)
PPy	Polypyrrole
PSEPT	Polyhedral skeletal electron pair theory
QM	Quantum mechanics
SANS	Small-angle neutron scattering
SAXS	Small-angle X-ray scattering
SDS	Sodium dodecyl sulfate
SEC	Size exclusion chromatography
SEP	Skeletal electron pairs
SLS	Static light scattering
SI	Supporting information
ss-NMR	Solid-state nuclear magnetic resonance
TGA	Thermogravimetric analysis
THF	Tetrahydrofuran
UCST	Upper critical solution temperature
UV-Vis	Ultraviolet-visible
WAXS	Wide-angle X-ray scattering

Preface

This dissertation consists of the studies on the self-assembly of boranes and caboranes, the interactions between metallacarborane and polymers, and the preparation of polymeric nanoparticles with COSAN. This research was conducted in the Boron cluster laboratory of my supervisor, Dr. Pavel Matějíček, which is part of the Soft Matter group of prof. Karel Procházka, at the Department of Physical and Macromolecular Chemistry at Charles University in Prague, from September 2013 to April 2017. Thanks to MŠMT/DAAD funding (7AMB16D007/ 57220012), I could also spend three months in the group of prof. Michael Gradzielski at Technical University in Berlin and the group of Dr. Reinhard Miller at Max Planck Institute for Colloids and Interfaces in Gölm, where I mainly studied metallacarboranes behavior at water/air interface by different tensiometry techniques.

The first chapter, theoretical background, covers the basis of borane, carborane and metallacarborane chemistry with the focus on boron cluster compounds, their application as well as the behavior in the solution. To understand self-assembly of boron cluster, self-assembly of amphiphiles and hydrophobic effect is briefly explained. The chapter 2 deals with fundamentals of characterization methods that I mostly worked with, materials, and experimental set-up. In the next part, I introduce the research aims (Chapter 3) followed by the results presented as the collection of six, thematiclly ordered, publications (Chapter 5). In these, where I am the first author, my contribution was in preparation of the nanoparticles, conducting most of the experiments and writing manuscripts. In two publications, where I am not the first author, my contribution was in measurements of dynamic light scattering, solubility determinations, Cryo-TEM micrograph analyzes and ^{1}H NMR measurements.

In the presented publications, other authors also contributed. Besides supervisor Dr. Matějíček and advisor Dr. Uchman, the other members of our department are acknowledged: Dr. Tošner measured and helped with NMR measurements (DOSY, NMR, $^{1}H\{^{11}B\}$, ^{11}B) and discussions. Dr. Kalíkova measured HPLC of boranes. Other members of the department, who are not coauthors of presented publications, are also acknowledged: Dr. Štěpánek for helpful comments and ideas, Dr. Hybelbauerová for some of NMR experiments, Mgr. Vrbata for HPLC measurements, and Karolina Štoudková for sample preparation and conductivity measurements.

Many results came also from the cooperation with other Czech or foreign groups: Dr. Zhigunov (Institute of Macromolecular Chemistry, AVČR, Prague) carried out SAXS and WAXS experiments. Prof. Teixidor, Prof. Viñas, Dr. Tarrés and Msc. González-Cardoso (Institut de Ciencia de Materials de Barcelona, Bellaterra, Spain) synthesized and characterized dumbbells and carried out MALDI-TOF MS measurements. Dr. Ruokolainen, Dr. Nykanen, Dr. Reza (Department of Applied Physics Nanotalo, Aalto University, Finland) and Dr. Kereïche (Institute of Cellular Biology and Pathology, First Faculty of Medicine, Charles University) provided Cryo-TEM micrographs. Prof. Hoogenboom and Dr. Verbraeken (Department of Organic and Macromolecular chemistry, Faculty of Sciences, Ghent University) synthesized

poly(2-methyl-2-oxazoline)-*block*-poly(2-*n*-propyl-2-oxazoline). Prof. Gradzielski (Stranski-Laboratorium für Physikalische Chemie und Theoretische Chemie, Institut für Chemie, Technical University, Berlin) provided tensiometry instrument and participated in discussion. Dr. Hänninen, Prof. Sillanpää (Department of Chemistry, University of Jyväskylä, Finland) carried out X-ray structure determination. Dr. Cígler and Dr. Pramanik (Institute of Organic Chemistry and Biochemistry, AVČR, Prague) purified borane samples. This research would also not be possible without the financial support of the Department of Physical and Macromolecular Chemistry, the Grant Agency of Charles University (GAUK 512214) and the Czech Science Foundation (P205/14-14608S; P208/17-00648S).

1 Theoretical background

1.1 Introduction

Boron, the fifth element of the periodic table, is the only non-metal of Group 13. Its first isolation was carried out by H. Davy,[1] J. L. Gay-Lussac and L. J. Thénard[2] in 1808 from the mineral borax, which had been known for centuries for the preparation of glazes and glasses. The name boron was proposed by Davy, who used the word combination of the natural source of boron and the similarity to carbon, i.e. bor(ax + carb)on. The first synthesized compounds were trivalent, such as trihalides or borates, behaving as expected, but later synthesis of boranes brought a mystery of strange type of bonding, which was finally revealed by W. Lipscomb[3]. In 1976 he was awarded the Nobel Prize in Chemistry "for his studies on the structure of boranes illuminating problems of chemical bonding".

Boron has been often compared to its neighbors in periodic table – carbon and silicon. Similarly, boron forms covalent, molecular compounds, but it differs in having one less valence electron than the number of valence orbitals. Because of this “handicap”, boron was often vaguely labeled as electron deficient. However, a disadvantage turned out to be an advantage, and specific boron bonding has provided a great diversity in borane chemistry. Moreover, synthesis of the first carboranes in the 1950’s opened the door to even greater possibilities and many carboranes and metallacarboranes have found their potential use in various applications, from the wheels of nano-cars to the treatment of cancer.

1.2 Boron

Pure boron flourishes with structural complexity of its allotropic modifications. In comparison to other elements of Group 13, which adopt metallic bonding, the small size and high ionization energies of boron result in covalent bonding. The main structural unit of boron allotropes is the B_{12} icosahedron with 12 vertices and 20 triangular faces. Even amorphous boron contains randomly bonded icosahedra.[4] Above 1000°C, crystalline boron can be obtained with its four major polymorphs: α-rhombohedral and β-rhombohedral, α-tetragonal and β-tetragonal. The simplest form is the α-rhombohedral modification with nearly regular B_{12} icosahedra in slightly deformed cubic close packing.[5] New boron allotropes were described just recently. γ-orthorombic phase with NaCl-type arrangement of B_{12} icosahedra and B_2 pairs was prepared in 2009.[6] Furthermore, carbon analogues of fullerene and graphene were prepared in 2014. Fullerene-like structure, called borospherene (B_{40}^-), is a cluster with not spherical but rather baseball shape.[7] Graphene-like structure, called borophene (B_{36}^- and neutral B_{36} is a quasiplanar two-dimensional sheet with a hexagonal hole in the middle.[8] Generally, crystalline boron is an extremely hard with low density, low electrical conductivity and very high melting point. For example, the most stable, β-rhombohedral, allotrope has melting point 2092°C.

Boron has two naturally occurring isotopes, ^{10}B (20%) and ^{11}B (80%). Each isotope has nuclear spin, which can be used in NMR spectroscopy, especially for ^{11}B. Isotope ^{10}B with its high neutron capture cross section found its application in BNCT treatment of cancer (chapter 1.7.1). The electronegativity of boron is 2.0 (according to Pauling scale), which is lower than the values for hydrogen (2.2) and for carbon (2.6). This fact has important consequences for the discussion on bonding, weak interactions and reactions in boron chemistry. The chemical properties of boron are mostly influenced by its small size, high ionization energy and the similarity in electronegativity with carbon and hydrogen. This leads to unusually extensive number of boron compounds, which can be divided into five main groups:[9]

- metal borides;
- boranes (boron hydrides) including carboranes and metallacaboranes;
- boron trihalides and their adducts and derivatives;
- oxo-compounds including polyborates, borosilicates, peroxoborates, etc.;
- organoboron compounds and B–N compounds.

Boron is potentially essential nutrient, which can be found in foods of plant origin and has an important role in metabolism.[10,11] Knowledge of functions and metabolism of boron is currently limited, partially because of challenges in the analysis of boron in food and body.[12]

1.3 Boranes

Numerous neutral or anionic boranes (B_nH_m or $[B_nH_m]^{x-}$) have been prepared since the first synthesis in 1912.[13] The most important periods in history of borane science has been always connected with the potential applications and financial support. It reached its zenith in 1950s during an industrial effort of U.S. government to develop borane-based aircraft and rocket fuels.[14] Combustion of boranes released much higher energies compared to hydrocarbons but the combustion products (solid boron oxides and nitrides) negatively affected jet and rocket engines. Hence, this project was abandoned and stocks of boranes remained with the possibility of converting them into other useful materials. This period created a solid basis for the future development of borane and carborane chemistry.

Boranes can be classified according to the structure into 5 classes:[9]

- *closo*-boranes $[B_nH_n]^{2-}$ (from Greek for "cage") with closed *n*-cornered polyhedral clusters;
- *nido*-boranes B_nH_{n+4} (from Latin for "nest") with non-closed structures in which the B atoms occupy *n* corners of an (*n* + 1)-cornered polyhedron;
- *arachno*-boranes B_nH_{n+6} (from Greek for "spider's web") with even more open clusters in which the B atoms occupy *n* contiguous corners of an (*n* + 2)-cornered polyhedron;
- *hypho*-boranes B_nH_{n+8} (from Greek for "net") with the most open clusters in which the B atoms occupy *n* corners of an (*n* + 3)-cornered polyhedron;
- *conjuncto*-boranes B_nH_{n+8} (from Latin for "I join together") with structures formed by linking two (or more) clusters together.

Most widely studied borane is probably *nido*-decaborane, $B_{10}H_{14}$, mostly because of its potential use as fuel. Among the most studied *closo*-boranes are decaborate $[B_{10}H_{10}]^{2-}$ and mainly icosahedral dodecaborate $[B_{12}H_{12}]^{2-}$, structurally parent units of large number of derivatives. In the following text, characteristic features, such as bonding and aromaticity, are explained. The synthesis and the possible derivatives can be found in the literature.[9]

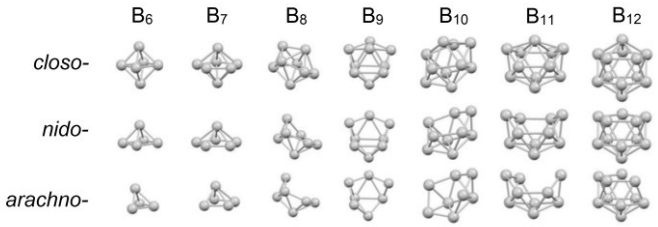

Figure 1.1. The structural relationships between *closo*-, *nido*- and *arachno*- clusters noted by Williams[15] which were the stimulus for the development of Wade's rules.[16] Adapted from ref. 17.

1.3.1 Multicenter bonding

Two main types of boron bonding can be found in boron compounds: classical 2c-2e (two-center, two-electron) B–B σ-bonds and unique multicenter bonds, which are typical for boron chemistry. The former is created occasionally, when a boron atom accepts an electron. It leads to molecules similar to those of carbon with classical 2c-2e σ-bonds, such as BH_4^-, analog of CH_4. Most boron compounds have multicenter bonds, which can bound in two ways, B–B–B or B–H–B. This ability of boron is a result of its low electronegativity and four valence orbitals occupied only by three valence electrons. Because of this "lack" of electrons, multicenter bonding has been sometimes incorrectly called "electron deficient". Theories of borane bonding have been extensively developed and explained mostly by W. Lipscomb and his group (Nobel Prize in Chemistry, 1976).[3]

Diborane, B_2H_6, is the simplest compound with two 3c-2e (three-center, two-electron) B–H–B bonds. Two boron and one hydrogen atom supply three orbitals, one from each atom. These orbitals form one bonding and two antibonding molecular orbitals and the bonding orbital is filled by two electrons. In general, *n*-atomic borane has *n* atomic orbitals and *n*/3 bonding molecular orbitals, which are filled by 2*n*/3 electrons. When this, localized bond, description is applied to *closo*-borane clusters, for example $[B_{12}H_{12}]^{2-}$, several bond arrangements can satisfy the electron-orbital balance requirements leading to many resonance forms. In heteroboranes, such as carboranes, the situation becomes even more complicated. Thus, it was necessary to extend localized-bond treatment by electron-delocalization methods, which could handle many compositions and structures. On the basis of Limpscomb's topological theory, molecular orbital studies and the knowledge of icosahedron and deltahedron patterns in boranes[15] (Figure 1.1), K. Wade proposed a set of rules, which showed a correlation of geometric structure with the available number of skeletal electrons in each system.[16] The Wade's rules (or the Wade-Mingos rules, formally also known as the polyhedral skeletal electron pair theory, PSEPT) consider that clusters are constructed from building-block units such as BH or CH, supplying a given number

of electrons to the skeletal framework and in most molecules, these units use three orbitals for bonding to its neighbors. For example, BH unit has four electrons of which two are used in B−H and two for skeletal framework (two-electron donor). The total number of these skeletal electron pairs (SEP) determine the geometry of boron clusters. For *closo*-boranes $[B_nH_n]^{2-}$, boron atoms occupy all *n* corners of an *n*-cornered polyhedron and the structure requires (*n* + 1) SEP. Wade's rules can be also extended to carboranes and metallacarboranes.[17]

1.3.2 Cluster aromaticity

Aromaticity is not limited only to organic chemistry, but also boranes, especially *closo*-boranes and carboranes are accepted as aromatic compounds, specifically 3D-aromatic (also called superaromatic, spherical or σ-aromatic).[18] This phenomenon has been explained theoretically[19,20] and also confirmed experimentally by high stability, magnetic properties and NMR measurements of boron cluster compounds as well as undergoing reactions typical for aromatic compounds. Aromaticity stabilization tends to increase with increasing cluster size, especially boranes with 6 and 12 vertexes show very high stability. Most studies on aromaticity were focused on closed clusters of boranes and carboranes, but also open *nido*- and *arachno*-species show aromaticity, although lower than that of *closo*-boranes.[21]

Borane structure diagrams

Structure diagrams with the skeletal boron (or carbon) atoms, typically having five or six neighbors including hydrogen or other attached substituents (Figure 1.1 and 1.2), may look confusing and indicating too many two-electron pair bonds. Comparing to classical organic diagrams, multicenter bonding and spherical aromaticity has to be considered in boranes (and also carboranes). In borane diagrams, connecting line between two atoms does not explicitly indicates the pair of electrons. Instead, these lines show the geometry only.

1.3.3 Chemical properties

Many smaller and open boranes are very reactive and several are spontaneously flammable in air. On the other hand, most *closo*-boranes $[B_nH_n]^{2-}$ and their carborane analogues are exceptionally stable. The reason behind the high reactivity of smaller boranes is hydrogen-richness associated with the presence of B–H–B and BH_2 groups, which can be mostly found in lower hydrides. An important contribution to stabilization is spherical aromaticity. Many *closo*-boranes are thus very stable, robust and not degraded when heated even to 600°C. It is worth noting, that $[B_{12}H_{12}]^{2-}$ is claimed to be the most stable molecule known to chemistry, withstanding temperatures above 800°C.[21]

Chemical reactions of boranes are strongly directed by electron charge density. Highest density occurs at boron atoms at apical position (axial, below and above the plane), which is the preferred site of electrophilic attack. Conversely, boron atoms involved in B–H–B bonding are the preferred site of nucleophilic attack because of the lowest electron charge density. In acid-base reactions, bridge hydrogens are more reactive than terminal ones.

1.4 Carboranes

Carboranes (in formal nomenclature carbaboranes) are boranes with one or more carbon atoms in the cluster framework. To avoid inclusion of some organoboranes, carboranes are more exactly defined as carbon-boron clusters of four or more vertices in which non-classical (electron-delocalized multicenter) bonding plays a significant role.[21] The majority of carboranes have two carbon atoms in the cluster framework, which originates from their usual synthesis from alkynes.

Study of carboranes started even before the synthesis of such compounds, when Lipscomb, Hoffmann and others theoretically predicted existence of polyhedral carboranes.[22] The first icosahedral carboranes had actually been industrially prepared in the 1950s under U.S. program developing fuels, but carboranes were not reported in literature until 1963.[23] Since then, many synthetic routes have been reported, for example pyrolysis of boranes and alkynes, or the reaction in a silent electric discharge. Other synthetic approaches provide carboranes with one to four carbon atoms (or even more in some metallacarboranes). Numerous synthesized carboranes varies in cluster size, shape, carbon location and number of carbon atoms. Many *nido*-, *arachno*- and *hypho*-carboranes have been synthesized and studied, but the focus of this thesis is on *closo*-carboranes, which are the most numerous and the most stable carboranes.

1.4.1 Dicarbadodecaborane

Among the first synthesized and most studied carboranes is *closo*-1,2-dicarbadodecaborane, 1,2-$C_2B_{10}H_{12}$ (*ortho*-carborane), which is the most common carborane and thousands of derivatives have been synthesized with huge potential. It is very stable, but on heating above 425°C it is converted to even more stable isomer 1,7-$C_2B_{10}H_{12}$ (*meta*-carborane). At the temperatures higher than 600°C, further isomerization results in isomer 1,12-$C_2B_{10}H_{12}$ (*para*-carborane; Figure 1.2). Mechanism of this isomerization was explained as the cooperative diamond-square-diamond rearrangement, in which icosahedral triangles converts to squares of cuboctahedral intermediate.[24] In general, the most stable carborane isomers are those with the furthest separation between the carbon atoms in the framework because of the mutual repulsion between electropositive carbon nuclei.

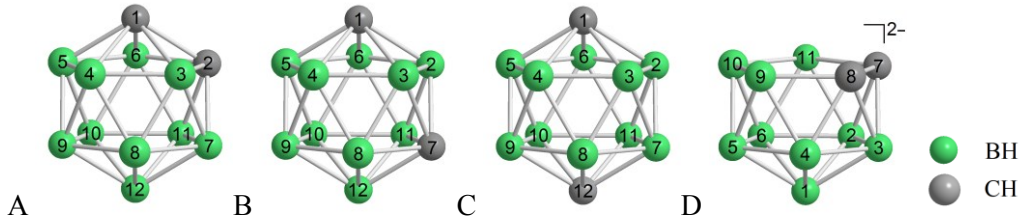

Figure 1.2. Structures of carboranes: (A) 1,2-$C_2B_{10}H_{12}$, (B) 1,7-$C_2B_{10}H_{12}$, (C) 1,12-$C_2B_{10}H_{12}$ and (D) *nido*-$[7,8\text{-}C_2B_9H_{11}]^{2-}$ (dicarbollide)

It is noteworthy that carborane synthesis often leads to the isolation of thermo-dynamically less stable structure because of kinetically stabilized structures. For example, many

metallacarboranes are prepared under low-energy conditions and their thermodynamically favored isomers have never been isolated.

Ortho-carborane and its derivatives are very stable toward degradation by acids and oxidants under a wide range of conditions, which allows chemists to use great variety of reactions without changing the icosahedral cage.[25] In carboranes, the C–H groups tend to be more polar than the B–H, the hydrogens of the C–H groups are thus weakly acidic and can be easily removed by nucleophile, resulting in C-substituted derivatives. Other approaches can also lead to B-substituted derivatives. *Closo*-carboranes can be specifically degraded to *nido*-carboranes, usually removing the BH vertex next to the two CH vertices. Degradation of $C_2B_{10}H_{12}$ by base, followed by deprotonation leads to *nido*-carboranes $[7,8\text{-}C_2B_9H_{11}]^{2-}$ and $[7,9\text{-}C_2B_9H_{11}]^{2-}$, which structurally reminds the cyclopentadiene anion well-known for metal complexation. Similar function of these *nido*-carboranes led to the discovery of the metallacarboranes (chapter 1.5).

1.4.2 1-carbadodecaborate

1-carbadodecaborate, $[CB_{11}H_{12}]^-$, is another important carborane and its self-assembly is described in the results section of this thesis (chapter 5.2). It is very stable and resistant to degradation but comparing to neutral $C_2B_{10}H_{12}$ it is polar and highly soluble in water, which makes it potentially useful in medical applications, such as BNCT (chapter 1.7.1). $[CB_{11}H_{12}]^-$ anion and its conjugates are very weakly coordinating and can form stable salts with extremely reactive cations, leading to very strong Brønsted acids, strong oxidants and cationic catalysts[26] (chapter 1.7.2). They are among the least nucleophilic anions of modern chemistry. It is worth noting that $H[CHB_{11}Cl_{11}]$ is the strongest pure Brønsted acid presently known.[27] Nevertheless, it was labeled as ”strong yet gentle”[28] because it does not oxidate or decompose other compounds as a result of their very low nucleophilicty and chemical inertness. In general, weakly coordinating properties of some carboranes arise from the large anion size, delocalized negative charge, and in case of halide conjugates, the shield of the halide substituents.[28]

1.4.3 Icosahedron stability

Note that both neutral $C_2B_{10}H_{12}$ (all the isomers) and anion $[CB_{11}H_{12}]^-$ are isoelectronic with icosahedral $[B_{12}H_{12}]^{2-}$ anion with 26 electrons. This motif also closely relates to allotropes of pure boron incorporating B_{12} icosahedra. The icosahedron is apparently to boron what the hexagon is to carbon. Extraordinary stability of B_{12} icosahedron led synthetic chemists to the term “icosahedral barrier”, expressing challenges in the synthesis of *supra*-icosahedral boranes (clusters with more than 12 vertices).[29] Nevertheless, this barrier was surmounted long ago by the “addition” of metal atoms (13- to 15-vertex clusters) and very recently by carbon atom generating 13-vertex cluster with C_2B_{11} unit.[30] However, B_{13} cluster is still waiting for its first synthesis.

1.5 Metallacarboranes

The extraordinary ability of carboranes to incorporate metal atoms led to the synthesis of metallacarboranes (or metallocarboranes), which have become the great subarea of boron chemistry. Since the first synthesis by Hawthorne in 1965,[31] carborane complexes of nearly all of the transition metals and many lanthanides have been synthesized and described. They can be efficiently produced by the reaction of transition metal ion with open-cage carborane substrate. All *nido*- and *arachno*-carboranes and heteroboranes form complexes with transition metal ions.[21] The most frequently used carborane ligands are *nido*-[7,8-RR'$C_2B_9H_9$]$^{2-}$ and *nido*-[7,9-RR'$C_2B_9H_9$]$^{2-}$, also called dicarbollide (Figure 1.2D), yielding icosahedral *closo*-MC_2B_9. When metal is complexed by two carbollide moieties, bis(dicarbollyl) complex, (RR'$C_2B_9H_9$)$_2$M, with sandwich-like structure, is formed. These compounds are very stable and metal-dicarbollyl binding remains intact over a wide range of conditions.

Dicarbollide complexation of metals has been often compared with that of cyclopentadiene in metallocenes. Metallacarborane surpassed metallocenes in many ways, such as stronger σ bonding and accommodation of variable metal oxidation states stabilized by electron delocalization. In some metallacarboranes, reduction or oxidation of metal influence the structure. For example, nickel bis(dicarbollide) can turn from *transoid* conformation to *cisoid* via oxidation of Ni(III) to Ni(IV).[32] Similarly, iron (II) bis(dicarbollide) is *transoid* but the protonated complex is converted to a *cisoid* configuration.[33] Possible control of rotational motion suggests the preparation of nanomachines and applications in microengineering.

Numbering of clusters

Numbering of carboranes is based on IUPAC general rules, which recommend to number successive rings in a clockwise manner around the highest symmetry axis. Atoms of highest atomic number are given the highest priority. One can be confused applying these rules on metallacarboranes (see COSAN structures, Figure 1.3). This exception says that for icosahedral metallacarboranes in which one or more boron vertexes are replaced by metal atoms, the numbering system is the same as that of the parent carborane (compare 1,2-$C_2B_{10}H_{12}$ and *nido*-[7,8-$C_2B_9H_{11}$]$^{2-}$ in Figure 1.2).

1.6 Cobalt bis(dicarbollide)

Anions [*commo*-3,3'-Co(III)(1,2-$C_2B_9H_{11}$)$_2$]$^-$ and [*commo*-2,2'-Co(III)(1,7-$C_2B_9H_{11}$)$_2$]$^-$ were among the first metallacarboranes synthesized[31] and the most studied member of carboranes with hundreds of synthesized derivatives. In literature, several names of these compounds can be found, such as cobalt bis(dicarbollide), cobaltabisdicarbollide, bis(dicarbollyl)cobaltate(–1), as well as trivial abbreviation COSAN (from CObalt SANdwich), which is used only for 1,2-isomer. From 48 topologically possible isomers, only these two are currently known (Figure 1.3). The classical way of the synthesis includes partial degradation of *ortho*-carborane with base into *nido*-[7,8-$C_2B_9H_{12}$]$^-$ followed by its deprotonation and reaction with $CoCl_2$.[31,34] Overall charge

of COSAN is 1– and numerous counterions have been used for the preparation of COSAN salts: various metals and ammonium cations, piperidinium, pyridinium, triphenylmethylium, hydrazinium, as well as protonated amino acids, glucosamines, amides, etc.[34] Most of these salts are well soluble in water and many organic solvents and the solubilities depends on the type of counterion and substituents. [35,36] Interesting exceptions are ammonium and alkyl-ammonium salts, which are well-known for their low solubility.[36] Cosan anion is strongly hydrophobic and one of the least coordinating anions.[37]

Cosan shows the absorbance maximum at $\lambda \approx 300$ nm, which can be conveniently used in UV-Vis colorimetric determination of concentration. The second absorption peak lies at $\lambda \approx 450$ nm, which causes yellow-orange color.[38,III] In infrared (IR) and Raman spectrum COSAN shows intense peak at 2570 cm^{-1} that corresponds to B–H stretching frequency and intense bands in the low-frequency IR region, originating from metal-ligand skeleton stretching modes.[39]

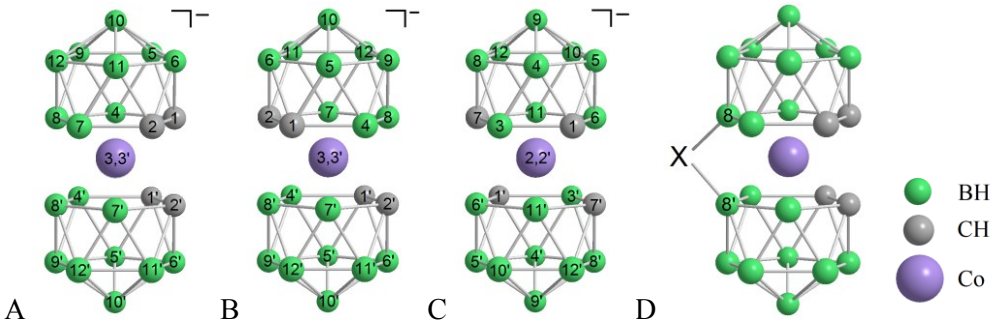

Figure 1.3. Structure of cobalt bis(dicarbollide) anions: (A) *cisoid*-[3,3'-Co(1,2-$C_2B_9H_{11})_2]^-$; (B) *transoid*-[3,3'-Co(1,2-$C_2B_9H_{11})_2]^-$; (C) [2,2'-Co(1,7-$C_2B_9H_{11})_2]^-$; (D) 8,8'-bridged 3,3'-Co(1,2-$C_2B_9H_{11})_2$ derivative (X = I, OMe, OEt, SMe, SEt, SH, NH_2, etc.)

1.6.1 Conformations

Many crystal and molecular COSAN structures have been determined since 1967,[40] but the location of carbon atoms was not revealed until 1982.[41] It was found that the two dicarbollide ligands were mutually rotated by 37° with the two C–C edges in close proximity (*cisoid* conformation; Figure 1.3), and the orientation of C_2B_9 faces on the two ligands was almost parallel (dihedral angle 3.7°). Relative energies of COSAN rotamers computationally studied by Buhl et al.[42] are shown in Figure 1.4. The minima at $\theta = 180°$ (*transoid*) and $\theta = 108°$ (*gauche*) are very similar in energy, and the rotamer with $\theta \approx 36°$ (*cisoid*) is slightly less stable, by about 10 kJ mol^{-1}. These minima are separated by three distinct transition states and the barriers between them are low (less than 37 kJ mol^{-1}), which indicates facile rotation about the B10−B10' axis. Recent study showed that although the most stable rotamer in vacuum is *transoid*, COSAN anion in majority of crystal structures prefers *cisoid* conformation, which is probably stabilized by dihydrogen bonds.[43] In COSAN derivatives, conformations can also be affected by *exo*-skeletal substituents and type of counterion.[43]

Transoid-[3,3'-Co(1,2-$C_2B_9H_{11})_2]^-$ is not the most stable form of cobalt bis(dicarbollide) because the other positional isomers with nonadjacent carbon atoms were found to be even lower in energy. The 1,7-isomer, [2,2'-Co(1,7-$C_2B_9H_{11})_2]^-$, was identified as the most stable with the energetic global minimum 121 kJ mol^{-1} lower than the energy of *transoid* conformation of COSAN.[42]

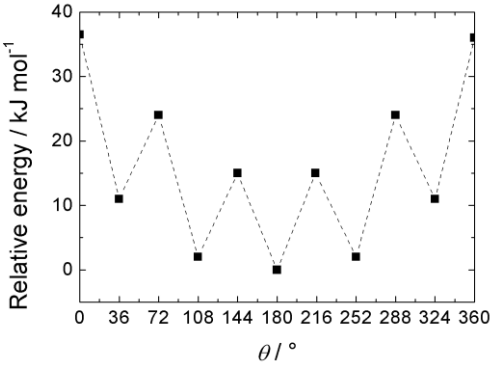

Figure 1.4. Schematic energy profile of free COSAN in vacuum for rotation about the B10–B10' axis (θ: 8'-3-10-8 dihedral angle). Adapted from ref. 42.

1.6.2 Electron distribution and reactivity

Cobalt atom in COSAN has a formal charge 3+, which can undergo reversible one-electron reduction or oxidation. Reduction leads to the brown cobalt (II) anion [3,3'-Co(1,2-$C_2B_9H_{11})_2]^{2-}$ which can revert back to yellow-orange [3,3'-Co(1,2-$C_2B_9H_{11})_2]^-$.[44] Higher negative charge of carbon atoms causes different reactivity for C and B (Figure 1.5). Boron atoms can also differ in their polarity depending on their position. The closer the boron atom is to the carbon in cluster framework, the more positive it is. Different reactivity of carbon and boron gives opportunity to the rich derivative chemistry. For example, well studied halogenation of COSAN proceeds at the boron atoms with maximum electron density and the sequential order of chlorination of COSAN was found to be in this order: B8 = B8' > B9 = B9' = B12 = B12' > B10 = B10'.[45] The chemical stability of 8,8'- and 8,8',9,9',12,12'-halogeno derivatives is even higher in comparison with the parent COSAN[34] and their dicarbollide ligands have *transoid* conformation.[46]

In general, substitution reactions at carbon atoms are similar to those in classical organic chemistry, whereas modification at boron atoms with hydrides was a challenge for decades. At present, two approaches help boron chemist to modify borane clusters at boron atoms. In the first one, a primary substituent (–I, –OH, –SH, $–NH_2$) is introduced to carborane cluster and this substituent can be subsequently modified.[47,48] Besides classical mono-substitution, COSAN also provides 8,8'-bridged derivatives, especially charge compensated ones (Figure 1.3D). The mechanism of this characteristic feature of COSAN was described as electrophile-induced nucleophilic substitution.[49] In the second approach, borane cluster is modified by cyclic oxonium ring, which can be opened by various nucleophiles. This approach leads to a great variety of COSAN derivatives with a flexible spacer containing various terminal functional

groups. These groups can conjugate with other molecules, such as biomolecules (nucleotides, porphyrins, saccharides) or second carborane cluster.[50] Large number of COSAN conjugates were synthesized with potential use in extraction (Chapter 1.7.2), for example, COSAN with simple oligo(ethylene oxide)[51] and crown ether[52] derivatives. The study of self-assembly and cationic selectivity of the compounds incorporating two COSAN molecules connected by hydrophilic $–O(CH_2CH_2O)_2$ spacer, also called dumbbells, is presented in the paper II (chapter 5.3).

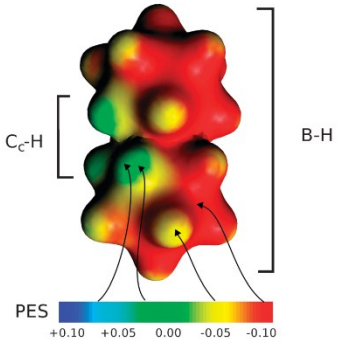

Figure 1.5. Electrostatic potential on the van der Waals surface of the *cisoid* rotamer of $[3,3'\text{-}Co(1,2\text{-}C_2B_9H_{11})_2]^-$.[43]

1.7 Applications of boron cluster compounds

1.7.1 Medical applications

Boron cluster compounds have several specific properties, which lead to tailored synthesis of new drugs. For instance, the size of icosahedral cluster is comparable to that of adamantane and larger than benzene ring used in various drugs. The volume occupied by $C_2B_{10}H_{12}$ is approximately 40% larger than that of rotating benzene.[53] Moreover, attachment of substituents on clusters enable three-dimensional arrangement with various angles. Furthermore, some substituted carborane clusters show chirality,[54] which can be used for the preparation of even more specific types of drugs. The use of boron clusters in medicine is also extended by their lipophilic and hydrophobic character, and their high thermal and chemical stability in various environments, which allows them to survive in many biological systems without degradation.

Boron cluster drugs can be divided into two classes.[55] The first class consists of physiologically inert compounds, principally carriers of boron used in Boron Neutron Capture Therapy, BNCT (chapter 1.7) and radiodiagnostics. In the second class, there are physiologically active compounds, which are compatible with binding sites of biological targets.

Boron Neutron Capture Therapy (BNCT)

The most known medical application of boranes is BNCT, the treatment of cancer based on the nuclear reaction of nonradioactive ^{10}B and low-energy thermal neutrons. This reaction produces an α-particle, $^4He^{2+}$, and a $^7Li^{3+}$ ion together with 2.31 MeV of kinetic energy and a 480 keV photon:

$$^{10}B + n\ (0.025\ eV) \rightarrow \alpha + {}^{7}Li^{3+}\ (2.31\ MeV) + \gamma\ (0.48\ MeV)$$

These high-energy ions can travel one cell diameter (5–9 μm) and selectively kill tumor cells loaded by sufficient quantities of ^{10}B. The great advantage of ^{10}B isotope is in its neutron capture cross-section with the value 4–7 orders of magnitude higher than that of the elements present in tissues. Until recently developed neutron source for NCT,[56] the research of BNCT was limited to the presence of nuclear reactors and thus, most clinical studies and trials have come from United States, Japan, Finland and few other European countries.[57] Two boron drugs have been used clinically, a dihydroxyboryl derivative of phenylalanine called boronophenylalanine and sodium mercaptododecaborate (also called borocaptate) or "BSH" ($Na_2B_{12}H_{11}SH$; Figure 1.6). Many other types of ^{10}B compounds have been studied, mostly icosahedral boranes and carboranes, which provide 10 times higher concentration of boron than single-boron compounds. One of the most important requirements for ^{10}B carriers is selective delivery to tumor cells while keeping the ^{10}B concentration in the normal surrounding cells low to minimize the damage to normal tissue. Therefore, many studies have been focused on the improved selectivity of boron delivery agents by incorporating them into tumor-targeting molecules, such as peptides, proteins, antibodies, nucleosides, sugars, porphyrins, liposomes, as well as nanoparticles.[57-59]

Physiologically active boron cluster compounds

An important potential application of boron cluster compounds is HIV protease inhibition by metal complexes. Cosan (chapter 1.6) and its various derivatives were found to be potent, specific and selective competitive inhibitors of HIV protease.[60] Protein crystallography of protease together with COSAN revealed that two COSAN molecules bound to the hydrophobic pocket of protease. Hence, various compounds incorporating two COSAN connected via linkers of distinct types and length have been synthesized and studied (Figure 1.6B).[61]

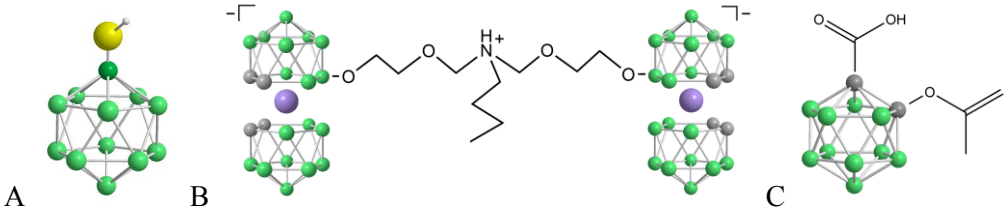

Figure 1.6. Structures of boron cluster drugs: (A) sodium mercaptododecaborate, $[B_{12}H_{11}SH]^{2-}$; (B) sodium hydrogen butylimino bis-8,8-[5-(3-oxa-pentoxy)-3-cobalt bis(1,2-dicarbollide)]diate; (C) asborin (color coding is the same as in Figure 1.3)

Several other boron cluster pharmacophores have been synthesized, in most cases, as carborane analogs to already known drugs. For example, asborin, which is a carborane analog of aspirin, uses *ortho*-carborane instead of phenyl group (Figure 1.6C).[62] Several other carboranes containing drugs have been studied, such as flufenamic acid and diflunisal analogs, antifolates analogs, [5,5]-*trans*-lactone thrombin inhibitor, inhibitors of hypoxia-inducible

factors, COX inhibitors, purinergic receptor ligands, carbonic anhydrase inhibitor and analog of anesthetic lidocaine.[55]

Biomolecules conjugated with highly hydrophobic carboranes or metallacarboranes often show low solubility in water[35] and tend to form aggregates.[63,64] Thus, effective drug delivery systems and deeper understanding of self-assembly of boranes and carboranes can help to reach the full potential of these drugs.

1.7.2 Other applications

Extraction agents

The largest-scale application of carborane chemistry in industry is extraction of metals from nuclear waste.[64-66] The separation of valuable and biotoxic elements from spent nuclear fuel is important for both economic and ecological reasons. The excellent properties of COSAN and its derivatives perfectly satisfy the requirements of extraction agents in separation processes of nuclear waste. Cosan, as a low-nucleophilic, low-coordinating anion, provides also good solubility of its conjugated acids and most of their salts in medium-polarity solvents such as ethers or nitrosolvents, to which they can be extracted from the water phase together with alkali metal cations. In addition, great chemical and thermal stability of COSAN was improved by chlorine substitution and chloro-protected derivative, $[3,3'\text{-}Co(1,2\text{-}C_2B_9H_8Cl_3)_2]^-$ was able to survive the strongly acidic environment of extraction process (3 M HNO_3) without the formation of undissociated COSAN acid. Chloro-substituted COSAN derivative thus became industrially essential for routine recovery of $^{137}Cs^+$ and $^{90}Sr^{2+}$.[67] The heavy alkali metal cations can be extracted by the COSAN reagents without additives.[68] For extraction of M^{2+} ions, actinides and lanthanides, it is necessary to use additives, such as polyethylene oxide, crown ethers or organic phosphonates.[69,70] The best selectivity toward desired metal cations occurred in nitrobenzene, however, it is ecologically unfriendly.

Chloro-substituted COSAN and its derivatives were first applied to solvent extraction of radionuclides in the 1970s by Czech workers. This research was followed by an industrial support and the first plant testing in Russia in 1985. After decades, various combinations of derivatives and additives has been studied to improve extraction effectivity and specificity. In last few years, attention has turned to synergistic approaches that use COSAN together with other effective complexing agents and bifunctional COSAN derivatives have been synthesized.[71] These complexes, and others of similar design, are highly efficient in extracting lanthanides and actinides from nuclear waste.

Catalysis

Analogy of metallacarboranes with metallocenes already indicated possibilities of new catalytic systems. Additionally, greater versatility and robustness of the metallacarboranes facilitated catalyst tailoring to specific needs and recovering intact. Most attention has centered on homogeneous catalysis of organic processes and various *exo*-metallated, metallacarboranes catalysts have been synthesized and studied.[21] Some carborane anions have found their use in catalysis because of their nearly noncoordinating anions. For example, $Li[CB_{11}Me_{12}]$ affords Li^+

in an extremely active form that catalyzes the rearrangement of pericyclic hydrocarbons[72] as well as the radical polymerization of terminal alkenes[73] and isobutylene.[74] Lithium salt of COSAN catalyzes the conjugate addition of silyl ketene acetals to hindered α,β-unsaturated carbonyls[75] as well as nucleophilic substitution on allylic acetates.[76] Other effective catalyst is also $H[CHB_{11}Cl_{11}]$, the strongest known superacid.[27]

Polymeric and nanostructured materials

Thermal and chemical stability, aromaticity, and versatility to be chemically modified make icosahedral carborane clusters attractive as synthetic building blocks in material science. Various types of dendritic,[77] thermally stable,[78,79] light-emitting,[80] conducting[81] or coordination polymers[82] containing caboranes have been synthesized.

Photophysical studies of some boron cluster compounds revealed their interesting properties, such as luminescence.[83] Incorporation of these clusters into conjugated polymers leads to new materials with improved optoelectronic properties. The most used icosahedral cluster in this field is dicarbadodecarborane, and its influence on the emission properties has been studied in star-shaped molecules,[84] π-conjugated organic systems[85,86] and polymers.[87]

Other studies of carborane-containg polymeric materials have been focused on conducting organic polymers (COPs). For the activation of polypyrrole-based COP, COSAN anion has been used as doping agent resulting in enhanced thermal stability and overoxidation threshold.[81,88] The polymerization of pyrrole, bonded through a diether to COSAN anion, produced a self-doped COP with even higher overoxidation resistance.[89]

Concerning building blocks of nanostructures, carboranes found an extraordinary use as wheels of molecular machines. Originally employed fullerenes were replaced by *para*-carboranes because of their higher solubility and suitable photophysical properties. A variety of *para*-carboranyl-wheeled molecules has been synthesized including the nanocar, the nanocaterpillar, and the trigonal nanocar.[90]

1.8 Self-assembly of boron cluster compounds

Self - assembly has been defined as spontaneous association of molecules into defined geometry under a defined condition.[91] This thermodynamic process is described by the resulting equilibrium between the molecules and the self-assembled aggregates. Self-assembly has become broad term frequently used in description of various systems, for example self-assembly of surfactants, block copolymers, monolayers, nanoclusters, nanotubes and nanowires and even larger building blocks.[92] Spontaneous association is also abundant in many biological systems, such as the formation of membranes by lipids. In this thesis, only self-assembly of boron cluster compounds and self-assembly of surfactants are discussed because of their similarities. It is worth mentioning, that classical self-assembly in colloidal chemistry deals only with noncovalent interactions. Comparing to covalent bonds, they are relatively weak but can be numerous. To understand the self-assembly of boranes and carboranes, the basis on noncovalent

interactions need to be explained. It should be also noticed, that many boranes and heteroboranes are anions and their electrostatic interactions play an important role.

1.8.1 Noncovalent interactions of boron cluster compounds

Classical hydrogen bond, which can be schematically depicted as X–H···Y, is relatively strong, directional and specific noncovalent interaction. X–H represents the hydrogen donor and Y is electronegative atom, such as halogen, O, N or S, whereas X is more electronegative atom than H. "Electron deficiency" makes boron cluster compounds poor H-bond acceptor and the partial negative charge of hydrogens make them also bad H-bond donors. Therefore, this type of bonding has never been observed in boranes.[93]

Weak hydrogen (non-conventional) bonds are considerably weaker than classical hydrogen bonds and are formed, when the H-bond donor is C–H[94] (C–H···O, N, Cl) and/or the H-bond acceptor is the electron density of aromatic molecules (N, O, C–H···π).[95] This bonding is well-known in peptides, crystals and biological systems. In carboranes, the presence of weak hydrogen bonding (such as C–H···O, N, S, halogen and P) has been reported in the crystal structures of carborane derivatives[96] and C–H···π bonding was found in carborane systems with benzene rings.[97] Useful tool for identifying this type of bonding is IR spectroscopy. For example, IR band of *ortho*-carborane C–H group shows the low-frequency shift and broadening on hydrogen bonding with DMSO.[39]

Dihydrogen bond **(DHB)** is energetically weaker interaction than classical hydrogen bond (1–7 kcal mol^{-1}) occurring between proton donors Y–H (Y = N, O, S, C) and σ-bonding electron pair of M–H bonds in hydrides (M = electropositive atom, such as B, alkali, or transition metal). In heteroboranes, spectroscopic and structural experimental evidence was found for C−H···H−B, N−H···H−B, O−H···H−B, and S−H···H−B DHB types.[93] DHB interaction origins from both electrostatic and dispersion, and its energy increases with acidity of donor proton. DHB was found to help stabilizing structures of carborane in crystals,[98] materials,[99] in the systems with biomolecules[100] and even with water.[101] These interactions play an important role in medicinal applications and in the preparation of nanoparticles and nanocomposite described in chapter 1.9 and the papers IV–VI.

σ-hole bonding is the interaction of halogen or chalcogen atom X in some molecules (R–X) with electron donor (Lewis basis). Depending on the type of X atom, this bonding is called halogen, chalcogen or pnictogen bonding. In halogen bonds (Cl, Br, I), the three pairs of halogen unshared electrons form a belt of negative electrostatic potential around its central region with a positive "σ-hole" on the outermost portion of its surface, centered around the R−X axis.[102] This σ-hole interacts with negative regions of other molecules. Chalcogen bond (S···π) was found in the structure of phenyl-substituted thiaborane.[103]

Interactions with biomolecules

With the growing potential of carborane clusters in medicinal use, the studies of interactions between borane clusters and biomolecules becomes important. For example, in the complex of $[CB_{11}H_{12}]^-$ anion and amino acids, studied by quantum mechanics (QM) methods as a model

system of COSAN with HIV protease (chapter 1.7.1), DHB was found to be the dominant interaction.[100] DHB stabilized these complexes by 4.2–5.8 kcal mol^{-1} per interaction and the interaction was preferably formed by the hydrogen atoms of lower carborane hemisphere (i.e. the part of the cage opposite to the carbon atom). Another study of COSAN-peptide interactions revealed, that the stabilization energies of the complexes can be increased by introducing *exo*-skeletal substitutions and by increasing the total negative charge of the cage.[104] Furthermore, in conjunction with the X-ray structure analysis, calculations suggested that COSAN in the active site of protease is present with its sodium counterion, with limited rotary motion.[105]

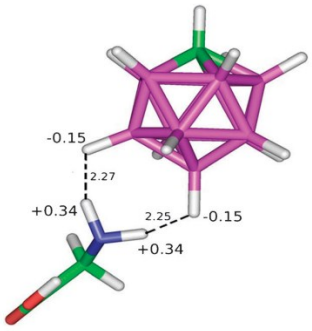

Figure 1.7. Interaction between $[CB_{11}H_{12}]^-$ and glycine via two dihydrogen bonds. Partial charges on the interacting hydrogens as well as distances in Å are shown.[100,61]

1.8.2 Hydrophobic effect

Hydrophobic effect is a tendency for the hydrophobic part of molecule or particle to avoid contact with water. The molecular mechanism of this effect has been a source of great discussion. Nevertheless, the generally accepted view is that its molecular origin is based on significant structural changes of the water surrounding apolar groups. This structuring of water (also called the iceberg formation)[106,107] was proved by the slower molecular motion of the water molecules around solute.[109] It causes a decrease in entropy whereas the enthalpy change upon a hydrocarbon transferring into water is negligible. Hence, this transfer is associated with a large and positive Gibbs free energy change, ΔG, according to:

$$\Delta G\,(\text{large}) = \Delta H\,(\text{small}) - T\Delta S\,(\text{large and negative}) \qquad (1.1)$$

where ΔH is enthalpy change, T is thermodynamic temperature, and ΔS is entropy change. Because of large positive ΔG, hydrophobic molecules have low solubility and they tend to minimize the contact with water by aggregation.

The classical hydrophobic effect, the model described above, is entropically driven. On the other hand, several observations of protein-ligand recognition[109] or membrane binding of amphiphiles[110] revealed a thermodynamic processes with a large enthalpic driving force ($\Delta H_o \ll 0$; $T\Delta S \ll 0$). This specific complexation has been called nonclassical hydrophobic effect.[111] Although the explanation has remained obscure, the hydration of each interacting partner is apparently crucial. Therefore, in case of boron cluster compounds, the unusual hydration can be the reason of their hydrophobicity.

Boranes – hydrophobic or amphiphilic?

The origin of boranes and carboranes strong hydrophobicity has been explained as the result of the presence of partial negative charge on hydrogens, which prevents them from classical hydrogen bonding with water molecules. Although DHB between water molecules and borane hydride occurs (Figure 1.8),[101] this interaction is much weaker than the classical hydrogen bonding and therefore, boranes prefer to avoid the contact with water. The influence of hydrogens on the borane hydrophobicity has been confirmed with the findings that the hydrophobic character can be modulated by the substituents, such as hydroxyl, amine or carboxylic group, which decreases hydrophobicity of conjugates.[55]

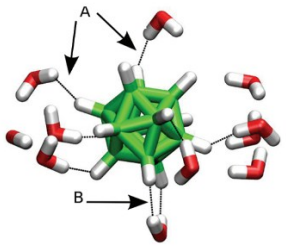

Figure 1.8. Snapshot from simulations showing some of the water molecules around the $[B_{12}H_{12}]^{2-}$ cluster forming two types (A and B) of O−H···H−B dihydrogen bonds.[101]

In one of the publications included in this thesis,[II] we studied solution behavior of several boranes and carboranes. Extensive study revealed that all the studied compounds in water showed unexpected behavior similar to amphiphiles (chapter 1.8.3), such as formation of multimolecular aggregates and lowering of surface tension of water. Detailed study of these "stealth amphiphiles" is presented in the paper II (chapter 5.2).

Among the studied compounds, COSAN has attracted most attention recently. Several studies have tried to describe and explain COSAN solution behavior.[112-118] High solubility of COSAN in both water and organic solvents has already indicated two-faces of COSAN solution behavior. Among the first evidences of amphiphilic behavior is the study from 2001 showing surface activity of COSAN.[112] Later computational studies of molecular dynamics of COSAN at water/organic solvent interface showed that COSAN accumulates at interface and forms small aggregates.[113-115] Subsequently, experimental evidences of COSAN aggregation[116,117] (chapter 1.8.4) supported self-assembly predictions. Other similarities of COSAN with surfactants showed the study of electrolysis behavior and foam formation.[118] Nevertheless, COSAN amphiphilicity is still controversial and has been explained in many ways. The presence of CH groups in the middle of the peanut shaped COSAN led to the new term in the literature, θ-amphiphile.[117,119] However, this concept lacks the evidence of localized hydrophobic and hydrophilic regions. Moreover, partially positively charged CH groups were supposed to participate in classical hydrogen bonding with water, but preliminary results showed that water molecules preferred the hydrogen bonding with each other than with CH group of COSAN.

1.8.3 Self-assembly of amphiphiles

One of the most widely studied self-assembly processes is the micellization of surfactants. In this chapter, micellization of amphiphiles is briefly described because this association shows many similarities with the self-assembly of COSAN (chapter 1.8.4).

Amphiphilic molecules have both a hydrophilic and a hydrophobic part (usually a hydrocarbon chain). The terms amphiphile and surfactant are often used interchangeably. The word *surfactant* originates from surface-active agent referring to a key property of surfactants, which is their tendency to adsorb at air-water interface and consequently to lower the surface tension of water. This is an important aspect of the use of surfactants in detergents. Surfactants can be divided into two groups: nonionic, ionic (cationic or anionic) and zwitterionic surfactants.[91] Their solution behavior is controlled by the hydrophobic effect, which leads to the formation of spherical particles – micelles. They consist of the hydrophobic core, which is shielded from water by the surrounding corona formed by the hydrophilic groups. Nevertheless, some low-molecular mass compounds, such as ethanol, are surface active and amphiphilic but they do not form classical micelles. Besides spherical micelles, various other morphologies and shapes are possible, for example cylindrical micelles, vesicles or lamellar structures. The morphology of assemblies depends on the concentration, as well as the geometry of amphiphile and the resulting force between the polar head groups.[120] These parameters are involved in the critical packing parameter, p, defined as

$$p = \frac{v}{a_0 l_c} \tag{1.2}$$

in which a_o is the area per molecule at the aggregate surface, v is the volume of the hydrophobic chain, and l_c is the maximum length of this chain. The area per molecule, a_0, increases if the repulsive forces between polar head groups predominate. The values of the critical packing parameter are mostly lower than one, for example for spherical micelles $p < 1/3$.

Micellization occurs in the solutions with concentrations higher than critical micelle concentration, CMC (critical micelle concentration). Addition of surfactant above the CMC increase only the micelle concentration but not the concentration of unimer. CMC can be determined by several methods, such as surface tension, light scattering, isothermal titration calorimetry, conductometry, NMR (both ^{1}H NMR change of chemical shifts and diffusion coefficients from DOSY experiments) or fluorescence.

Various micellization models have been proposed. The most common one, closed association model,[121] assumes a dynamic equilibrium between the unassociated unimers and the molecules associated in an aggregate. This model involves CMC, where certain physical properties of the solution show a sharp change. The micelles are practically monodisperse and finite-size. Alternatively, the open association model assumes multiple equilibrium, continuous growth of the aggregates, and the absence of a well-defined CMC.[122,123]

For ionic surfactants, the counterion dissociation plays a significant role. Because of the counterions, macroscopic phase separation becomes entropically very unfavorable and ionic surfactant tends to form small micelles. Thermodynamics of micellization, described by the

closed association model, assumes that micelles M are formed by *n* surfactant molecules S, which have *m* counterions G:

$$n\mathrm{S} + m\mathrm{G} = (\mathrm{S}_n\mathrm{G}_m)^z = \mathrm{M}^z \tag{1.3}$$

where *z* is the charge or the valence of the micelles. The standard Gibbs free energy change, ΔG^0, for the micellization of equation 1.3 can be obtained from the well-known thermodynamic result:

$$\Delta G^0 = -RT\ln K = -RT(\ln X_\mathrm{M} - n\ln X_\mathrm{S} - m\ln X_\mathrm{G}) \tag{1.4}$$

in which *R* is gas constant, *T* is thermodynamic temperature, *K* is equilibrium constant and X_i is mole fraction. If we define ΔG^0_mic as the standard Gibbs free energy change of micellization per mole of amphiphile, then:

$$\Delta G^0_\mathrm{mic} = -\frac{RT}{n}\ln K = -RT\left(\frac{1}{n}\ln X_\mathrm{M} - \ln X_\mathrm{S} - \frac{m}{n}\ln X_\mathrm{G}\right) \tag{1.5}$$

Finally, for large *n* equation 1.5 is reduced to:

$$\Delta G^0_\mathrm{mic} = (1+\beta)RT\ln X_\mathrm{CMC} \tag{1.6}$$

where $\beta = m/n$ and is called the degree of counterion binding to micelle (or counterion condensation). For example, classical ionic surfactant, sodium dodecyl sulfate, SDS, is in water fully dissociated without any ion-pairs. Above the CMC, the charge density on micelles is very high and approximately 80% of sodium cations ($\beta = 0.8$) condense at the surface and compensate the surface charge.[124] Furthermore, addition of salt decreases the CMC because the added electrolyte reduces the repulsion between polar head groups of ionic surfactant molecules.

At very high concentrations, amphiphiles can self-assemble into lyotropic liquid crystalline phases, which is the phase that lacks the full three-dimensional translational order of molecules on a crystal lattice. The term “lyotropic” refers to the fact that the phase is formed by amphiphiles under appropriate conditions of concentration, temperature and pressure. Lyotropic phases with one-dimensional translational order, which consists of amphiphiles bilayers are called lamellar phases. These can, under certain conditions, curve into closed shell structures called vesicles, which are commonly used in cosmetics and in many potential applications of drug delivery.

Amphiphilic properties are important for a much broader group of compounds than only surfactant systems. Various macromolecules show both hydrophilic and hydrophobic regions, for example block and grafted copolymers, proteins, lipopolysaccharides, DNA, cellulose or Pickering emlusions.[125] Amphiphilic behavior can be also achieved by a specific coating of the nanoparticles, which have been mostly prepared for stabilizing water/oil emulsions.[126]

1.8.4 Self-assembly of COSAN

Formation of different assemblies in aqueous solution of COSAN relates to hydrophobic or amphiphilic character (chapter 1.8.2) and has been observed experimentally by various techniques. Diffusion coefficient from DOSY NMR shows two concentration regions divided by critical aggregation concentration, CAC (11 mM for Na[COSAN]): unimers below CAC, and small assemblies of 5 molecules above CAC.[I] In addition, scattering techniques revealed the presence of large aggregates.[116,117] Bauduin et al. interpreted the large particles in H[COSAN] solution as monolayer vesicles with COSAN molecules oriented orthogonally to the shell surface.[117] However, results from SAXS,[I] interfacial tension[112] and molecular dynamics simulations[114] show that typical COSAN orientation at the water/air and water/oil interface is rather parallel. In addition, later findings showed that the fraction of these larger aggregates is probably less than 5–10%. Moreover, non-negligible fraction of nanobubbles in COSAN solution was detected by LS,[I] which makes the clear description of this system even more difficult. Other details concerning this topic are described in the paper I (chapter 5.1).

Interestingly, at very high concentrations lyotropic lamellar phase is formed in solution of iodine COSAN derivative, H[I_2COSAN].[119] The authors even concluded that lamellar phase seems to be a general property of COSAN. This phase consists of monomolecular sheets, which are connected via dihydrogen bonds oriented perpendicularly to the surface of the layer.

The main aggregation driving force of COSAN self-assembly has been often referred to dihydrogen bonds between B–H and C–H but since borane clusters without C–H were found to aggregate similarly (see chapter 5.2) it is rather nonspecific hydrophobic effect that causes the association of COSAN.

Self-assembly has been also observed in the aqeous solutions of COSAN derivatives, such as conjugates with porphyrine,[127,64] nucleoside,[63] fluorescein[38] and short oxyethylene chain.[III] For porphyrine-COSAN conjugates, the interaction between negatively charged COSAN and the protonated porphyrine moiety was suggested as the reason for the aggregation.[127] The study of nucleoside-COSAN conjugates revealed, that aggregation is strongly enhanced by the presence of amino groups leading to the formation of zwitterions, which are sparingly soluble in the aqueous solution. In addition, all COSAN-containing compounds were found to be almost insoluble in buffers containing molecules bearing amino groups that are currently used in biology-oriented studies.[63] All these studies can help to understand solution behavior of carborane drugs and to prepare better drug delivery carriers.

1.9 Coassembly of COSAN

In the studies of COSAN interaction with macromolecules, we have used the term coassembly, which is mainly used for the formation of nanostructures based on the interaction of polymers with usually low-molecular-weight agents, for example polyelectrolytes with ions.[128] Majority of the COSAN coassembly studies are focused on potential medicinal use, in which the substance formulated alongside the active ingredient, is called excipient. It helps in stabilizing the dispersion, enhancing solubility and controlling drug release. Several studies have been

conducted with an emphasis on solubilization and long-term stability of COSAN and its derivatives after mixing with polymers,[129,130] cyclodextrines,[131,38] human serum albumin,[129] surfactants[129] and phospholipid bilayers.[38] These excipients improve solubilization and lower size of the aggregates, and some authors claimed that these excipients suppressed COSAN self-assembly. However, these phenomena were not described on the molecular and interaction level and after the next findings the issue of COSAN self-assembly was found to be much more complex. In this chapter, some of the previously studied COSAN systems are described and divided into two main groups – solid composites and coassembly in aqueous solution.

1.9.1 Solid composites

An important study from our group by Matějíček et al. showed that Na[COSAN] interacts with widely used hydrophilic polymer, poly(ethylene oxide), PEO, leading to insoluble nanocomposite with uniquely organized structure (Figure 1.9).[132-134] This precipitate obviously differs from pure COSAN by its red color. The COSAN clusters and sodium cations are evenly dispersed within the PEO matrix with long-range order and the immobilized PEO does not contain any crystalline polymeric domains. QM calculations revealed that part of the hydrogens of CH_2 units of PEO are involved in DHB with hydrogens attached to B10 and B10' of COSAN (6.3 kcal mol^{-1}; Figure 1.9B). Further contribution is caused by the attractive interaction between Na^+ and PEO oxygens (19 kcal mol^{-1}).

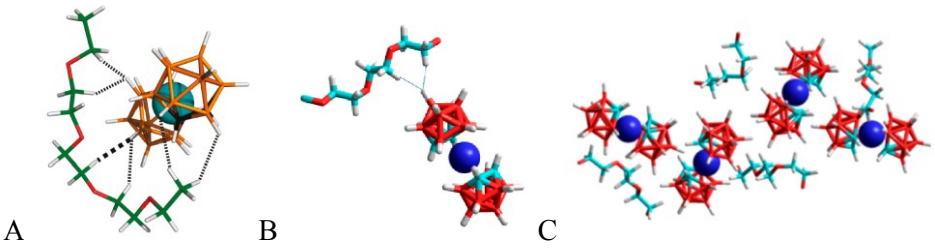

Figure 1.9. (A) Optimized structure of COSAN and PEO pentamer complex based on QM calculations with possible interactions;[133] (B) Structural motif of COSAN with PEO in PEO/Na^+/COSAN composite estimated from 2D NMR spectra;[134] (C) The proposed structure of PEO/Na^+/COSAN composite.[134]

Another COSAN composite was formed by poly(2-vinylpyridine), P2VP, and poly(4-vinylpyridine), P4VP (Figure 1.10A).[134] Comparing to flexible PEO chain with low glass temperature (T_g), P2(4)VP chains have higher T_g and they are more rigid and positively charged. In acidic aqueous solution, completely protonized polymers P2(4)VP and Na[COSAN] formed amorphous orange precipitate P2(4)VP/H^+/COSAN. In this case, the driving interaction is direct electrostatic attraction between polycation P2(4)VP and COSAN anions. This attraction is stronger than DHB between PEO and COSAN, therefore accumulated quantity of COSAN within the composite is larger. Direct contact between COSAN and $N{=}(H)^+$ was observed in P4VP but not in P2VP, indicating that charge position in polymer isomers has an important impact on COSAN location. This charge position influences COSAN orientation: in P2VP it is

parallel, but in P4VP perpendicular to the polymer chain. Comparing to PEO/Na^+/COSAN composite, the chains are covered not only by bulky COSAN, but also smaller chloride anions, which fill the unoccupied spots and compensate the rest of positive charges on the polymer chain (Figure 1.10B,C).

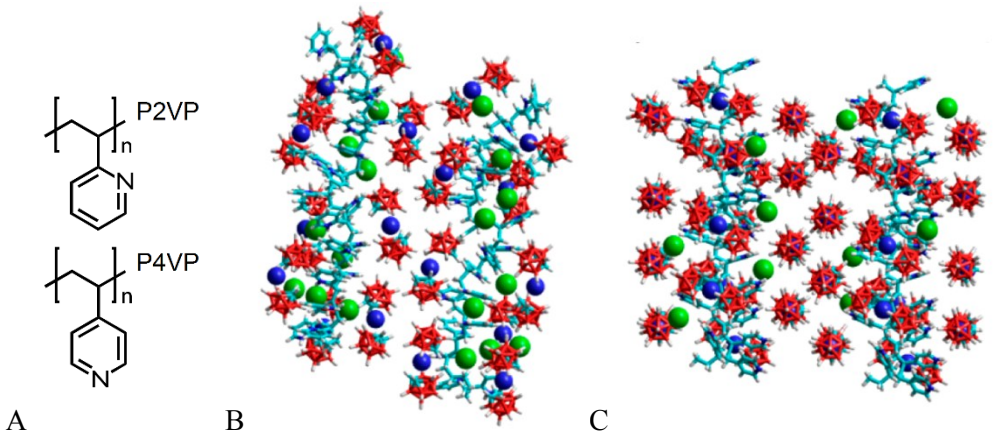

Figure 1.10. (A) Structures of poly(2-vinylpyridine), P2VP, and poly(4-vinylpyridine), P4VP; (B) idealized structure of P2VP/H^+/COSAN composite; (C) idealized structure of P4VP/H^+/COSAN composite[134] (color coding: green = Na^+, cyan = polymer, red = dicarbollide of COSAN, blue = cobalt).

In all three polymeric nanocomposites (PEO, P2VP, P4VP) uniaxial rotational motions of COSAN molecules was observed. This COSAN motion is more extensive than those of polymer segments, resembling the system of rigid polymeric stator and COSAN mobile rotator. Such systems are called amphidynamic and have a potential use as molecular machines.

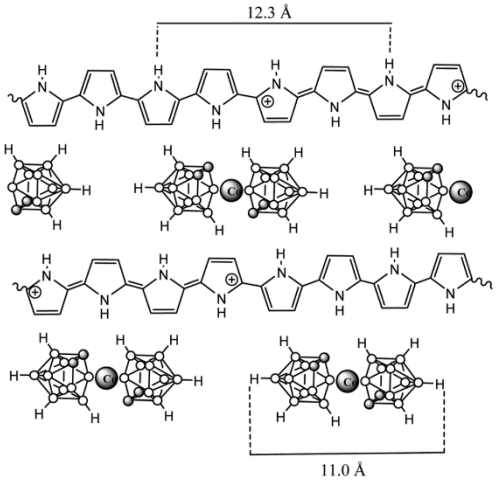

Figure 1.11. Graphical representation of the PPy/COSAN polymer.[135]

Several studies were focused on the composites of polypyrrole (PPy) with COSAN or other carboranes, in the search of the new conducting organic polymers (COPs) using carboranes as the low-coordinating doping anions (Chapter 1.7.2).[88,89,135] PPy/COSAN composite was prepared via electropolymerization of the monomer in the presence of Cs[COSAN].[81] X-ray photoelectron analysis showed that there are four PPy segments per each COSAN anion

(Figure 1.11). Retention of COSAN anions within the polymeric matrix was supposed to be caused by hydrophobicity, large size and multiple binding properties of COSAN.[135]

1.9.2 Coassembly in solution

The PEO/COSAN interaction turned out to be a useful tool for preparing nanoparticles with diblock copolymer of PEO and hydrophilic block which can solubilize PEO/COSAN complex. Therefore, poly(ethylene oxide)-*block*-poly(methacrylic acid), PEO–PMA, was used to prepare nanoparticles with PEO/Na[COSAN] core and pH-responsive shell of polyanionic PMA.[132] Particle composition depends on salt concentration and COSAN can diffuse from/into the nanoparticle after the salinity change. These particles also represent the first polymeric nanoparticles in which hydrophilic PEO forms the core. However, PMA block lacks biocompatibility and the potential biochemical use is thus limited.

To stabilize PEO/COSAN complex in water we decided to use hydrophilic poly(2-alkyl-2-oxazoline)s, POX, which become useful alternative to PEO in various application and provide biocompatibility, variety of side-chain modifications and thermoresponsivity.[136] First, we used block copolymer of PEO with poly(2-ethyl-2-oxazoline), PEO–PEtOx.[130] Cosan was found to interact also with PEtOx block, but PEtOx/Na[COSAN] complex was water soluble. PEO−PEtOx/Na[COSAN] nanoparticles in 0.1M NaCl solution were homogenous without core-shell structure because PEO and PEtOx blocks were intermixed and cross-linked by COSAN molecules. PEO–PEtOx was also mixed with COSAN derivatives, which effectively inhibited HIV, and the polymer was found to interact with all of them manifesting in decrease of particles size and increase of COSAN solubility. However, *in vitro* experiments revealed that the inhibitors binded to PEO−PEtOx too strongly and the polymeric nanoparticles "competed" with HIV protease for inhibitor molecules. The inhibition activity is therefore deteriorated.

In later studies, we used star-like copolymer 4-arm poly(ethylene oxide)-*block*-poly(2-methyl-2-oxazoline), $[PEO–PMeOx]_4$, to compare the intraction of COSAN with polymers of different morphology.[IV,V] $[PEO–PMeOx]_4$/Na/COSAN nanoparticles had multicompartment structure comparing to homogenous spheres of linear polymer. We also found out that strength of interaction between COSAN and POX can be controlled by the cation of present salt, as we observed different structures of particles in Li^+, Na^+ and K^+ salt. In addition, comparison of POX with different alkyl group shows increase in interaction strength in following order: methyl, ethyl and *n*-propyl. The assemblies POX/COSAN can be also modulated by the temperature because some POX show thermoresponsivity.[VI] Hence, the POX polymers provide excellent properties for preparing various types of COSAN nanoparticles for drug delivery. Detailed study on the interactions between POX and COSAN is presented in the papers IV, V and VI (chapters 5.4, 5.5 and 5.6).

References

[1] Davy, H. *Philos. Trans. R. Soc. Lond.* **1809**, *99*, 39.

[2] Gay-Lussac, J. L.; Thénard, L. J. *Ann. Chim. Phys.* **1808**, *68*, 169.

[3] Lipscomb, W. N. The boranes and their relatives. In *Chemistry 1971-1980*; Frangsmyr, T., Ed.; World Scientific Publishing Co. Pte. Ltd.: Singapore, 1993; p. 224.

[4] Delaplane, R. G.; Dahlborg, U.; Graneli, B.; Fischer, P.; Lundström, T. *J. Non-Cryst. Solids* **1988,** *104*, 249.

[5] Fujimori, M.; Nakata, T.; Nakayama, T.; Nishibori, E.; Kimura, K.; Takata, M.; Sakata, M. *Phys. Rev. Lett.* **1999**, *82*, 4452.

[6] Zarechnaya, E. Y.; Dubrovinsky, L.; Dubrovinskaia, N.; Miyajima, N.; Filinchuk, Y.; Chernyshov, D.; Dmitriev, V. *Sci. Technol. Adv. Mater.* **2009**, *9*, 044209.

[7] Zhai, H. J.; Zhao, Y. F.; Li, W. L.; Chen, Q.; Bai, H.; Hu, H. S.; Piazza, Z. A.; Tian, W. J.; Lu, H. G.; Wu, Y. B.; Mu, Y. W.; Wei, G. F.; Liu, Z. P.; Li, J.; Li, S. D.; Wang, L. S. *Nat. Chem.* **2014**, *6*, 727.

[8] Piazza, Z. A.; Hu, H. S.; Li, W. L.; Zhao, Y. F.; Li, J.; Wang, L. S. *Nat. Commun*. **2014**, *5*, 3113.

[9] Greenwood, N. N.; Earnshaw A. *Chemistry of the elements, second edition*; Pergamon Press: Oxford, 1984; p. 139.

[10] World Health Organization. *Trace elements in human nutrition and health*; World Health Organization: Geneva, 1996; p. 175.

[11] Nielsen, F. H. *Nutr. Rev.* **2008**, *66*, 183.

[12] Samman, S.; Foster, M.; Hunter, D. The Role of Boron in Human Nutrition and Metabolism. In *Boron Science: New Technologies and Applications*; Hosmane, N. S., Ed.; CRC Press: New York, 2012; p. 73.

[13] Stock, A. *Hydrides of Boron and Silicon*; Cornell University Press: Ithaca, New York, 1933.

[14] Hughes, R. L.; Smith, I. C.; Lawless, E. W. *In Production of the Boranes and Related Research*; Holzmann, R. T., Ed.; Academic Press: New York, 1967.

[15] Williams, R. E. *Inorg. Chem.*, **1971**, *10*, 210

[16] Wade, K. *J. Chem. Soc. D* **1971**, 792.

[17] Welch, A. J. *Chem. Commun*., **2013**, *49*, 3615.

[18] Schleyer, R.; Najafan, K. Are polyhedral boranes, carboranes and carbocations aromatic? In *The Borane, Carborane, Carbocation Continuum*; Casanova, J., Ed.; John Wiley and Sons, Inc.: New York, 1998; p. 169.

[19] Lipscomb, W. N. *Boron Hydrides*; Benjamin: New York, 1963.

[20] King, R. B. *Chem. Rev.* **2001**, *101*, 1119.

[21] Grimes, R. N. *Carboranes, Second Edition*. Academic Press: London, 2011; p.18.

[22] Hoffmann, R.; Lipscomb, W. N. *J. Chem. Phys.* **1962**, *36*, 3489.

[23] Fein, M. M.; Bobinski, J.; Mayes, N.; Schwartz, N.; Cohen, M. S. *Inorg. Chem.* **1963**, *2*, 1111.

[24] Lipscomb, W. N. *Science* **1966**, *153*, 373.

[25] Kalinin, V. N.; Olshevskaya, V. A. *Russ. Chem. Bull.* **2008**, *57*, 815.

[26] Korbe, S.; Schreiber, P. J.; Michl, J. *Chem. Rev*. **2006**, *106*, 5208.

[27] Juhasz, M.; Hoffmann, S.; Stoyanov, E.; Kim, K. C.; Reed, C. A. *Angew. Chem. Int. Ed*. **2004**, *43*, 5352.

[28] Reed, C. A. *Chem. Commun.* **2005**, *13*, 1669.
[29] Grimes, R. N. *Angew. Chem. Int. Ed*. **2003**, *42*, 1198.
[30] Burke, A.; Ellis, D.; Giles, B. T.; Hodson, B. E.; Macgregor, S. A.; Rosair, G. M.; Welch, A. J. *Angew. Chem.* **2003**, *115*, 235.
[31] Hawthorne, M. F.; Young, D. C.; Wegner, P. A. *J. Am. Chem. Soc*. **1965**, *87*, 1818.
[32] Hawthorne, M. F.; Zink, J. I.; Skelton, J. M.; Bayer, M. J.; Liu, C.; Livshits, E.; Baer, R.; Neuhauser, D. *Science* **2004**, *303*, 1849.
[33] Bühl, M.; Hnyk, D.; Macháček, J. *Inorg. Chem.* **2007**, *46*, 1771.
[34] Sivaev, I. B.; Bregadze, V. I. *Collect. Czech. Chem. Commun.* **1999**, *64*, 783.
[35] Rak, J.; Dejlová, B.; Lampová, H.; Kaplánek, R.; Matějíček, P.; Cígler, P.; Král, V. *Mol. Pharm.* **2013**, *10*, 1751.
[36] Plešek, J.; Baše, K.; Mareš, F.; Hanousek, F.; Štíbr, B.; Heřmánek, S. *Collect. Czech. Chem. Commun.* **1984**, *49*, 2776.
[37] Reed, C. A.; Guiset, F. *J. Am. Chem. Soc.* **1996**, *118*, 3281.
[38] Uchman, M.; Jurkiewicz, P.; Cígler, P.; Grüner, B.; Hof, M.; Procházka, K.; Matějíček, P. *Langmuir* **2010**, *26*, 6268.
[39] Leites, L. A. *Chem. Rev.* **1992**, *92*, 279.
[40] Zalkin, A.; Hopkins, T. E.; Templeton, D. H. *Inorg. Chem*. **1967**, *6*, 1911.
[41] Borodinsky, L.; Sinn, E.; Grimes, R. N. *Inorganic Chemistry* **1982**, *21*, 1686.
[42] Bühl, M.; Hnyk, D.; Macháček, J. *Chem. Eur. J.* **2005**, *11*, 4109.
[43] Juárez-Pérez, E. J.; Núñez, R.; Viñas, C.; Sillanpää, R.; Teixidor, F. *Eur. J. Inorg. Chem*. **2010**, 2385.
[44] Chamberlin, R. M.; Scott, B. L.; Melo, M. M.; Abney, K. D. *Inorg. Chem*. **1997**, *36*, 809.
[45] Farràs, P.; Viñas, C.; Teixidor, F. *J. Organomet. Chem.* **2013**, *747*, 119.
[46] Sivý, P.; Preisinger, A.; Baumgartner, O.; Valach, F.; Koreň, B.; Matel, L. *Acta Cryst. C* **1986**, *42*, 28.
[47] Peymann, T.; Knobler, C. B.; Hawthorne, M. F. *Inorg. Chem*. **1998**, *37*, 1544.
[48] Peymann, T.; Lork, E.; Gabel, D. *Inorg. Chem*. **1996**, *35*, 1355.
[49] Jelinek, T.; Štibr, B.; Mareš, F.; Plešek, J.; Heřmánek, S. *Polyhedron* **1987**, *6*, 1737.
[50] Semioshkin, A. A.; Sivaev, I. B.; Bregadze, V. I. *Dalton Trans*. **2008**, *8*, 977.
[51] Plešek, J.; Grüner, B.; Heřmánek, S.; Báča, J.; Mareček, V.; Jänchenová, J.; Lhotský, A.; Holub, K.; Selucký, P.; Rais, J.; Císařová, I. *Polyhedron* **2002**, *21*, 975.
[52] Grüner, B.; Plešek, J.; Báča, J.; Dozol, J. F.; Lamare, V.; Císařová, I.; Bělohradský, M.; Čáslavský, J. *New J. Chem*. **2002**, *26*, 867.
[53] Scholz, M.; Hey-Hawkins, E. *Chem. Rev*. **2011**, *111*, 7035.
[54] Plešek, J. *Inorg. Chim. Acta* **1999**, *289*, 45.
[55] Lesnikowski, Z. *J. Med. Chem*. **2016**, *59*, 7738.
[56] Harling, O.K. *Appl. Radiat. Isot*. **2009**, *67*, S7.
[57] Barth, R. F.; Vicente, M. H.; Harling, O. K.; Kiger, W. S.; Riley, K. J.; Binns, P. J.; Wagner, F. M.; Suzuki, M.; Aihara, T.; Kato, I.; Kawabata, S. *Radiat. Oncol.* **2012**, *7*, 146.
[58] Soloway, A. H.; Tjarks, W.; Barnum, B. A.; Rong, F. G.; Barth, R. F.; Codogni, I. M.; Wilson, J. G. *Chem. Rev*. **1998**, *98*, 1515.
[59] Bregadze, V. I.; Sivaev, I. B. Polyhedral Boron Compounds for BNCT. In *Boron Science: New Technologies and Applications*; Hosmane, N. S., Ed.; CRC Press: New York, 2012; p. 181.

[60] Cígler, P.; Kožíšek, M.; Řezáčová, P.; Brynda, J.; Otwinowski, Z.; Pokorná, J.; Plešek, J.; Grüner, J.; Dolečková-Marešová, L.; Máša, M.; Sedláček, J.; Bodem, J.; Kräusslich, H. G.; Král, V.; Konvalinka, J. *Proc. Natl. Acad. Sci.* **2005**, *102*, 15394.

[61] Řezáčová, P.; Cígler, P.; Matějíček, P.; Lepšík, M.; Pokorná, J.; Grüner, B.; Konvalinka, J. Medicinal Application of Carboranes: Inhibition of HIV Protease. In *Boron Science: New Technologies and Applications*; Hosmane, N. S., Ed.; CRC Press: New York, 2012; p. 41.

[62] Scholz, M.; Bensdorf, K.; Gust, R.; Hey-Hawkins, E. *ChemMedChem* **2009**, *4*, 746.

[63] Matějíček, P.; Cígler, P.; Olejniczak, A. B.; Andrysiak, A.; Wojtczak, B.; Procházka, K.; Lesnikowski, Z. *Langmuir* **2008**, *24*, 2625.

[64] Hao, E.; Sibrian-Vazquez, M.; Serem, W.; Garno, J. C.; Fronczek, F. R.; Vicente, M. G. H. *Chem. Eur. J.* **2007**, *13*, 9035.

[65] Grüner, B.; Rais, J.; Selucký, P.; Lučaníková, M. Recent Progress in Extraction Agents Based on Cobalt Bis(Dicarbollides) for Partitioning of Radionuclides from High-Level Nuclear Waste. In *Boron Science: New Technologies and Applications*; Hosmane, N. S., Ed.; CRC Press: New York, 2012; p. 463.

[66] Plešek, J. *Chem. Rev*. **1992**, *92*, 269.

[67] Rais, J.; Kyrš, M.; Heřmánek, S. Czech. Patent 153 933, 1974.

[68] Rais, J.; Selucký, P.; Kyrš, M. *J. Inorg. Nucl. Chem*. **1976**, *38*, 1376.

[69] Rais, J.; Šebestová, E.; Selucký, P.; Kyrš, M. *J. Inorg. Nucl.* **1976**, *38*, 1742.

[70] Podzimek, I.; Kyrš, M.; Rais, J.; Vaňura, P. *Polyhedron* **1983**, *2*, 331.

[71] Mikulášek, L.; Grüner, B.; Dordea, C.; Rudzevich, V.; Böhmer, V.; Haddaoui, J.; Hubscher-Bruder, V.; Arnaud-Neu, F.; Čáslavský, J.; Selucký, P. *Eur. J. Org. Chem*. **2007**, *28*, 4772.

[72] Moss, S.; King, B. T.; de Meijere, A.; Kozhushkov, S. I.; Eaton, P. E.; Michl, J. *Org. Lett*. **2001**, *3*, 2375.

[73] Vyanakaram, K.; Barbour, J. B.; Michl, J. *J. Am. Chem. Soc*. **2006**, *128*, 1510.

[74] Volkis, V.; Mei, H.; Shoemaker, R. K.; Michl, J. *J. Am. Chem. Soc*. **2009**, *131*, 3132.

[75] Dubay, W. J.; Grieco, P. A.; Todd, L. J. *J. Org. Chem*. **1994**, *59*, 6898.

[76] Grieco, P. A.; DuBay, W. J.; Todd, L. J. *Tetrahedron Lett* **1996**, *37*, 8707.

[77] Viñas, C.; Núñez, R.; Teixidor, F.. Large Molecules Containing Icosahedral Boron Clusters Designed for Potential Applications. In *Boron Science: New Technologies and Applications*; Hosmane, N. S., Ed.; CRC Press: New York, 2012; p. 701.

[78] Kimura, H.; Okita, K.; Ichitani, M.; Sugimoto, T.; Kuroki, S.; Ando, I. *Chem. Mater.* **2003**, *15*, 355.

[79] Zhou, Q.; Mao, Z.; Ni, L.; Chen, J. *J. Appl. Polym. Sci.* **2007**, *104*, 2498.

[80] Nagata, Y.; Chujo, Y. *Macromolecules* **2008**, *41*, 2809.

[81] Masalles, C.; Borrós, S.; Viñas, C.; Teixidor, F. *Adv. Mater.* **2000**, *12*, 1199.

[82] Hardie, M. J. *J. Chem. Crystallogr.* **2007**, *37*, 69.

[83] Jelliss, P. A. Photoluminescence from Boron-Based Polyhedral Clusters. In *Boron Science: New Technologies and Applications*; Hosmane, N. S., Ed.; CRC Press: New York, 2012; p. 355.

[84] Dash, B. P.; Satapathy, R.; Gaillard, E. R.; Maguire, J. A.; Hosmane, N. S. *J. Am. Chem. Soc*. **2010**, *132*, 6578.

[85] Kokado, K.; Chujo, Y. *J. Org. Chem.* **2010**, *76*, 316.

[86] Ferrer-Ugalde, A.; Juárez-Pérez, E. J.; Teixidor, F.; Viñas, C.; Sillanpää, R.; Pérez-Inestrosa, E.; Núñez, R. *Chem. Eur. J.* **2012**, *18*, 544.

[87] Kokado, K.; Tokoro, Y.; Chujo, Y. *Macromolecules* **2009**, *42*, 2925.
[88] Masalles, C.; Borrós, S.; Viñas, C.; Teixidor, F. *Adv. Mater*. **2002**, *14*, 449.
[89] Masalles, C.; Llop, J.; Viñas, C.; Teixidor, F. *Adv. Mater.* **2002**, 14, 826.
[90] Morin, J. F.; Sasaki, T.; Shirai, Y.; Guerrero, J. M.; Tour, J. M. *J. Org. Chem.* **2007**, *72*, 9481.
[91] Lee, Y. S. *Self-Assembly and Nanotechnology*; John Wiley & Sons, Inc.: Hoboken, New Jersey, 2008.
[92] Ozin, G.; Arsenault, A. *Nanochemistry – A Chemical Approach to Nanomaterials*; The Royal Society of Chemistry: Cambridge, 2005.
[93] Sedlak, R.; Fanfrlík, J.; Pecina, A.; Hnyk, D.; Hobza, P.; Lepšík, M. Noncovalent Interactions of Heteroboranes. In *Boron – The Fifth Element*; Hnyk, D.; McKee, M. L., Ed.; Springer International Publishing: Switzerland, 2015; p. 219.
[94] Taylor, R.; Kennard, O. *J. Am. Chem. Soc*. **1982**, *104*, 5063.
[95] Meyer, E. A.; Castellano, R. K.; Diederich, F. *Angew. Chem. Int. Ed.* **2003**, *42*, 1210.
[96] Fox, M. A.; Hughes, A. K. *Coord. Chem. Rev*. **2004**, *248*, 457.
[97] Blanch, R. J.; Williams, M.; Fallon, G. D.; Gardiner, M. G.; Kaddour, R.; Raston, C. L. *Angew. Chem. Int. Ed.* **1997**, *36*, 504.
[98] Campbell, J. P.; Hwang, J. W.; Young, V. G.; Von Dreele, R. B.; Cramer, C. J.; Gladfelter, W. L. *J. Am. Chem. Soc*. **1998**, *120*, 521.
[99] Planas, J. G.; Viñas, C.; Teixidor, F.; Comas-Vives, A.; Ujaque, G.; Lledós, A.; Light, M. E.; Hursthouse, M. B. *J. Am. Chem. Soc*, **2005**, *127*, 15976.
[100] Fanfrlík, J.; Lepšík, M.; Horinek, D.; Havlas, Z.; Hobza, P. *Chem. Phys. Chem*. **2006**, *7*, 1100.
[101] Karki, K.; Gabel, D.; Roccatano, D. *Inorg. Chem.* **2012**, *51*, 4894.
[102] Clark, T.; Hennemann, M.; Murray, J. S.; Politzer, P. *J. Mol. Model.* **2007**, *13*, 291.
[103] Fanfrlík, J.; Přáda, A.; Padělková, Z.; Pecina, A.; Macháček, J.; Lepšík, M.; Holub, J.; Růžička, A.; Hnyk, D.; Hobza, P. *Angew. Chem. Int. Ed.* **2014**, *53*, 10139.
[104] Fanfrlík, J.; Hnyk, D.; Lepšík, M.; Hobza, P. *Chem. Phys. Chem.* **2007**, *9*, 2085.
[105] Fanfrlík, J.; Brynda, J.; Řezáč, J.; Hobza, P.; Lepšík, M. *J. Phys. Chem. B*. **2008**, *112*, 15094.
[106] Frank, H. S.; Evans, M. W. *J. Chem. Phys.* **1945**, *13*, 507.
[107] Shinoda, K. *J. Phys. Chem.* **1977**, *81*, 1300.
[108] Yamaguchi, T.; Matsuoka, T.; Koda, S. *J. Chem. Phys.* **2004**, *120*, 7590.
[109] Bingham, R.; Bodenhausen, G.; Findlay, J. H. B. C.; Hsieh, S.-Y.; Kalverda, A. P.; Kjellberg, A.; Perazzolo, C.; Phillips, S. E. V.; Seshadri, K.; Turnbull, W. B.; Homans, S. W. *J. Am. Chem. Soc*. **2004**, *126*, 1675.
[110] Seelig, J.; Ganz, P. *Biochem*. **1991**, *30*, 9354.
[111] Syme, N. R.; Dennis, C.; Phillips, S. E.; Homans, S. W. *ChemBioChem* **2007**, *8*, 1509.
[112] Popov, A.; Borisova, T. *J. Colloid Interface Sci.* **2001**, *236*, 20.
[113] Chevrot, G.; Schurhammer, R.; Wipff, G. *J. Phys. Chem. B* **2006**, *110*, 9488.
[114] Chevrot, G.; Schurhammer, R.; Wipff, G. *Phys. Chem. Chem. Phys.* **2007**, *9*, 1991.
[115] Chevrot, G.; Schurhammer, R.; Wipff, G. *Phys. Chem. Chem. Phys.* **2007**, *9*, 5928.
[116] Matějíček, P.; Cígler, P.; Procházka, K.; Král, V. *Langmuir* **2006**, *22*, 575.
[117] Bauduin, P.; Prevost, S.; Farràs, P.; Teixidor, F.; Diat, O.; Zemb, T. *Angew. Chem., Int. Ed.* **2011**, *50*, 5298.
[118] Viñas, C.; Tarrés, M.; González-Cardoso, P.; Farràs, P.; Bauduin, P.; Teixidor, F. *Dalton Trans.* **2014**, *43*, 5062.

[119] Brusselle, D.; Bauduin, P.; Girard, L.; Zaulet, A.; Viñas, C.; Teixidor, F.; Ly, I.; Diat, O. *Angew. Chem. Int. Ed.* **2013**, *52*, 12114.

[120] Israelachvili J. N. *Intermolecular and surface forces*. London: Harcourt Brace and Company; 1992.

[121] Blandamer, M. J.; Cullis, P. M.; Soldi, L. G.; Engberts, J.; Kacperska, A.; Vanos, N. M.; Subha, M. C. S. *Adv. Colloid Interface Sci.* **1995**, *58*, 171.

[122] Nyrkova, I. A.; Semenov, A. N. *Eur. Phys. J. E: Soft Matter Biol. Phys.* **2005**, *17*, 327.

[123] Klíčová, L. U.; Sebej, P.; Stacko, P.; Filippov, S. K.; Bogomolova, A.; Padilla, M.; Klan, P. *Langmuir* **2012**, *28*, 15185.

[124] Marcolongo, J. P.; Mirenda, M. *J. Chem. Educ.* **2011**, *88*, 629.

[125] Chevalier, Y.; Bolzinger, M. A. *Colloids Surf. A Physicochem. Eng. Asp.* **2013**, *439*, 23.

[126] Kalashnikova, I.; Bizot, H.; Cathala, B.; Capron, I. *Biomacromolecules* **2012**, *13*, 267.

[127] Kubat, P.; Lang, K.; Cígler, P.; Kožíšek, M.; Matějíček, P.; Janda, P.; Zelinger, Z.; Procházka, K.; Král, V. *J. Phys. Chem. B* **2007**, *111*, 4539.

[128] Zhong, S.; Cui, H. G.; Chen, Z. Y.; Wooley, K. L.; Pochan, D. *J. Soft Matter* **2008**, *4*, 90.

[129] Rak, J.; Kaplánek, R.; Král, V. *Bioorg. Med. Chem. Lett.* **2010**, *20*, 1045.

[130] Ďorďovič, V.; Uchman, M.; Procházka, K.; Zhigunov, A.; Pleštil, J.; Nykanen. A.; Ruokolainen, J.; Matějíček, P. *Macromolecules* **2013**, *46*, 6881.

[131] Rak, J.; Jakubek, M.; Kaplánek, R.; Matějíček, P.; Král, V. *Eur. J. Med. Chem.*, **2011**, *46*, 1140.

[132] Matějíček, P.; Zedník, J.; Ušelová, K.; Pleštil, J.; Fanfrlík, J.; Nykänen, A.; Ruokolainen, J.; Hobza, P.; Procházka, K. *Macromolecules* **2009**, *42*, 4829.

[133] Matějíček, P.; Brus, J.; Zhigunov, A.; Pleštil, J.; Uchman, M.; Procházka, K.; Gradzielski, M. *Macromolecules* **2011**, *44*, 3847-3855.

[134] Brus, J.; Zhigunov, A.; Czernek, J.; Kobera, L.; Uchman, M.; Matějíček, P. *Macromolecules* **2014**, *47*, 6343.

[135] Núñez, R.; Romero, I.; Teixidor, F.; Viñas, C. *Chem. Soc. Rev*. **2016**, *45*, 5147.

[136] Hoogenboom, R. *Angew. Chem., Int. Ed*. **2009**, *48*, 7978.

2 Experimental section

2.1 Characterization methods

The behavior and the structure of the boron cluster compounds assemblies and the coassemblies with polymers, have been characterized mainly by the following instrumental techniques:

- Light scattering: DLS, SLS, SAXS, SANS
- Nuclear magnetic resonance: ^{1}H, ^{1}H $\{^{11}B\}$ and ^{11}B NMR, DOSY
- Microscopy: Cryo-TEM, AFM
- Calorimetry: ITC
- Surface tension: Profile Analysis Tensiometry

Detailed description of each technique can be found in abundant literature and reviews. Herein, the focus is only on the instruments that I mostly worked with.

2.1.1 Light scattering

Static light scattering (SLS)

When a monochromatic light interacts with a matter, it leads to the scattering of electromagnetic waves because of the induction of an oscillating electric dipole in the radiated matter. This secondary light scatters to all directions and its electric dipole has a momentum $\boldsymbol{m}$, which depends on polarizability α and electric field vector $\boldsymbol{E}$ of the incident radiation.[1,2] From the relations of these parameters, the scattered intensity $I(q)$ can be derived and expressed as:

$$I(q) = \frac{16\pi^4\alpha^2 I_0 cos\theta}{\lambda^4 r^2} \tag{2.1}$$

where α is the polarizability of the molecules, I_0 is the intensity of the incident light, θ is scattering angle, λ is the wavelength of the used light in vacuum, r is the distance from the scattering sample to the detector and q is scattering vector defined as:

$$q = \frac{4\pi n_0 \sin\left(\frac{\theta}{2}\right)}{\lambda} \tag{2.2}$$

where n_0 is the refractive index increment of the solvent. Measurements of static light scattering (SLS) provide values of normalized scattering intensity for given angle, called Rayleigh ratio, which is defined as:

$$R(q) = \frac{I(q)r^2}{I_0} \tag{2.3}$$

According to Debye's theory,[3] polarizability α is dependent on the refractive index increment of the sample with respect to the solvent and on the osmotic pressure of the solution, π. Using these relations, we can rewrite scattering intensity from equation 2.1 as the very important Zimm equation:

$$\frac{Kc}{R(q)} = \frac{1}{MP(q)} + 2A_2c + \dots \tag{2.4}$$

where K is contrast factor, $P(q)$ is form factor, M is molar mass of particles, A_2 is second virial coefficient, providing a quantitative measure for the solute particle-solvent interactions. Second virial and following coefficients originate from extension of van't Hoff relation for osmotic pressure and concentration. In ideal solution (in the absence of specific interactions between solvent and solute molecules) A_2 is equal zero. Contrast factor can be also described as a scattering power of one individual solute particle and is defined as:

$$K = \frac{4\pi^2 n_0^2}{\lambda_0^4 N_\mathrm{A}} \left(\frac{\partial n}{\partial c}\right)^2 \tag{2.5}$$

where N_A is Avogadro constant and $\frac{\partial n}{\partial c}$ is refractive index increment of the sample with respect to the solvent. For the particles larger than $\lambda/20$, several of oscillating dipoles are created simultaneously within a particle. Consequently, some of the emitted waves show a phase difference, which leads to a nonisotropic angular dependence of the scattered light intensity. This interference pattern of intraparticular scattered light, also called particle form factor $P(q)$, is characteristic for size and shape of the scattering particle. For the low θ values, particle form factor can be expressed with series expansion:

$$P(q) = 1 - \frac{1}{3} q^2 R_\mathrm{g}^2 + \dots = \sim \frac{1}{1 + \frac{1}{3} q^2 R_\mathrm{g}^2} \tag{2.6}$$

where R_G is radius of gyration. For very dilute solutions of particles of size smaller than $\lambda/20$, the phase difference is negligible and the scattering intensity is independent of the scattering angle (form factor in eq. 2.4 is formally 1).

Zimm equation (eq. 2.4) is routinely used to determine the molar mass, the radius of gyration, and the second virial coefficient. For polydisperse samples, Zimm analysis provide the weight average of molar mass and the z-average of squared radius of gyration. The refractive index increment of many particles is unknown and difficult to obtain. In such cases, the light scattering intensity extrapolated to zero scattering angle can be evaluated as the measure proportional to molar mass of particles.

Dynamic light scattering (DLS)

Particles in solution show a random motion caused by thermal density fluctuations of the solvent. Because of these temporal concentration fluctuations, the interference and the resulting scattered intensity also change with time. This motion can be described by van Hove self-correlation

function $G_s(\boldsymbol{r},\tau)$, which defines the probability of finding a given scattering particle at time $t + \tau$ at position $\boldsymbol{r}$, if the same particle previously at time t has been located at position $\mathbf{0}$:

$$G_s(\boldsymbol{r},\tau) = < n(\mathbf{0},t)n(\boldsymbol{r},t+\tau) >_{V,T} \tag{2.7}$$

where $n(\boldsymbol{r},t)$ is the local number density of scattering particles and the average < > is taken both over the whole scattering volume and the total measuring time. Using a hardware correlator, these fluctuations of concentration are transormed by Fourier transformation into first-order autocorrelation function (or also dynamic structure factor), $g_1(q,t)$:

$$g_1(q,t) = \int G_s(\boldsymbol{r},\tau)\exp(i\boldsymbol{q}\boldsymbol{r})\,dr \tag{2.8}$$

For isotropic diffusive particle motion (random walk model) $g_1(q,t)$ can be expressed as:

$$g_1(q,t) = \exp(-D_S q^2 \tau) \tag{2.9}$$

where D_s is self-diffusion coefficient. Consequently, the hydrodynamic radius of the scattering particle, R_H, can be determined using Stokes-Einstein equation:

$$D = \frac{kT}{f} = \frac{kT}{6\pi\eta R_H} \tag{2.10}$$

where k is Boltzmann constant, T is thermodynamic temperature, f is friction of solution, and η is viscosity of solvent.

The autocorrelation function $g_1(q,t)$ can be experimentally obtained by DLS measurement. For SLS experiments, the average scattered intensity $<I(q,t)>$ is measured, on the other hand, DLS requires the fluctuating intensity $I(q,t)$, which is measured as the normalized intensity autocorrelation function $g_2(q,t)$, defined as:

$$g_2(q,\tau) = \frac{< I(q,t)I(q,t+\tau) >}{< I(q,t)^2 >} \tag{2.11}$$

and is related to the amplitude autocorrelation function $g_1(q,t)$ via the Siegert relation:

$$g_2(q,\tau) = 1 + \beta|g_1(q,t)|^2 \tag{2.12}$$

where β is a correction factor. For monodisperse samples, autocorrelation function is a single exponential with decay rate $\Gamma = D_s q^2$. Analysis of non-monodisperse samples (with low polydispersities) is also possible, for example, by the so-called cumulant analysis, which is based on a series expansion of $g_1(q,t)$. In this case, self-diffusion coefficient is q-dependent (changes with angle θ) and therefore is called apparent diffusion coefficient $D_{app}(q)$. The true average diffusion coefficient $<D_s>_z$, which is a z-average, is determined by extrapolation of the apparent diffusion coefficient towards zero scattering vector and vanishing concentration.

Other scattering techniques

The magnitude of the scattering vector q defines the observational length scale of the light scattering experiment. The larger q becomes, the smaller the length scale and the sample details observed. Hence, the use of the wavelengths shorter than that of visible light can give additional information on the structure. For example, in Small-Angle X-ray Scattering (SAXS),[4] X-rays with wavelengths ~0.1 nm are scattered by the electrons of atoms. In Small-Angle Neutron Scattering (SANS),[5] neutrons are scattered by the atoms nuclei. In SAXS experiment, the scattered intensity $\Delta I(q)$ of the particle can be summarized as:

$$\Delta I(q) = K \cdot P(q) \cdot S(q) \tag{2.13}$$

where K is constant, which consists of the particle contrast, volume, and concentration. The form factor $P(q)$ reflects the shape and the internal density distribution of the particles. The structure $S(q)$ carries the information about particle-particle distances and degree of order. This additional interference causes wave or peak in the scattered intensity profile. For the pronounced peak, the position of its maximum (q_{peak}) indicates the distance (d_{Bragg}) between the aligned particles by using Bragg's law:

$$d_{\text{Bragg}} = \frac{2\pi}{q_{\text{peak}}} \tag{2.14}$$

Analysis of the experimentally obtained scattering data is performed by nonlinear fitting of the scattered intensity profiles to various models.

2.1.2 NMR spectroscopy

Nuclear magnetic resonance (NMR)[6] is a physical phenomenon in which nuclei in a magnetic field absorb and re-emit electromagnetic waves. Only isotopes, which contain an odd number of protons and/or neutrons, in other words, they have nonzero nuclear spin, are active in NMR. The spin angular momentum, $\boldsymbol{I}$, is characterized by the nuclear spin quantum number, I. The nuclei that have nonzero spin angular momentum also have nuclear magnetic moments, $\boldsymbol{\mu}$, which is related to $\boldsymbol{I}$ via the relation:

$$\boldsymbol{\mu} = \gamma \boldsymbol{I} \tag{2.15}$$

in which the gyromagnetic ratio, γ, is a characteristic constant for a given nucleus. By convention, the value of the z-component of vector $\boldsymbol{I}$ is defined as:

$$I_z = \hbar m_{\text{I}} \tag{2.16}$$

where $\hbar$ is reduced Planck constant and m_{I} is magnetic quantum number, defined as $m_{\text{I}} = (-I, -I + 1, ..., I - 1, I)$. Thus, I_z has $2I + 1$ possible values. In the presence of an external magnetic field with the magnetic field vector $\boldsymbol{B}$, the spin states of the nucleus have energies given by:

$$E = -\boldsymbol{\mu} \cdot \mathbf{B} \tag{2.17}$$

In an NMR spectrometer, the static external magnetic field is directed by convention along the *z*-axis of the laboratory coordinate system. For this geometry, equation 2.17 reduces to

$$E = -\gamma I_z B_0 = -\gamma m_I \hbar B_0 \tag{2.18}$$

in which B_0 is the static magnetic field strength. In other words, applying magnetic field causes the split of nuclear energy levels according their magnetic quantum number m_I (also called Zeeman effect). By analogy with other areas of spectroscopy, transitions between Zeeman levels can be stimulated by applied electromagnetic radiation. For example, when $I = ½$, then $m_I = \pm ½$ and thus, the photon energy, ΔE, required to excite a transition between the two states is:

$$\Delta E = -\hbar \gamma B_0 \tag{2.19}$$

By Planck's Law, the frequency of the electromagnetic radiation, which can be absorbed, is given by:

$$\omega = \frac{\Delta E}{\hbar} = \gamma B_0, \quad \nu = \frac{\omega}{2\pi} = \frac{\gamma B_0}{2\pi} \tag{2.20}$$

where ω is angular frequency (in radians per second) and ν is frequency (in Hz), also called the Larmor frequency.

A general feature of NMR spectroscopy is that the observed resonance frequencies depend on the local environments of individual nuclei and are referred to as chemical shifts, δ. This phenomenon arises from the motions of electrons induced by the external magnetic field. These electrons generate secondary magnetic fields, which results in effect called nuclear shielding, σ. Then, the effective magnetic field, B_{eff}, is decreased:

$$B_{\text{eff}} = B_0(1 - \sigma) \tag{2.21}$$

In practice, chemical shifts are measured in parts per million (ppm) relative to a reference resonance signal from a standard molecule:

$$\delta = \frac{\nu - \nu^{\text{ref}}}{\nu^{\text{ref}}} \times 10^6 = (\sigma^{\text{ref}} - \sigma) \times 10^6 \tag{2.22}$$

in which ν and ν_{ref} are the frequencies of the signal of interest and the reference signal, respectively. Chemical shifts are independent of the static magnetic field strength and in the form of NMR spectrum, they provide information about the structure of the molecule. Besides the analyze of molecular structure, chemical shifts can provide further information, such as the detection of aggregation. When molecules assemble in solution, the nuclear shielding can change and cause different shift than that of unaggregated molecules (see Figure I.3 in chapter 5.1).

Most used type of NMR spectroscopy is ^{1}H experiment which provide characterization of various organic molecules. For polymers, the polydispersity and the numerous slightly different protons cause the broadening of ^{1}H NMR signals and thus the interpretation of the

polymers structure is complicated. However, polymers have also benefited from NMR spectroscopy[7] but in a somewhat different manner, such as tacticity determination, monomer sequence analysis of copolymers, analysis of end groups and irregular linkages. For the results of this thesis, we often used ^{1}H NMR spectra to determine the fraction of immobilized polymeric segments.[8] This concept has been extensively studied for polymer adsorptions on the solid surfaces.[9,10] When polymers in solution adsorb onto a surface, there is a decrease in intensity of the NMR peaks. Where separate populations of bound and unbound polymer segments occur, the immobilized segments appear as broad peaks or broad background in the spectra. In ^{1}H NMR, peak broadening can be so extensive compared to the width of the peaks of the mobile species, that the signal from the immobilized segments cannot be distinguished from the background.

An important NMR technique used in this thesis is the diffusion NMR, which is also referred to as Self-Diffusion or Diffusion Ordered SpectroscopY (DOSY).[11] Diffusion NMR experiments resolve different compounds in a mixture based on their different diffusion coefficients. The measurement is based on the combination of radio-frequency pulses with magnetic field gradients. Using magnetic gradient, molecules can be spatially encoded, based on their position in the tube. If they move after the encoding, during the diffusion time that follows in the pulse sequence, their new spatial position can be decoded with a second gradient. Pulsed-field gradient technique afford a powerful tool not only for studying molecular diffusion and particle size but also for providing structural information when the diffusion is restricted.

2.1.3 Tensiometry

The surface tension[12] of liquids is caused by the attractive forces between the molecules, mainly by dispersion, dipole-dipole, dipole-induced dipole forces, and hydrogen bonding. In the bulk liquid, a molecule is surrounded by the same attractive forces in all directions, whereas for a molecule at the surface this attraction is lacking in one direction. This asymmetry is the origin of the surface energy and the surface tension thus relates to the cohesive forces in a liquid. According to the second molecular explanation, the distances between the molecules close to the surface are larger and therefore, they have a larger energy.

The surface tension of liquids causes the formation of drops, which tends to shape them into spheres, as this is the form of lowest surface energy. The surface tension can be described by the energies emerging from the two opposing forces: surface energy and pressure-volume energy. Employing the geometry of the drop, the surface tension γ can be expressed by the Young-Laplace equation:

$$\Delta P = \gamma \left(\frac{1}{R_1} + \frac{1}{R_2} \right) \tag{2.23}$$

where R_1 and R_2 are the main radii of the drop curvature (for a spherical drop $R_1 = R_2$) and ΔP is the pressure difference across the fluid interface. Equation 2.23 also reveals that the pressure increases as the drop size decreases.

Water has relatively high surface tension (72.8 mN m^{-1} at 20°C) caused by high attraction of water molecules via hydrogen bonds. This tension can be affected by added component in one of three different ways. (i) Organic water-soluble molecules, such as ethanol, normally decrease the surface tension monotonically with increasing concentration because of preferential adsorption of the organic molecules at the liquid–air interface. (ii) Electrolytes normally increase the surface tension because there is a negative adsorption of the ions at the surface (depletion from the surface). Similarly, very hydrated molecules, such as sucrose and glucose, also give a positive increment to the surface tension. (iii) Surfactants show a large decrease in surface tension at very low concentrations up to the CMC because of strong adsorption of the surfactants at the surface. Above the CMC, the surface tension is constant because all additional surfactant forms new micelles, thus keeping the surfactant unimer concentration constant.

For the adsorption at the surface of liquid, Gibbs defined the surface as the position where the solvent concentration is half between that in the solvent and in the vapor. Then the surfactant adsorption Γ, also called the surface excess, relates to the surface tension through the Gibbs equation:

$$\Gamma = -\frac{1}{nRT}\frac{\mathrm{d}\gamma}{\mathrm{dln}a} \tag{2.24}$$

where a is the activity of the surfactant in the bulk solution and n is a constant (n = 1 for the nonionic surfactants and n > 1 for ionic surfactants).[13] The surfactant adsorption is thus obtained from the slope of a plot of the surface tension versus the logarithm of concentration. Assuming monolayer adsorption, the adsorbed amount is inversely proportional to the cross-sectional area per adsorbed molecule (A_S). To obtain the γ values, and consequently Γ and A_S, several methods can be used, such as pendant drop method, ring and plate tensiometry or maximum bubble pressure tensiometry. In this thesis, the surface tension data were obtained by the pendant drop tensiometry,[14] which offers a simple solution for determining γ of liquid by the analysis of the shape of a pendant drop and by iterative fitting the Young-Laplace equation to the coordinates of a drop or bubble (also called profile analysis tensiometry, PAT). This method can be used for the liquid/air or liquid/liquid interfaces, as well as the measurements of dynamic surface tension $\gamma(t)$.[15,16]

2.2 Materials

2.2.1 Boron cluster compounds

Sodium decaborate, $Na_2[B_{10}H_{10}]$, sodium dodecaborate, $Na_2[B_{12}H_{12}]$, potassium 1-carbadodecaborate, $K[CB_{11}H_{12}]$, sodium mercaptododecaborate, $Na_2[B_{12}H_{11}SH]$ or $Na_2[BSH]$, and cesium salt of anion [3-cobalt(III) bis(1,2-dicarbollide)](–1), $Cs[3,3'\text{-}Co(C_2B_9H_{11})_2]$, Cs[COSAN], were purchased from Katchem Ltd. (Czech Republic). All the structures are shown in Figure 2.1. Cs[COSAN] was converted to $Na[COSAN].4H_2O$ by extraction described by Plešek.[17] The $[NMe_4]$[COSAN] salt was prepared by precipitation of Na[COSAN] with $[NMe_4]Cl$ in water. Solubilities of Na[COSAN], Li[COSAN], H[COSAN], K[COSAN] and $[NMe_4]$[COSAN] in water were determined by UV-Vis (ε(280nm) = 32012 M^{-1} cm^{-1}) and gave the following results: 1509 mM, 1175 mM, 846 mM, 747 mM and 0.019 mM, respectively. Samples of the boron cluster compounds for NMR, ITC, LS, and conductivity experiments in paper I and II were prepared by dissolution of boron cluster compound in water or heavy water (D_2O).

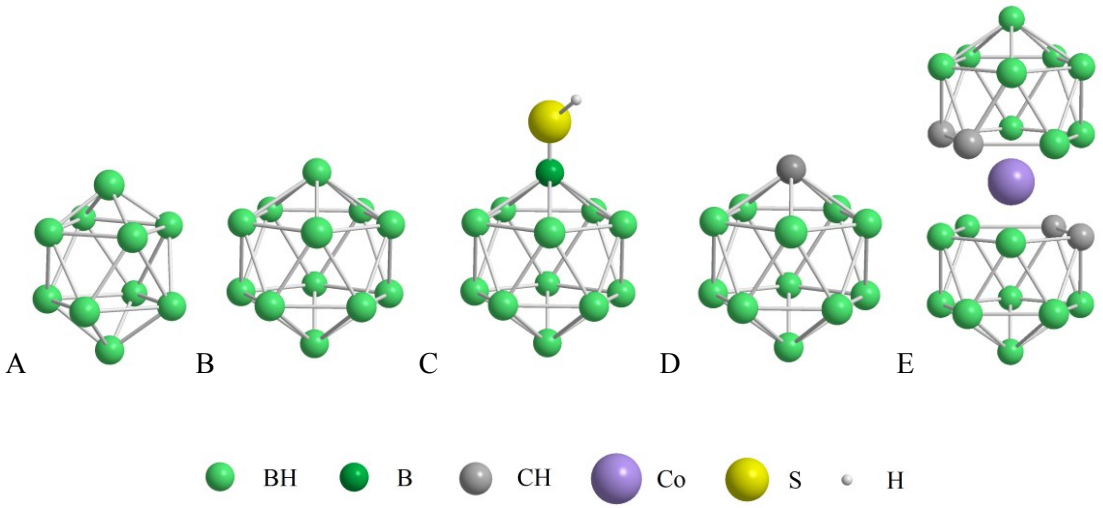

Figure 2.1. Structure of the studied boron cluster compounds: (A) $[B_{10}H_{10}]^{2-}$, (B) $[B_{12}H_{12}]^{2-}$, (C) $[B_{12}H_{11}SH]^{2-}$, (D) $[CB_{11}H_{12}]^{-}$, and (E) $[3,3'\text{-}Co(C_2B_9H_{11})_2]^{-}$.

Preparation of Na[COSAN], Li[COSAN] and K[COSAN]

The cationic exchange resin (Amberlite IR120, H form) was purchased from Acros Organics. For the study in paper V, Cs[COSAN] was converted to Na[COSAN], Li[COSAN] and K[COSAN] according the following procedure: first, we charged the resin by passing 250 mL of 3 M HCl followed by rinsing with water. The column was loaded by lithium (or potassium respectively) cation by passing 3M MCl for preparation of M[COSAN] (M = Li, Na, and K) solution through resin, and then rinsed by around 500 mL of water (the eluent was tested if it contains traces of MCl by $AgNO_3$ solution). Solid Cs[COSAN] was dissolved in a mixture of acetonitrile/water (50:50) and this solution (around 100 mL) was passed repeatedly through (drop by drop) a cation exchanging resin loaded with desired cation. The solvent was finally evaporated and the crude product was leave to dry in a dessicator overnight. Cationic exchange

was also confirmed by capillary zone electrophoresis. Water content in M[COSAN] for M = Na, Li, K was determined by TGA to be 16%, 13%, and 0% (w/w), respectively.

Purification and conversion

Samples of $Na_2[B_{10}H_{10}]$, $Na_2[B_{12}H_{12}]$ and $Na_2[BSH]$ contained traces of triethylammonium cation. Further, $Na_2[B_{10}H_{10}]$, $Na_2[B_{12}H_{12}]$, $Na_2[BSH]$ and $K[CB_{11}H_{12}]$ contained certain amount of sodium (potassium) carbonate [4–10 % (w/w)], and also crystal water (~20 %). Triethylammonium was removed by cation exchange column chromatography as follows. A 25 cm×2 cm column was filled with strongly acidic cation exchange resin Amberlite IR120 resin (Sigma-Aldrich) suspended in deionized H_2O. Then 200 mL of 3 M HCl was run through the column, followed by 750 mL of deionized H_2O. After acid conditioning, 250 mL of 15 % NaCl (for $Na_2[B_{12}H_{12}]$ and $Na[CB_{11}H_{12}]$) or 15% Na_2SO_4 (for $Na_2[B_{10}H_{10}]$) solution was passed through the column, followed by 1000 mL of deionized H_2O. After conversion to the sodium form, 100 mg sample of borane, dissolved in 2 mL of H_2O, was loaded on the column. The column was eluted with deionized H_2O (100 mL). The eluted aqueous solution was collected and lyophilized to a solid residue.

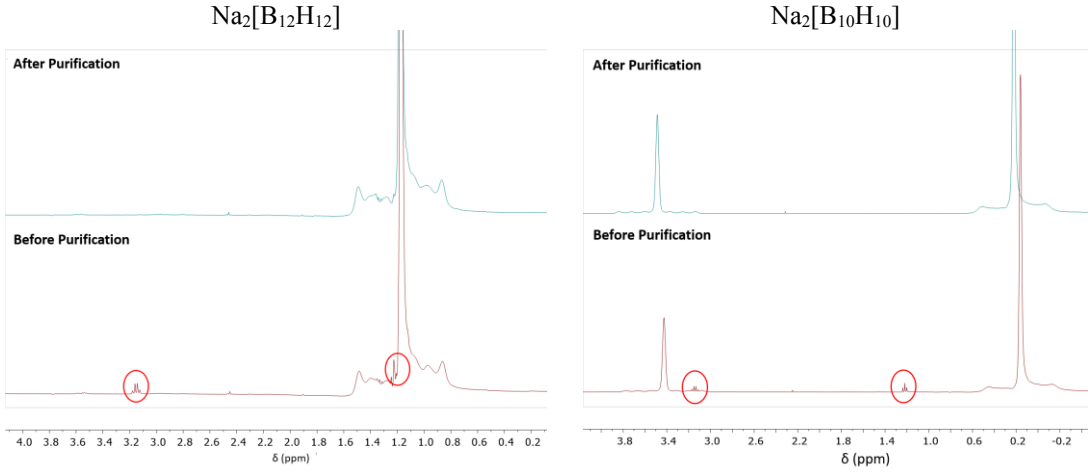

Figure 2.2. NMR spectra of purified $Na_2[B_{12}H_{12}]$ and $Na_2[B_{10}H_{10}]$.

Characterization of purified boron cluster compounds

The purified boranes and carboranes were characterized using MS, NMR and elemental analysis. Interestingly, we observed that even traces of Cl^- ions present on the ionex can react with the $[B_{10}H_{10}]^{2-}$ anion. We used therefore Na_2SO_4 for equilibration of the column, which completely prevented this undesirable side reactivity.

ESI MS provided following results: $[B_{12}H_{12}]^{2-}$ calculated $[M]^{2-}$ 71.11, found 71.1; $[B_{10}H_{10}]^{2-}$ calculated $[M–H^-+H^+]^-$ 118.18, found 118.2, $[M+Na^+]^-$ calculated 141.17, found 141.2; $[CB_{11}H_{12}]^{2-}$ calculated $[M]^-$ 143.20, found 143.2.

The ^1H NMR $\{^{11}B\}$ spectra measured in D_2O revealed the presence of small amounts of triethylammonium cation which was reliably removed using the ionic exchange chromatography.

The ^{1}H NMR $\{^{11}B\}$ spectra for $Na_2[B_{12}H_{12}]$ and $Na_2[B_{10}H_{10}]$ before and after purification are shown in Figure 2.2.

The $K[CB_{11}H_{12}]$ did not contain triethylammonium impurity, however, we converted a part of the sample to the $Na[CB_{11}H_{12}]$ by the same procedure as used for boranes. We estimated the content of H_2O in the all samples using elemental analysis. The calculated weight percents of H_2O are: 26.6 % for $Na_2[B_{12}H_{12}]$, 23.1 % for $Na_2[B_{10}H_{10}]$ and 19.6 % for $Na[CB_{11}H_{12}]$. The $Na[CB_{11}H_{12}]$ sample contained also Na_2CO_3 (11.1 %) impurity, which originates from the supplier (originally as K_2CO_3) and cannot be removed by the used procedure. For both boranes, the amounts of other mineral salt impurities were less than 4 %.

2.2.2 Dumbbells

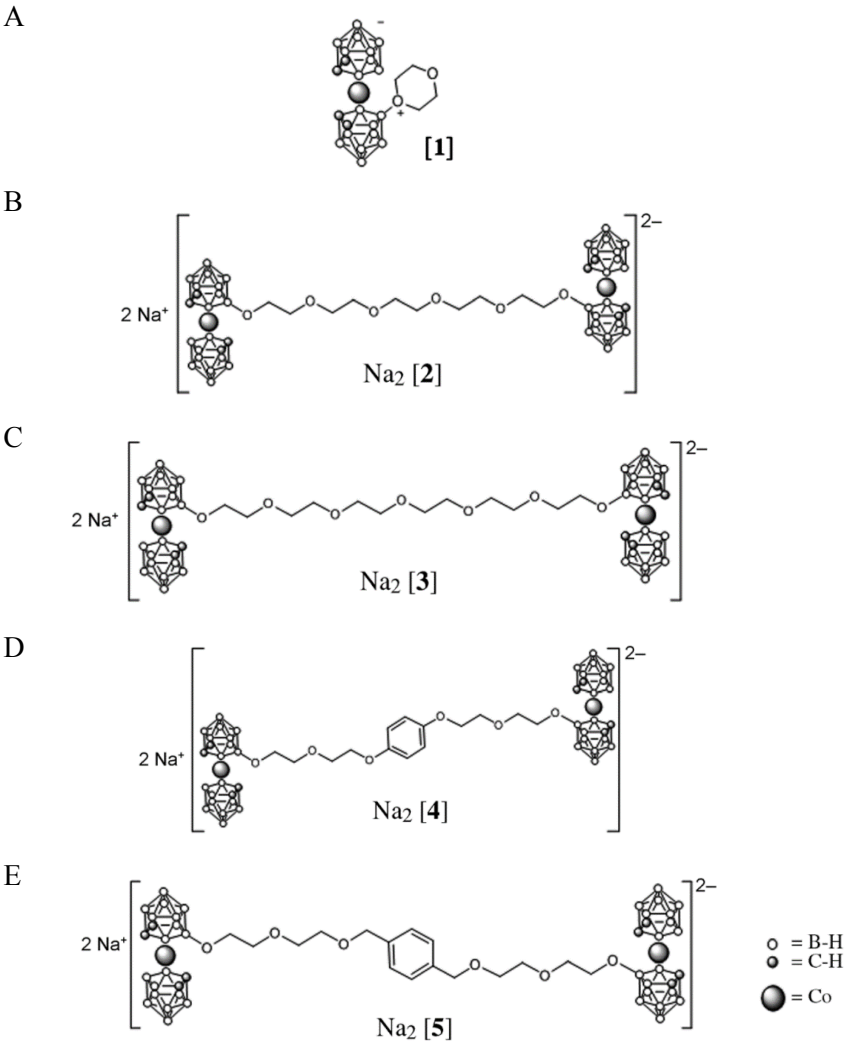

Figure 2.3. Structures of (A) cobaltabisdicarbollide dioxanate [**1**] and (B) dumbbells: Na_2[**2**], (C) Na_2[**3**], (D) Na2[**4**], (E) Na_2[**5**].

The compounds, in which two COSAN anions are connected by oligo(ethylene oxide) linker, were called dumbbells. All the structures are shown in Figure 2.3. Solvents and agents for the

synthesis of dumbbells, such as anhydrous dioxane, boron trifluoride etherate, ethyl acetate, diethylene glycol, LiCl, NaCl, KCl, RbCl, CsCl and NH_4Cl (grade I > 99%) were purchased from Sigma-Aldrich. Hydrocloric acid (37%) was purchased from Carlo Erba Reagents. All other solvents used were obtained from Carlo Erba SDS and purified by distillation under nitrogen atmosphere from sodium and benzophenone as indicator. The cationic exchanging resin used (Amberlite IR120, H form) was purchased from Acros Organics.

Synthesis and characterization of dumbbells

Cobaltabisdicarbollide dioxanate, [**1**], has been synthesized according to a well-established procedure,[18] starting from the commercially available cesium salt of cobalt bisdicarbollide. Synthesis of Na_2[**2**] and Na_2[**3**] is described below. Compounds Na_2[**4**][19] and Na_2[**5**][20] have been synthesized as reported.

Synthesis of Na_2[2]

The synthesis of Na_2[**2**] is outlined in Scheme 2.1.

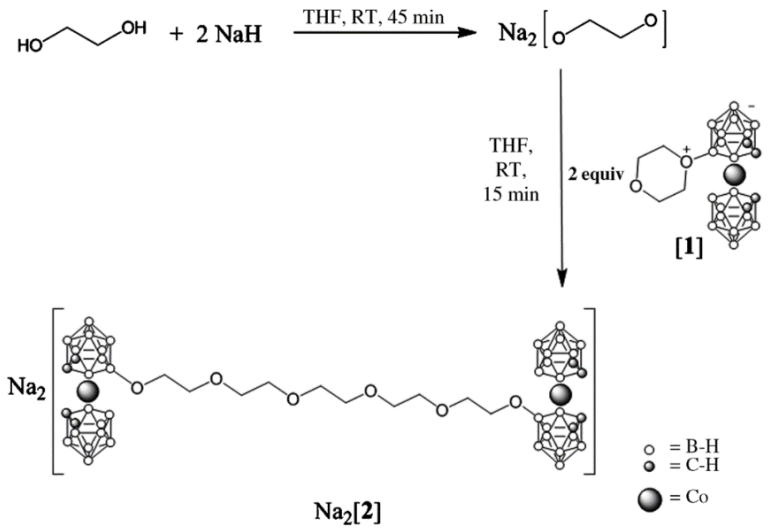

Scheme 2.1. Synthetic route for the preparation of Na_2[2].

Ethylene glycol (10 µL, 0.37 mmol) was added to a stirring solution of NaH (15.2 mg, 0.78 mmol) in dry THF (5 ml) under a nitrogen atmosphere over 15 min at room temperature. Then, [3,3'-Co(8-$C_4H_8O_2$-1,2-$C_2B_9H_{10}$)(1',2'-$C_2B_9H_{11}$)] (150 mg, 0.78 mmol) was added to the reaction flask and was stirred for an additional 2.5 hours at room temperature. Once finished, a final Et_2O/H_2O/NaCl extraction was performed. The organic fraction was evaporated under vacuum and purified by preparative layer chromatography with ethyl acetate as the eluent (R_f = 57) to give Na_2[**2**] (159.5 mg, 72%).

^{1}H NMR (300 MHz, CD_3COCD_3), δ: 4.15 (brs, 4H, C_c-H), 4.11 (brs, 4H, C_c-H), 3.80-3.60 (m, 20H, -CH_2-O-). ^{1}H{^{11}B}-NMR (300 MHz, CD_3COCD_3), δ: 4.15 (brs, 4H, C_c-H), 4.11 (brs, 4H, C_c-H), 3.80-3.60 (m, 20H, -CH_2-O-), 2.90 (brs, 3H, B-H), 2.70 (brs, 3H, B-H), 2.04

(brs, 3H, B-H), 1.84 (brs, 2H, B-H), 1.69 (brs, 1H, B-H), 1.62 (brs, 2H, B-H), 1.54 (brs, 2H, B-H), 1.46 (brs, 1H, B-H). ^{11}B-NMR (96 MHz, CD_3COCD_3), δ: 25.12 (s, 1B, B-O), 6.73 (d, ^{1}J(B,H)=125, 1B, B-H), 1.75 (d, ^{1}J(B,H)=139, 1B, B-H), -1.18 (d, ^{1}J(B,H)=165, 1B, B-H), -3.43 (d, 2B, B-H), -5.87 (d, ^{1}J(B,H)=134, 6B, B-H), 15.96 (d, ^{1}J(B,H)=151, 2B, B-H), -19.10 (d, ^{1}J(B,H)=154, 2B, B-H), 20.62 (d, 1B, B-H), -27.22 (d, ^{1}J(B,H)=144, 1B, B-H). ^{13}C{^{1}H}-NMR (75 MHz, CD_3COCD_3), δ: 72.05 (-O-CH_2), 71.68 (-O-CH_2), 69.76 (-O-CH_2), 69.37 (-O-CH_2), 68.08 (-O-CH_2), 53.44 (C_c-H), 46.59 (C_c-H).

FTIR (ν in cm^{-1}): 3044.60 (w, υ(C_c-H)), 2916.43 (w, υ(C-H)), 2837.60 (w, υ(C-H)), 2529.53 (s, υ(B-H)), 1699.11 (w, υ(C=O), coord. acetone), 1200–900 (s, υ(C-O)).

MALDI-TOF-MS (m/z (%)): 904.17 (100) [*M*–Na]; elemental analysis calculated (%) for $Na_2C_{18}B_{36}O_6H_{62}Co_2 \cdot 1.6C_3H_6O$: C 26.83, H 7.09; found, C 26.90, H 7.22.

Synthesis of Na_2[3]

The same procedure and amounts as those for Na_2[**2**] were used, but starting from diethylene glycol instead of ethylene glycol: diethylene glycol (10 µl, 0.37 mmol), NaH (15.2 mg, 0.78 mmol), dry THF (5 ml) and [**1**] (150 mg, 0.78 mmol) were utilized to obtain Na_2[**3**] (167.6 mg, 94%). R_f = 56.

^{1}H NMR (300 MHz, CD_3COCD_3) δ = 4.18 (brs, 4H, C_c-H), 4.13 (brs, 4H, C_c-H), 3.90-3.50 (m, 24H, -CH_2-O-). ^{1}H{^{11}B}-NMR (300 MHz, CD_3COCD_3, δ): 4.18 (brs, 4H, C_c-H), 4.13 (brs, 4H, C_c-H), 3.90-3.50 (m, 24H, -CH_2-O-). 2.91 (brs, 3H, B-H), 2.71 (brs, 3H, B-H), 2.06 (brs, 3H, B-H), 1.86 (brs, 2H, B-H), 1.70 (brs, 1H, B-H), 1.64 (brs, 2H, B-H), 1.55 (brs, 2H, B-H), 1.46 (brs, 1H, B-H). ^{11}B-NMR (96 MHz, CD_3COCD_3, δ): 25.25 (s, 1B, B-O-), 6.80 (d, ^{1}J(B,H)=127, 1B, B-H), 1.77 (d, ^{1}J(B,H)=140, 1B, B-H), -1.16 (d, ^{1}J(B,H)=152, 1B, B-H), -3.43 (d, 2B, B-H), -5.80 (d, ^{1}J(B,H)=139, 6B, B-H), 15.97 (d, ^{1}J(B,H)=151, 2B, B-H), -19.05 (d, ^{1}J(B,H)=155, 2B, B-H), 20.75 (d, 1B, B-H), -27.36 (d, ^{1}J(B,H)=108, 1B, B-H). ^{13}C-NMR (75 MHz, CD_3COCD_3, δ): 71.54 (-B-O-CH_2-), 69.11 (-O-CH_2-), 68.84 (-O-CH_2-), 68,76 (-O-CH_2-), 68.36 (-O-CH_2-), 53.01 (C_c-H), 46.68 (C_c-H).

IR (ATR, cm^{-1}): 3046.12 (w, υ(C_c-H)), 2920.78 (w, υ(C-H)), 2873.71 (w, υ(C-H)), 2533.33 (s, υ(B_c-H)), 1685.10 (s, υ(C=O), coordinated acetone), 1200–900 (s, υ(C-O)).

MALDI-TOF-MS *m*/*z* (%): 948.16 (100) [M–Na]; elemental analysis calculated (%) for $Na_2C_{20}B_{36}O_7H_{66}Co_2 \cdot 1.3\ C_3H_6O$: C 27.41, H 7.10; found, C 27.45, H 7.04.

Crystals of Na_2[**3**] were obtained through a diffusion method at room temperature. The product was dissolved in CH_2Cl_2 and few drops of acetone then heptane were slowly added on top as an insoluble layer.

Cation exchange: syntheses of M_x[dumbbell]

To obtain the desired cation for each dumbbell, different from the initial one, approximately 100 mg of starting compound Na_2[**2**], Na_2[**3**], Na_2[**4**] and Na_2[**5**], was dissolved in a minimum volume of EtOH. A saturated aqueous solution of [NMe_4]Cl was added to the EtOH solution, leading to the complete precipitation of the dumbbell-like compound, with 2 [NMe_4]$^+$ units. Then, the water-insoluble compound in a mixture of acetonitrile/water (50:50) was passed

repeteadly through a cation exchanging resin, priorly loaded with the desired cation. The solvent was finally evaporated. The partial or complete solubilization of the new salt in distilled water and the disappearance of the $[NMe_4]^+$ peaks in the ^1H NMR indicate that complete exchange of the desired alkaline ion has been successful. Salts of H^+, Li^+, Na^+, Rb^+, Cs^+ and $[NMe_4]^+$ for each dumbbell were obtained. The concentration of saturated dumbbells solutions was estimated byUV-Vis spectroscopy from extinction coefficient determined for sodium and lithium dumbbells, $\varepsilon(307\ nm) = 36\ 585\ M^{-1}\ cm^{-1}$.

2.2.3 Polymers

All structures of studied polymers are shown in Figure 2.4. In the papers IV and V, we studied the homo-arm star double-hydrophilic diblock copolymer [poly(ethylene oxide)-*block*-poly(2-methyl-2-oxazoline)]$_4$, [PEO–PMeOx]$_4$, linear double-hydrophilic diblock copolymers poly(ethylene oxide)-*block*-poly(2-ethyl-2-oxazoline), PEO–PEtOx and PEO–PEtOx(2), and linear double-hydrophilic triblock copolymer poly(2-ethyl-2-oxazoline)-*block*-poly(ethylene oxide)-*block*-poly(2-ethyl-2-oxazoline), PEtOx–PEO–PEtOx (structures in Figure 2.4). These polymers were purchased from Polymer source, Inc. (Dorval, Quebec, Canada). Results of [PEO–PMeOx]$_4$ and PEO–PEtOx samples described in the main text, while data on other two samples are shown in Supporting information only. As provided by Polymer Source, all the block copolymers have been prepared from PEO pre-polymers (mPEO for diblocks, PEO for triblock, and PEO star with pentaerythritol core for 4-arm star) with desired molar mass and low dispersity by additional polymerization of POX blocks. In paper VI, we used the newly synthesized block copolymer poly(2-methyl-2-oxazoline)-*block*-poly(2-*n*-propyl-2-oxazoline), PMeOx−PPrOx. The synthetic procedure is described below.

The poly(2-ethyl-2-oxazoline) linear homopolymer, PEtOx, was purchased from Aldrich with the weight averaged relative molecular weight 5×10^4. The linear poly(ethylene oxide), PEO, was purchased from Fluka with the weight-averaged relative molecular weight 41.5×10^3 and $Đ = 1.10$.

Synthesis of PMeOx–PPrOx

All reagents for the polymer synthesis were obtained from Sigma-Aldrich. Monomer synthesis and polymerizations as well as the synthesis and characterization of PMeOx and PPrOx homopolymers were performed as described elsewhere.[21-23] Briefly, both monomers, MeOx and PrOx were fractionally distilled over BaO under argon atmosphere. Acetonitrile was purified over aluminum oxide by means of a solvent purification system from J. C. Meyer and directly tapped in the glove box (Vigor). The polymerization mixture was prepared in the glove box. The polymerization was conducted in a 20 ml Biotage vial with stir bar, which was dried overnight in the oven (220°C). The duration of the polymerization was calculated from previously reported propagation rates. A solution of methyl 4-toluenesulfonate (initiator; 75.4 µL), acetonitrile (solvent; 8.54 ml) and MeOx (1.69 ml, 1.34 mol/L) was prepared and polymerized in the microwave synthesizer at 140°C (Biotage Initiator Sixty with IR temperature probe). After full

conversion of MeOx, the microwave vial was transferred back to the glovebox, where PrOx (4.76 ml, 2.76 mol/L) was added and heated again to 140°C in the microwave. After polymerization the polymer solution was cooled down to 0°C and 1 ml of a 1 M KOH in methanol was added under stirring and left overnight at room temperature. The resulting block copolymer with hydroxyl end groups was precipitated twice in cold (0°C) diethyl ether and filtrated off after each precipitation and was dried in the vacuum oven at 50°C. All manipulations for the polymerizations were carried out in a VIGOR Sci-Lab SG 1200/750 Glovebox System with a water and oxygen concentration ≤ 0.1 ppm and < 0.5 ppm, respectively. For the polymerizations, a Biotage Initiator EXP Microwave System with Robot Sixty auto sampler was used. During the polymerizations, the microwave synthesizer operated at a constant set temperature which was monitored by an IR-sensor.

A

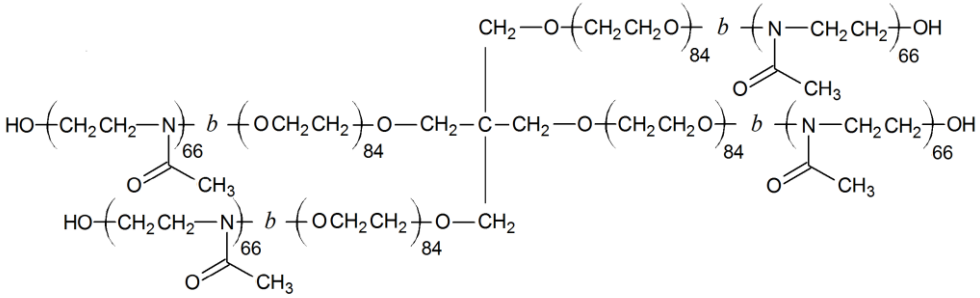

B

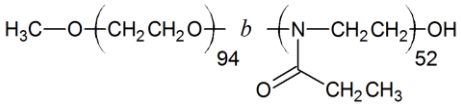

C

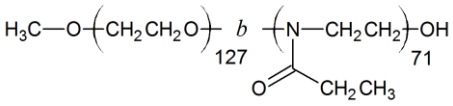

D

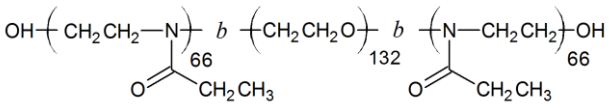

E

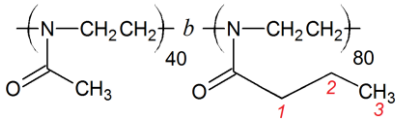

Figure 2.4. Structures of the studied polymers: (A) $[PEO–PMeOx]_4$, (B) PEO–PEtOx, (C) PEO–PEtOx(2), (D) PEtOx–PEO–PEtOx and (E) PMeOx–PPrOx

Characterization of polymers

We characterized all the block copolymers PEO–PEtOx, PEO–PEtOx(2), PEtOx–PEO–PEtOx and $[PEO–PMeOx]_4$ by standard GPC and NMR measurements, and the results are summarized in Table 2.1. M_n of all blocks were calculated by comparing of PEO and POX signals with the terminal group signals as shown in NMR spectra for PEO–PEtOx and $[PEO–PMeOx]_4$ below (Figure 2.5). GPC measurements were used for determination of dispersity ($Đ$) of block copolymers; all the chromatograms were monomodal. While PEO–PEtOx, PEO–PEtOx(2) and PEtOx–PEO–PEtOx samples are of a linear architecture, $[PEO–PMeOx]_4$ macromolecule has a star-like shape with the pentaerythritol "core" and with four PMeOx blocks on the periphery. Lengths of PEO and POX blocks in all the studied samples are comparable, and PEO blocks are always longer; (PEO in the range 84–128 segments, and POX in the range 51–71 segments). The overall dispersities of block copolymers are fairly high (1.5–1.8), and it is given mainly by POX blocks, since PEO prepolymers had dispersities only ~1.1.

Table 2.1. Characterization of block copolymers based on ^{1}H NMR and GPC measurements.

	M_n(PEO), NMR	M_n(POX), NMR	w(PEO), NMR	$Đ$, GPC
PEO-PEtOx	4100	5100	0.45	1.8
$[PEO-PMeOx]_4$	4×3700	4×5600	0.40	1.5
PEO-PEtOx(2)	5600	7000	0.44	1.8
PEtOx-PEO-PEtOx	4500	2×5000	0.31	1.6

In paper VI, PMeOx macro-initiator and the newly synthesized block copolymer PMeOx–PPrOx were characterized by standard SEC and obtained value of polydispersity was $Đ$ = 1.09 and molar mass M_n = 16 210, which was calculated against poly(methyl methacrylate) (PMMA) standards from PSS. NMR spectrum is shown in Figure 2.6.

Sample preparation in paper IV and VI

The light scattering (LS) titration experiments for monitoring of the nanoparticle formation were carried out as follows: Stock aqueous solution of Na[COSAN] (0.0245 M) was consecutively added to PEO–PEtOx or $[PEO–PMeOx]_4$ solutions (2 g/L, 5 mL) in 0.154 M NaCl. The solutions during the titration process were analyzed by a measuring of light scattering.

The samples for SAXS/SANS study were prepared by quick addition of Na[COSAN] solution in 0.154 M NaCl to 200 μL of relatively concentrated PEO–PEtOx solution (10 g/L) in 0.154 M NaCl.

The samples for NMR study were prepared by mixing of calculated amount of solid Na[COSAN] with 1 mL of PEO–PEtOx$^{[IV]}$ (PMeOx–PPrOx)$^{[VI]}$ solution (10 g/L) in 0.154 M NaCl in D_2O to obtain mixtures with COSAN-to-polymer segment ratio ξ = 0.015, 0.045 and 0.150. Small amount (1 μL) of *t*-BuOH was added to the solutions as an internal standard.

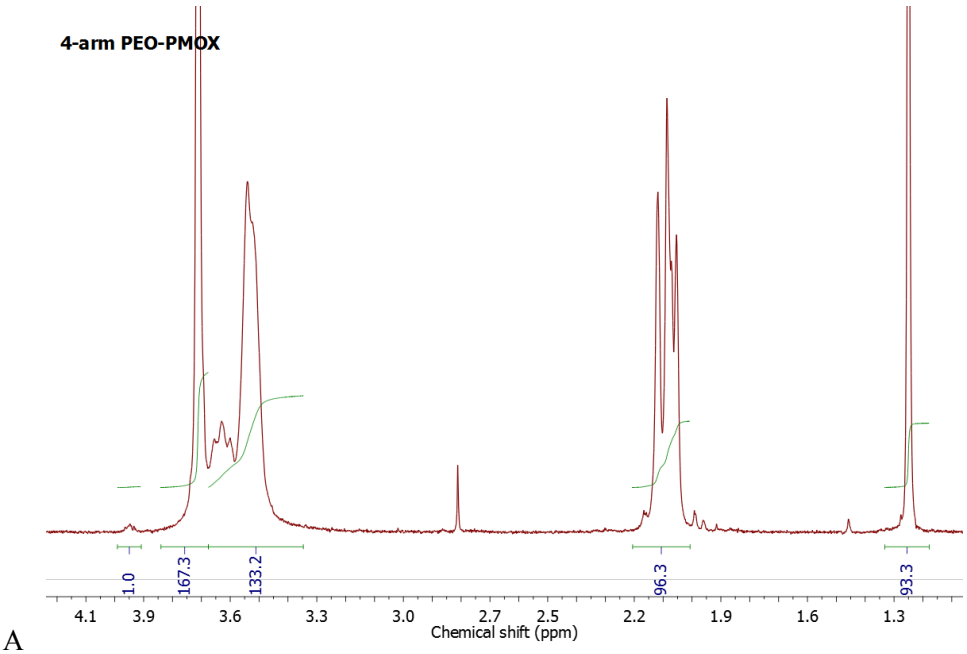

A

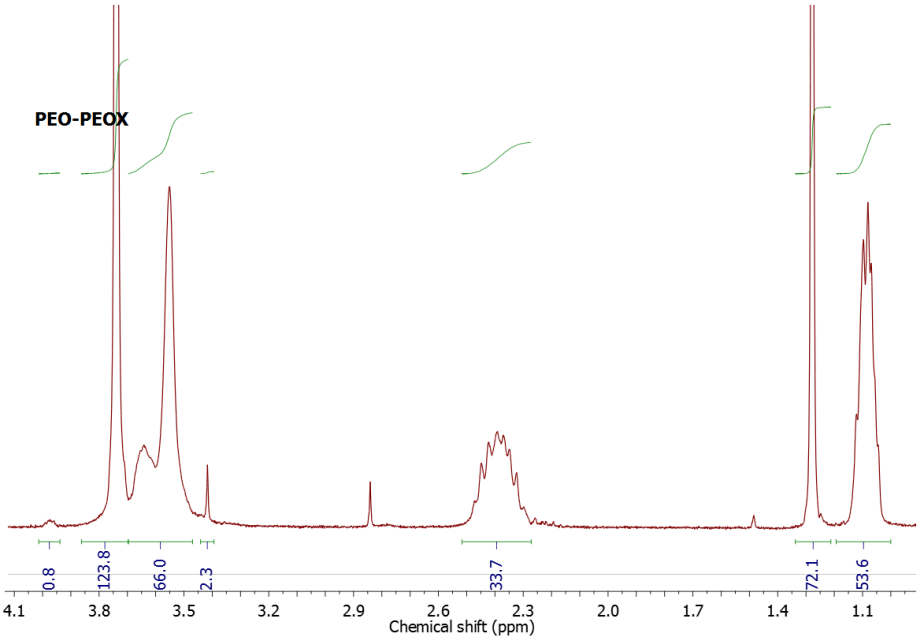

B

Figure 2.5. Representative ^{1}H NMR spectrum and signal assignment for (A) $[PEO–PMeOx]_4$: HO-$C\underline{H}_2C\underline{H}_2$-N (end group) 3.95; O-$C\underline{H}_2C\underline{H}_2$ 3.7; N-$C\underline{H}_2C\underline{H}_2$ 3.65-3.4; NCO-$C\underline{H}_3$ 2.1; internal standard *t*-BuOH 1.25. (B) for PEO–PEtOx: HO-$C\underline{H}_2CH_2$-N (terminal group) 3.95; O-$C\underline{H}_2C\underline{H}_2$ 3.7; N-$C\underline{H}_2C\underline{H}_2$ 3.65-3.4; $C\underline{H}_3$-O (terminal group) 3.4; NCO-$C\underline{H}_2CH_3$ 2.4; internal standard *t*-BuOH 1.25; NCO-$CH_2C\underline{H}_3$ 1.1.

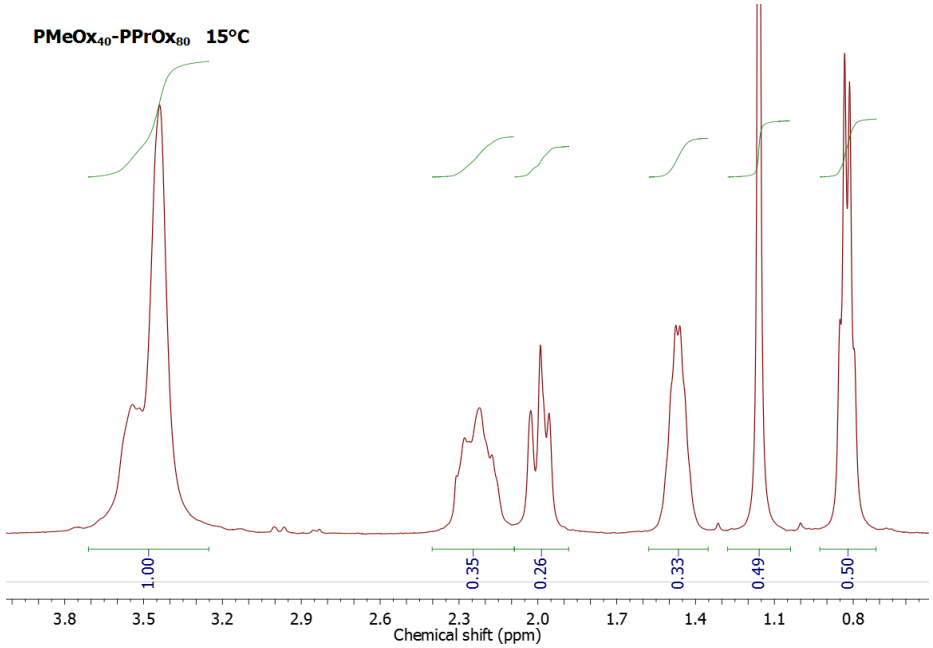

Figure 2.6. Representative ^{1}H NMR spectrum and signal assignment for PMeOx–PPrOx at 15°C: 3.5 ppm – ETHYLENE backbone –C$\underline{H_2}$C$\underline{H_2}$– of both PMeOx and PPrOx; 2.2 ppm – PROPYL 1 CO–C$\underline{H_2}$– of pendant propyl group of PPrOx; 2.0 ppm – METHYL CO–C$\underline{H_3}$ pendant methyl group of PMeOx; 1.5 ppm – PROPYL 2 –C$\underline{H_2}$– of pendant propyl group of PPrOx; 1.1 ppm – internal standard *t*-BuOH; 0.8 ppm – PROPYL 3 –C$\underline{H_3}$ of pendant propyl group of PPrOx.

Sample preparation in paper V

The samples of PEO–PEtOx copolymers with M[COSAN] in 0.154 M MCl (M stands for Na, Li and K) for light scattering, NMR, SANS and cryo-TEM analysis were prepared as follows: the copolymer was dissolved in 0.154 M MCl. The stock aqueous solution of M[COSAN] (0.0245 M) in 0.154 M MCl or solid M[COSAN] were added to the polymer solutions in desired metallacarborane-to-polyme segment ration, ξ. For NMR measurements, a small amount of *t*-buthyl alcohol (1 μL) was added to the solutions as an internal standard. The sample of PEO−PEtOx/Li[COSAN] (polymer concentration 10 g/L, $\xi = 0.045$) in 0.154 M LiCl was used for ITC and NMR titrations, where the nanoparticle dispersion was titrated by 0.154 M LiCl, NaCl and KCl solution.

2.3 Experimental set-up

Nuclear Magnetic Resonance Spectroscopy (NMR)

^{1}H NMR spectra were measured on a Varian ^{UNITY}*INOVA* 300 in deuterium oxide (99.5 %; Chemotrade, Leipzig, Germany). Spectra were referenced to the solvent signal (4.80 ppm). ^{1}H $\{^{11}B\}$ and ^{11}B NMR data were recorded on Bruker Avance III 600 MHz spectrometer at 25°C.

Measurements of translational diffusion coefficients (DOSY) were performed with the double stimulated echo experiment with bipolar pulse field gradients. The pulse sequence has been optimized to suppress flow and convection artifacts as well as eddy current effects. The use of bipolar gradients removes possible modulation of the intensity decay curves by chemical exchange occurring between the sites with different chemical shifts. The gradients were 1 ms long with 16 different linearly spaced amplitudes spanning the range 0–60 G cm^{-1}, and the diffusion time was 1 s. The calibration was done using a standard sample of 1 % H_2O in D_2O (doped with $GdCl_3$), for which the value of the HDO diffusion coefficient at 25°C is 1.9×10^{-9} m^2 s^{-1}. All data processing and fitting of the diffusion coefficients has been done using the spectrometer software (Topspin 2.1, Bruker).

Dynamic Light Scattering (DLS) and Static Light Scattering (SLS)

The light scattering setup (ALV, Langen, Germany) consisted of a 633 nm He-Ne laser, an ALV CGS/8F goniometer, an ALV High QE APD detector, and an ALV 5000/EPP multibit, multitau autocorrelator. DLS data analysis was performed by fitting the measured normalized intensity autocorrelation function $g_2(t) = 1 + \beta|g_1(t)|^2$, where $g_1(t)$ is the electric field correlation function, t is the lag-time and β is a factor accounting for deviation from the ideal correlation. An inverse Laplace transform of $g_1(t)$ with the aid of a constrained regularization algorithm (CONTIN) provides the distribution of relaxation times, $\tau A(\tau)$. Effective angle- and concentration-dependent hydrodynamic radii, $R_H(q,c)$, were obtained from the mean values of relaxation times, $\tau_m(q,c)$, of individual diffusive modes using the Stokes-Einstein equation. To obtain true hydrodynamic radii, the data have to be extrapolated to a zero scattering angle. Since the refractive index increment, dn/dc, is unknown for almost all samples, we evaluated in such cases only the light scattering intensity extrapolated to zero scattering angle as the measure proportional to molar mass of polymeric nanoparticles.

Small Angle X-ray Scattering (SAXS)

In chapters 5.1, 5.4 and 5.6, SAXS experiments were performed using a pinhole camera (Molecular Metrology SAXS System) attached to a microfocused X-ray beam generator (Osmic MicroMax 002) operating at 45 kV and 0.66 mA (30 W). The camera was equipped with a multiwire gas-filled area, detector with an active area diameter of 20 cm (Gabriel design). Two experimental setups were used to cover the q range of 0.005–1.1 Å^{-1}. Scattering vector, q, is defined as: $q = (4\pi/\lambda)\sin\theta$, where λ is the wavelength and 2θ is the scattering angle. The scattering intensities were put on absolute scale using a glassy carbon standard.

In chapter 5.2, the investigations by small angle X-ray (SAXS) method were carried out on Rigaku instrument. It has a pinhole camera attached to a rotating anode X-ray high-flux beam generator (MicroMax 007-HF), which operates at 40 kV and 30 mA (1200 W). The camera was equipped with a multiwire, gas-filled area detector with an active area diameter of 20 cm. Two experimental chambers were used to cover the Q-range of 0.006–1.4 Å.

Small Angle Neutron Scattering (SANS)

The neutron experiments were performed at YuMO spectrometer with two detectors system mode (Dubna, Russia). The beam was collimated to a diameter of 14 mm on the sample and the covered q range was 0.07–0.2 $Å^{-1}$. The solution was placed into Hellma standard cells with the thickness of 1 mm in the direction of neutron beam. The obtained spectra were put on absolute intensity scale using vanadium scatterer. Spectra were normalized by the standard procedure using SAS software.

Electrophoretic light scattering

The measurements were carried out with a Nano-ZS Zetasizer (Malvern Instruments, UK). Zeta-potential values were calculated from electrophoretic mobilities (averages of 15 to 100 measurements) using the Smoluchowski approximation.

Isothermal Titration Calorimetry (ITC)

ITC measurements were performed with an Isothermal Titration Calorimeter (Nano ITC), TA Instruments – Waters LLC, (New Castle, USA). The microcalorimeter consists of a reference cell and a sample cell (24K Gold). The sample cell was connected to a 50 µL syringe. The syringe needle was equipped with a flattened, twisted paddle at the tip, which ensures continuous mixing of the solutions in the cell rotating at 250 rpm. Titrations were carried out by consecutive injections from the syringe into the sample cell. We carefully tuned experimental conditions to reach the minimum of noise prior the measurements. The differential heat of mixing was determined for discrete changes of composition. The raw heat changes were analyzed by NITPIC software to obtain ITC thermograms, from which ΔH^{agg}, ΔH^{mic} and CMC^{ITC} were determined.

Cryogenic Transmission Electron Microscopy (Cryo-TEM)

A Jeol JEM-3200 FSC microscope was used for the Cryo-TEM imaging. 200 mesh copper grids with holey carbon foil Quantifoil, R2/1, were treated with oxygen and hydrogen plasma (Gatan, Model 950 Advanced Plasma System, time 30 s, target vacuum 70 mTorr, target power 50W, O_2 gas flow 27.5 sccm, H_2 gas flow 6.4 sccm) prior to sample preparation. Plasma treated grid was placed into FEI Vitrobot having room temperature and 100 % relative humidity. 1 µl of sample solution was applied on the grid and the Vitrobot was set to execute one two seconds blotting with 2.0 mm offset. 1:1 liquid propane-ethane mixture cooled to –180°C was used for vitrification. The vitrified sample was cryo-transferred into the microscope and continuously cooled during the imaging process at –188°C. Micrographs were recorded with Gatan Ultrascan

4000 camera operating microscope at bright field mode, at 300 kV acceleration voltage and with Omega type in-column energy filter set to 0–20 eV energy-loss range (zero-loss imaging).

Atomic force microscopy (AFM)

AFM measurements were performed in the semicontact (tapping) mode under ambient conditions using a scanning probe microscope Digital Instruments NanoScope dimensions 3 equipped with a Nanosensors silicon cantilever. The nanoparticles were deposited from very dilute solutions (ca. 0.01 g/L) on a freshly cleaved mica surface. The samples were left to dry in a vacuum oven.

Surface tension measurement

Surface tension was measured by means of pendant drop method using: DataPhysics OCA–15 plus, Dynamic Contact Angle from DataPhysics Instrument GmbH, Fildestadt. Video based measurement instrument for static and dynamic contact angle. Needles Nordson EFD® with appropriate diameter were used.

Conductometry

Conductivity was measured with precision conductivity equipment consisting of a Radiometer apparatus CDM230 and a conductivity cell. All measurements were carried out at 25°C. From the plot of specific conductivity, κ, on concentration, degree of micelle ionization, β, was determined.

X-ray structure determination

The data collection was performed with Agilent SuperNova dual wavelength diffractometer equipped with Atlas CCD area detector using Cu-Kα radiation with the CrysAlisPro program package. Analytical numeric correction using multifaceted crystal was performed as implemented in CrysAlisPro program. The structure was solved by direct methods by using the SHELXS-97 program or the SIR-97 program and the full-matrix least squares refinements on F^2 were performed using the SHELXL-97 program. The figure was drawn with Diamond 3 program. The heavy atoms were refined anisotropically. Rest of the CH and BH hydrogen atoms were included at the calculated distances with fixed displacement parameters from their host atoms (1.2 or 1.5 times of the host atom).

MALDI-TOF Mass Spectroscopy (MALDI-TOF MS)

The negative mode was utilized on a Brucker Biflex instrument (N_2 laser; λ_{exc} 337 nm, pulses of 0.5 ns), ion source of 20 000 kV (Uis1) and 17 500 kV (Uis2), without matrix. The intensity of the laser was fixed at the 30%.

Electrospray Ionisation Mass Spectrometry (ESI-MS)

Mass spectra were obtained on a Q-Tof micro (Waters) in ESI negative mode.

Infrared spectroscopy (IR)

IR spectra (ν, cm^{-1}; Attenuated total reflection) were obtained on a Shimadzu FTIR-8300 spectrophotometer.

UV-Vis spectroscopy

UV-Vis absorption spectra were carried out with SPECORD S600, Analytik Jena, Germany, diode-array spectrometer.

High-Performance Liquid Chromatography (HPLC)

Measurements were analyzed with Atlantis® dC18 5µm, 4.6×150 mm (Waters) column by gradient elution as follows: 0–2 min acetonitrile/water 10:90; 2–5 min linear gradient up to acetonitrile/water 80:20 (temperature 20ºC, rate 1 mL/min, detection UV-Vis at 200 nm, injection 20 µL).

Size-Exclusion Chromatography (SEC)

Measurements were performed on an Agilent 1260-series HPLC system equipped with a 1260 online degasser, a 1260 ISO-pump, a 1260 automatic liquid sampler (ALS), a thermostated column compartment (TCC) at 50°C equipped with two PLgel 5 µm mixed-D columns in series, a 1260 diode array detector (DAD) and a 1260 refractive index detector (RID). The used eluent was dimethylacetamide (DMA) containing 50 mM of lithium chloride at an optimized flow rate of 0.593 ml/min. The spectra were analyzed using the Agilent Chemstation software with the GPC add on.

Elemental analyses

Elemental analyses were performed using a Carlo Erba EA1108 microanalyzer.

References

[1] Schärtl, W. *Light Scattering from Polymer Solutions and Nanoparticle Dispersions*; Springer: Berlin, 2007.

[2] Brown, W. *Light Scattering: Principles and Developement*; Calendron Press: Oxford, 1996.

[3] Debye, P. *J. Phys. Colloid Chem.* **1947**, *51*, 18.

[4] Schnablegger, H.; Singh, Y. *The SAXS Guide – Getting acquainted with the principles*; Anton Paar GmbH: Austria, 2013.

[5] Lindner P.; Zemb, T. *Neutrons, X-Rays and Light: Scattering methods applied to soft condensed matter*; Elsevier: North-Holland, 2002.

[6] Cavanagh, J.; Fairbrother, W. J.; Palmer, A. G.; Rance, M.; Skelton, N. J. *Protein Spectroscopy Principles and Practice, Second Edition*; Elsevier Academic Press: San Diego, California, 2007.

[7] Hatada, K.; Kitayama, T. *NMR Spectroscopy of Polymers*; Springer-Verlag Berlin Heidelberg, 2004

[8] Kawaguchi, S.; Winnik, M. A.; Ito, K. *Macromolecules* **1996**, *29*, 4465.

[9] Blum, F. D. *Colloids Surf.* **1990**, *45*, 361.
[10] Cosgrove, T.; Griffiths, P. C. *Adv. Colloid Interface Sci.* **1992**, *42*, 175.
[11] Johnson, C. S. *Prog. Nucl. Magn. Reson. Spectrosc.* **1999**, *34*, 203.
[12] Kronberg, B.; Holmberg, K.; Lindman, B. *Surface Chemistry of Surfactants and Polymers*; John Wiley & Sons, Ltd.: Chichester, 2014; p. 231.
[13] Gibbs, J. W. *Papers of J. Willard Gibbs, 2 vols.*; Bumstead, H. A. and van Name, R. G., Ed., Longmans Green, London, 1906 (Reprinted by Dover, New York, 1961).
[14] Berry, J. D.; Neeson, M. J.; Dagastine, R. R.; Chan, D. Y.; Tabor, R. F. *J. Colloid Interface Sci.* **2015**, *454*, 226.
[15] Dukhin; S. S.; Kretzschmar, G.; Miller, R. Dynamics of Adsorption at Liquid Interfaces: Theory, Experiment, Application, In *Studies in Interface Science, Vol. 1*; Möbius, D. and Miller, R., Ed., Elsevier: Amsterdam, 1995.
[16] Mucic, N.; Javadi, A.; Kovalchuk, N. M.; Aksenenko, E. V.; Miller, R. *Adv. Colloid Interface Sci.* **2011**, *168*, 167.
[17] Plešek, J.; Baše, K.; Mareš, F.; Hanousek, F.; Štíbr, B.; Heřmánek, S. *Collect. Czech. Chem. Commun.* **1984**, *49*, 2776.
[18] Teixidor, F.; Pedrajas, J.; Rojo, I.; Viñas, C.; Kivekäs, R.; Sillanpää, R.; Sivaev, I.; Bregadze, V.; Sjöberg, S. *Organometallics*, **2003**, *22*, 3414.
[19] Keller, S.; Vargas, C.; Zhao, H. Y.; Piszczek, G.; Brautigam, C. A.; Schuck, P. *Anal. Chem.* **2012**, *84*, 5066.
[20] Farràs, P.; Teixidor, F.; Kivekäs, R.; Sillanpää, R.; Viñas, C.; Grüner, B.; Cisarova, I. *Inorg. Chem.* **2008**, 47, 9497.
[21] Hoogenboom, R.; Thijs, H. M.; Jochems, M. J.; van Lankvelt, B. M.; Fijten, M. W.; Schubert, U. S. *Chem. Commun.* **2008**, *44*, 5758.
[22] Wiesbrock, F.; Hoogenboom, R.; Leenen, M.; van Nispen, S. F.; van der Loop, M.; Abeln, C. H.; van den Berg, A. M. J.; Schubert, U. S. *Macromolecules* **2005**, *38*, 7957.
[23] Verbraeken, B.; Monnery, B. D.; Lava, K.; Hoogenboom, R. *Eur. Polym. J.* **2017**, *88*, 451.

3 Research aims

The research of carboranes in the laboratory of my supervisor Dr. Matějíček began more than ten years ago and the main stimulus was the discovery of the inhibition of HIV protease by cobalt bis(dicarbollide), COSAN, and its conjugates. Besides that, other potential applications have been known mostly related to medicine. However, the understanding of the behavior of COSAN and other boron cluster compounds in water and salt was unclear. Because the aggregation of boron drugs can influence the potential medical use, we focused on the amphiphilicity of cluster compounds. Furthermore, we searched for the most suitable drug delivery carriers of COSAN. In summary, the aims of this thesis were:

- The clarification of the hydrophobic or amphiphilic character of boron cluster compounds.

- The description of the self-assembly processes of various boron cluster compounds and their conjugates in water.

- The preparation of polymeric carriers of COSAN and the study of the interactions between COSAN and block copolymers. Additionaly, the focus was on the stimuli, which can be used for the drug release.

4 List of papers

Thematically ordered research papers included in the dissertation thesis:

[I] Classical amphiphilic behavior of nonclassical amphiphiles:
A comparison of metallacarborane self-assembly with SDS micellization.
Uchman, M.; Ďorďovič, V.; Tošner, Z.; Matějíček, P.
Angewandte Chemie – International Edition **2015**, *54*, 14113–14117.

[II] Stealth amphiphiles: Self-assembly of polyhedral boron clusters.
Ďorďovič, V.; Tošner, Z.; Uchman, M.; Zhigunov, A.; Reza, M.; Ruokolainen, J.; Pramanik, G.; Cígler, P.; Kalíkova, K.; Gradzielski, M.; Matějíček, P.
Langmuir **2016**, *32*, 6713–6722.

[III] Aqueous self-assembly and cation selectivity of cobaltabisdicarbollide dianionic dumbbells.
Tarrés, M.; Viñas, C.; González-Cardoso, P.; Hanninen, M.; Sillanpää, R.; Ďorďovič, V.; Uchman, M.; Teixidor, F.; Matějíček, P.
Chemistry – A European Journal **2014**, *20*, 6786–6794.

[IV] Compartmentalization in hybrid metallacarborane nanoparticles formed by block copolymers with star-like architecture.
Ďorďovič, V.; Uchman, M.; Zhigunov, A.; Nykanen, A.; Ruokolainen, J.; Matějíček, P.
ACS Macro Letters **2014**, *3*, 1151–1155.

[V] Cation-sensitive compartmentalization in metallacarborane containing polymer nanoparticles.
Ďorďovič, V.; Uchman, M.; Reza, M.; Ruokolainen, J.; Zhigunov, A.; Ivankov, O.; Matějíček, P.
RSC Advances **2016**, *6*, 9884–9892.

[VI] Tuning of thermoresponsivity of poly(2-alkyl-2-oxazoline) block copolymer by interaction with surface active and chaotropic metallacarborane anion.
Ďorďovič, V.; Verbraeken, B.; Hogenboom, R.; Kereiche, S.; Matějíček, P.; Uchman, M. (submitted **2017**)

Papers not included in the dissertation thesis:

Hybrid nanospheres formed by intermixed double-hydrophilic block copolymer poly(ethylene oxide)-*block*-poly(2-ethyloxazoline) with high content of metallacarboranes.
Ďorďovič, V.; Uchman, M.; Procházka, K.; Zhigunov, A.; Pleštil, J.; Nykanen. A.; Ruokolainen, J.; Matějíček, P.
Macromolecules **2013**, *46*, 6881–6890.

5 Results

5.1 Paper I

Classical amphiphilic behavior of nonclassical amphiphiles: A comparison of metallacarborane self-assembly with SDS micellization*

Abstract

The self-assembly of metallacarboranes, a peculiar family of compounds exhibiting surface activity and resembling molecular-scale Pickering stabilizers, has been investigated by comparison to the micellization of sodium dodecylsulfate (SDS). These studies have shown that molecules without classical amphiphilic topology but with an inherent amphiphilic nature can behave similarly to classical surfactants. As shown by NMR techniques, the self-assembly of both metallacarboranes and SDS obey a closed association model. However, the aggregation of metallacarboranes is found to be enthalpy-driven, which is very unusual for classical surfactants. Possible explanations of this fact are outlined.

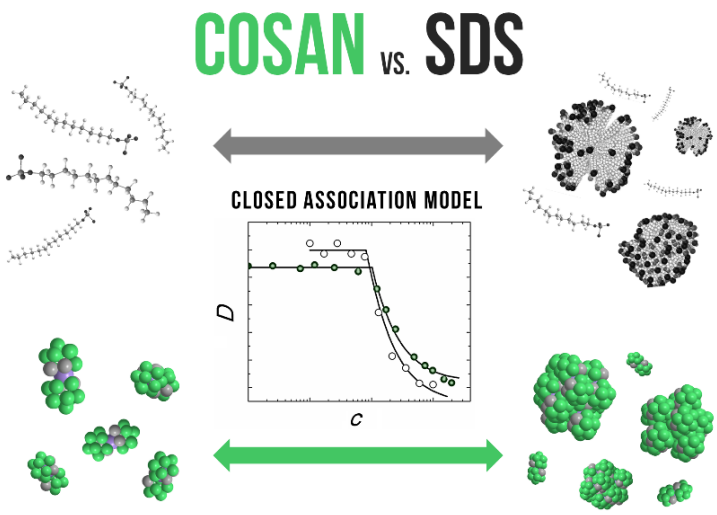

* In slightly modified version published as: Uchman, M.; Ďorďovič, V.; Tošner, Z.; Matějíček, P.: Classical Amphiphilic Behavior of Nonclassical Amphiphiles: A Comparison of Metallacarborane Self-Assembly with SDS Micellization, *Angewandte Chemie – International Edition* **2015**, *54*, 14113–14117.

Introduction

Metallacarboranes, such as the [3,3'-Co($C_2B_9H_{11}$)$_2$]$^-$ anion, also known as the COSAN anion (Figure I.1A), are boron cluster compounds containing metal cations (for example, Co, Ni, and Fe) sandwiched by two dicarbollide clusters.[1] Thanks to their unique properties,[2–4] they have been employed, for example, in radioactive ion extraction[5] and also in biomedical, application-oriented research.[6–9] As a result of the presence of hydridic B–H vertices and charge delocalization, the COSAN anion exhibits surface activity[10–12] and has an amphiphilic character. As a result, it accumulates at interfaces and is soluble in both oil and water.[13] With this in mind, it is not surprising that metallacarboranes self-assemble in water in spite of their unusual molecular structure.[14–21]

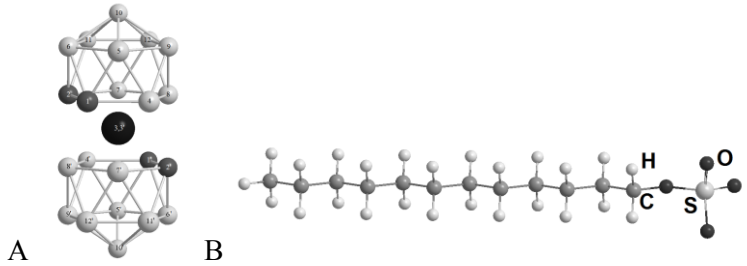

Figure I.1. The structures of anions of (A) Na[COSAN] and (B) sodium dodecylsulfate (SDS). Cluster-vertex color coding in (A): B–H = light gray, C–H = dark gray, Co = black

In this Communication, we compare the association behavior of Na[COSAN] with the most studied ionic surfactant – sodium dodecylsulfate (SDS; Figure I.1B). Unlike Na[COSAN], the molecule of SDS has classical amphilphilic topology, consisting of a long aliphatic tail and a small, charged head group. The closed association model describes the solution behavior of such compounds.[22,23] Our aim is to show that even molecules with an unusual molecular structure can follow the rules established for classical surfactants. Furthermore, unusual and unexpected features of metallacarboranes in solution will be outlined and explained.

Results and discussion

Direct proof that Na[COSAN] can be included in a broader family of surfactants is shown in Figure I.2. Both curves exhibit two breaks in the semilogarithmic plot.[24–26] The curve at lower concentration indicates the point at which the compound starts to accumulate at the interface. It is assigned to $1/K_{aw}$ (where K_{aw} is the air–water partition coefficient), which is a measure of hydrophobicity. Thus, SDS is more hydrophobic than Na[COSAN]. The second break is usually attributed to the critical aggregation (micelle) concentration (denoted CAC or CMC), assuming that the formation of micelles does not cause a further decrease of the γ value.

It is useful to compare the slopes of the two γ versus ln(c) curves, as the slope is proportional to the surface excess Γ. This is shown in Figure I.S1 in the Supporting Information (SI) and the value of the surface area per molecule (A_S) is calculated. It is evident that Na[COSAN] accumulates to a lesser extent than SDS at the interface. Furthermore, the Na[COSAN] adsorption is a continuous process without an abrupt formation of compact

monolayers or "2D aggregates". This continuous adsorption process is demonstrated by the fact that the area occupied by one molecule decreases continuously (with increasing concentration) from a relatively large value (4–5 nm^2) to a limiting value of A_S(Na[COSAN]) = 0.98 nm^2, which indicates a preferential parallel orientation of the cluster axis to the plane of the interface[11] (a main axis of length 1.1 nm and a semiaxis of length 0.6 nm in COSAN).

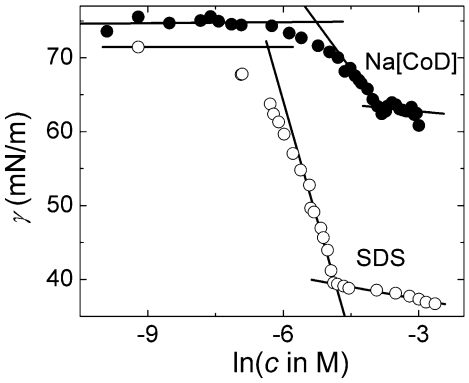

Figure I.2. Surface tension (γ) of Na[COSAN] and SDS aqueous solutions as a function of ln(c). Data for SDS taken from the literature.[24,25]

With the help of earlier data,[10,11] the molecular picture of Na[COSAN] at the interface can be interpreted as follows: While aliphatic tails of SDS are exposed to air forming a fairly compact monolayer (the A_S(SDS) value essentially does not change with c), bulky COSAN are concentrated on the aqueous side of the interface.[10] The clusters slightly repel each other without forming regular monolayers.[11] Cations play a substantial role here, because their hydration energy stabilizes the clusters at the interface.[11]

Considering the fairly low surface activity and the bulkiness of the clusters, we can argue that metallacarboranes should be taken as molecular-scale Pickering stabilizers[27] rather than surfactants (see their ability to stabilize nanobubbles reported below). Nevertheless, it will be shown that Na[COSAN] does self-assemble in pure water in a very similar manner to classical surfactants, whereas Pickering stabilizers generally cannot do so.

In our first paper investigating the aggregation of metallacarboranes in 2006, the principle method employed was a light scattering technique.[14] Later on, we realized that NMR spectroscopy was a more suitable tool for studying intermolecular interactions and thermal motions of metallacarboranes.[28] Concentration-dependent ^{1}H {^{11}B} NMR spectra of Na[COSAN] over a concentration range of 0.25–200 mm are shown in Figure I.S2. Significant shifts of resonance signals are evident around the CAC value. The most pronounced changes are observed for the CH1,2 and BH6 signals (Figure I.3A; see Figure 1.3 for molecular labelling), revealing the strong influence of mutual interactions in this area of the clusters. Similar but substantially weaker trends were observed for the α-CH2 groups of SDS around the CMC (Figure I.3B).[28,29]

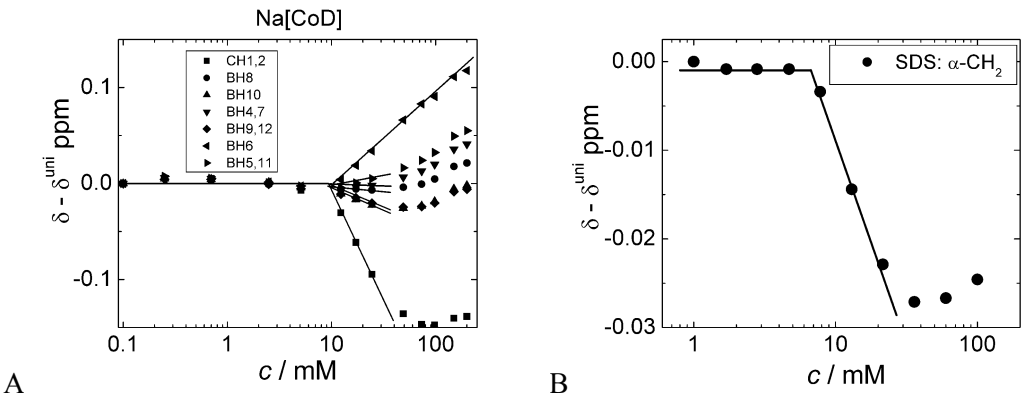

Figure I.3. Changes in the relative chemical shifts for signals in (A) the $^{1}H\{^{11}B\}$ NMR spectra of Na[COSAN] and (B) the ^{1}H NMR spectra of SDS as a function of concentration at 25°C. Chemical shift changes for (A) specific CH and BH moieties of Na[COSAN] (see Figure 1.3 for numbering scheme) and (B) α-CH2 of SDS (taken from the literature)[28] are recorded. Each data point is referenced to the chemical shift of the unimer (δ_{uni}) for the highest dilution of compounds, that is, where only unimers appear.

The similarities between the solution behaviors of SDS and Na[COSAN] run even deeper. We carried out DOSY ^{1}H NMR experiments to detect thermal self-diffusion of COSAN. The results for Na[COSAN] and SDS diffusion are compared in Figure I.4, where experimental points were fitted according to the model of closed association (a simple mathematical model and the results of the fitting procedure are shown in the NMR section of SI). The fitted data unambiguously indicate that self-assembly of both surfactants can be satisfactorily described by the same model.[22,23]

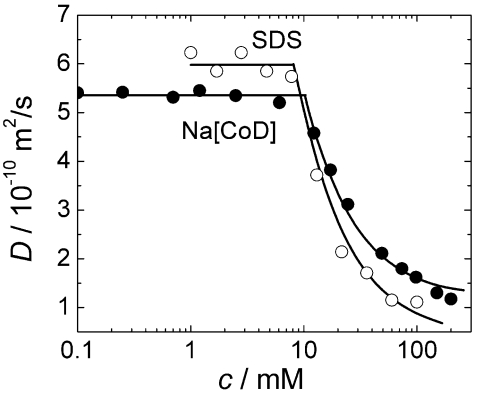

Figure I.4. Diffusion coefficients (D) obtained from ^{1}H DOSY NMR experiments at 25°C for the CH1,2 signals of Na[COSAN] plotted as a function of concentration. The corresponding diffusion coefficients for the α-CH2 resonance signals of SDS were obtained from previous reports.[28] Data fitted by the closed association model (see Equations 5.1.2 and 5.1.3 in SI).

Despite a similar size and mechanism of formation, the structure of the metallacarborane associates is hardly comparable to a classical micelle with a hydrophobic core and a charged layer at the micellar surface. Small-angle X-ray scattering (SAXS) data show that the

aggregation number of Na[COSAN] is very low (N^{agg} = 5) as compared to SDS (N^{agg} = 62). Furthermore, the average distance between centers of gravity of neighboring clusters within aggregates 0.59 nm (calculated from correlation peaks in SAXS curves) indicates that a parallel orientation of COSAN (a semiaxis of length 0.6 nm) is preferred.

Plots of both the CAC values for Na[COSAN] and the CMC values for SDS against temperature (see Figure I.S3) have a classical shape.[30,31] The temperature dependence of the CAC is useful to calculate the free energy of aggregation. Thermodynamic parameters like the free energy, enthalpy, and entropy of aggregation (ΔG^{agg}, ΔH^{agg}, and ΔS^{agg}, respectively) allow us to better understand the mechanism of the self-assembly process. An important parameter to evaluate the ΔG^{agg} value is the degree of counterion binding to micelles (β). The β value is almost zero for Na[COSAN], but rises to around 80% for SDS micelles.[31] For more details, see the thermodynamics section in SI.

To complete a thermodynamic description of the self-assembly of Na[COSAN], a method for the direct determination of the ΔH^{agg} values is needed. With this in mind, isothermal temperature calorimetry (ITC) experiments were run at various temperatures, where a concentrated Na[COSAN] solution was slowly titrated into pure water.[32,33] The aggregates were decomposed into COSAN unimers and the measured process corresponded to deaggregation. The raw data is shown in Figure I.5. ITC is an exceptionally sensitive method that detects mutual interactions and the redistribution of nanostructures.[34] The presence of single, sharp endothermic peaks in Figure I.5 proves that "micelle" deaggregation is the only process occurring during Na[COSAN] dilution. Considering the data, it is found that the ΔH^{agg} value only slightly depends on temperature and is exothermic (around –13 kJ mol^{-1}).

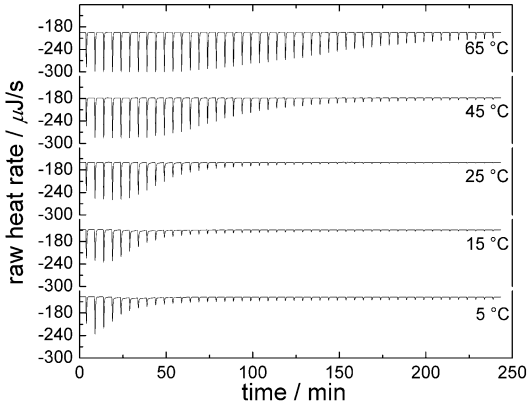

Figure I.5. Raw ITC data for the deaggregation process during the titration of Na[COSAN] (120 mM) into pure water at various temperatures.

From the free energy and enthalpy of aggregation we calculated also the ΔS^{agg} value. All the thermodynamic parameters for Na[COSAN] and SDS micellization are shown in Figure I.6 and Figure I.S4, respectively. In both cases, the ΔG^{agg} value is negative and almost independent of temperature. Both enthalpy and entropy terms are usually dependent on

temperature (see Figure I.S4), and compensate each other as demonstrated in the so-called compensation plot[35] (see Figure I.S5 and further comments in SI).

The micellization of classical hydrocarbon and fluorocarbon surfactants is typically explained as an entropy-driven process (see Figure I.S4 for SDS) since the driving force is the classical hydrophobic effect, resulting from gains in entropy caused by the release of solvent molecules.[36,37] This is not the case for Na[COSAN], for which the entropy contribution is, in fact, negligible (Figure I.6), pointing to a nonclassical hydrophobic effect.[38,39] An explanation for the dominant role of the enthalpy term is not straightforward (see SI for comments). Even though the model for the B–H···H–C dihydrogen bond[40] sounds attractive (it is consistent with a parallel orientation of clusters within the aggregates and with the NMR spectral changes in Figure I.2A), such a bond has not yet been directly proven in metallacarborane solutions. Considering the current state of knowledge, we prefer an explanation based on a nonspecific hydrophobic action[36–39] with a predominant role for (de)hydration of the cluster (see the sections on compensation plots and enthalpy-driven association in SI).

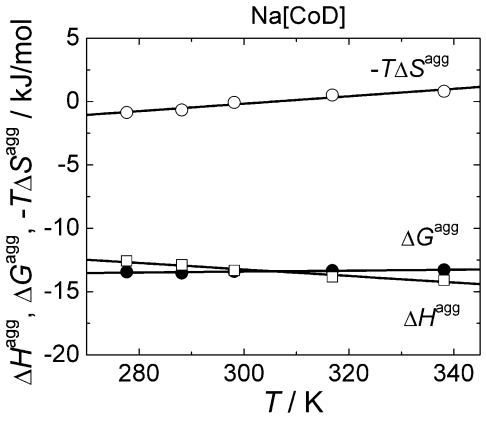

Figure I.6. Thermodynamic parameters (ΔG^{agg}, ΔH^{agg}, and $-T\Delta S^{agg}$) of Na[COSAN].

Finally, the above-described Na[COSAN] associates are compared with large spherical nanoparticles. These large nanoparticles were first detected using light-scattering (LS) techniques in our laboratory in 2006[14] and were subsequently interpreted as monolayer vesicles in 2011 and subsequent years.[17, 18, 41] Spherical nanoparticles are sufficiently large for LS, but they are beyond the detection limit of DOSY experiments. The DOSY technique is, however, suitable for detection of low-molar-mass molecules in complex mixtures, which do not scatter light.

It was recently reported for solutions of surface-active polymers that a “slow mode” (that is, large particles) could be detected even for non-associating compounds by LS.[42] This result was interpreted as the stabilization of nanobubbles by the surfactant. Thus, the surface-active COSAN clusters would be packed at the surface of nanobubbles[12] in the same way that they are located in vesicles, according to the model proposed by Bauduin et al.,[12,17] making them almost indistinguishable by scattering techniques. In our current LS study (see the results in Figure I.S6 with further comments), we confirmed the presence of single molecules, small micelle-like aggregates, and spherical nanoparticles in solution. The fraction of large particles

is, however, very low (less than 1%; see the cryo-TEM analysis in Figure I.S7), and it is significantly less than what we claimed in 2006.[14] Their inner structure is still unclear, since the cryo-TEM image in Figure I.S7 is hardly comparable to that of true vesicles with an interior area of lighter density.[41] We also observed a non-negligible fraction of nanobubbles by LS, which are most likely stabilized by Na[COSAN]. This supports the above-mentioned theory that metallacarboranes should be taken not only as surfactants, but also as molecular-scale Pickering stabilizers.[27]

In summary, it is evident that a metallacarborane cluster, despite its peculiar shape and structure, behaves like a classical surfactant in many cases. The formation of more complex structures like lamellae, vesicles, or worm-like particles can also be detected for Na[COSAN] as well as for SDS.[43] Furthermore, both compounds can form complexes with cationic polyelectrolytes and also with electroneutral poly(ethylene oxide) (PEO), as previously described.[44, 45] The main differences between behavior of Na[COSAN] and SDS were found in the thermodynamics of their self-assembly in water.

Supporting Information

Surface Tension (The Gibbs-adsorption-isotherm approach)

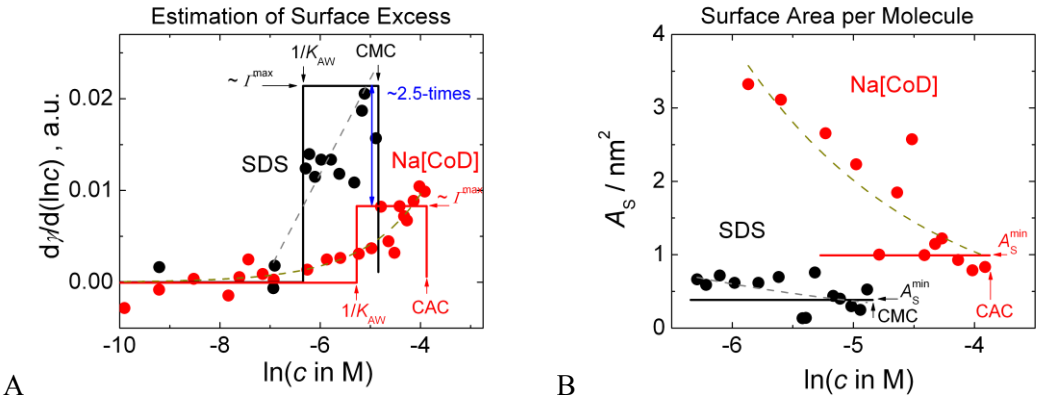

Figures I.S1. (A) 1st derivative of γ vs. ln$c$ plot, which is proportional to surface excess, Γ, for SDS (black) and Na[COSAN] (red) of experimental points below CAC/CMC and linear fits from Figure I.1. The value of Γ is proportional to number of surfactant molecules accumulated at the interface. Close to CAC/CMC, there are ca. 2.5-times more molecules of SDS than Na[COSAN] at the interface. (B) the average area occupied by a molecule at the interface, A_S, derived from dγ/d(ln$c$) values for SDS (black) and Na[COSAN] (red). Close to CMC/CAC, the values of limiting coverage is as follows: A_S(Na[COSAN]) = 0.98 nm^2 and A_S(SDS) = 0.38 nm^2. Arrows denote the breaks in γ dependences: the first one is related to K_{AW} (air-water partition coefficient), which is a term describing the affinity of a compound for the interface (it is a measure of hydrophobicity), and the second one assigns the value of CMC/CAC. K_{aw}(Na[COSAN]) = 200, K_{aw}(SDS) = 570, *cac*(Na[COSAN]) = 20 mM, *cmc*(SDS) = 8 mM. The experimental points are fitted by an exponential function (dash lines).

^{1}H and DOSY NMR spectroscopy

Fitting of diffusion coefficients from DOSY NMR by the closed association model

The concentration dependent effective diffusion coefficient, D, can be expressed as the number weighted summation of contributions from all the species in solution, D_i, with corresponding fraction f_i.

$$D = \sum_i f_i D_i \qquad (5.1.1)$$

In the closed association model, there are only single molecules below CAC. Above CAC, there is a mixture of single molecules, with concentration equal to *cac*, and aggregates, size of which does not depend on concentration. Thus, it reads:

$$D = D_1; c \leq cac \qquad (5.1.2)$$

$$D = \left[\frac{cac}{c}\right] D_1 + \left[\frac{c - cac}{c}\right] D_{\text{agg}}; c > cac \qquad (5.1.3)$$

where c is analytical concentration, cac is the value of critical aggregation concentration (11 mM for Na[COSAN] at 25°C), D_1 is a diffusion of single molecule, and D_{agg} is a diffusion of aggregates. From fitting of experimental data (Figure I.3) and using Stokes-Einstein equation, we calculated hydrodynamic radii, R_H, of Na[COSAN] molecules (unimers), 0.37 nm, and self-assemblies, 1.85 nm, at 25ºC.

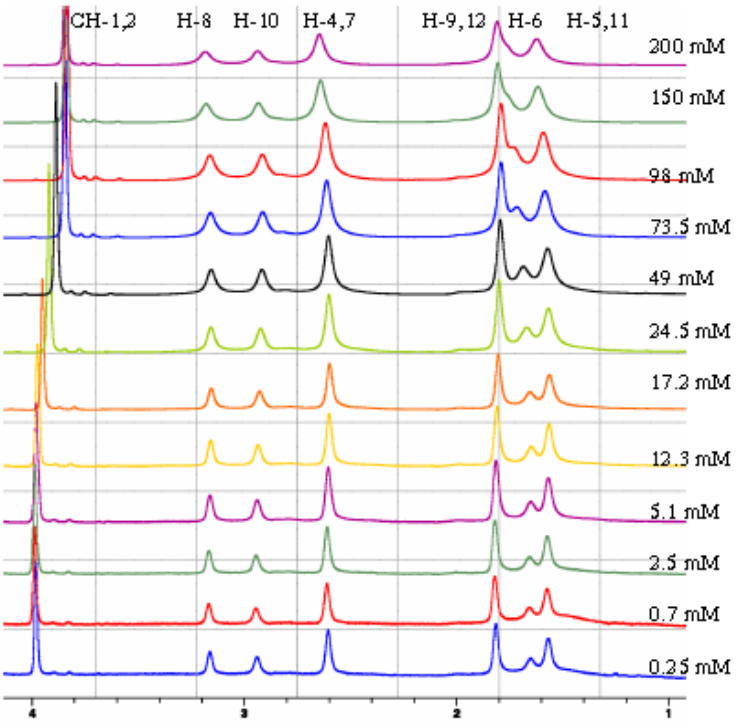

Figure I.S2. ^{1}H $\{^{11}B\}$ NMR spectra of Na[COSAN] for concentrations 0.25–200 mM. The signals are assigned to corresponding CH or BH groups.

Thermodynamics

For calculation of free energy of micellization (aggregation), simplified equation

$$\Delta G^0_{\text{mic}} = (1 + \beta) RT \ln X_{\text{CMC}} \qquad (5.1.4)$$

is commonly used, where β is a degree of counterion binding to micelles (estimated from conductivity measurements), and X_{CMC} is a value of CMC expressed as molar ratio. It can be used only for SDS, where aggregation number N^{agg} = 62 is high enough to be neglected, and β is as high as 80% for SDS micelles indicating substantial condensation of Na^+ to the micelles.[44] For Na[COSAN], N^{agg} = 5 was determined by SAXS, and it is too low to be neglected in estimation of ΔG^{agg}. The value of β was measured by conductometry, and it is close to zero for

Na[COSAN] indicating that there are no Na^+ cations incorporated within the aggregates. For calculation of free energy of aggregation we utilized an approach proposed by Lim et al.[30]

$$\frac{G^0_{\mathrm{mic}}}{RT} = \left[\left(1+\frac{m}{n}-\frac{1}{n}\right)\ln X_{\mathrm{CMC}}\right] + \left[\frac{1}{n}\ln\frac{n(n+m)(2n+2m-1)}{n+m-2}\right] + \left[\left(1+\frac{m}{n}-\frac{1}{n}\right)\ln\frac{1}{\nu_S}\frac{(n+m)(2n+2m-1)}{(n+m-1)(n+m+1)}\right] \quad (5.1.5)$$

where parameters *m* and *n* stand for number of condensed counterions on a micelle and number of surfactant molecules in a micelle, respectively, and $\nu_S = 1$ for uni-univalent surfactant. Thus, it stands for Na[COSAN] "micelles": $m = 0$ and $n = 5$.

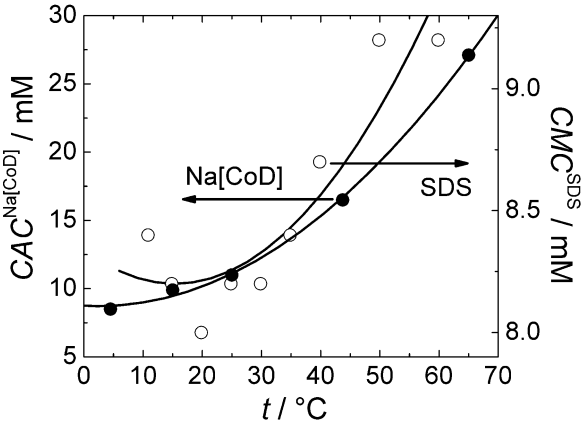

Figure I.S3. Concentration dependence of critical aggregation/micelle concentration, CAC/CMC, of Na[COSAN] (black points and left *y*-axis) and SDS (hollow points and right *y*-axis) obtained by DOSY NMR. Data for SDS taken from literature.[31]

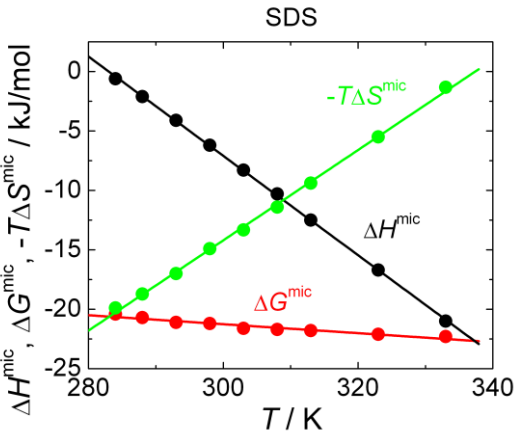

Figure I.S4. Thermodynamic potentials (ΔG^{mic}, ΔH^{mic} and $-T\Delta S^{mic}$) of SDS association.[31]

Enthalpy driven association of Na[COSAN]

The interpretation of dominance of the enthalpy term is not straightforward (corresponding references are in the main text). (i) One possible explanation can be a presence of B–H···H–C

dihydrogen bond within the aggregates, which is strong enough to overwhelm the electrostatic repulsion between anionic clusters. Even though the existence of such bond has been predicted in literature, supported by parallel orientation of COSAN clusters in various systems (solid state and lyotropic lamellar phase) and also by significant shift of CH1,2 signals in NMR spectra (see Figure I.2A), it has never been proven directly.

(ii) Another interpretation of the enthalpy driven association is related to already-mentioned "nonclassical hydrophobic effect" first described for binding of ligands into hydrophobic protein pockets, where hydrophobic action accompanied by changes of the solute solvation is enthalpy driven process.

(iii) Further, it was found for hydrophobic objects dispersed in water, that the contribution of entropy and enthalpy term to the hydration free energy and to the attractive interaction among them strongly depends on their size. Association of amphiphiles can be thus both entropy and enthalpy driven depending on dimensions of associating molecules. COSAN cluster with longitudinal axis length around 1.1 nm is large enough that it already belongs to objects where associative attraction can be enthalpy driven.

Compensation plot

From intercept of the compensation plot ($\Delta S^{agg} = 0$), we obtained a value of ΔH^*(Na[COSAN]) = –13.4 kJ mol^{-1} and ΔH^*(SDS) = –21.9 kJ mol^{-1}, which are related to "chemical part" of micellization process and it is equal to pure solute-solute interaction. Compensation temperature (slope of the compensation plot), T_c(Na[COSAN]) = 264 K reflects "desolvation part" of the micellization process, i.e., dehydration of COSAN clusters, and it is exceptionally low as compared to classical surfactants like SDS (T_c(SDS) = 307 K).

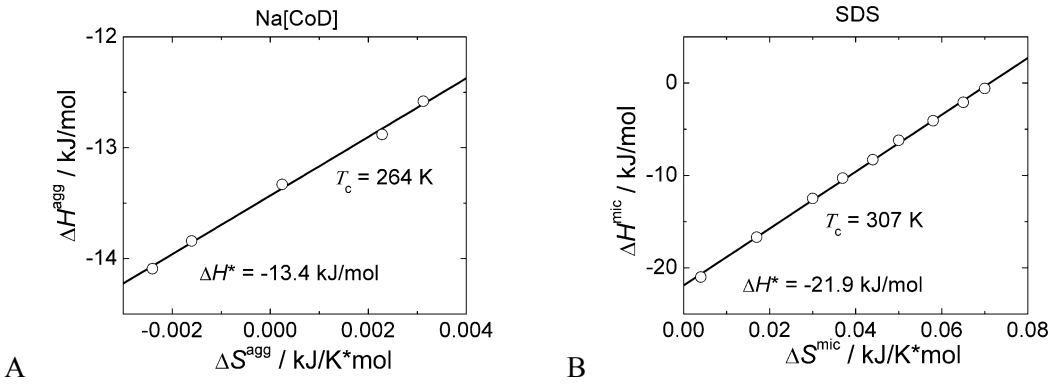

Figure I.S5. Compensation plot of Na[COSAN] (A) and SDS (B) micellization.

Light Scattering Analysis

In the first set of samples, we prepared fresh Na[COSAN] solutions for LS study, where the presence of nanobubbles cannot be excluded. In the second step, the solutions were treated by the methods proposed for destruction of nanobubbles (filtration and heating).[42] As the third set of samples, we carried out dialysis experiment, where concentrated Na[COSAN] solution were leave to penetrate into semipermeable tube filled with degassed water. Thus, only single clusters

could go through. Large spherical nanoparticles cannot penetrate inside the dialysis tube, but they can form inside since if they are in equilibrium with single molecules.

There are three types of Na[COSAN] nanoparticles detected by dynamic light scattering, DLS, as three independent modes. Two of them are in equilibrium: 1) mixture of single molecules and small "micelles" (<R_H> = 0.4 nm; curves 1 and 1' in Figure I.S6A, and first peak in Figure I.S6B), 2) spherical nanoparticles that are in equilibrium with other forms of Na[COSAN] (<R_H> = 38 nm; curves 2 and 2' in Figure I.S6A, and second peaks in Figure I.S6B). The third one is not in equilibrium: 3) mixture of nanobubbles, dirt and large aggregates that are not in equilibrium (<R_H> = 200 nm; curve 3 in Figure I.S6A, and third peaks in Figure I.S6B), because simple filtering and heating can remove it. We interpret it as nanobubbles or large undefined agglomerates, because it does not form inside the dialysis tube, and thus are not in equilibrium with single molecules, aggregates, and spherical nanoparticles.

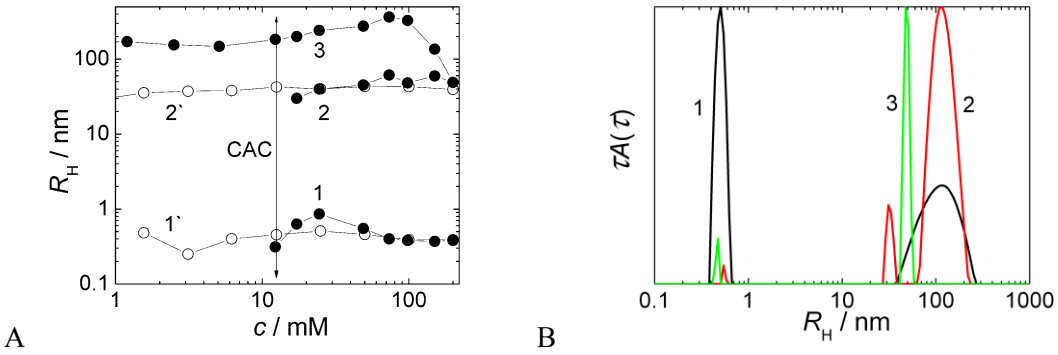

Figure I.S6. (A) Dependence of hydrodynamic radius, R_H, (from DLS) on Na[COSAN] concentration for untreated solutions (black points) and after treatment (hollow points). Fast mode (curves 1 and 1') is assigned to single molecules and small aggregates in equilibrium. First slow mode (curves 2 and 2') is assigned to spherical nanoparticles in equilibrium, and second slow mode (curve 3) is related to large nanoparticles that are not in equilibrium with other forms of Na[COSAN] molecules.
(B) Distribution of hydrodynamic radii of 50 mM Na[COSAN] solutions from "dialysis" experiment: inside dialysis tube (curve 1, black), outside dialysis tube (curve 2, red), and outside dialysis tube after filtration (curve 3, green).

Cryo-TEM analysis

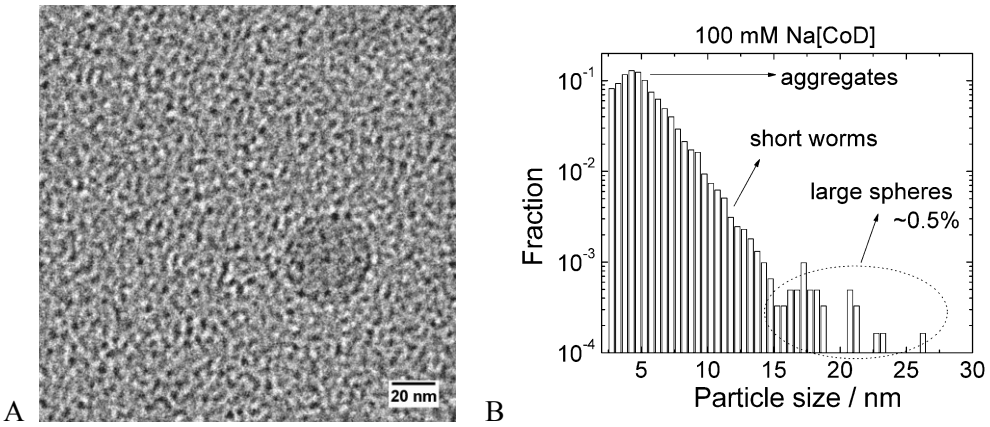

Figure I.S7. (A) Representative cryo-TEM micrograph of the Na[COSAN] spherical nanoparticle accompanied by small aggregates, and (B) a nanoparticle size analysis in 100 mM solution.

Acknowledgements

P.M. would like to acknowledge the financial support of the Czech Science Foundation (P205/14–14608S). We thank Janne Ruokolainen (Aalto University, Finland) for cryo-TEM measurements, Josef Pleštil (IMC CAS, Prague) for SAXS measurements and interpretation, Michael Gradzielski (TU Berlin) for fruitful discussions, and Sara A. Thibodeau for her critical proofreading.

References

[1] M. F. Hawthorne, D. C. Young, T. D. Andrews, D. V. Howe, R. L. Pilling, A. D. Pitts, M. Reintjes, L. F. Warren, P. A. Wegner, *J. Am. Chem. Soc.* **1968**, *90*, 879.

[2] I. B. Sivaev, V. I. Bregadze, *Collect. Czech. Chem. Commun.* **1999**, *64*, 783.

[3] R. N. Grimes, in *Carboranes*, Academic Press, London, **2011**.

[4] J. Plesek, *Chem. Rev.* **1992**, *92*, 269.

[5] B. Gruner, J. Rais, P. Selucky, M. Lucanikova, in *Boron Science: New Technologies and Applications* (Ed.: N. S. Hosmane) CRC, New York, **2012**, pp 463–490.

[6] D. Gabel, *Pure Appl. Chem.* **2015**, *87*, 173.

[7] M. Scholz, E. Hey-Hawkins, *Chem. Rev.* **2011**, *111*, 7035.

[8] Z. J. Lesnikowski, *Collect. Czech. Chem. Commun.* **2007**, *72*, 1646.

[9] P. Rezacova, P. Cigler, P. Matejicek, M. Lepsik, J. Pokorna, B. Gruner, J. Konvalinka, in *Boron Science: New Technologies and Applications* (Ed.: N. S. Hosmane) CRC, New York, **2012**, pp. 41-70.

[10] G. Chevrot, R. Schurhammer, G. Wipff, *J. Phys. Chem. B* **2006**, *110*, 9488.

[11] A. Popov, T. Borisova, *J. Colloid Interface Sci.* **2001**, *236*, 20.

[12] P. M. Gassin, L. Girard, G. Martin-Gassin, D. Brusselle, A. Jonchere, O. Diat, C. Vinas, F. Teixidor, P. Bauduin, *Langmuir* **2015**, *31*, 2297.

[13] J. Rak, B. Dejlova, H. Lampova, R. Kaplanek, P. Matejicek, P. Cigler, V. Kral, *Mol. Pharm.* **2013**, *10*, 1751.

[14] P. Matejicek, P. Cigler, K. Prochazka, V. Kral, *Langmuir* **2006**, *22*, 575.

[15] P. Matejicek, P. Cigler, A. B. Olejniczak, A. Andrysiak, B. Wojtczak, K. Prochazka, Z. Lesnikowski, *Langmuir* **2008**, *24*, 2625.

[16] M. Uchman, P. Jurkiewicz, P. Cigler, B. Gruner, M. Hof, K. Prochazka, P. Matejicek, *Langmuir* **2010**, *26*, 6268.

[17] P. Bauduin, S. Prevost, P. Farras, F. Teixidor, O. Diat, T. Zemb, *Angew. Chem. Int. Ed.* **2011**, *50*, 5298.

[18] D. Brusselle, P. Bauduin, L. Girard, A. Zaulet, C. Vinas, F. Teixidor, I. Ly, O. Diat, *Angew. Chem. Int. Ed.* **2013**, *52*, 12114.

[19] P. Bauduin, T. Zemb, *Curr. Opin. Colloid Interface Sci.* **2014**, *19*, 9.

[20] C. Vinas, M. Tarres, P. Gonzalez-Cardoso, P. Farras, P. Bauduin, F. Teixidor, *Dalton Trans.* **2014**, *43*, 5062.

[21] M. Tarres, C. Vinas, P. Gonzalez-Cardoso, M. M. Hanninen, R. Sillanpaa, V. Dordovic, M. Uchman, F. Teixidor, P. Matejicek, P. *Chem. Eur. J.* **2014**, *20*, 6786.

[22] H. Wennerstrom, B. Lindman, *Micelles. Physical Chemistry of Surfactant Association. Phys. Rep.* **1979**, *52*, 1.

[23] I. A. Nyrkova, A. N. Semenov, *Eur. Phys. J. E* **2005**, *17*, 327.

[24] P. H. Elworthy, K. J. Mysels, *J. Colloid Interf. Sci.* **1966**, *21*, 331.

[25] C. H. Chang, E. I. Franses, *Colloids Surf., A* **1995**, *100*, 1.

[26] F. M. Menger, A. L. Galloway, M. E. Chlebowski, *Langmuir* **2005**, *21*, 9010.

[27] Z. Du, M. P. Bilbao-Montoya, B. P. Binks, E. Dickinson, R. Ettelaie, B. S. Murray, L*angmuir* **2013**, *19*, 3106.

[28] J. H. Lin, W. S. Chen, S. S. Hou, *J. Phys. Chem. B* **2013**, *117*, 12076.

[29] P. D. T. Huibers, *Langmuir* **1999**, *15*, 7546.

[30] H. U. Kim, K. H. Lim, *Bull. Korean Chem. Soc.* **2003**, *24*, 1449.

[31] J. P. Marcolongo, M. Mirenda, *J. Chem. Educ.* **2011**, *88*, 629.

[32] M. Uchman, S. Pispas, L. Kovacik, M. Stepanek, *Macromolecules* **2014**, *47*, 7081.

[33] M. Uchman, M. Gradzielski, B. Angelov, Z. Tosner, J. Oh, T. Chang, M. Stepanek, K. Prochazka, *Macromolecules* **2013**, *46*, 2172.

[34] O. Mertins, R. Dimova, *Langmuir* **2011**, *27*, 5506.

[35] L. J. Chen, S. Y. Lin, C. C. Huang, *J. Phys. Chem. B* **1998**, *102*, 4350.

[36] D. Chandler, *Nature* **2005**, *437*, 640.

[37] R. Zangi, *J. Phys. Chem. B* **2011**, *115*, 2303.

[38] N. R. Syme, C. Dennis, S. E. V. Phillips, S. W. Homans, *ChemBioChem* **2007**, *8*, 1509.

[39] A. Biela, N. N. Nasief, M. Betz, A. Heine, D. Hangauer, G. Klebe, *Angew. Chem. Int. Ed.* **2013**, *52*, 1822.

[40] P. Farras, E. J. Juarez-Perez, M. Lepsik, F. Luque, R. Nunez, F. Teixidor, *Chem. Soc. Rev.* **2012**, *41*, 3445.

[41] C. Verdia-Baguena, A. Alcaraz, V. M. Aguilella, A. M. Cioran, S. Tachikawa, H. Nakamura, F. Teixidor, C. Vinas, *Chem. Comm.* **2014**, *50*, 6700.

[42] J. Q. Wang, *Macromolecules* **2015**, *48*, 1614.

[43] M. Almgren, J. C. Gimel, K. Wang, G. Karlsson, K. Edwards, W. Brown, K. Mortensen, *J. Colloid. Interf. Sci.* **1998**, *202*, 222.

[44] B. Z. Shang, Z. Wang, R. G. Larson, *J. Phys. Chem. B* **2008**, *112*, 2888.

[45] J. Brus, A. Zhigunov, J. Czernek, L. Kobera, M. Uchman, P. Matejicek, *Macromolecules* **2014**, *47*, 6343.

5.2 Paper II

Stealth Amphiphiles:
Self-Assembly of Polyhedral Boron Clusters*

Abstract

This is the first experimental evidence that both self-assembly and surface activity are common features of all water-soluble boron cluster compounds. The solution behavior of anionic polyhedral boranes (sodium decaborate, sodium dodecaborate, and sodium mercaptododeca-borate), carboranes (potassium 1-carbadodecaborate), and metallacarboranes (sodium [cobalt bis(1,2-dicarbollide)]} was extensively studied, and it is evident that all the anionic boron clusters form multimolecular aggregates in water. However, the mechanism of aggregation is dependent on size and polarity. The series of studied clusters spans from a small hydrophilic decaborate resembling hydrotrope to a bulky hydrophobic cobalt bis(dicarbollide) behaving like a classical surfactant. Despite their pristine structure resembling Platonic solids, the nature of anionic boron cluster compounds is inherently amphiphilic – they are stealth amphiphiles.

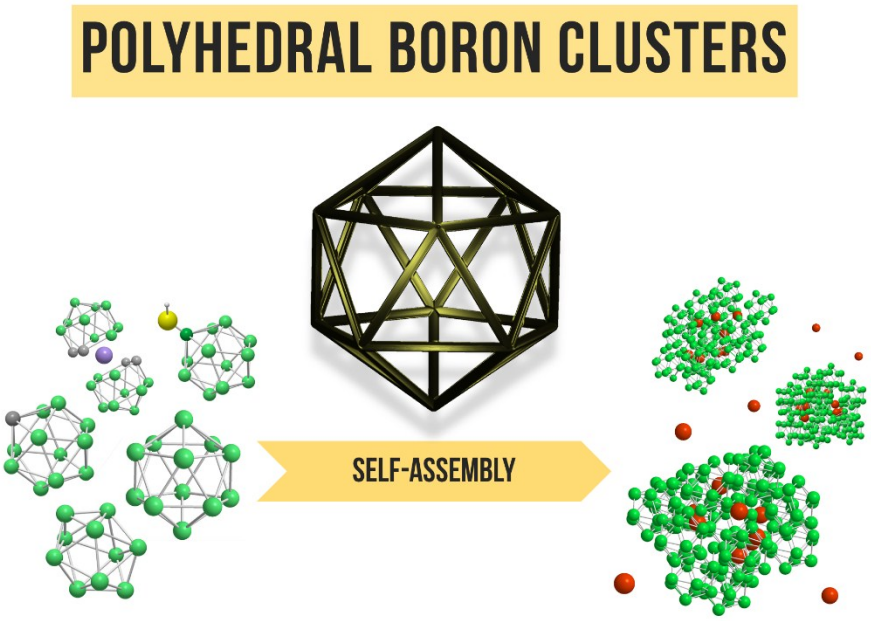

* In slightly modified version published as: Ďorďovič, V.; Tošner, Z.; Uchman, M.; Zhigunov, A.; Reza, M.; Ruokolainen, J.; Pramanik, G.; Cígler, P.; Kalíkova, K.; Gradzielski, M.; Matějíček, P.: Stealth Amphiphiles: Self-Assembly of Polyhedral Boron Clusters. *Langmuir* **2016**, *32*, 6713–6722.

Introduction

Self-assembly of low-molar mass compounds, for instance, surfactants, is a well-known and thoroughly understood process,[1-4] and no surprises in this field are expected. An iconic example of such behavior is a micellization of soaps such as sodium dodecyl sulphate (SDS) into spherical micelles obeying a mechanism of closed association.[5] The self-assembly process is intimately related to surface activity, which is necessary but not sufficient for micellization in solution. Ethanol, for example, is surface active and has an amphiphilic structure; however, it does not form micelles in solution, so it is not a surfactant. Although multimolecular associations were detected in alkanol/water mixtures, their loose structure distinguishes them from classical surfactant micelles.[6-8] Surface active compounds usually are amphiphilic. They have an affinity for both water and oil, expressed for example, by the empirical parameter HLB, hydrophile-lipophile balance.[4,9] The surface activity stems from the amphiphilic molecular structure. Typical surfactants have simultaneously hydrophobic and hydrophilic parts of their molecules, such as the long hydrophobic tail and small hydrophilic head in the SDS. In cases in which the hydrophobic part of an amphiphile is too small, such compounds behave like hydrotropes rather than surfactants.[10-15] It has, however, been demonstrated that there is no sharp border between these two kinds of amphiphiles (see the work of Hopkins Hatzopoulos et al. describing surface activity and association of *p*-*n*-alkybezoate series differing in the length of the alkyl tail spanning from "true hydrotrope" and alkyl hydrotrope to "true surfactant").[13] A hydrotrope is defined as a compound with the ability to increase the solubility of insoluble compounds in water regardless of the molecular structure of the hydrotrope.[10] As a "side effect", even hydrotropes can form micelles or at least nonmicellar aggregates, although it is not related to their action on hydrophobe solubility.[11]

A nonclassical surfactant with unusual amphiphilic structure that aggregates in water has been described in literature.[16-22] Cobalt bis(dicarbollide) anion, COSAN, is surface active and amphiphilic and exhibits a self-association in water that is comparable to classical micellization, though the anion does not have an amphiphilic topology like SDS (hydrophilic head with hydrophobic tail).[23] The origin of the aggregation is still controversial in the literature. One interpretation assumes the existence of dihydrogen bond (B–H···H–C) within the aggregates that is strong enough to overwhelm the electrostatic repulsion between the anionic clusters.[24] Another theory is more general[23] and takes into consideration a non-classical hydrophobic effect.[25-29]

According to the former approach, boron clusters without C–H groups like dodecaborate should not aggregate in water, and such compounds are predicted to be non-surface active, nonamphiphilic and nonhydrotropic, behaving like SO_4^{2-} anion in aqueous solutions.[24] In this work, we will show that this rule fails for anionic *closo*-boranes and that self-assembly, amphiphilicity, and surface activity are common features of anionic *closo*-boranes, carboranes and metallacarboranes pointing to hydrophobic[23] or chaotropic[30] effects as driving forces in the self-assembly. We studied the solution behavior of sodium decaborate, $Na_2[B_{10}H_{10}]$, sodium dodecaborate, $Na_2[B_{12}H_{12}]$, potassium and sodium 1-carbadodecaborate, $K(Na)[CB_{11}H_{12}]$, and sodium mercaptododecaborate, $Na_2[BSH]$, and compared it with the already extensively studied

sodium [3-cobalt(III) bis(1,2-dicarbollide)], Na[COSAN], (structure of all studied molecules shown in Figure 2.1). The species mentioned above are typical examples of anionic *closo*-boron cluster compounds that exhibit exceptional stability and are very water-soluble. Their structure and properties have been described in detail in the literature.[31-36] Here, we should emphasize that boron-containing molecules have attracted more attention in recent years, and some of them are already used in medical applications.[37-41] The best-known example is BSH, which is used clinically as a boron delivery agent in BNCT for the treatment of cancers.[42,43]

With regard to the molecular structure of boron clusters, a typical example, dodecaborate anion, $[B_{12}H_{12}]^{2-}$, is a symmetric object with delocalized charge, with a shape resembling a Platonic solid. Because of its "pristine" structure, one would not expect an aggregation tendency or surface activity. However, recent findings of Gabel et al. indicate that its solution behavior is surprisingly rich. This conclusion was reached because dodecaborate acts as a hydrophilic but superchaotropic anion in water solution.[30,44-47] It means that water molecules are less structured and more "lipophilic" around such anions than they are in bulk water. Association of chaotropes with cyclodextrins is explained not in terms of hydrophobic action but as so-called chaotropic effect because it is driven by enthalpy. However, closer inspection of anionic boron clusters consisting of hydrophobic B–H vertices with delocalized charge tells us that their nature is "schizophrenic". It is at once hydrophobic and water-soluble, and the balance of both contributions is dependent on size and charge (compare with the concept of HLB for classical surfactants mentioned above). We therefore assume that boron cluster compounds are amphiphilic, including rather hydrophilic decaborate as well as bulky and fairly hydrophobic cobalt bis(dicarbollide) – we call them stealth amphiphiles.

In our experimental study, we used techniques like nuclear magnetic resonance spectroscopy (NMR), cryo-transmission electron microscopy (cryo-TEM), tensiometry, conductometry, and calorimetry to reveal and describe self-assembly of boron cluster compounds in water. A mechanism of aggregation is proposed and compared with that of cobalt bis(dicarbollide).

Results and Discussion

The fact that metallacarboranes (like Na[COSAN]) can aggregate in water is already well established in the boron cluster chemist community.[16-24] Mechanism of formation of small aggregates (sometimes called "micelles")[20] has been already extensively studied, and it obeys the closed association model with critical aggregation concentration (CAC).[23] Besides small aggregates, large monolayer vesicles form spontaneously in water solutions of cobalt bis(dicarbollides), which is unparalleled in colloidal science.[20,21] Despite the predictions,[21] an abundance of such layered nanostructures is fairly low in dilute solutions.[23]

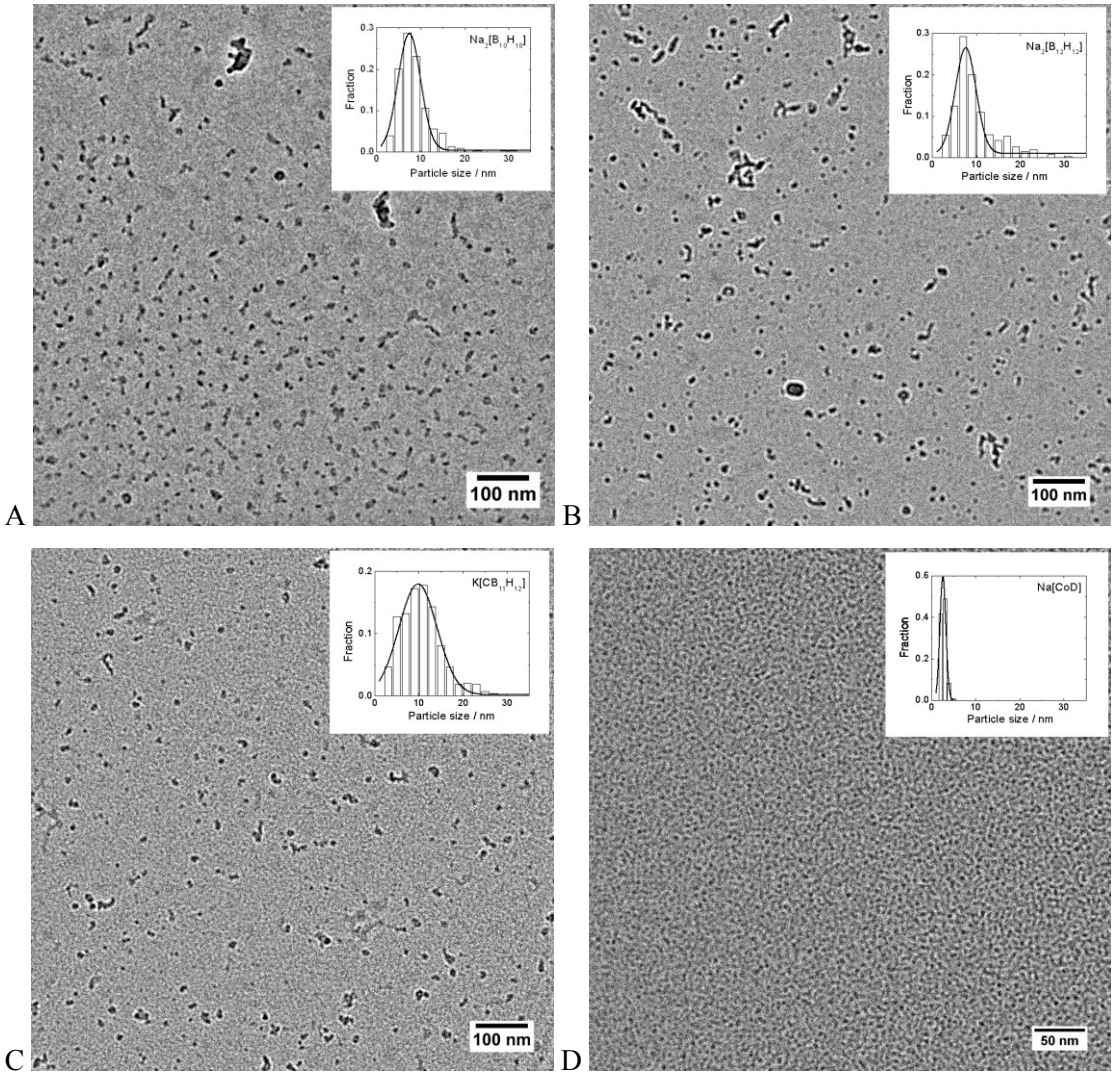

Figure II.1. Typical cryo-TEM micrographs and corresponding nanoparticle size distributions of 0.7 M aqueous solutions of (A) $Na_2[B_{10}H_{10}]$, (B) $Na_2[B_{12}H_{12}]$, and (C) $K[CB_{11}H_{12}]$ and (D) a 0.1 M solution of Na[COSAN].

An aggregation of simple *closo*-(carb)borane clusters $[B_{10}H_{10}]^{2-}$, $[B_{12}H_{12}]^{2-}$ and $[CB_{11}H_{12}]^{-}$ has been considered as highly improbable.[24] However, after careful inspection of more concentrated samples (from 0.1 to 2 M), we revealed nanoparticles based on self-assembly. For visualization of such aggregates, we successfully utilized a cryo-TEM imaging. Unfortunately, very high density of aggregates prevents the chance of obtaining high-quality and high-resolution micrographs because of overlapping of the nanostructures in thin ice layers. However, panels A and C of Figures II.1 are micrographs of 0.7 M solutions of $Na_2[B_{10}H_{10}]$, $Na_2[B_{12}H_{12}]$ and $K[CB_{11}H_{12}]$ respectively, together with size distributions of polydisperse nanoparticles (average diameters of 7.5 ± 5.1, 7.7 ± 5.0 and 9.8 ± 8.7 nm, respectively). For comparison, we also show micrograph of Na[COSAN] aggregates (Figure II.1D), which are smaller (diameter of 2.6 ± 1.3 nm) and evidently have a different morphology. We also analyzed the areas in which the aggregates form a uniform layer (see cryo-TEM micrographs of

$Na_2[B_{12}H_{12}]$ solutions in Figure II.S1A,B). It is evident that the aggregates consist of small domains with diameter of approximately 2–3 nm.

To determine the mechanism of aggregation, NMR spectroscopy is a suitable method.[48–52] Information on the self-diffusion of boron clusters can be directly obtained from $^1H\{^{11}B\}$ DOSY NMR experiments. A concentration dependence of effective diffusion coefficients, D, of four boron clusters and cobalt bis(dicarbollide) is shown in panles A and C of Figure II.2, respectively (corresponding hydrodynamic radii, R_H, in panles B and D of Figure II.2). In $^1H\{^{11}B\}$ and $^{11}B\{^1H\}$ NMR spectra, we observed concentration-dependent changes of chemical shifts, δ, with trends comparable to those observed by DOSY NMR (see spectra and relative chemical shifts in Figures II.S2 and II.S3).

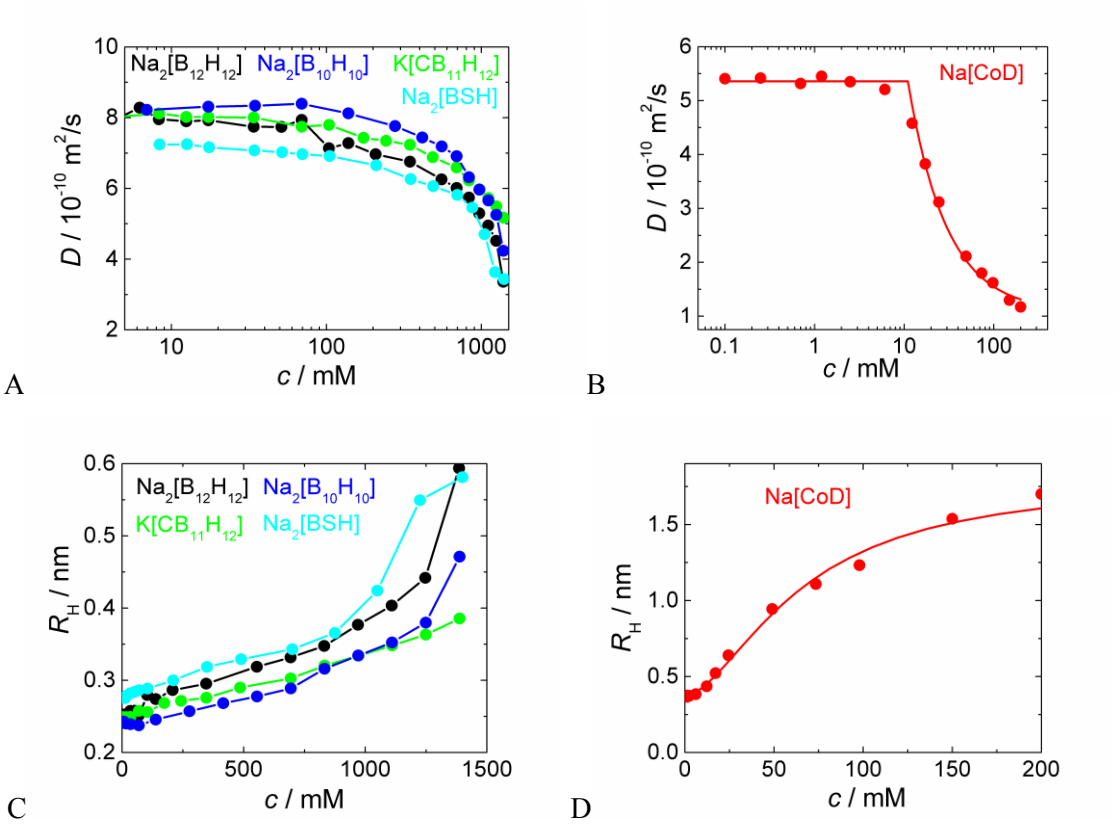

Figure II.2. Diffusion coefficients (A and B) and corresponding hydrodynamic radii (C and D) as functions of concentration obtained from (A and C) ^1H $\{^{11}B\}$ DOSY NMR of $Na_2[B_{10}H_{10}]$, $Na_2[B_{12}H_{12}]$, $K[CB_{11}H_{12}]$, and $Na_2[BSH]$, and (B and D) ^1H DOSY NMR of Na[COSAN]. Curve of Na[COSAN] diffusion fitted by equations of closed association model (see equations in SI).

It is interesting to compare trends for Na[COSAN] with those for other boron clusters. While the metallacarborane aggregation can be assigned to the closed association model,[23] it is not definitively the case for description of *closo*-(car)boranes self-assembly. Effective diffusion coefficients decrease almost linearly with increasing concentration above ~70 mM (CAC). A surprisingly small value of R_H for single molecules (~0.25 nm) indicates that a hydration shell is very thin for the borane clusters.[44] Furthermore, the effect of aggregate growth seems to be very weak. The value of R_H increases by only 0.2 nm in the broad concentration range. To

explain that, it is useful to express the concentration-dependent effective diffusion coefficients as the number-weighted summation of contributions from all the aggregation forms in solution (for details and equations, see SI).[53,54]

In the case of Na[COSAN] (Figure II.2B), there are only single clusters below the CAC (with R_H ca. 0.4 nm), and a mixture of single clusters with aggregates, the size of which does not depend on concentration (R_H ca. 1.8 nm), above the CAC. Keeping in mind that metallacarboranes fully dissociate in water and counterions are not condensed on the aggregates due to relatively low charge density of bulky metallacarborane cluster, the Na[COSAN] aggregates cannot grow beyond a certain limit due to electrostatic restrictions.[20,23]

In the case of small boron clusters, we assume that the aggregation number grows with an increasing concentration without a limit (Figure II.2A), which resembles the isodesmic association model employed for a self-assembly of dyes,[55-58] or progressive association model proposed for alcohols or for some hydrotropes.[1,10,14] The trend is almost identical for all the samples regardless of exoskeletal substitution (BSH) or the presence of endoskeletal C–H unit in $[CB_{11}H_{12}]^-$ anion. It is clear that the presence of C–H group has an only minor effect on the self-assembly process.

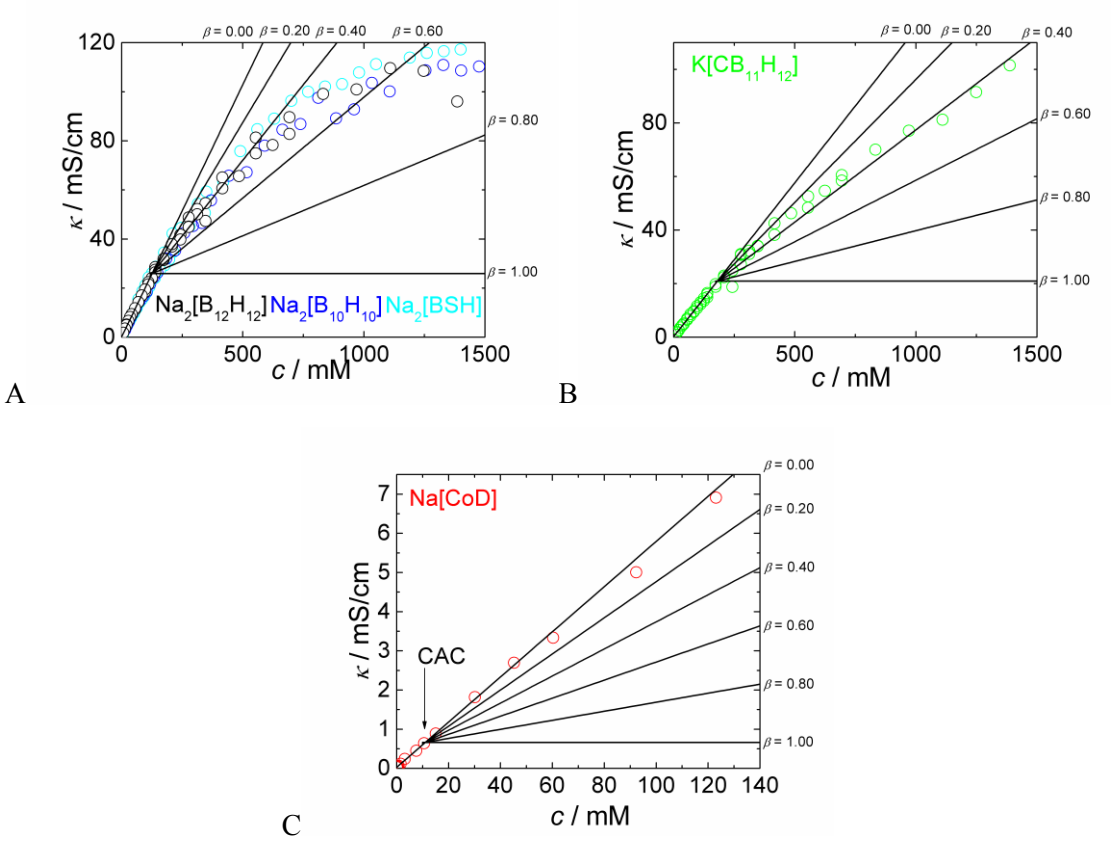

Figure II.3. Plot of specific conductivity, κ, as a function of concentration for solutions of (A) $Na_2[B_{10}H_{10}]$, $Na_2[B_{12}H_{12}]$, $Na_2[BSH]$, (B) $K[CB_{11}H_{12}]$, and (C) Na[COSAN]. Lines within the graphs indicate hypothetical κ dependences with values of β from 0 to 1.

Cations are supposed to effectively condense within the aggregates, thereby compensating the charge of the boron cluster in the nanoparticles. Thus, the aggregation

mechanism is not closed but open.[5] After certain simplification, we estimated the fractions of aggregated molecules of the clusters (further details in SI and Figures II.S4 and II.S5). Hence, mild changes of diffusion coefficients with concentration can be satisfactorily explained by an assumption there are single clusters accompanied by a broad distribution of multimolecular aggregates with the fraction up to 50% in the concentration range of 0.1–1.5 M.

Bearing in mind the dimensions of the clusters (diameter of $[B_{12}H_{12}]^{2-}$ anion being ~0.6 nm), we found counterions had to be incorporated into aggregates larger than several nanometers as already assumed above. Useful information about that was obtained from conductivity and SAXS measurements. Ionic boron clusters are considered to behave as strong electrolytes in water. Dependence of molar conductivity, λ, on concentration should and actually does follow the Kohlrausch law: $\lambda = \lambda^0 - K\sqrt{c}$, where λ^0 is molar conductivity at infinite dilution, K is the Kohlrausch coefficient, and c is the concentration (Figure II.S6). A plot of the specific conductivity, κ, on concentration is commonly used for estimation of CAC (position of the break in the curve) and to calculate the fraction of condensed counterions, β, where $\beta = 1 - \alpha$ and α is the ratio of the slopes after and before CAC.[59] It is shown in panels A–C of Figures II.3 for all the studied boron clusters, where lines in the graphs are constructed for estimation of β.

The break indicating the CAC is not evident for Na[COSAN] (Figure II.3E), even though the CAC has been determined unambiguously to be ~11 mM by several methods (NMR and ITC). Only possible explanation is that counterions are repelled by the aggregates and $\beta = 0$. For the other cases, the dependencies (Figures II.3A,B) are not linear, but a continuous bending above 150 mM is observed rather than the sharp break. This is consistent with the scenario in which the aggregation number increases with concentration above CAC (~70 mM) and counterions start to become incorporated within the larger aggregates at the break point in the conductivity plot (~150 mM).

For metallacarborane aggregates, it has been already reported that a correlation peak at 1.07 ± 0.04 $Å^{-1}$ in SAXS/WAXS and SANS curves[20,23] is indicative of a direct cluster-cluster contact in a parallel orientation, excluding thus the presence of cations in the inner parts of the aggregate. In a SAXS/WAXS study of small (car)borane clusters, we detected at the most three correlation peaks in concentrated solutions of $Na_2[B_{10}H_{10}]$, $Na_2[B_{12}H_{12}]$, $Na_2[BSH]$ and $K[CB_{11}H_{12}]$. The first one in WAXS region (not shown) is observed at 2.1 $Å^{-1}$ in the broad concentration range for all the samples, and it can be assigned to intercluster distances (~3 Å, which is smaller than the cluster size). More interesting is an observation of the second peak in the WAXS region around 1.3 $Å^{-1}$ for $Na_2[B_{12}H_{12}]$, $Na_2[BSH]$ and $K(Na)[CB_{11}H_{12}]$, and around 1.55 $Å^{-1}$ for $Na_2[B_{10}H_{10}]$ (see "region I" in panels A and B of Figure II.4). Its position is also independent of concentration, but it appears above 250 mM. It is thus related to the formation of aggregates. The peak proves a direct cluster-cluster contact in the aggregates; it is 5.5, 4.9 and 3.9 Å for $[CB_{11}H_{12}]^-$, $[B_{12}H_{12}]^{2-}$ and $[B_{10}H_{10}]^{2-}$, respectively. The distances are slightly shorter than maximal H···H distance in the cluster (~6 Å for dodecaborate). It has a physical meaning only if there is no direct –H···H– contact pointing to a hydrophobic effect rather than a bond formation.

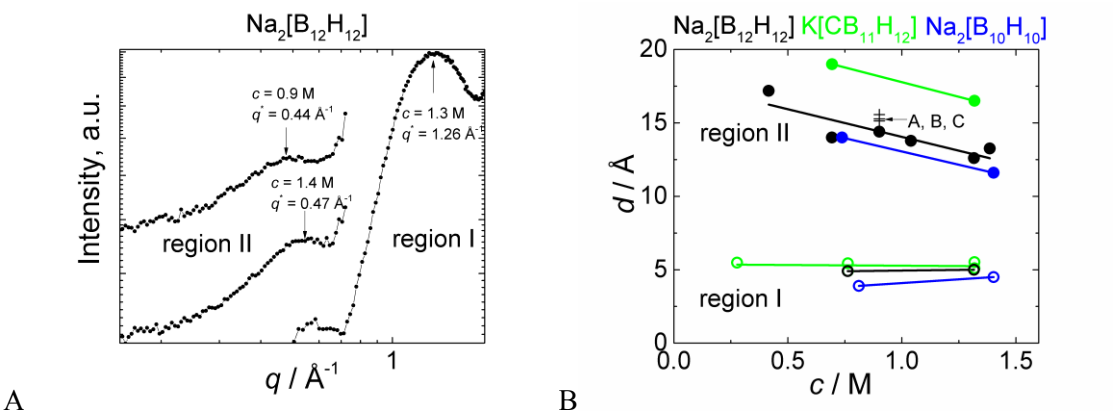

Figure II.4. (A) Typical SAXS (region II) and WAXS (region I) curves for $Na_2[B_{12}H_{12}]$ solutions with concentrations indicated within the graph, where positions of correlation peaks change with concentration in region I, but they are constant in region II. (B) Dependence of Bragg spacing, *d*, calculated from positions of correlations peaks in SAXS (region II) and WAXS (region I) curves for $Na_2[B_{12}H_{12}]$, $Na_2[B_{10}H_{10}]$ and $K[CB_{11}H_{12}]$ solutions (The Bragg spacing for 0.7 M $Na[CB_{11}H_{12}]$: 22.4 Å not shown). Three crosses with almost the same position indicated as A, B, and C correspond to three 0.9 M $Na_2[B_{12}H_{12}]$ solutions prepared by different procedures as described in the text.

The correlation peaks have been observed also in SAXS curves (region II in Figure II.4). The peak positions are sensitive to concentration and cation (see Figure II.4B). Similar concentration-dependent interparticle correlations were observed also for proteins because of mutual electrostatic interactions without the necessity of a microphase separation.[60] Because of the high ionic strength (screening of electrostatic forces) and of the cation sensitivity (significant differences between sodium and potassium salts of carbadodecaborate), we assume the aggregate formation (the microphase separation) as confirmed also by other methods. Therefore, we proposed the model of borane aggregates as shown in Figure II.5. It assumes the formation of spherical or wormlike domains formed by the clusters surrounded by the cloud of counterions. An alternative but less probable model assuming two populations of borane clusters (located on the surface and in the inner parts of the aggregates) is shown in Figure II.S7. From the Guinier region of SAXS curves we estimated the size of the aggregates in the range of few tens of nanometers that is in agreement with cryo-TEM results.

From results mentioned above, it is clear that all the boron cluster compounds undergo a self-assembly process in solution. The inner structure of such aggregates still represents a challenge and requires further research. To determine whether the aggregation is thermodynamically or kinetically controlled, we prepared three solutions of $Na_2[B_{12}H_{12}]$ at the same concentration (0.9 M), but by three different procedures: (A) dilution of concentrated sample (1.8 M), (B) direct dissolution of crude sample, and (C) thickening of dilute solution (0.45 M). The results are shown in Figure II.4B as crosses assigned as A, B, and C. Because all three results overlap within the experimental error and are in line with the change in concentration (black line), we assume that the aggregation is most likely thermodynamically controlled.

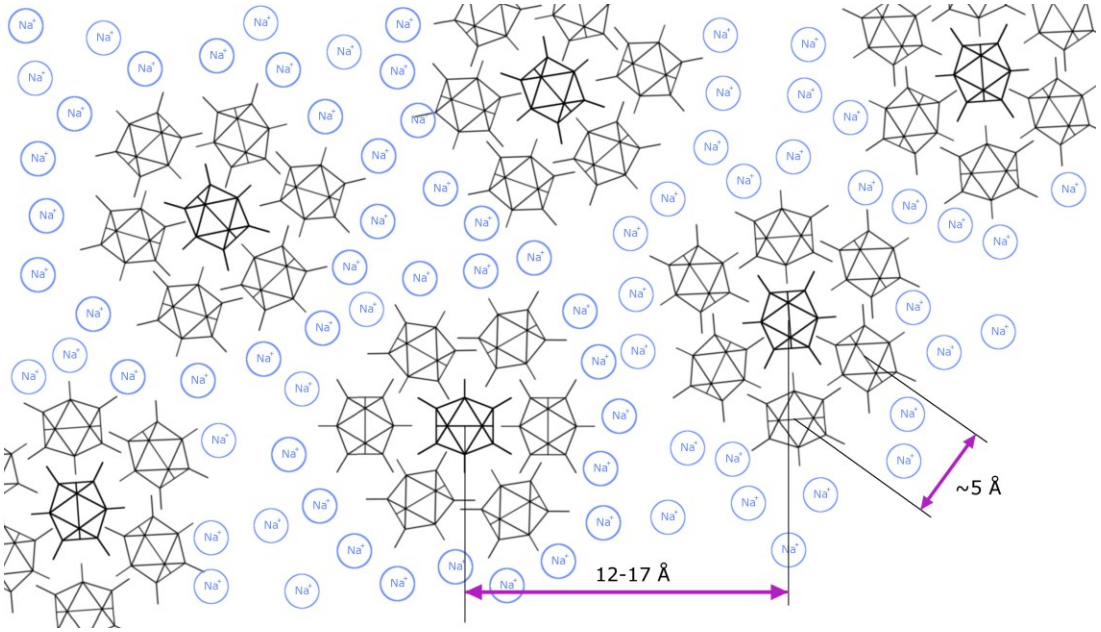

Figure II.5. Proposed structure of $Na_2[B_{12}H_{12}]$ aggregates assuming a formation of domains of borane clusters exhibiting a direct contact with each other. The domains with diameter ~2 nm (confirmed by cryo-TEM) are surrounded by a cloud of cations. Distances between the domains slightly increase with borane concentration.

We directly measured the enthalpy of (de)aggregation of $Na_2[B_{12}H_{12}]$ and $K[CB_{11}H_{12}]$ by ITC (see Figures II.S8A–D). The value of ΔH^{agg} is in both cases close to zero (between –2 and 2 kJ/mol). For dodecaborate, it, furthermore, switches from exo- to endothermic with temperature. This means that the enthalpy term is almost negligible. We know from our previous work that thermodynamics of Na[COSAN] self-assembly is markedly different.[23] It is highly exothermic and thus an enthalpy-controlled process as evidenced by ITC results (see the comparison of ΔH^{agg} for related systems in Figure II.S8E). It indicates that the driving force for the aggregation is a hydrophobic effect even for fairly hydrophilic clusters like dodecaborate.[23]

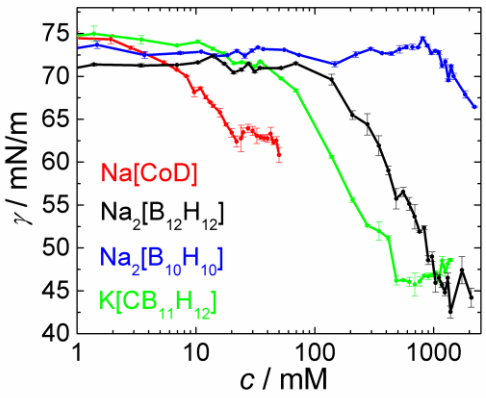

Figure II.6. Surface tension, γ, as a function of concentration for $Na_2[B_{10}H_{10}]$, $Na_2[B_{12}H_{12}]$, $K[CB_{11}H_{12}]$, and Na[COSAN] aqueous solutions.

The last part of the paper focuses on the surface activity of boron cluster compounds. For Na[COSAN], it has been observed and described several times,[16-24] but it has not been expected for other boranes.[24] Nevertheless, an accumulation near the water-air interface and surface activity is anticipated for large anions in the literature.[61] We measured the surface tension, γ, of $Na_2[B_{10}H_{10}]$, $Na_2[B_{12}H_{12}]$, $K[CB_{11}H_{12}]$, and Na[COSAN] solutions by means of the pendant drop method (shown in Figure II.6). The concentration dependence of γ for typical surfactants exhibits two breaks in the semilogarithmic scale resembling a letter Z (for a detailed analysis of the γ curves, see Figure II.S9A–D).[62] The first one, for the lowest concentration, is a measure of hydrophobicity of the compound. It is closely related to K_{aw} (air-water partition coefficient), which is a term describing the affinity of a compound for the interface. The boron clusters can be thus arranged according to hydrophobicity as follows: Na[COSAN] > $K[CB_{11}H_{12}]$ > $Na_2[B_{12}H_{12}]$ > $Na_2[B_{10}H_{10}]$. This is in agreement with the results of preliminary HPLC experiments with a hydrophobic stationary phase (see Figure II.S10).

After the break, the compounds start to accumulate at the interface, which manifests itself by the positive surface excess and consequently by a decrease of surface tension. The most surprising is a considerable surface activity of small boron clusters. However, it occurs only at fairly high concentrations (> 100 mM). From the slope between the breaks, it is possible to calculate the average area occupied by a molecule at the interface, A_S, according to the Gibbs adsorption isotherm.[63] We obtained the following limiting values of A_S for Na[COSAN], $K[CB_{11}H_{12}]$, $Na_2[B_{12}H_{12}]$ and $Na_2[B_{10}H_{10}]$: 0.98, 0.78, 0.94 and 1.54 nm^2, respectively (for the concentration dependence of A_S, see Figure II.S11), with factor n values of 2, 2, 3 and 3, respectively.[63] We included this factor in the calculation of A_S, because counterions should accompany the boron cluster at the interface. Furthermore, the large values of A_S indicate that boron clusters slightly repel each other without forming compact monolayers.[23]

The second break in γ versus ln c plot usually assigned to the CAC or CMC. That is the case for only Na[COSAN] in our study. For Na[COSAN], the break position is roughly in agreement with the value of the CAC estimated by NMR and ITC (11 mM at 25°C). On the other hand, $Na_2[B_{12}H_{12}]$, $K[CB_{11}H_{12}]$ also exhibit the break around 1 M. No such break has, however, been observed by other methods [from DOSY experiments, the CAC should be around 70 mM (see Figure II.2A)]. However, a closer inspection of γ curves for $Na_2[B_{12}H_{12}]$ in normal and semilogarithmic representations (see Figure II.S12A,B) reveals that the break is probably apparent and the whole curve can be fitted by a smooth exponential function. The fact that surface tension does not further decrease with concentration at elevated concentrations should be related to significant nonideality of the solution rather than a microphase separation (aggregation).[64] It means that the activity of borane clusters changes only slightly with increasing concentration in solutions above 1 M.

In the previous paragraphs, we demonstrated that all the studied boron cluster compounds do aggregate in water. We can divide the studied compounds into two groups.

(i) COSAN cluster. Its solution behavior is partly comparable to that of classical surfactants like SDS, and metallacarboranes can thus be called surfactants. It forms small "micelles" above the CAC.[23] Preliminary experimental results for borane $K[B_{21}H_{18}]$ (the

intermediate of which is *anti*-$B_{18}H_{22}$, which exhibits interesting photophysics),[65] indicate that this compound most likely belongs to this family. It has shape, size, and charge comparable to COSAN, but does not contain C–H units. Its nanoparticles as seen by cryo-TEM resembles metallacarborane spherical nanoparticles[20,23] (Figure II.S13). Furthermore, the $[B_{21}H_{18}]^-$ anion and COSAN are the only ones among the boron clusters that are known to form an insoluble nanocomposite with PEO.[66,67] We are planning an extensive study of this compound in our future research. However, it is evident that the formation of B–H···H–C dihydrogen bonds is not the main driving force for aggregation of boron cluster anions. Instead, size and shape do matter.

(ii) The second group comprises "small" anionic clusters like dianionic (do)decaborates and monoanionic 1-carbadodecaborate. Their surface charge density is fairly high because of relatively small dimensions, and the charge is 2– as compared to bulky 1– for COSAN and $[B_{21}H_{18}]^-$. We believe that it stands behind the fact that aggregation takes place at a concentration much higher than that in the case of Na[COSAN]. Furthermore, it is the reason why counterion condensation could occur. Consequently, the mechanism of aggregate formation does not obey the closed association model but rather the isodesmic model (stepwise growth or progressive association model). They are surface active, but does not resemble surfactants but rather hydrotropes.[10,13] Unfortunately, this statement is based on an analogy only[13] and it is not yet supported by an experimental observation of hydrotrope action.[10]

The driving force for the aggregation of boron cluster compounds is quite difficult to elucidate on the molecular level. It is certainly related with a hydrophobic nature of B–H vertices that cannot form a classical hydrogen bond. The hydrophobic effect should thus be considered as a general driving force. Two types of hydrophobic effects have been decribed in the literature: classical and nonclassical.[25-29,68] The former is closely related to entropy of water molecules, while the latter is explained by the enthalpy contribution of water (heat of hydration). Further, it is known that the water structure in the vicinity of hydrophobic objects depends on their size,[69,70] and the dimensions of boron clusters (~1 nm) are just at the borderline.

Conclusions

Solution behavior of decaborate, dodecaborate, 1-carbadodecaborate, mercaptododecaborate and cobalt bis(dicarbollide) anions was extensively studied by NMR, conductivity, tensiometry, microscopy, calorimetry, and scattering methods. All the experiments indicate that the boron clusters form multimolecular aggregates in solution and are surface active despite the absence of a hydrophobic tail as compared to classical surfactants. The studied compounds comprise the boron cluster compounds of various hydrophile-lipophile balances: from small and hydrophilic decaborate with a high charge density resembling hydrotropes or chaotropic anions to bulky and hydrophobic metallacarborane behaving like classical surfactant. However, a nature of all of them is inherently amphiphilic as demonstrated by surface tension measurements.

The series can be divided into two groups: (i) bulky metallacarborane with a prolonged molecule, the aggregation of which is driven by enthalpy and obeys the mechanism of closed association with small aggregation number and no condensed counterions,[9] and (ii) small and

highly symmetric *closo*-(carb)boranes, which aggregate most likely according the progressive association model with a relatively high aggregation number without an electrostatic restriction due to the effective counterion condensation. Furthermore, aggregation takes place regardless of the exoskeletal substitution (BSH) or the presence of C–H units within the cluster ($[CB_{11}H_{12}]^-$). The driving force for all the processes mentioned above is closely related to a nonclassical hydrophobic effect.

The boron cluster compounds as a family of stealth amphipiles open new possibilities for the rational design of self-organized structures that might be exploited in nanotechnology.

Supporting Information

Cryo-TEM imaging of inner structure of aggregates

A

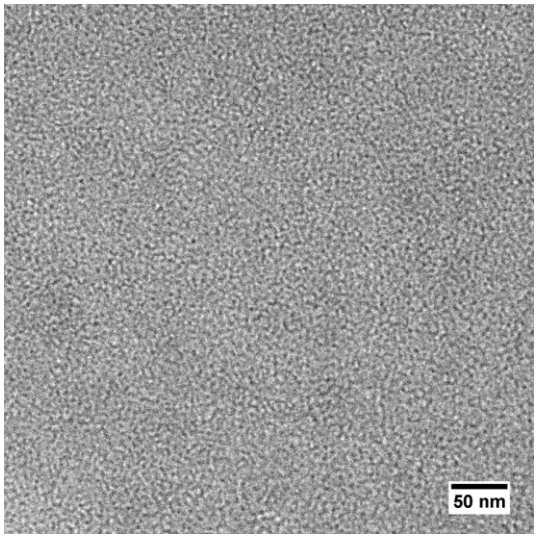

B

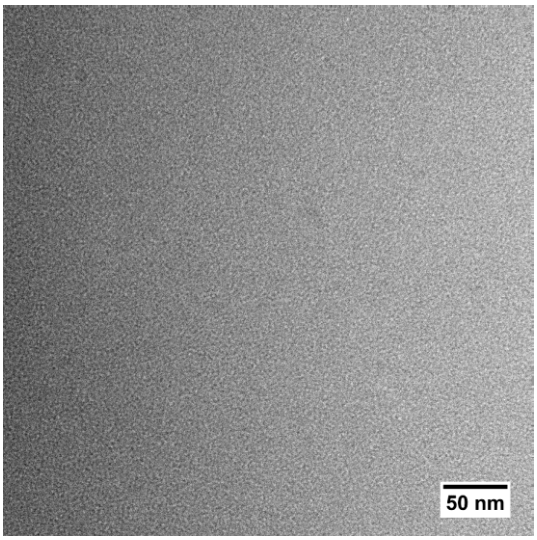

Figure II.S1. Cryo-TEM micrograph of (A) 0.3 M and (B) 1.1 M $Na_2[B_{12}H_{12}]$ solutions in the areas, where the aggregates overlap forming a continuous layer. Average diameters of dark nanostructures within the aggregates are 3.2 nm and 2.3 nm, respectively.

NMR spectra

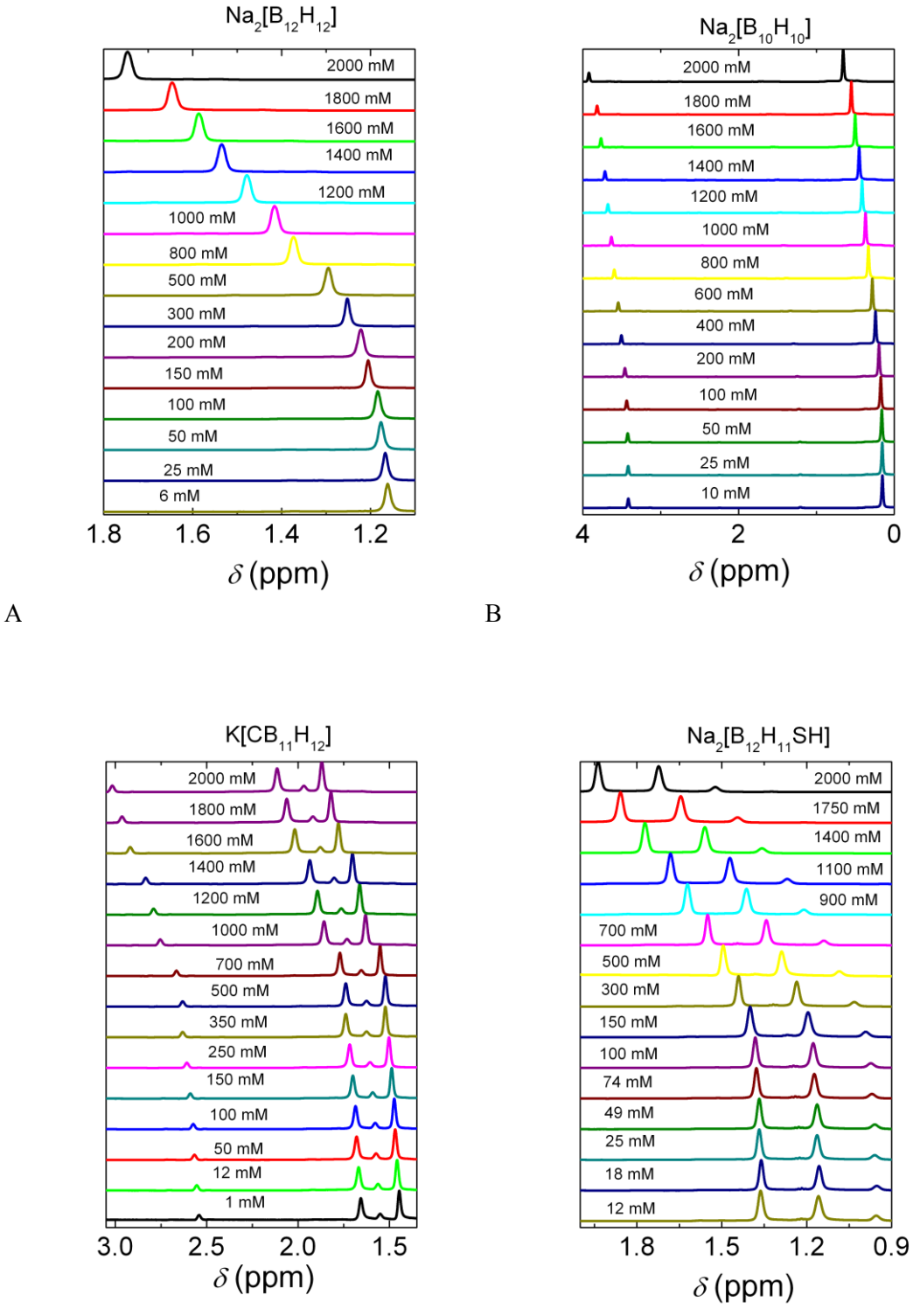

Figure II.S2. ^{1}H $\{^{11}B\}$ NMR spectra of $Na_2[B_{12}H_{12}]$, $Na_2[B_{10}H_{10}]$, $K[CB_{11}H_{12}]$, and $Na_2[BSH]$ in heavy water; corresponding concentrations (of raw samples) given in the graphs.

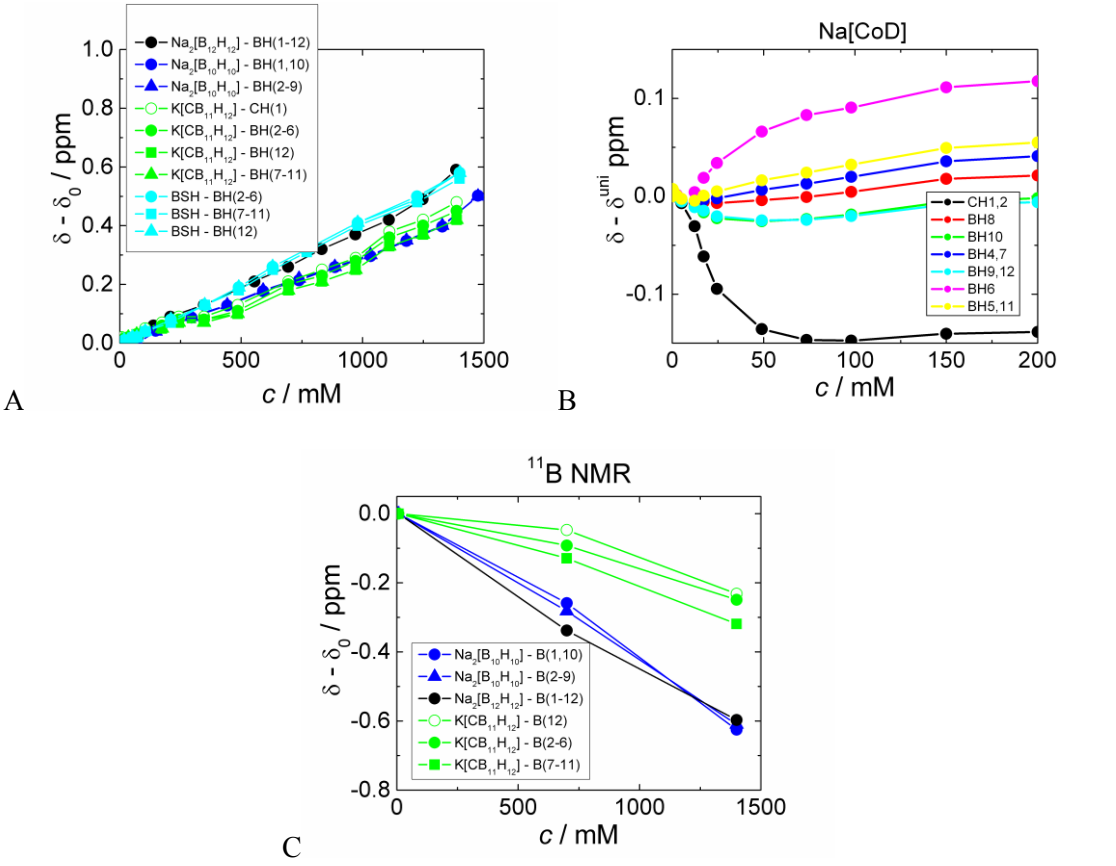

Figure II.S3. Relative chemical shifts in ^{1}H $\{^{11}B\}$ NMR spectra of (A) $Na_2[B_{12}H_{12}]$, $Na_2[B_{10}H_{10}]$, $K[CB_{11}H_{12}]$ and $Na_2[BSH]$, and (B) Na[COSAN], and in (C) ^{11}B $\{^{1}H\}$ NMR spectra of $Na_2[B_{12}H_{12}]$, $Na_2[B_{10}H_{10}]$ and $K[CB_{11}H_{12}]$; signal assigned to corresponding atoms.

Fraction of molecules involved in aggregation

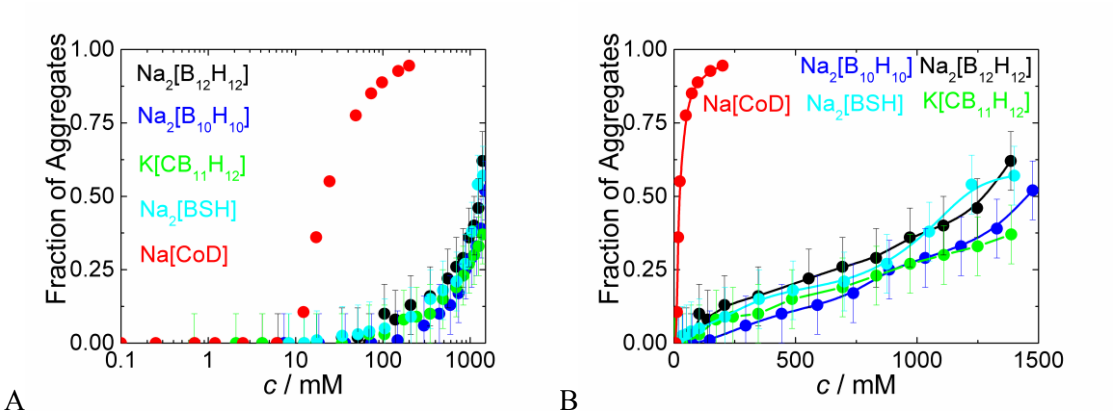

Figures II.S4. Fraction of molecules involved in aggregation, f_{agg}, calculated from DOSY NMR data at 25ºC for Na[COSAN] according eq. 5.2.4 and for $Na_2[B_{12}H_{12}]$, $Na_2[B_{10}H_{10}]$, $K[CB_{11}H_{12}]$ and $Na_2[BSH]$ according eq. 5.2.6; (A) semi-log and (B) normal representation.

Mean diffusion coefficient, D, which is known directly from DOSY NMR experiments, can be expressed like the number weighted summation of contributions from all the aggregation forms in solution:

$$D = \sum_i f_i D_i \tag{5.2.1}$$

For Na[COSAN] the fraction of aggregated molecules, f_{agg}, is calculated according the closed association model:

$$D = D_1; c \leq cac \tag{5.2.2}$$

$$D = \left[\frac{cac}{c}\right] D_1 + \left[\frac{c - cac}{c}\right] D_{\mathrm{agg}}; c > cac \tag{5.2.3}$$

and thus

$$f_{\mathrm{agg}} = \frac{c - cac}{c} \tag{5.2.4}$$

where c is analytical concentration, cac is critical aggregation concentration, D_1 is diffusion of single molecule, and D_{agg} is diffusion of aggregates.

For other boranes ($Na_2[B_{12}H_{12}]$, $Na_2[B_{10}H_{10}]$, $K[CB_{11}H_{12}]$, and $Na_2[BSH]$), it assumes that solutions contain concentration dependent mixture of single clusters with diffusion coefficient D_1 and multimolecular aggregates with radius R_{agg}, where diffusion coefficient of the aggregates D_{agg} can be calculated from R_{agg} according Stokes-Einstein relation. For D it reads:

$$D = f_1 D_1 + f_{\mathrm{agg}} D_{\mathrm{agg}} \tag{5.2.5}$$

and thus

$$f_{\mathrm{agg}} = \frac{D - D_1}{D_{\mathrm{agg}} - D_1} \tag{5.2.6}$$

where D and D_1 are directly known from DOSY NMR, and the values of D_{agg} and R_{agg} can be estimated from cryo-TEM micrographs (see Figure II.1). Dependence of f_{agg} on R_{agg} is plotted in Figure II.S4 for a broad range of sample concentration. For estimation of the fraction of aggregated molecules (as shown in Figure II.S3), we used the mean values from cryo-TEM analysis (diameter close to 10 nm). However, it is evident that f_{agg} is only weakly dependent on R_{agg} for aggregates above 2 nm.

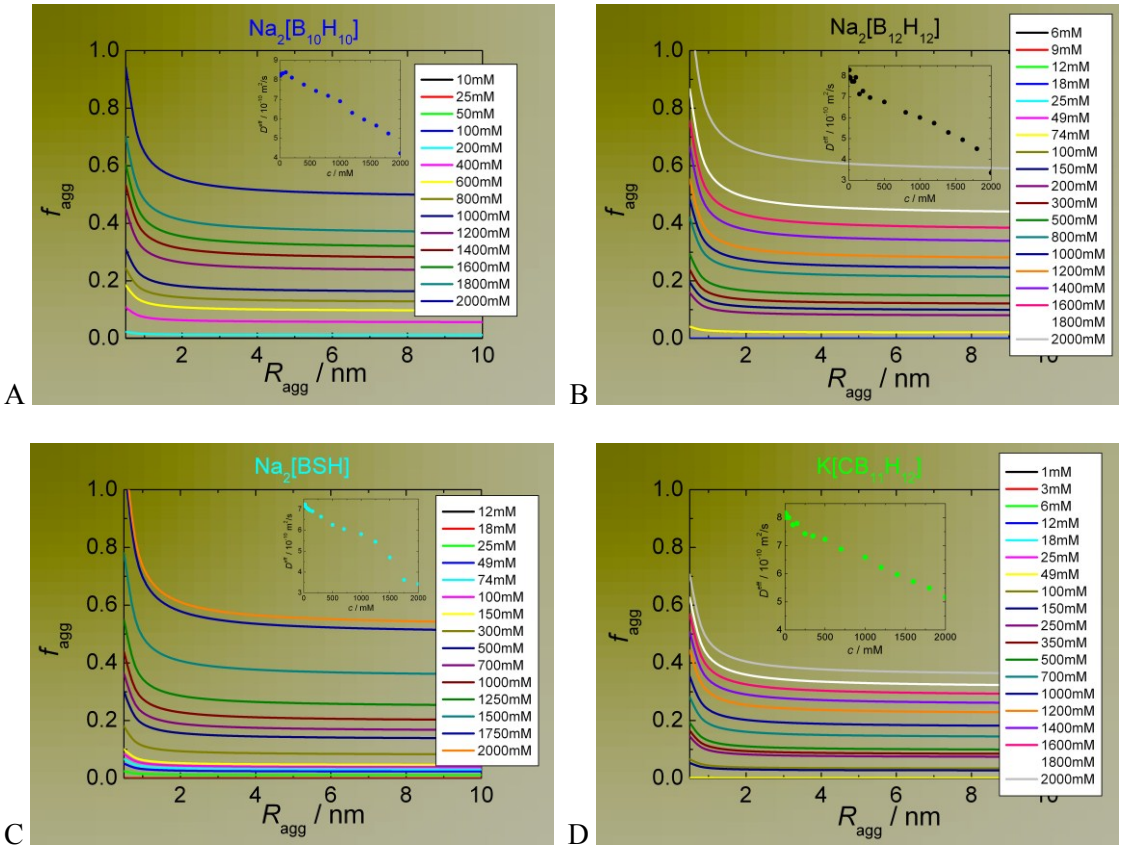

Figure II.S5. Fraction of molecules involved in aggregation, f_{agg}, for (A) $Na_2[B_{10}H_{10}]$, (B) $Na_2[B_{12}H_{12}]$, (C) $Na_2[BSH]$ and (D) $K[CB_{11}H_{12}]$ as a function of radius of the aggregates for various sample concentrations.

Conductivity

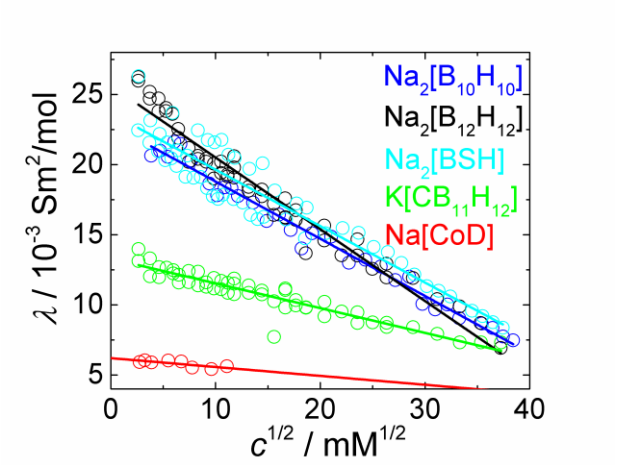

Figure II.S6. Expression of Kohlrausch law as a plot of molar conductivity, λ, against $c^{1/2}$ for $Na_2[B_{12}H_{12}]$, $Na_2[B_{10}H_{10}]$, $K[CB_{11}H_{12}]$, $Na_2[BSH]$), and Na[COSAN].

Structure model of borane aggregates

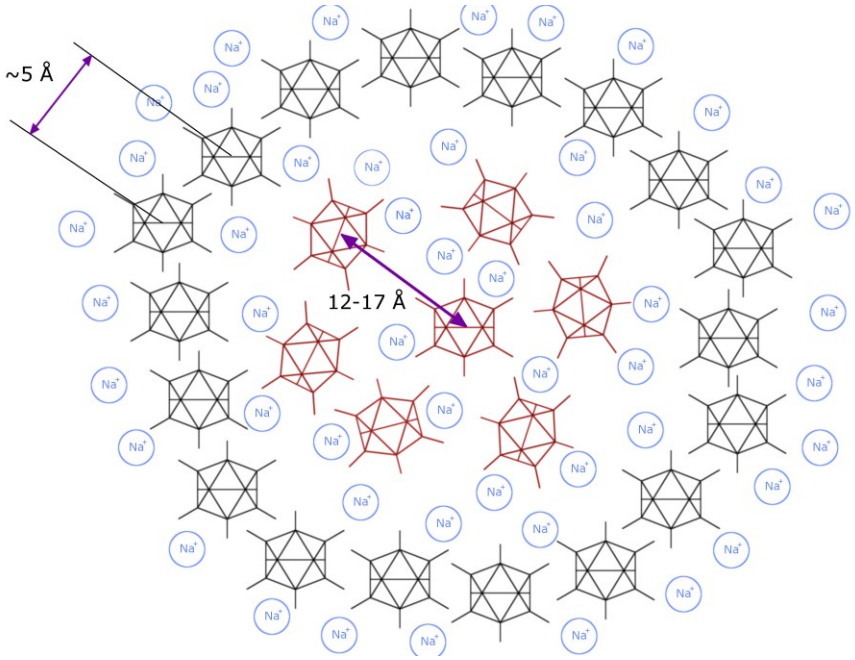

Figure II.S7. Alternative model of the structure of $Na_2[B_{12}H_{12}]$ aggregates that assumes incorporation of counterions into the inner parts of the aggregates ($[B_{12}H_{12}]^{2-}$ depicted by black and red structures; counterions shown in blue). This assumption would lead to two fractions of borane clusters: (i) clusters located on the surface of the aggregates (in black) in direct contact with each other related to the correlation peak in WAXS curves (region I), and (ii) clusters located in the inner parts of the aggregates (in red) that are surrounded by counterions related to correlation peaks in SAXS curves (region II).

ITC

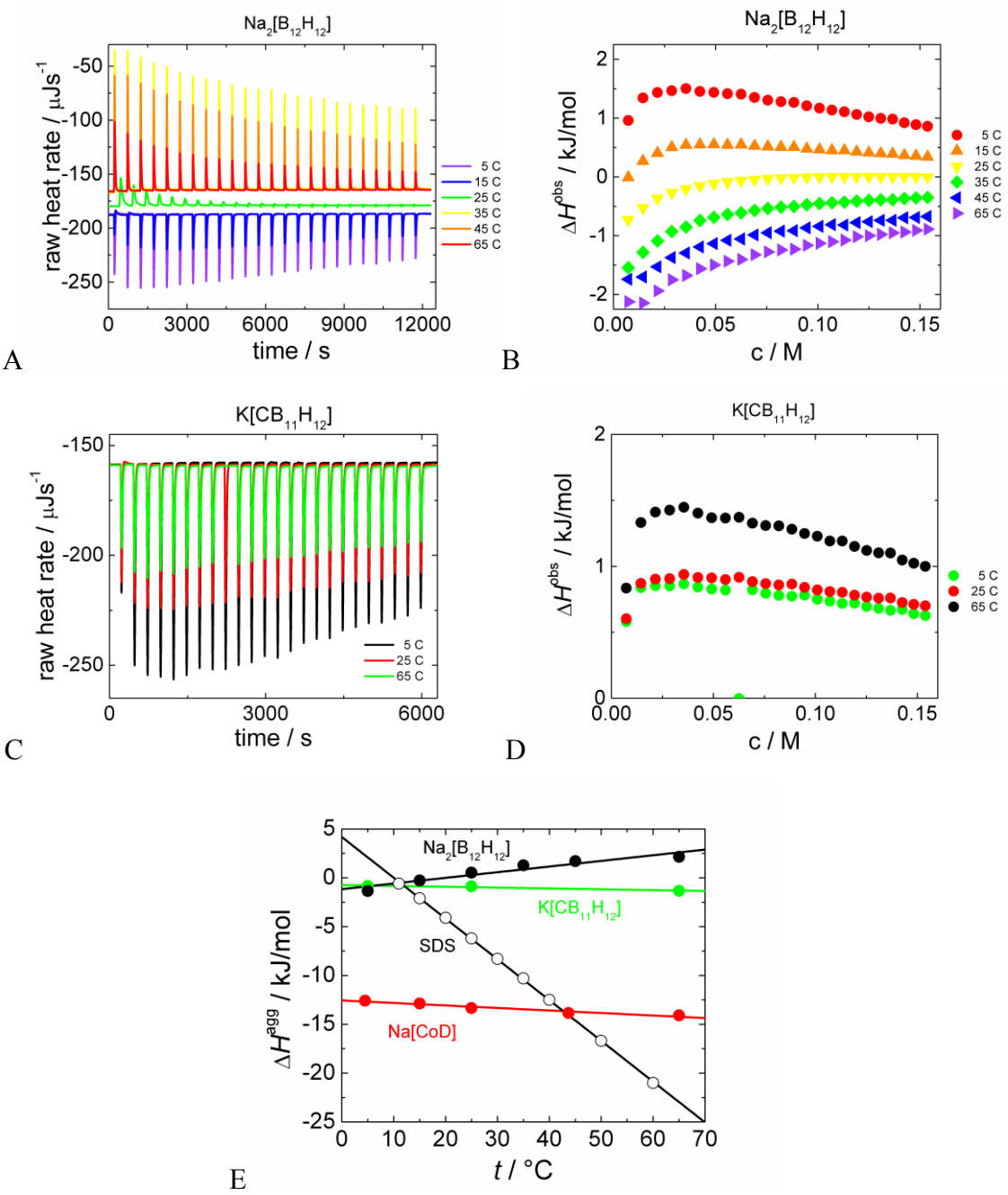

Figure II.S8. ITC (A, C) raw data and (B, D) thermograms for titration of concentrated (A, B) $Na_2[B_{12}H_{12}]$ and (C, D) $K[CB_{11}H_{12}]$ solutions into pure water, where ΔH^{obs} corresponds to the heat of deaggregation. (E) Comparison of heats of aggregation, ΔH^{agg}, at various temperatures for $Na_2[B_{12}H_{12}]$ and $K[CB_{11}H_{12}]$ estimated from thermograms (B and D, respectively), and for Na[COSAN] and SDS from our previous work.

Surface tension and HPLC

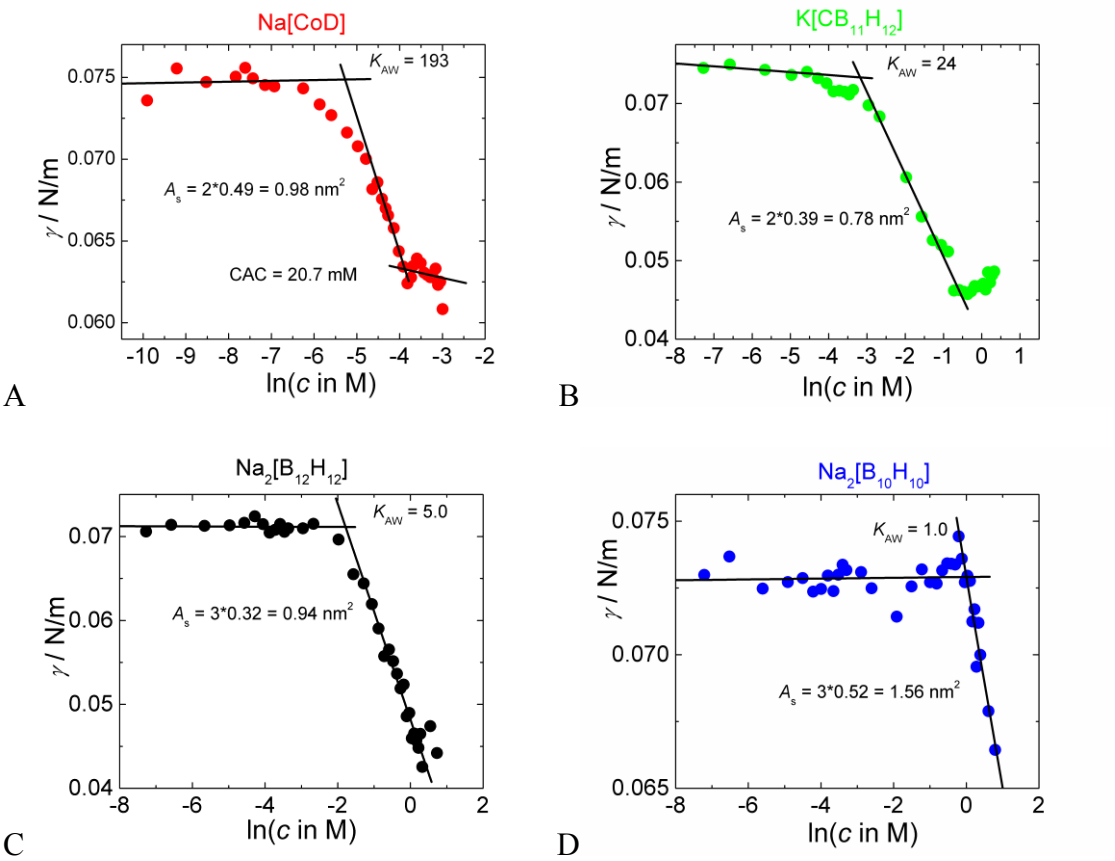

Figure II.S9. Surface tension, γ, as a function of concentration for (A) Na[COSAN], (B) $K[CB_{11}H_{12}]$, (C) $Na_2[B_{12}H_{12}]$, and (D) $Na_2[B_{10}H_{10}]$ aqueous solutions with evaluation according Gibbs adsorption isotherm (surface area per one molecule).

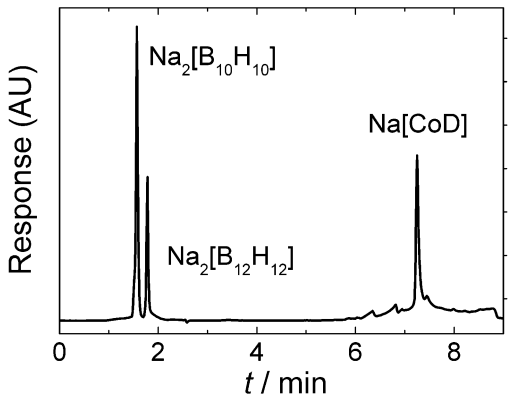

Figure II.S10. HPLC chromatogram for Na[COSAN], $Na_2[B_{12}H_{12}]$, and $Na_2[B_{10}H_{10}]$ indicating that Na[COSAN] is much more hydrophobic than (do)decaborates, and $Na_2[B_{10}H_{10}]$ is slightly more hydrophilic than $Na_2[B_{12}H_{12}]$.

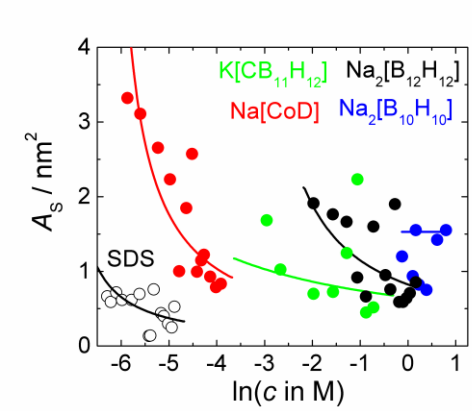

Figure II.S11. The average area occupied by a molecule at the air/water interface, A_S, derived from $d\gamma/d(\ln c)$ values for Na[COSAN] (red points), $K[CB_{11}H_{12}]$ (green points), $Na_2[B_{12}H_{12}]$ (black points), and $Na_2[B_{10}H_{10}]$ (blue points), where the values of limiting coverage is as follows: 0.98 nm^2, 0.78 nm^2, 0.94 nm^2, and 1.54 nm^2, respectively. Solid lines represent values of A_S calculated for polynomial fit of surface tension curves in Figure II.S10.

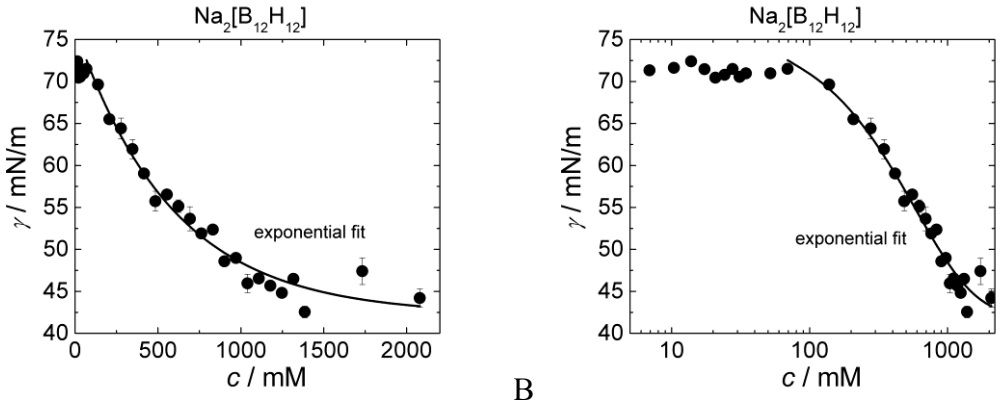

Figures II.S12. Exponential fit of the surface tension curve of $Na_2[B_{12}H_{12}]$ in (A) normal and (B) semi-log representation indicating that the "CAC break" is not real in this case.

Additional cryo-TEM imaging

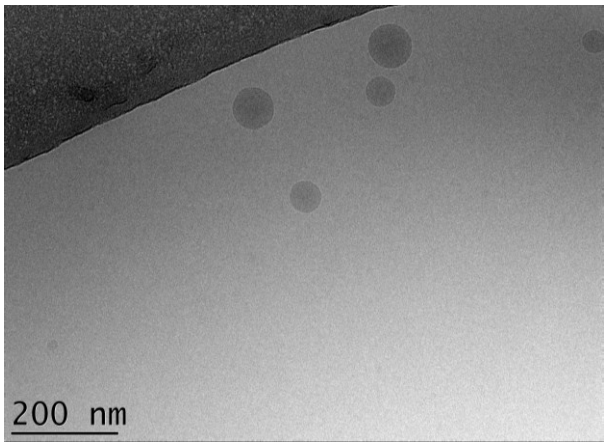

Figure II.S13. Cryo-TEM micrograph of 17 mM $K[B_{21}H_{18}]$ solution.

Acknowledgements

Authors would like to acknowledge the financial support of the Czech Science Foundation P205/14–14608S and the Ministry of Education of the Czech Republic 7AMB16DE007, and Karolína Štoudková for a kind assistance with most of experimental work. The gift of $K[B_{21}H_{18}]$ from Bohumir Gruner is gratefully acknowledged.

References

[1] Wennerstrom, H.; Lindman, B. Micelles–Physical-chemistry of surfactant association. *Phys. Rep.* **1979**, *52* (1), 1–86

[2] Nagarajan, R. Molecular packing parameter and surfactant self-assembly: The neglected role of the surfactant tail. *Langmuir* **2002**, *18* (1), 31–38.

[3] Nagarajan, R.; Ruckenstein, E. Theory of surfactant self-assembly – A predictive molecular thermodynamic approach. *Langmuir* **1991**, *7* (12), 2934–2969.

[4] Schramm, L. L.; Stasiuk, E. N.; Marangoni, D. G. 2 Surfactants and their applications. *Annu. Rep. Prog. Chem., Sect. C: Phys. Chem.* **2003**, *99*, 3–48.

[5] Nyrkova, I. A.; Semenov, A. N. Multimerization: Closed or open association scenario? *Eur. Phys. J. E: Soft Matter Biol. Phys.* **2005**, *17* (3), 327–337.

[6] Bodet, J.-F.; Davis, H. T.; Scriven, L. E.; Miller, W. G. Molecular self-diffusion in n-alkane-brine mixtures with small ethoxylated alcohols. *Langmuir* **1988**, *4* (2), 455–458.

[7] Zana, R.; Michels, B. Fluorescence probing and ultrasonic absorption study of the self-association of 1-butanol in aqueous solution. *J. Phys. Chem.* **1989**, *93* (6), 2643–2648.

[8] Zana, R. Aqueous surfactant-alcohol systems: A review. *Adv. Colloid Interface Sci.* **1995**, *57*, 1–64.

[9] Ganguli, A. K.; Ganguly, A.; Vaidya, S. Microemulsion-based synthesis of nanocrystalline materials. *Chem. Soc. Rev.* **2010**, *39* (2), 474–485.

[10] Kunz, W.; Holmberg, K.; Zemb, Th. Hydrotropes. *Curr. Opin. Colloid Interface Sci.* **2016**, *22* (2), 99-107.

[11] Booth, J. J.; Abbott, S.; Shimizu, S. Mechanism of hydrophobic drug solubilization by small molecule hydrotropes. *J. Phys. Chem. B* **2012**, *116* (51), 14915-14921.

[12] Eastoe, J.; Hopkins Hatzopoulos, M.; Dowding, P. J. Action of hydrotropes and alkyl-hydrotropes. *Soft Matter* **2011**, *7* (13), 5917-5925.

[13] Hopkins Hatzopoulos, M.; Eastoe, J.; Dowding, P. J.; Rogers, S. E.; Heenan, R.; Dyer, R. Are hydrotropes distinct from surfactants? *Langmuir* **2011**, *27* (20), 12346-12353.

[14] Boskovic, P.; Sokol, V.; Zemb, Th.; Touraud, D.; Kunz, W. Weak micelle-like aggregation in ternary liquid mixtures as revealed by conductivity, surface tension, and light scattering. *J. Phys. Chem. B* **2015**, *119* (30), 9933-9939.

[15] Bauduin, P.; Testard, F.; Zemb, Th. Solubilization in alkanes by alcohols as reverse hydrotropes or lyotropes. *J. Phys. Chem. B* **2008**, *112* (39), 12354-12360.

[16] Popov, A.; Borisova, T. *J. Colloid Interface Sci.* **2001**, *236* (1), 20-27.

[17] G. Chevrot, R. Schurhammer, G. Wipff, *J. Phys. Chem. B* **2006**, *110* (19), 9488-9498.

[18] P. Matejicek, P. Cigler, K. Prochazka, V. Kral, *Langmuir* **2006**, *22* (2), 575-581.

[19] Rezacova, P.; Cigler, P.; Matejicek, P.; Lepsik, M.; Pokorna, J.; Gruner, B.; Konvalinka, J. Medicinal Application of Carboranes: Inhibition of HIV Protease. In *Boron Science: New Technologies and Applications*; Hosmane, N. S., Ed.; CRC Press: New York, 2012; pp 41-70.

[20] Bauduin, P.; Prevost, S.; Farras, P.; Teixidor, F.; Diat, O.; Zemb, Th. A theta-shaped amphiphilic cobaltabisdicarbollide anion: Transition from monolayer vesicles to micelles. *Angew. Chem., Int. Ed.* **2011**, *50* (23), 5298–5300.

[21] Bauduin, P.; Zemb, Th. Perpendicular and lateral equations of state in layered systems of amphiphiles. *Curr. Opin. Colloid Interface Sci.* **2014**, *19* (1), 9-16.

[22] Gassin, P. M.; Girard, L.; Martin-Gassin, G.; Brusselle, D.; Jonchere, A.; Diat, O.; Vinas, C.; Teixidor, F.; Bauduin, P. Surface activity and molecular organization of metallacarboranes at the air-water interface revealed by nonlinear optics. *Langmuir* **2015**, *31* (8), 2297-2303.

[23] Uchman, M.; Dordovic, V.; Tosner, Z.; Matejicek, P. Classical amphiphilic behavior of nonclassical amphiphiles: A comparison of metallacarborane self-assembly with SDS micellization. *Angew. Chem., Int. Ed.* **2015**, *54* (47), 14113-14117.

[24] Vinas, C.; Tarres, M.; Gonzalez-Cardoso, P.; Farras, P.; Bauduin, P.; Teixidor, F. Surfactant behaviour of metallacarboranes. A study based on the electrolysis of water. *Dalton Trans.* **2014**, *43* (13), 5062–5068.

[25] Biela, A.; Sielaff, F.; Terwesten, F.; Heine, A.; Steinmetzer, T.; Klebe, G. Ligand binding stepwise disrupts water network in thrombin: Enthalpic and entropic changes reveal classical hydrophobic effect. *J. Med. Chem.* **2012**, *55* (13), 6094–6110.

[26] Malham, R.; Johnstone, S.; Bingham, R. J.; Barratt, E.; Phillips, S. E. V.; Laughton, C. A.; Homans, S. W. Strong solute-solute dispersive interactions in a protein-ligand complex. *J. Am. Chem. Soc.* **2005**, *127* (48), 17061–17067.

[27] Syme, N. R.; Dennis, C.; Phillips, S. E. V.; Homans, S. W. Origin of heat capacity changes in a "Nonclassical" hydrophobic interaction. *ChemBioChem* **2007**, *8* (13), 1509–1511.

[28] Bingham, R. J.; Findlay, J. B. C.; Hsieh, S. Y.; Kalverda, A. P.; Kjellberg, A.; Perazzolo, C.; Phillips, S. E. V.; Seshadri, K.; Trinh, C. H.; Turnbull, W. B.; Bodenhausen, G.; Homans, S. W. Thermodynamics of binding of 2-methoxy-3-isopropylpyrazine and 2-methoxy-3-isobutylpyrazine to the major urinary protein. *J. Am. Chem. Soc.* **2004**, *126* (6), 1675–1681.

[29] Biela, A.; Nasief, N. N.; Betz, M.; Heine, A.; Hangauer, D..; Klebe, G. Dissecting the hydrophobic effect on the molecular level: The role of water, enthalpy, and entropy in ligand binding to thermolysin. *Angew. Chem., Int. Ed.* **2013**, *52* (6), 1822–1828.

[30] Assaf, K. I.; Ural, M. S.; Pan, F.; Georgiev, T.; Simova, S.; Rissanen, K.; Gabel, D.; Nau, W. M. Water structure recovery in chaotropic anion recognition: High-affinity binding of dodecaborate clusters to γ-cyclodextrin. *Angew. Chem., Int. Ed.* **2015**, *54* (23), 6852–6856.

[31] Kaszynski, P. Four decades of organic chemistry of closo-boranes: A synthetic toolbox for constructing liquid crystal materials. A review. *Collect. Czech. Chem. Commun.* **1999**, *64* (6), 895–926.

[32] Sivaev, I. B.; Bregadze, V. I.; Sjoberg, S. Chemistry of closo-dodecaborate anion [B(12)H(12)](2-): A review. *Collect. Czech. Chem. Commun.* **2002**, *67* (6), 679–727.

[33] Plesek, J. Potential applications of the boron cluster compounds. *Chem. Rev.* **1992**, *92* (2), 269–278.

[34] Grimes, R. N. Metallacarboranes in the new millennium. *Coord. Chem. Rev.* **2000**, *200*, 773–811.

[35] Sivaev, I. B.; Bregadze, V. I. Chemistry of cobalt bis(dicarbollides). A review. *Collect. Czech. Chem. Commun.* **1999**, *64* (5), 783–805.

[36] Alexandrova, A. N.; Boldyrev, A. I.; Zhai, H. J.; Wang, L. S. All-boron aromatic clusters as potential new inorganic ligands and building blocks in chemistry. *Coord. Chem. Rev.* **2006**, *250* (21-22), 2811–2866.

[37] Grimes, R. N. In *Carborane in Medicine*; Grimes, R. N., Ed.; Academic Press: Oxford, 2011; pp 1053-1082.

[38] Sivaev, I. B.; Bregadze, V. V. Polyhedral boranes for medical applications: Current status and perspectives. *Eur. J. Inorg. Chem.* **2009**, *11*, 1433–1450.

[39] Scholz, M.; Hey-Hawkins, E. Carbaboranes as pharmacophores: Properties, synthesis, and application strategies. *Chem. Rev.* **2011**, *111* (11), 7035–7062.

[40] Gabel, D. Boron clusters in medicinal chemistry: perspectives and problems. *Pure Appl. Chem.* **2015**, *87* (2), 173–179.

[41] Lesnikowski, Z. J. Boron units as pharmacophores - New applications and opportunities of boron cluster chemistry. *Collect. Czech. Chem. Commun.* **2007**, *72* (12), 1646–1658.

[42] Soloway, A. H.; Tjarks, W.; Barnum, B. A.; Rong, F. G.; Barth, R. F.; Codogni, I. M.; Wilson, J. G. The chemistry of neutron capture therapy. *Chem. Rev.* **1998**, *98* (4), 1515–1562.

[43] Hideghety, K.; Sauerwein, W.; Wittig1, A.; Goetz, C.; Paquis, P.; Grochulla, F.; Haselsberger, K.; Wolbers, J.; Moss, R.; Huiskamp, R.; Fankhauser, H.; de Vries, M.; Gabel, D. Tissue uptake of BSH in patients with glioblastoma in the EORTC 11961 phase I BNCT trial. *J. Neuro-Oncol.* **2003**, *62* (1), 145–156.

[44] Karki, K.; Gabel, D.; Roccatano, D. Structure and dynamics of dodecaborate clusters in water. *Inorg. Chem.* **2012**, *51* (9), 4894–4896.

[45] Fan, P.; Stolte, S.; Gabel, D. Interaction of organic compounds and boron clusters with new silica matrices containing the phosphatidylcholine headgroup. *Anal. Methods* **2014**, *6* (9), 3045–3055.

[46] Gabel, D.; Awad, D.; Schaffran, T.; Radovan, D.; Daraban, D.; Damian, L.; Winterhalter, M.; Karlsson, G.; Edwards, K. The anionic boron cluster (B12H11SH)(2-) as a means to trigger release of liposome contents. *ChemMedChem* **2007**, *2* (1), 51–53.

[47] Fan, P.; Neumann, J.; Stolte, S.; Arning, J.; Ferreira, D.; Edwards, K.; Gabel, D. Interaction of dodecaborate cluster compounds on hydrophilic column materials in water. *J. Chromatogr. A* **2012**, *1256*, 98–104.

[48] Lin, J. H.; Chen, W. S.; Hou, S. S. NMR studies on effects of tetraalkylammonium bromides on micellization of sodium dodecylsulfate. *J. Phys. Chem. B* **2013**, *117* (40), 12076–12085.

[49] Nordstierna, L.; Furo, I., Stilbs, P. Mixed micelles of fluorinated and hydrogenated surfactants. *J. Am. Chem. Soc.* **2006**, *128* (20), 6704-6712.

[50] Cui, X. H.; Jiang, Y.; Yang, C. S.; Lu, X. Y.; Chen, H.; Mao, S. Z.; Liu, M. L.; Yuan, H. Z.; Luo, P. Y.; Du, Y. R. Mechanism of the mixed surfactant micelle formation. *J. Phys. Chem. B* **2010**, *114* (23), 7808–7816.

[51] Cui, X. H.; Mao, S. Z.; Liu, M. L.; Yuan, H. Z.; Du, Y. R. Mechanism of surfactant micelle formation. *Langmuir* **2008**, *24* (19), 10771–10775.

[52] Kumar, B. V. N. P.; Pryadharsini, S. U.; Prameela, G. K. S.; Mandal, A. B. NMR investigations of self-aggregation characteristics of SDS in a model assembled tri-block copolymer solution. *J. Colloid Interface Sci.* **2011**, *360* (1), 154–162.

[53] Leclercq, L.; Nardello-Rataj, V.; Turmine, M.; Azaroual, N.; Aubry, J. M. Stepwise aggregation of dimethyl-di-n-octylammonium chloride in aqueous solutions: From dimers to vesicles. *Langmuir* **2010**, *26* (3), 1716–1723.

[54] Basilio, N.; Garcia-Rio, L.; Martin-Pastor, M. Calixarene-based surfactants: evidence of structural reorganization upon micellization. *Langmuir* **2012**, *28* (5), 2404–2414.

[55] Lewis, M. S.; Knott, G. D. Simulation studies of self-associating systems – Discrimination between specific and isodesmic association. *Biophys. Chem.* **1976**, *5* (1-2), 171–183.

[56] Fernandes, A.; Bras, N. F.; Mateus, N.; de Freitas, V. A study of anthocyanin self-association by NMR spectroscopy. *New J. Chem.* **2015**, *39* (4), 2602–2611.

[57] Smulders, M. M. J.; Nieuwenhuizen, M. M. L.; de Greef, T. F. A.; van der Schoot, P.; Schenning, A. P. H. J.; Meijer, E. W. How to distinguish isodesmic from cooperative supramolecular polymerisation. *Chem. Eur. J.* **2010**, *16* (1), 362–367.

[58] Pianet, I.; Andre, Y.; Ducase, M. A.; Tarascou, I.; Lartigue, J. C.; Pinaud, N.; Fouquet, E.; Dufourc, E. J.; Laguerre, M. Modeling procyanidin self-association processes and understanding their micellar organization: A study by diffusion NMR and molecular mechanics. *Langmuir* **2008**, *24* (19), 11027–11035.

[59] Marcolongo, J. P.; Mirenda, M. Thermodynamics of sodium dodecyl sulfate (SDS) micellization: An undergraduate laboratory experiment. *J. Chem. Educ.* **2011**, *88* (5), 629–633.

[60] Haussler, W.; Wilk, A.; Gapinski, J.; Patkowski, A. Interparticle correlations due to electrostatic interactions: A small angle x-ray and dynamic light scattering study. I. Apoferritin. *J. Chem. Phys.* **2002**, *117* (1), 413-426.

[61] Sivan, U. The inevitable accumulation of large ions and neutral molecules near hydrophobic surfaces and small ions near hydrophilic ones. *Curr. Opin. Colloid Interface Sci.* **2016**, *22* (2), 1–7.

[62] Menger, F. M.; Galloway, A. L.; Chlebowski, M. E. Surface tension of aqueous amphiphiles. *Langmuir* **2005**, *21* (10), 9010–9012.

[63] Eastoe, J.; Dalton, J. S. Dynamic surface tension and adsorption mechanisms of surfactants at the air-water interface. *Adv. Colloid Interface Sci.* **2000**, *85* (2-3), 103–144.

[64] Strey, R.; Viisanen, Y.; Aratono, M.; Kratohvil, J. P.; Yin, Q.; Friberg, S. E. On the necessity of using activities in the Gibbs equation. *J. Phys. Chem. B* **1999**, *103* (43), 9112–9116.

[65] Cerdan, L.; Braborec, J.; Garcia-Moreno, I.; Costela, A.; Londesborough, M. G. S. A borane laser. *Nat. Commun.* **2015**, *6*, 5958.

[66] Matejicek, P.; Brus, J.; Jigounov, A.; Plestil, J.; Uchman, M.; Prochazka, K.; Gradzielski, M. On the structure of polymeric composite of metallacarborane with poly(ethylene oxide). *Macromolecules* **2011,** *44* (10), 3847–3855.

[67] Brus, J.; Zhigunov, A.; Czernek, J.; Kobera, L.; Uchman, M.; Matejicek, P. Control over the self-assembly and dynamics of metallacarborane nanorotors by the nature of the polymer matrix: A solid-state NMR study. *Macromolecules* **2014**, *47* (18), 6343–6354.

[68] Zangi, R. Driving force for hydrophobic interaction at different length scales. *J. Phys. Chem. B* **2011**, *115* (10), 2303–2311.

[69] Chandler, D. Interfaces and the driving force of hydrophobic assembly. *Nature* **2005**, *437* (7059), 640–647.

[70] Patel, A. J.; Varilly, P.; Jamadagni, S. N.; Acharya, H.; Garde, S.; Chandler, D. Extended surfaces modulate hydrophobic interactions of neighboring solutes. *Proc. Natl. Acad. Sci. U. S. A.* **2011**, *108* (43), 17678–17683.

5.3 Paper III

Aqueous self-assembly and cation selectivity of cobaltabisdicarbollide dianionic dumbbells*

Abstract

It was known that the anion [3,3'-Co($C_2B_9H_{11}$)$_2$]$^-$, COSAN, produces aggregates in water solution. These aggregates are interpreted to be the result of C–H···H–B interactions. In this work, we demonstrate that it is possible to generate aggregates even after the incorporation of additional functional groups to the COSAN units. The approach has been to join two COSAN anions by a linker that can adapt itself to perform as a crown ether. The linker has been chosen to have six oxygen atoms that is the ideal number for K^+ selectivity in crown ethers. It is demonstrated that the linker binds the alkaline metal ions with different affinities, thus showing a distinct degree of selectivity. The highest affinity is shown towards K^+ from a mix containing Li^+, Na^+, K^+, Rb^+ and Cs^+ that can be indicative of a *pseudo* crown ether performance of the dumbbell. One interesting possibility is that the COSAN anions at the two ends of the linker could perform as a *hook-and-loop* fastener to close the ring. This facet is intriguing and deserves further consideration for the possible applications it may have. The distinct affinity towards alkaline metal ions was corroborated by solubility studies and ITC thermograms. Further, cryo-TEM micrographs, along with light scattering results, reveal the existence of small self-assemblies and compact nanostructures ranging from spheres to single/multi-layer vesicles in the aqueous solutions. The studies reported here have shown that these dumbbells can be in water or lipophilic phases with different appearances, either molecules or aggregates, offering a distinct model as drug carriers.

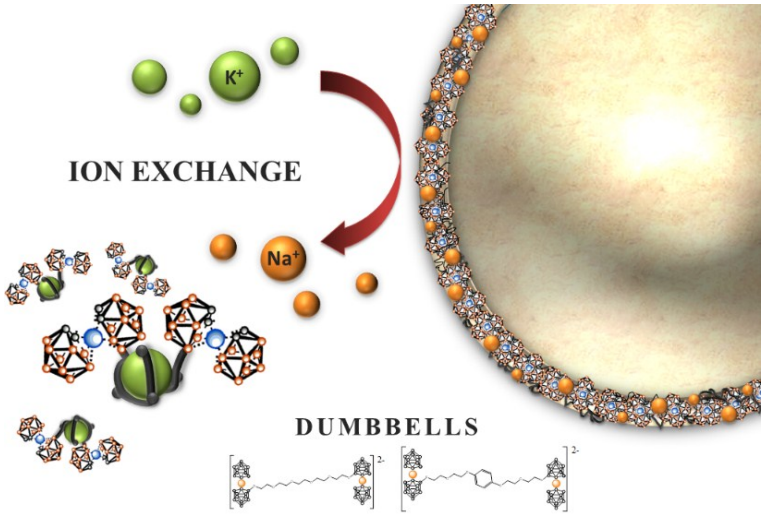

* In slightly modified version published as: Tarrés, M.; Viñas, C.; González-Cardoso, P.; Hanninen, M.; Sillanpää, R.; Ďorďovič, V.; Uchman, M.; Teixidor, F.; Matějíček, P.: Aqueous Self-Assembly and Cation Selectivity of Cobaltabisdicarbollide Dianionic Dumbbells, *Chemistry – A European Journal* **2014**, *20*, 6786–6794.

Introduction

The cobaltabisdicarbollide sandwich is a compound made of two $[C_2B_9H_{11}]^{2-}$ units that coordinate Co^{3+} in a η^5 way to generate $[3,3'\text{-}Co(C_2B_9H_{11})_2]^-$, COSAN.[1] Its properties are remarkable: It is monoanionic with a peculiar peanut shape with two globules that are responsible for distinguishing physico-chemical properties;[2] it is soluble in water and/or organic solvents depending on the cation; chemically and thermally stable in a large diversity of situations;[3] it has a plethora of B–H and C–H bonds that are at hand to generate many opportunities to produce hydrogen and dihydrogen bonds, that grant the anion a unique self-assembling capacity;[4] and COSAN can be substituted at carbon or at boron atoms. Similar to ferrocene, with which it shares key structural similarities, displays a rich reversible electrochemistry.[5] The anion itself was considered a weakly coordinating anion,[6] due to its low charge density,[7] that arises from its bulkiness and charge delocalization. However, over the past few years, several researchers have shown that some metallacarboranes behave similarly to a surfactant in aqueous solutions. Wipff and co-workers, interpreted by molecular dynamics methods that $[3,3'\text{-}Co(C_2B_9H_{11})_2]^-$ anions, although lacking amphiphilic topology, behave as anionic surfactants.[8] Later, some of us concluded, through a combination of static and dynamic light scattering (DLS) and microscopy methods, that COSAN, in aqueous solutions, organised in spherical aggregates with a radii of around 100 nm in a fairly monodisperse way. More recently, Bauduin et al. demonstrated by small- and wide-angle X-ray and neutron scattering that H[COSAN] formed monolayer vesicles at low concentrations in water.[2] Finally, it has been proven that minor changes in the molecular structure of COSAN induce major modifications in the solution behavior. The substitution of two B–H by two B–I units in the structure of COSAN leads to a lamellae lyotropic phase in the high concentration regime.[10] The former results have evidenced the self-organizing capacity of aqueous solutions of $[3,3'\text{-}Co(C_2B_9H_{11})_2]^-$ or its highly rigid derivatives, such as $[3,3'\text{-}Co(8\text{-}I\text{-}1,2\text{-}C_2B_9H_{10})_2]^-$. However, these results do not provide evidence to anticipate the aqueous behavior of metallacarborane containing molecules in which the self-organizing capacity of the borane molecule is partially hampered by functionalization.

Crown ethers are good at stabilizing alkaline cations: a crown ether with five oxygen atoms fits the size of Na^+ better to any other alkaline metal ion, while the one with six oxygen atoms prefers K^+ and crown ethers with four oxygen atoms are selective for Li^+.[11]

In 2003, it was reported that a good surrounding for Na^+ coordination was generated when both globules in COSAN were linked through the $C_{cluster}$ atoms by an $–S(CH_2CH_2O)_3S–$ spacer.[12] Upon complexation, the oxygen atoms are facing inwards towards the alkaline metal, whereas the exterior of the ring is hydrophobic.

Herein, we report on the alkaline ions extraction capacity and selectivity behavior of aqueous solutions of linear molecules in which their two ends are occupied by COSAN entities; the linker is made of ethylene oxide repeating units in similarity to those in crown ethers. These molecules have been named “dumbbells”. The end disposition of the COSAN entities allows the metallacarborane to make the full use of its self-assembling possibilities while still being connected to a second metallacarborane. The linker should not be against the formation of aggregates.[13] Finally, the number of oxygen atoms in the linker was chosen to be six, but in one

case was seven. Therefore, we expected that the dumbbell molecules synthesized would be best with K^+.

Results and dicussion

Solubility of dumbbell salts in aqueous solutions

Saturated solutions of Na^+, Li^+, K^+, H^+ and $[NMe_4]^+$ salts of dumbbells $[\mathbf{2}]^{2-}$, $[\mathbf{3}]^{2-}$, $[\mathbf{4}]^{2-}$ and $[\mathbf{5}]^{2-}$ in pure water, for one type of experiments, and in 0.154M chloride of corresponding cation (physiological saline; except $[NMe_4]^+$ salt), for a second type of experiments, were prepared. The solubility, S, in mM of all the samples was calculated from the absorbance at λ = 307 nm (COSAN band),[21] and it is shown in Figure III.1. Based on the dumbbells structures, the solubility product, $K_{sp} = [A^+]^2[B^{2-}] = 4S^3$, was calculated, in which A and B are corresponding cations and anions, respectively (shown as $pK_{sp} = -\log K_{sp}$ in Figure III.S1). The results in this section are only given on a qualitative level, because the aim is to distinguish what kinds of interaction and parts of the dumbbell molecule control its solution behavior.

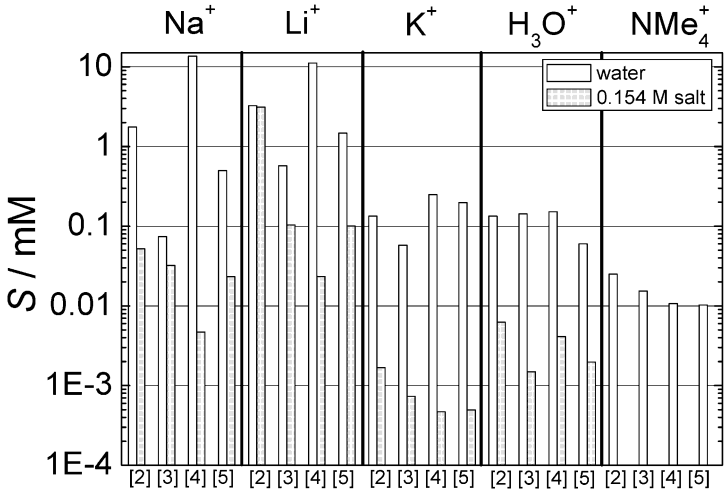

Figure III.1. Solubility of the dumbbells $[\mathbf{2}]^{2-}$, $[\mathbf{3}]^{2-}$, $[\mathbf{4}]^{2-}$ and $[\mathbf{5}]^{2-}$ (structures are given in Figure 2.3) with various counterions (Na^+, Li^+, K^+, H_3O^+, and $[NMe_4]^+$) in water (white columns) and in 0.154 M chloride of the corresponding cation except $[NMe_4]Cl$ (grey columns).

A more thorough description of Figure III.1 can be found in the Supporting Information (SI); however, a brief summary is given here. As expected, $[NMe_4]^+$ salts are the most insoluble and have a very minor influence from the linker. H^+, and surprisingly K^+ dumbbells are also sparingly soluble. The impact of the linker is almost negligible for dumbbells in acidic form. However, for potassium salts there is evidence of a dependence of the solubility on the linker, a phenomenon that is further enhanced for sodium and lithium dumbbells.[23] Na^+ and Li^+ dumbbells are the most soluble samples with pK_{sp} 8.4 ± 2.9 and 7.3 ± 1.6, respectively. The solubility decreases with increasing length of the polyethylene glycol (PEG) linker.

The solubility of all samples is substantially diminished in 0.154 M saline solutions of common cations, in which K^+ and H^+ dumbbells become almost insoluble (Figure III.1). This is

mainly due to the common ion effect.[23] For dumbbells in acid form, the solubility drops regardless of the nature of the linker in 0.154 M HCl. For potassium dumbbells, compounds with the *p*-phenylene subunits in the chain ([**4**]$^{2-}$ and [**5**]$^{2-}$) are more affected by the presence of KCl than those with purely PEG linker ([**2**]$^{2-}$ and [**3**]$^{2-}$). For sodium and lithium dumbbells, the impact of added salt is extremely broad (between 0.03 and 99%).

If we compare solubility of the dumbbells with those of parent COSAN salts in water (Figure III.S3), all dumbbells are less soluble in water than the corresponding COSAN salts. The most pronounced effect was observed for potassium salt and acid, which are otherwise very water soluble in the form of K[COSAN] and H[COSAN]. On the contrary, the decrease in solubility of $[NMe_4]^+$ dumbbells is almost negligible.

The explanation of the above-described trends is tightly related to the molecular structure of the molecules studied. The molecules contain the PEG chain, which is known to form a complex with several cations.[24] Although the COSAN cluster is highly hydrophobic, some of its salts are very water-soluble (i.e., H^+, Li^+, Na^+ and K^+). This is mainly due to the presence of a negative charge and the entropy of corresponding counterions. If the cations are immobilized for any reason, the solubility should drop substantially. These effects stand also behind the well-known aggregation of metallacarboranes in aqueous media.[2,4a,9,10]

In the case of dumbbells, the $[NMe_4]^+$ cation is expected to interact directly with negatively charged COSAN cluster, which results in the formation of insoluble complex, regardless of the presence of the linker. H_3O^+ interacts not only with COSAN cluster but also with highly negative oxygen atom attached directly to the cluster.[25] The presence of the linker, therefore, supports the decrease in solubility, but its nature is not such an important factor for H^+ and $[NMe_4]^+$, which is not the case for dumbbells of alkaline cations. For these cases, a partial complexation of Na^+, Li^+ and K^+ ions by the PEG linker is foreseen.

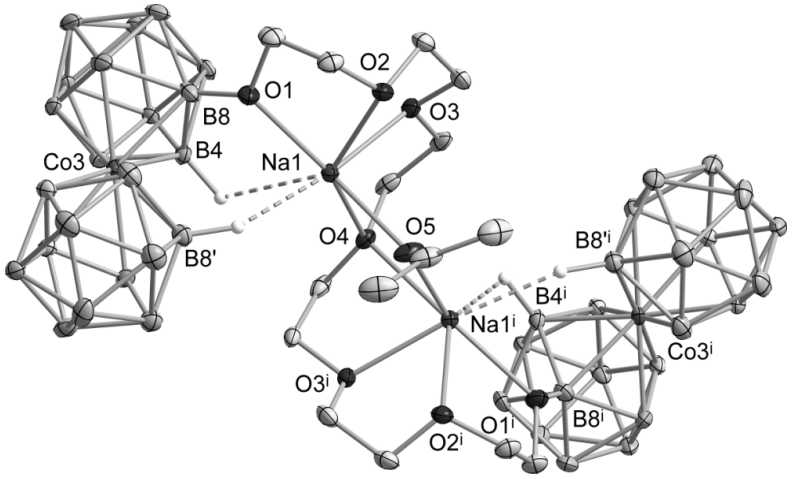

Figure III.2. The ORTEP drawing of the crystal structure of [Na_2[**3**](acetone)]. Thermal ellipsoids have been drawn at 20% probability level. CH and BH hydrogens that do not contribute to any weak interaction with sodium cations are omitted for clarity. Symmetry operation i: *–x*, *y*, 0.5*–z*.

To ascertain this prediction, crystals of Na_2[**3**] were grown. The solid-state structure of [Na_2(**3**)$_2$(acetone)] contains two cobaltabisdicarbollide units linked by 19-membered PEG chain with 7 ether oxygen atoms. Each sodium cation is surrounded by three oxygen atoms from the PEG linker with an additional bridging acetone molecule. The structure also contains two B−H···Na interactions to fulfil the coordination sphere of each sodium cation (Figure III.2).

The solubility is thus controlled by the length and chemical composition of the chain, the overall cation concentration, and the cation diameter. The affinity of K^+ to the PEG chain is the highest (see ITC and MALDI-TOF MS results below) among the studied alkaline cations, resulting in the low solubility of potassium dumbbells.

Aggregation of dumbbells in aqueous solutions

Previous work described that one typical feature of metallacarborane solutions in water is the presence of aggregates that could be detected by light scattering.[4a,9] In our DLS study on solutions of the dumbbell compound, we examined saturated solutions as well as the dependence of dumbbell and salt concentration. The observed trends are complex and difficult to interpret, which is typical for cobaltabisdicarbollide solutions.[4a] It is however clear that the aggregation behavior of the dumbbells is "metallacarborane-controlled" and that the presence of the linker has only a limited effect. This is in agreement with our previous studies on the self-assembly of COSAN and its conjugates.[4a,9,21,22] The sample and salt concentration dependence of hydrodynamic radius, R_H, of aggregates for various sodium and lithium dumbbells with sufficiently high solubility are shown in Figures III.S4–III.S7.

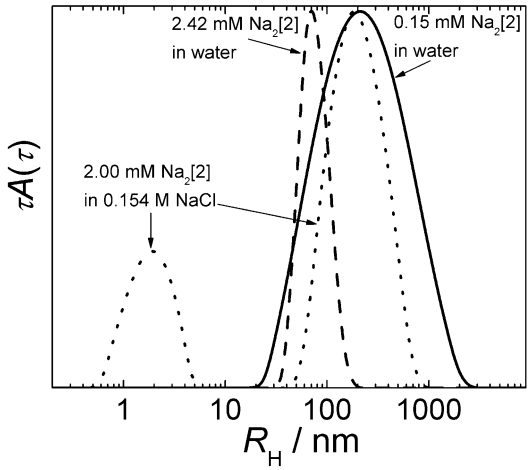

Figure III.3. Distribution of hydrodynamic radii, R_H, of Na_2[**2**] in water (solid and dash line) at various sample concentrations and in 0.154 M NaCl (dot line) obtained by DLS.

To generalize dependence from this detailed light-scattering study, we would like to show here DLS and cryo-TEM results of one sample only: Na_2[**2**]. All typical trends are demonstrated by the distribution of R_H of dumbbell aggregates in water and physiological saline solution (Figure III.3). One mode corresponding to the aggregates in a saturated solution in water (2.42 mM; Figure III.3, dashed line) can be seen. The mode shifts to higher radii with dilution by water (0.15 mM; Figure III.3, solid line). The most striking is the distribution for saturated

solution in saline (Figure III.3, dotted line). Two modes are observed: one is at around 200 nm (large aggregates) and the other is located at around 2 nm, which is close to the dimension of a single dumbbell molecule. This is the first time that we have observed a predominant fraction of such small nanoparticles in the solution of metallacarboranes by DLS.[4a] These small nanoparticles can be assigned to dumbbell associates consisting of only few molecules.

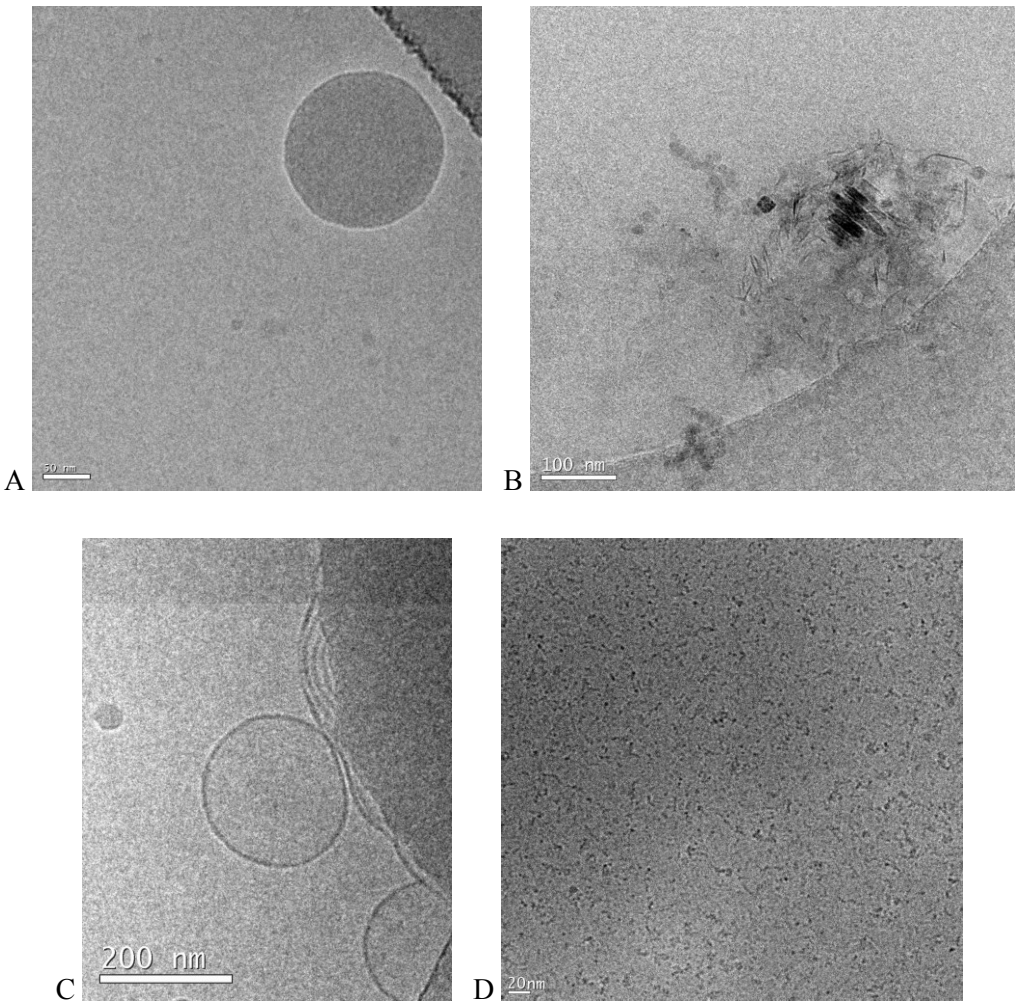

Figure III.4. Cryo-TEM micrographs of Na_2[**2**]: (A) 2.42 mM solution in water (scale bar: 50 nm); (B) 0.15 mM solution in water (scale bar: 100 nm); (C) 2.00 mM solution in 0.154 M NaCl (scale bar: 200 nm); and (D) a magnification of the image in C (scale bar: 20 nm).

Na_2[**2**] nanoparticles observed by DLS were visualized by cryo-TEM. In a saturated solution of Na_2[**2**] in water (Figure III.4A), there are compact spherical nanoparticles with dimensions comparable to the R_H distribution shown in Figure III.3 (dashed line). Diluted samples in water contain large polydisperse agglomerates (Figure III.4B) with evidence of lamellar structures; these findings are in agreement with our previous observations.[2,9a] The presence of salt leads to transformation of these nanospheres into large vesicle-like objects (Figure III.4C), consisting of layered dumbbell molecules[2,10] accompanied by very small particles with a worm-like shape (Figure III.4D). From cryo-TEM micrographs, it is evident that

the dumbbell molecules self-assemble into compact nano-objects in aqueous solutions, the structure of which could be tuned by the presence of salt.

Cation exchange

Once the influence of the coordinated cations to the dumbbell molecule in terms of water solubility and aggregation behavior was demonstrated, we tested the ability of particular dumbbells to exchange alkaline cations by means of MALDI-TOF. It is important to outline that the MALDI-TOF technique is used, in our hands, as a pseudo-quantitative analytical method. The samples have been prepared by a H_2O/Et_2O (10:10 mL) extraction of 10 mg of the dumbbell sample, with 100 equivalents of the desired alkaline chloride (LiCl, KCl, RbCl or CsCl). After shaking the mixture for 1 minute, the organic layer was analyzed by MALDI-TOF MS.

Our experience with borane anions indicates that MALDI-TOF MS is very good to detect mono-anions, but not for dianions. The dumbbells studied herein have two negative charges that are compensated in the salt with two alkaline cations. The incident ionizing laser of the MALDI-TOF mass spectrometer ionizes the molecule producing a mononegative species that is the result of the two negative charges of the DUMBBELL and one positive charge from the alkaline metal. This behavior allowed the study of the exchange ratio for each cation. The cobaltabisdicarbollides resist the intensity of the laser very well, and the spectra always appear very clearly. Only the heights in the same MALDI experiment are compared; never from two different MALDI experiments.

Cumulative experience through the years on analysis of incomplete reactions of cobaltabisdicarbollide and its derivatives, mainly halogenated species with other reagents, led us to observe that there is a parallel between ratio of heights in MALDI-TOF and ratio of concentrations obtained from ^{1}H NMR, particularly for the H–C_c cobaltabisdicarbollide region, near δ = 4–5 ppm. Moreover, we also demonstrated and reported the height/ratio relationship after comparing the MALDI-TOF MS and the square-wave voltammetry results, which is quantitative for a mixture of chlorinated cobaltabisdicarbollide salts.[26] All this prior studies are supportive that the height of the peaks in the same MALDI-TOF spectrum are proportional to the amount of each sample.

The application of MALDI-TOF MS to the extract in Et_2O led to the data shown in Figures III.S8–11. These data show that the initial alkaline cation (Na^+ in all cases) can be partly exchanged for any other alkaline metal (Li^+, K^+, Rb^+, and Cs^+) when used in a 100-fold excess. Notably, there are differences in the extent of cation exchange for particular dumbbells and alkaline cations. All the dumbbells studied exhibit an efficient exchange for K^+, Rb^+ and Cs^+, whereas this is not the case for Li^+. When sodium and lithium cations compete for the different dumbbells, without exception the dumbbells prefer to coordinate sodium, whereas for the other cations (K^+, Rb^+ and Cs^+), sodium is less favored. The general tendency shows that the larger cations are preferred to smaller ones.

As a further proof of concept that the heights of the mixtures are related to their ratio in the solution, we performed further extractions tests. Instead of extracting the Na_2[**4**] salt only once, as in the former experiments, we did it three times, always replacing the aqueous solution

of K^+ salt for a new one. After the three extractions, the MALDI-TOF MS results showed uniquely the $\{K[\mathbf{4}]\}^-$ signal, despite $\{Na[\mathbf{4}]\}^-$ being detectable. These experiments were also performed with the other three dumbbells. In some cases, after two contacts of 1 min each, for $Na_2[\mathbf{4}]$, total exchange occurred, whereas after three contacts practically all exchange occurred for $Na_2[\mathbf{2}]$, and a fourth contact would be advisable to remove the final traces of Na^+ for $Na_2[\mathbf{3}]$ and $Na_2[\mathbf{5}]$. That means that the cation exchange has taken place to completion, although not in only one batch; this again supports the relation between ratio of heights and ratio of concentrations (Figures III.S12–15).

Ion selectivity

To obtain information about the ion preference tendency, we performed the extraction experiment introduced in the previous section with a solution five different cations ("alkaline cationic mix"), each cation was in 1000-fold excess, instead of analyzing them individually. Figures III.5–III.8 show the MALDI-TOF mass spectra after 1 min of shaking the sodium dumbbell solutions, in diethyl ether, with the aqueous alkaline cationic mix. All measurements were carried out at the same laser intensity, so as not to alter the peak proportionality within each spectrum. The ion preference strongly depends on the nature of the linker in dumbbell molecules, which is in agreement with solubility data (Figure III.2 and Figure III.S1). The height of each MS envelop due to the cation trapped by dumbbell molecules (relative heights in %) calculated from the abundance of the corresponding peaks in the spectrum are summarised Table III.1.

Table III.1. Relative heights of alkaline cations in the MALDI-TOF spectra of various sodium dumbbells (Figure III.5–III.8).[a]

		Relative Amplitudes [%]				
		Li^+	Na^+	K^+	Rb^+	Cs^+
Ethylene glycol dumbbell	$Na_2[\mathbf{2}]$	4	8	33	27	28
Diethylene glycol dumbbell	$Na_2[\mathbf{3}]$	22	10	22	22	24
p-dihydroxybenzene dumbbell	$Na_2[\mathbf{4}]$	10	21	38	14	17
Dihydroxy-*p*-xylene dumbbell	$Na_2[\mathbf{5}]$	7	7	18	21	47

[a] Extracted in the water/Et_2O system against the alkaline cationic mix.

From the results given in Table III.1, it is possible to distinguish the following trends, depending on the dumbbell used. In the case of $Na_2[\mathbf{2}]$, the lithium and sodium ions have, by far, the lowest bonding interactions with the dumbbell, appearing in less than 10%, whereas potassium seems to be the most preferred cation (33%). Surprisingly, when the $Na_2[\mathbf{3}]$ dumbbell was used, all heights were near 20% (except Na^+); therefore, there is only weak cation selectivity. For $Na_2[\mathbf{4}]$, lithium has the lowest affinity and potassium is a favored at almost 40%. Finally, when using $Na_2[\mathbf{5}]$, lithium and sodium are again the less preferred ions (7% for each), whereas there is a strong affinity for caesium at nearly 50%.

This preference is related to the coordination number of each cation and the size of the metallacarborane-based dumbbells, which allow for better coordination for larger cations than for comparatively smaller ones.

Monitoring of cation exchange "in situ"

From the previous sections, it is reasonable to assume that alkaline cations are bound to the dumbbell molecules in aqueous solutions (especially within the compact nanoparticles). Furthermore, it is probable that such associates consist of several dumbbell molecules "glued" together by cations and through direct COSAN–COSAN interactions surrounded by a cloud of free cations. It is also clear that the cations differ in the preference to the dumbbell molecule (see the MALDI-TOF MS results). To directly prove our assumptions, we carried out ITC experiments, in which 1 mM of sodium and lithium ethylene glycol dumbbells were titrated against 16 mM NaCl, LiCl and KCl. The ion exchange of the low affinity cations of dumbbells by others with a higher preference is manifested by exothermic peaks in the raw ITC output (Figure III.S16). This experiment allows calculation of basic thermodynamic characterization data, such as the enthalpy of cation exchange and the corresponding stoichiometry.

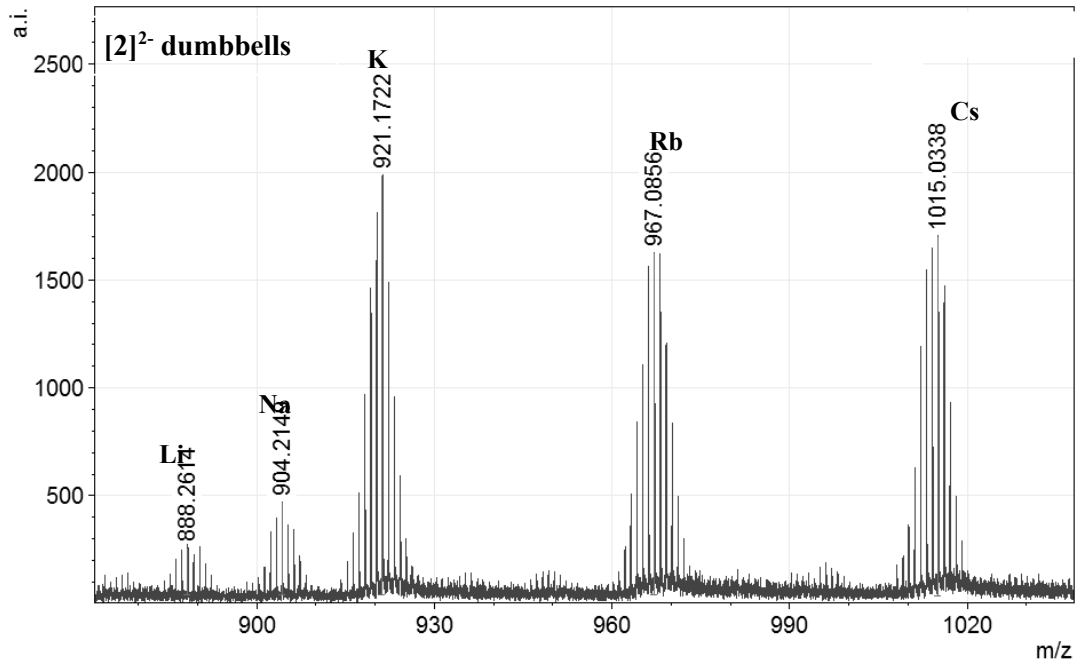

Figure III.5. MALDI-TOF mass spectrum of Na_2[**2**] with the five alkaline metals obtained after shaking the sodium dumbbell in diethyl ether against an alkaline cationic soup, in which each cation was 1000 times more concentrated than the starting dumbbell.

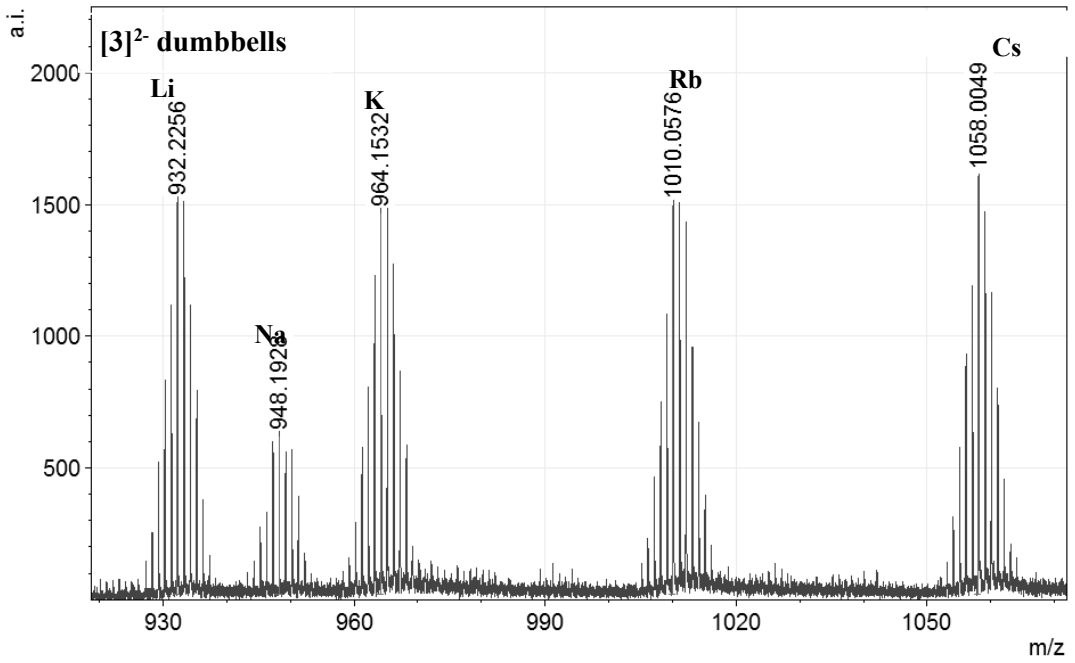

Figure III.6. MALDI-TOF mass spectrum of Na_2[**3**] with the five alkaline metals. Conditions are the same as outlined in Figure III.5.

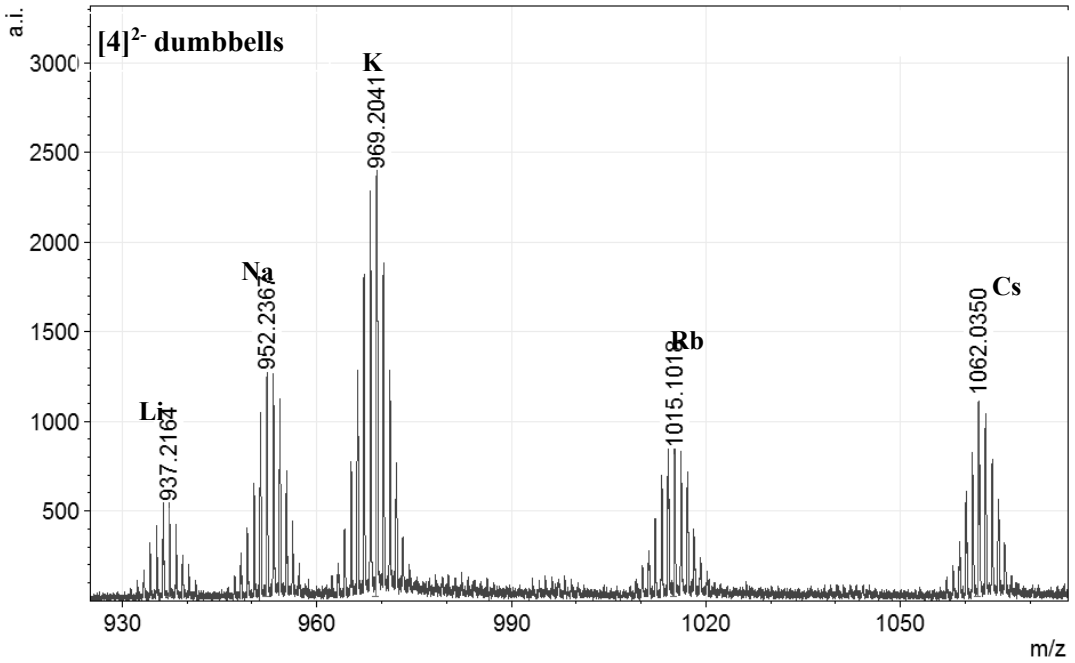

Figure III.7. MALDI-TOF mass spectrum of Na_2[**4**] with the five alkaline metals. Conditions are the same as outlined in Figure III.5.

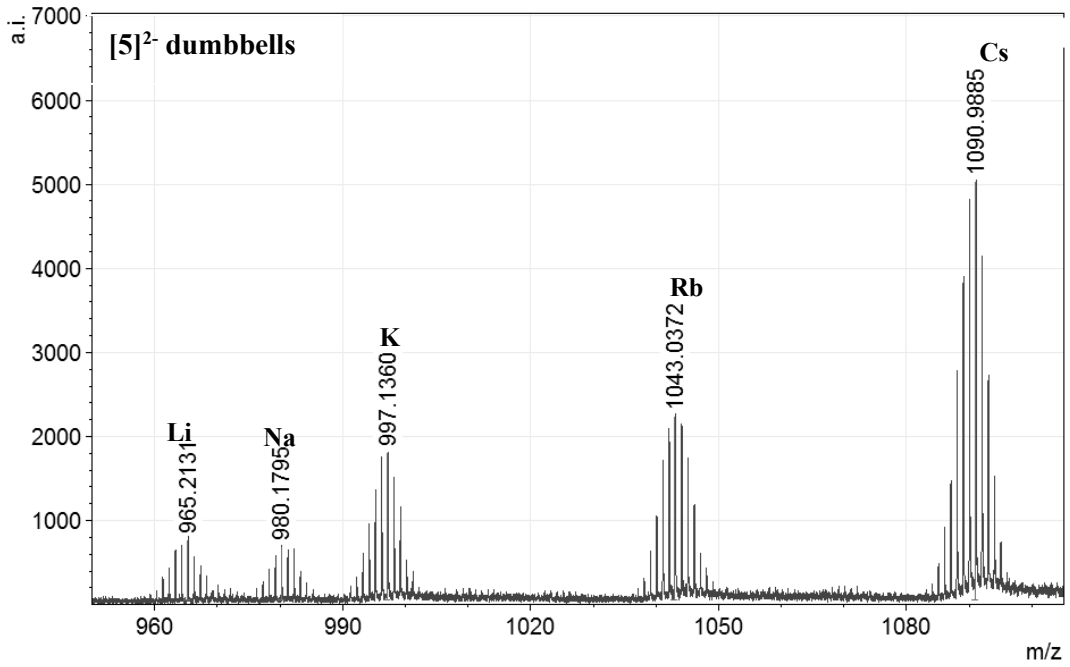

Figure III.8. MALDI-TOF mass spectrum of Na_2[**5**] with the five alkaline metals. Conditions are the same as outlined in Figure III.5.

The ITC curves for the exchange of Na^+ and Li^+ by K^+ (Figures III.9) demonstrate that K^+ cations bind directly to the dumbbell molecule; a process that is accompanied by the release of Na^+ or Li^+ to the bulk solution. The curves display three sequential steps with different positions and depths, which are in the range from –0.1 to –0.4 kJ mol^{-1}. Because the overall ΔH is fairly low, the process is probably driven by an entropy term.

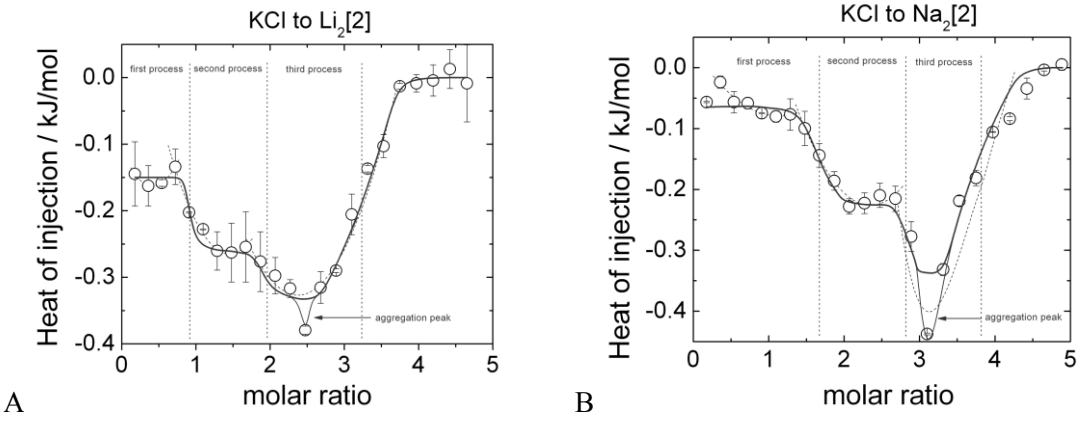

Figures III.9. ITC thermograms for 16 mM KCl titrated into 1 mM: (A) Li_2[**2**] and (B) Na_2[**2**]. The black dash lines (polynomial fits of experimental points) connecting the data are drawn only to guide the eye. The solid lines represent an attempt to model the data qualitatively by a three-site binding model according to ref. 28b. Evidence of three processes and the so-called "aggregation peak" detected by ITC is also demonstrated within the graphs. The vertical dotted lines indicate a stoichiometry of processes.

It is evident, that it does not obey a simple one-site binding model.[27] The steps in ITC curves correspond to three distinct processes (probably related to cation exchange at three

binding sites) with different affinities and $\Delta H^{exchage}$ values with respect to K^+.[28] This model describes the experimental dependences reasonably well (the solid lines in Figures III.9). Nevertheless, the presence of aggregation peak[13a] indicates that the third process could be accompanied by a rearrangement of dumbbell molecules. The binding sites can be assigned to the following parts of the dumbbell molecule: 1) PEG chain, 2) negatively charged parts of free COSAN hemisphere around B8, and 3) the oxygen attached to B8. Unfortunately, it is not possible to assign the processes in Figures III.9 to particular binding sites.

The stoichiometry of cation exchange is indicated by vertical lines in Figure III.9, for which the relative shift in Figure III.9B is probably caused by an incorrect estimation of the titrant concentration. As seen in Figure III.9, the expected 2:1 stoichiometry was not observed. The deviation is still unclear for us, and it will be the aim of our future research. It is probably related to the inner structure of dumbbell aggregates in solution, which could be different to those of the cation/anion ratio in the solid state.

Conclusions

COSAN anions are known to produce aggregations in water that can be modulated by salt concentration. We studied the capacity to generate aggregates after the incorporation of additional functional groups with the ultimate goal of producing molecular materials that self-assemble in water solution. The approach was to link two COSAN anions by a linker that could adapt itself to perform as a crown ether. The molecules looked like dumbbells because the bulky and compact COSAN anions were at each end of the linker. The four dumbbell-like COSAN conjugates differed in length and nature of the PEG linker. The linker was chosen to have six oxygen atoms in three of the four cases because it was the ideal number for K^+ selectivity in crown ethers. Water/diethyl ether extractions in combination with MALDI-TOF MS experiments demonstrated that, despite the existence of the two dense COSAN anions, the linker bound to the alkaline metal ions with different affinities; thus showing a distinct degree of selectivity. The highest affinity was shown towards K^+ from a mix containing Li^+, Na^+, K^+, Rb^+ and Cs^+; this could be an indication of a pseudo-crown ether performance of the dumbbell. This suggests that the COSAN anions at the two ends of the linker may perform as a hook-and-loop fastener to close the ring. This facet is intriguing and deserves further consideration for the possible applications it may have. The solubility values of Na^+, Li^+, K^+, H^+ and $[NMe_4]^+$ dumbbells were supportive of the extraction values and provided evidence that the dumbbells interacted with the different cations unevenly. Whereas ammonium and hydroxonium dumbbells were sparingly soluble with almost no interesting trends, alkaline dumbbells offered extremely varied solution behavior, depending on the composition of linker and dimensions of the alkaline cation. The ITC thermograms were also supportive of the selectivity of the dumbbells. When the Na^+ and Li^+ dumbbells were titrated with K^+, an exothermic process occurred. Careful study of the ITC thermograms provided evidence for three binding sites on the dumbbell molecules.

Concerning the capacity of these dumbbells to generate aggregates, cryo-TEM micrographs, together with light scattering results, revealed the presence of compact nanostructures in aqueous solutions, in which the morphology could be tuned by salt

concentration from spheres to single/multi-layer vesicles and small self-assemblies consisting of only several molecules.

These studies have shown that these dumbbells could have different appearances, either molecules or aggregates, in water or lipophilic domains. This is probably due to the capacity of the COSAN anions to produce multi C–H···H–B bonds, along with the PEG-type linker. These interactions permit an easy adjustment to the conditions of the aqueous medium and offer an alternative model as drug carriers that have not yet been considered.

Supporting Information

Solubility experiments

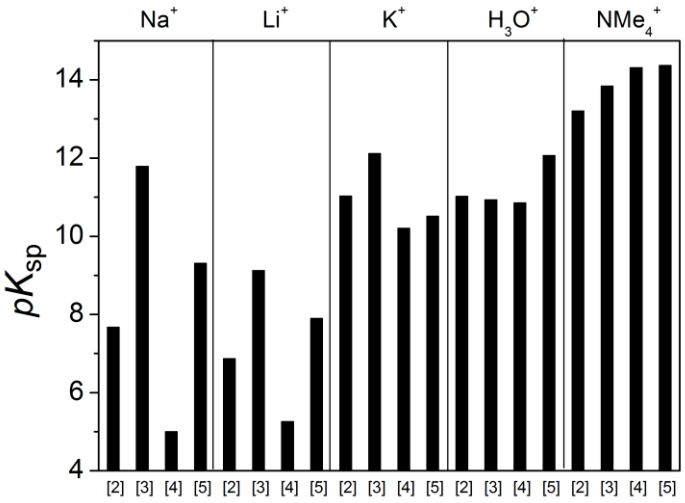

Figure III.S1. Solubility product of the dumbbells $[\mathbf{2}]^{2-}$, $[\mathbf{3}]^{2-}$, $[\mathbf{4}]^{2-}$ and $[\mathbf{5}]^{2-}$.

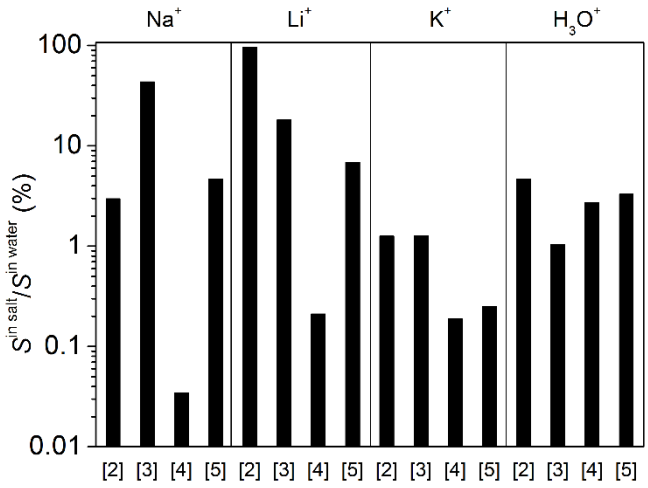

Figure III.S2. Solubility of dumbbells $[\mathbf{2}]^{2-}$, $[\mathbf{3}]^{2-}$, $[\mathbf{4}]^{2-}$ and $[\mathbf{5}]^{2-}$ in salt relative to that in pure water in %.

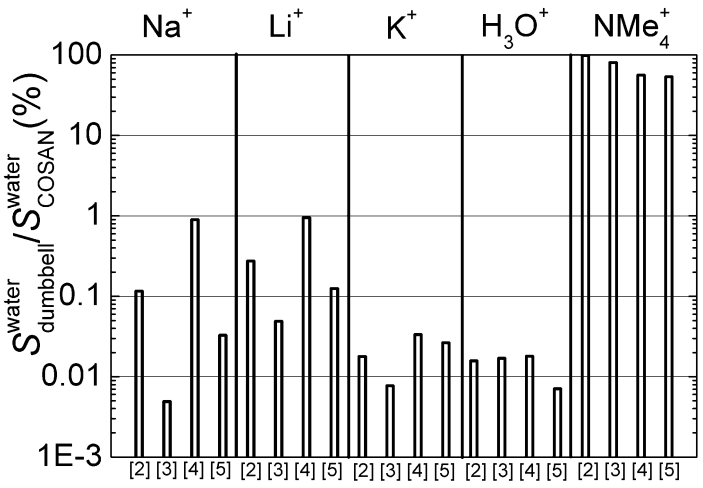

Figure III.S3. Solubility of dumbbells $[\mathbf{2}]^{2-}$, $[\mathbf{3}]^{2-}$, $[\mathbf{4}]^{2-}$ and $[\mathbf{5}]^{2-}$ in water relative to that of pure COSAN in %.

Descriptions of the solubility experiments

First, we focused on mean pK_{sp} values for dumbbells differing in counter-ions. As expected, $[NMe_4]^+$ salts are the most insoluble (pK_{sp} = 13.9 ± 0.5). It comes out that the influence of the linker is very minor because the variation of pK_{sp} values is very modest (± 0.5). H^+, and surprisingly K^+ dumbbells are also sparingly soluble with mean pK_{sp} 11.2 ± 0.6 and 11.0 ± 0.8, respectively. The impact of the linker is almost negligible for dumbbells in acid form. However, for potassium salts there is evidence of the effect, which is further enhanced for sodium and lithium dumbbells: the length and the nature of the chain have an impact on the solubility.[22] Na^+ and Li^+ dumbbells are the most soluble samples with pK_{sp} 8.4 ± 2.9 and 7.3 ± 1.6, respectively, where the value of pK_{sp} varies significantly with the nature of the linker. It is evident that the solubility decreased with an increase of the length of the PEG linker.

The solubility of all the samples is substantially diminished in 0.154 M saline solutions, where K^+ and H^+ dumbbells become almost insoluble (see Figure III.1). This is mainly due to the common ion effect.[23] Solubility in water and in saline solution is compared (Figure III.S2, where S^{salt} is divided by S^{water}). For dumbbells in acid form, the solubility drops few percents regardless of the nature of linker in 0.154 M HCl. For potassium dumbbells, it is evident that dumbbells with *p*-phenylene subunits in the chain ($[\mathbf{4}]^{2-}$ and $[\mathbf{5}]^{2-}$) are more affected by the presence of KCl than those with purely PEG linker ($[\mathbf{2}]^{2-}$ and $[\mathbf{3}]^{2-}$). For sodium and lithium dumbbells, the impact of added salt is extremely broad (between 0.03% and 99%), which is worth noticing.

If we compare solubility of the dumbbells with those of parent COSAN salts in water (Figure III.S3), we can estimate a role of the linker in the solution behavior of dumbbells. All the dumbbells are less soluble in water than the corresponding COSAN salts. The most pronounced suppression was observed for potassium salt and acid, which are otherwise very

water soluble in form of K[COSAN] and H[COSAN]. On the contrary, the decrease of $[NMe_4]^+$ dumbbells solubility is almost negligible.

Light scattering experiments

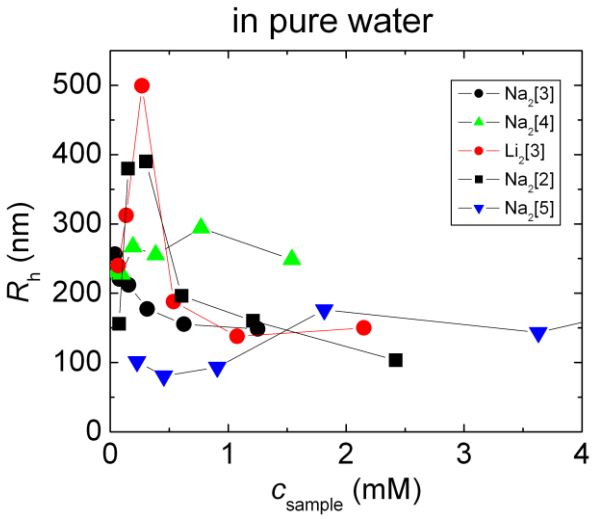

Figure III.S4. Concentration dependence of hydrodynamic radius, R_H, of aggregates of various dumbbells in pure water.

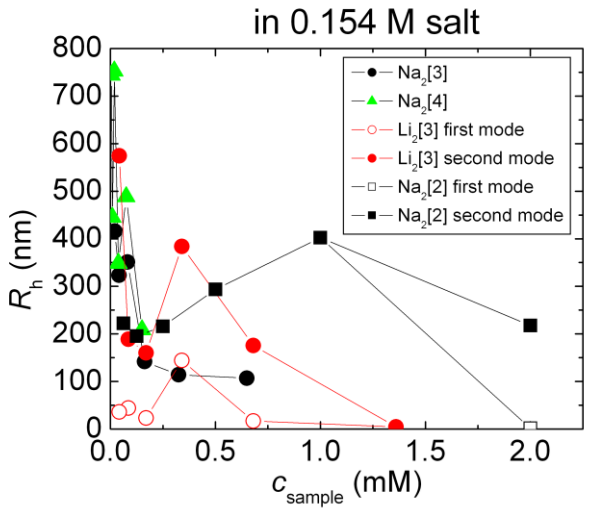

Figure III.S5. Concentration dependence of hydrodynamic radius, R_H, of aggregates of various dumbbells in 0.154 M NaCl or LiCl.

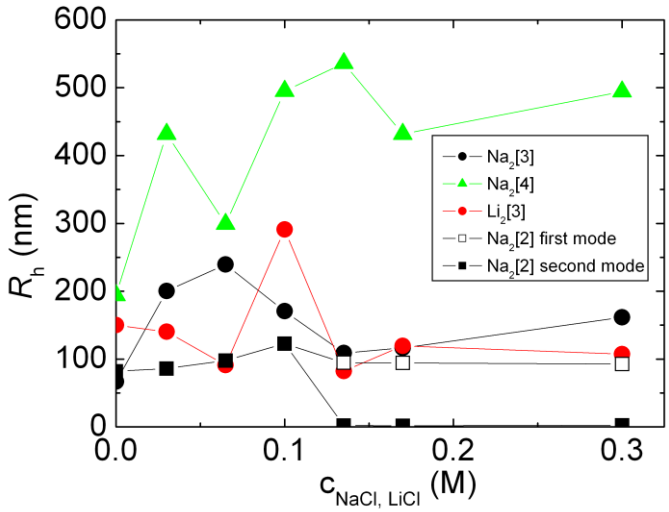

Figure III.S6. Dependence of hydrodynamic radius, R_H, of aggregates in saturated solutions of various dumbbells on addition of salt (NaCl or LiCl).

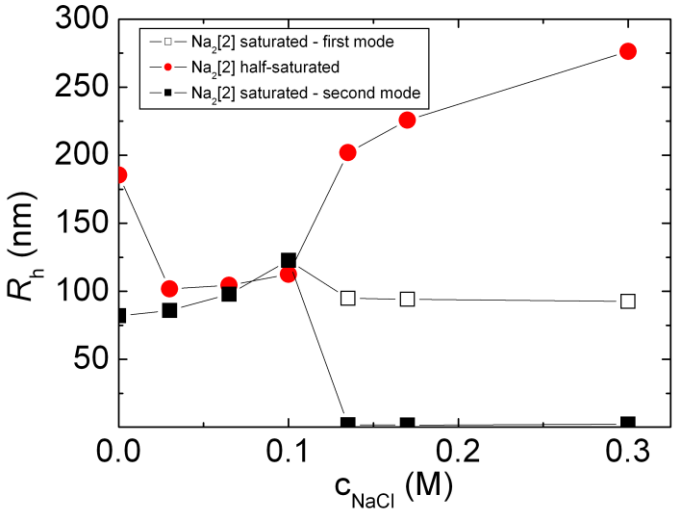

Figure III.S7. Dependence of hydrodynamic radius, R_H, of aggregates in saturated and half-saturated solution of Na_2[**2**] on addition of salt (NaCl or LiCl).

MALDI-TOF MS experiments

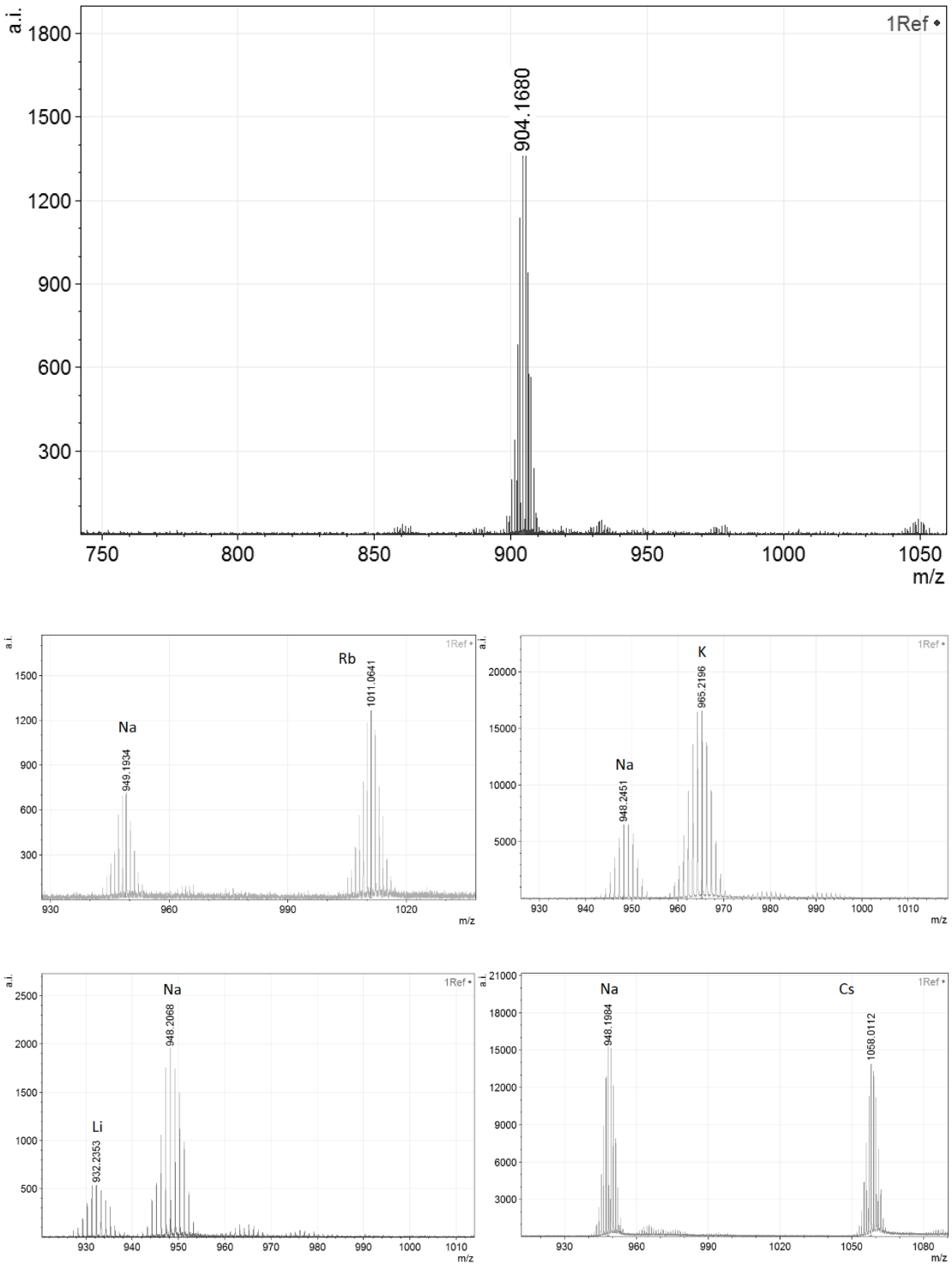

Figure III.S8. MALDI-TOF mass spectra of Na_2[**2**] and the corresponding cationic exchanges.

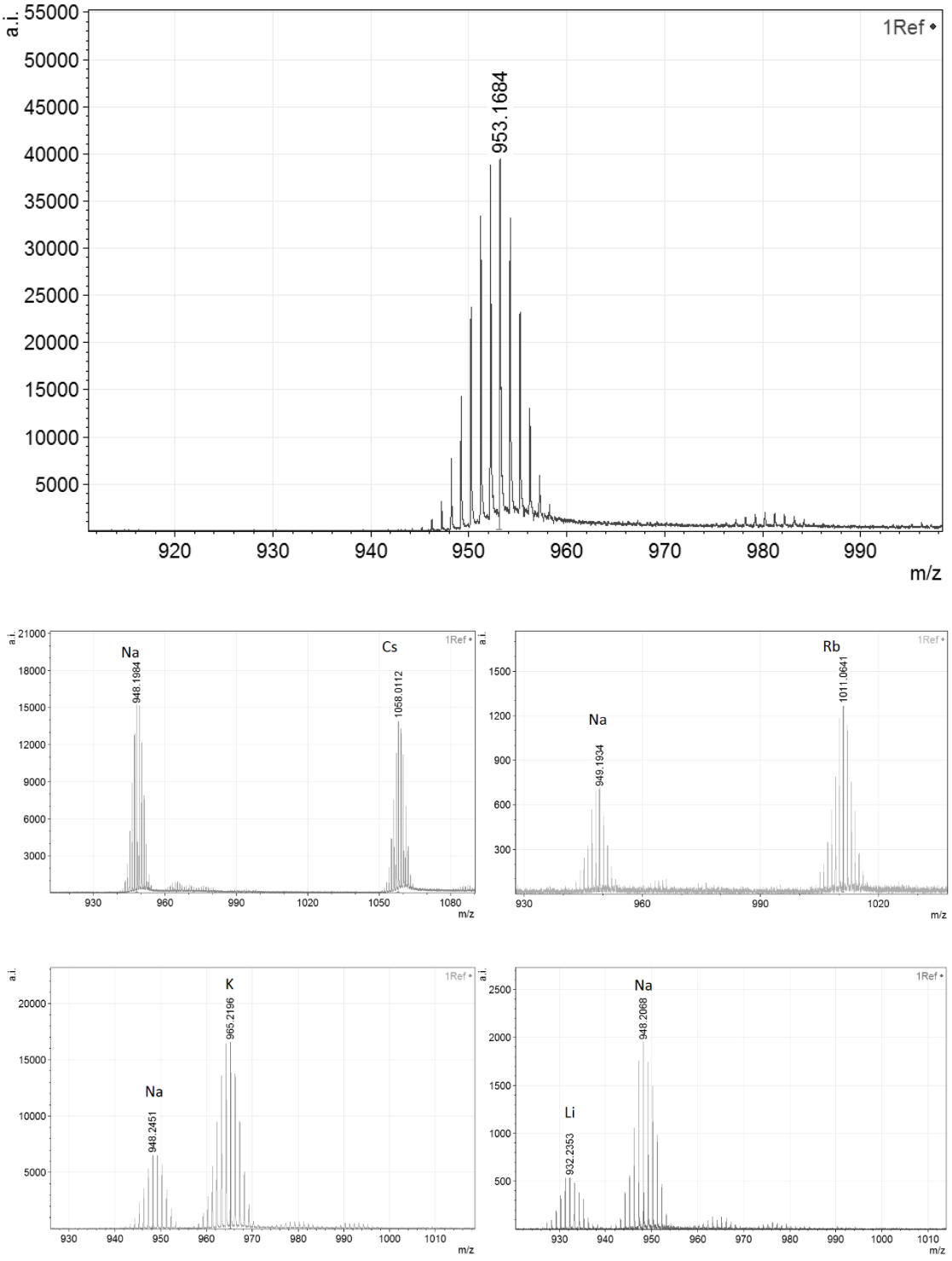

Figure III.S9. MALDI-TOF mass spectra of Na_2[**3**] and the corresponding cationic exchanges.

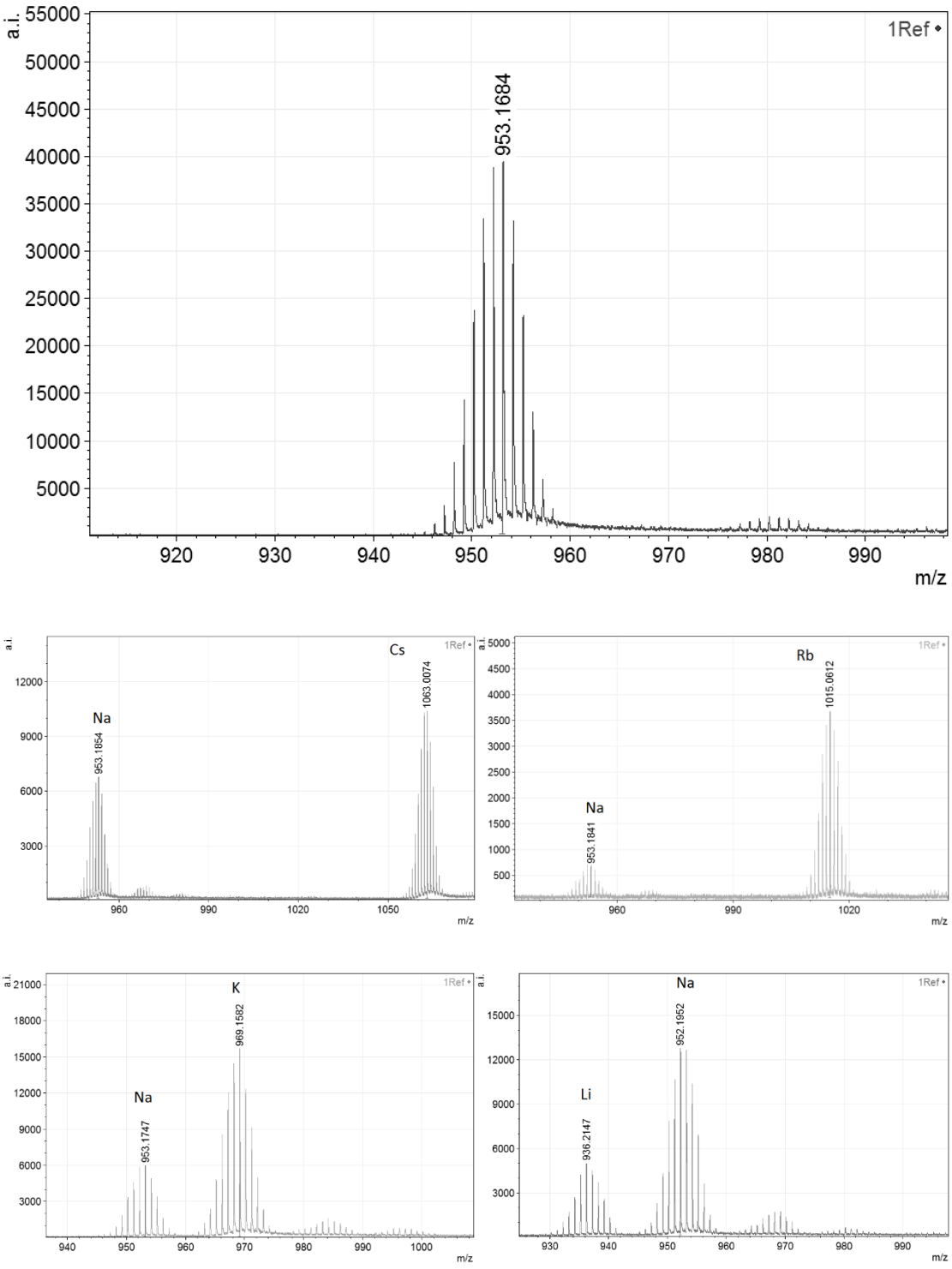

Figure III.S10. MALDI-TOF mass spectra of Na_2[**4**] and the corresponding cationic exchanges.

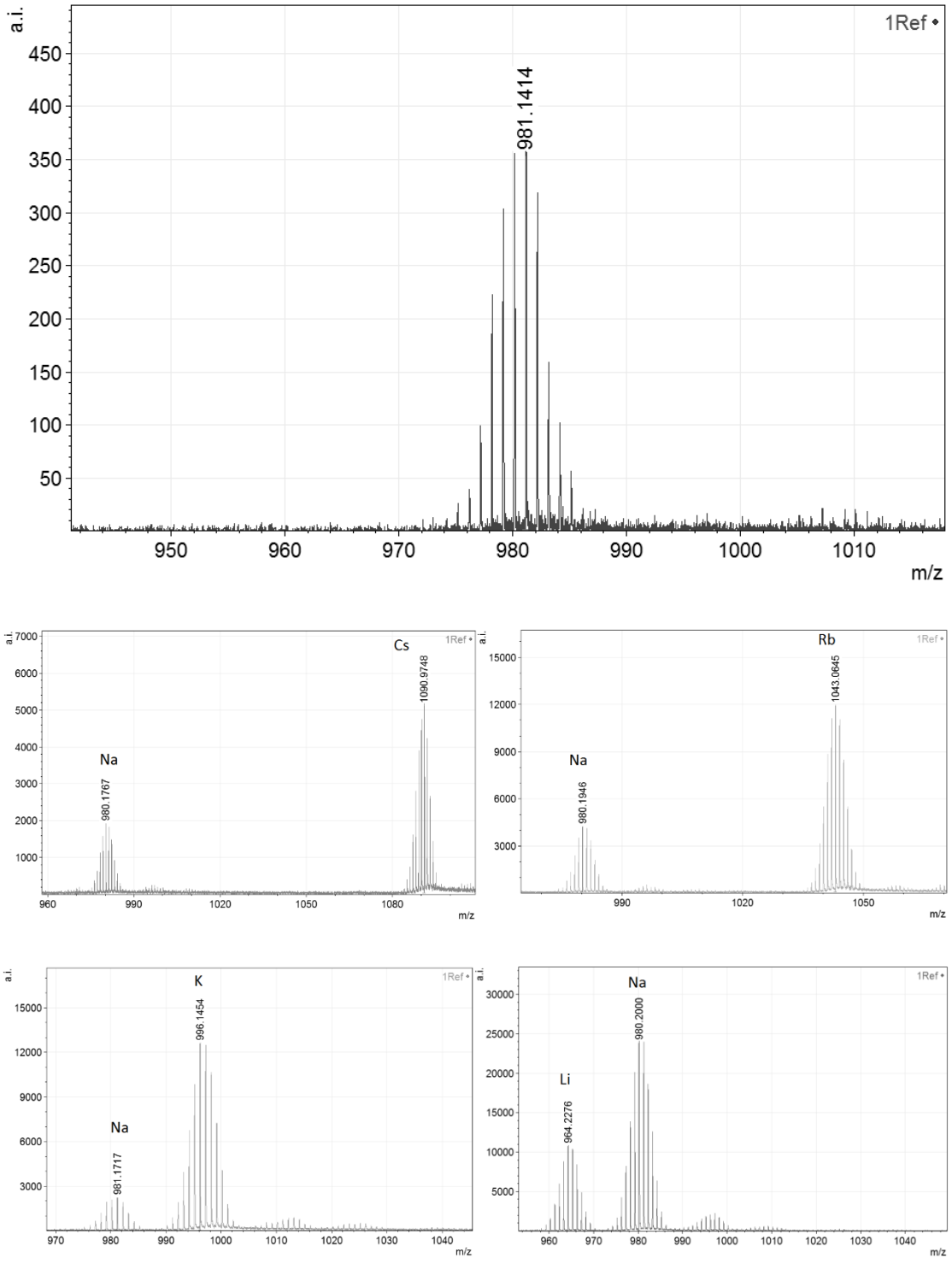

Figure III.S11. MALDI-TOF mass spectra of Na_2[**5**] and the corresponding cationic exchanges.

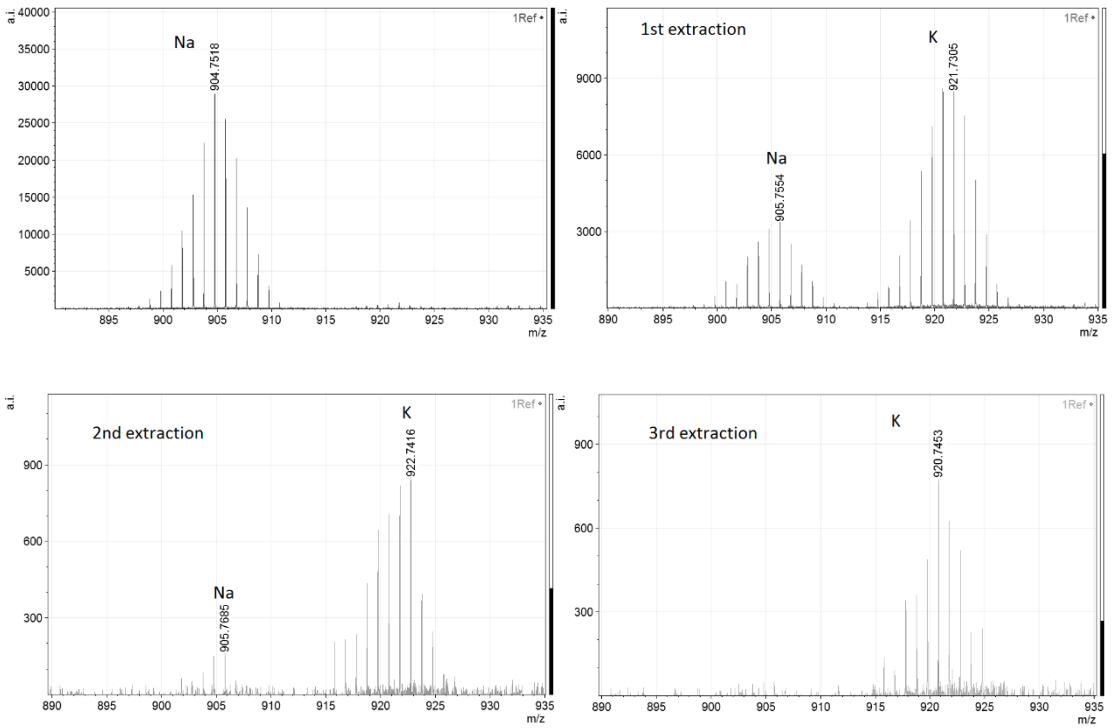

Figure III.S12. MALDI-TOF mass spectra of Na_2[**2**] with three consecutive extractions with 100 times excess of KCl.

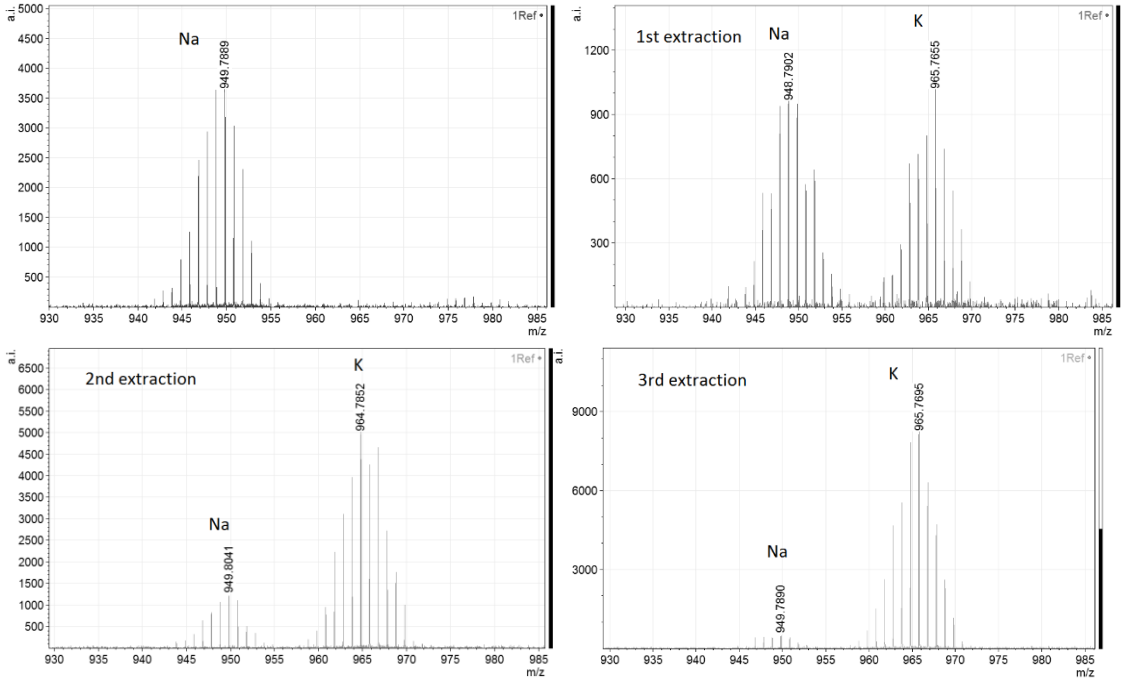

Figure III.S13. MALDI-TOF mass spectra of Na_2[**3**] with three consecutive extractions with 100 times excess of KCl.

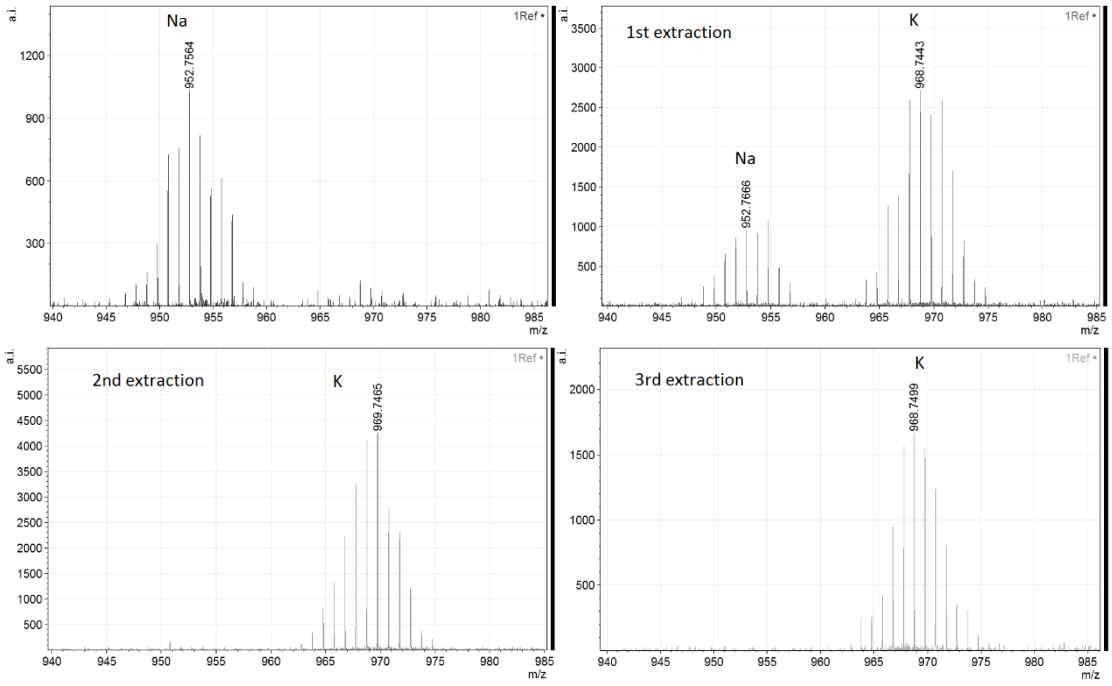

Figure III.S14. MALDI-TOF mass spectra of Na_2[**4**] with three consecutive extractions with 100 times excess of KCl.

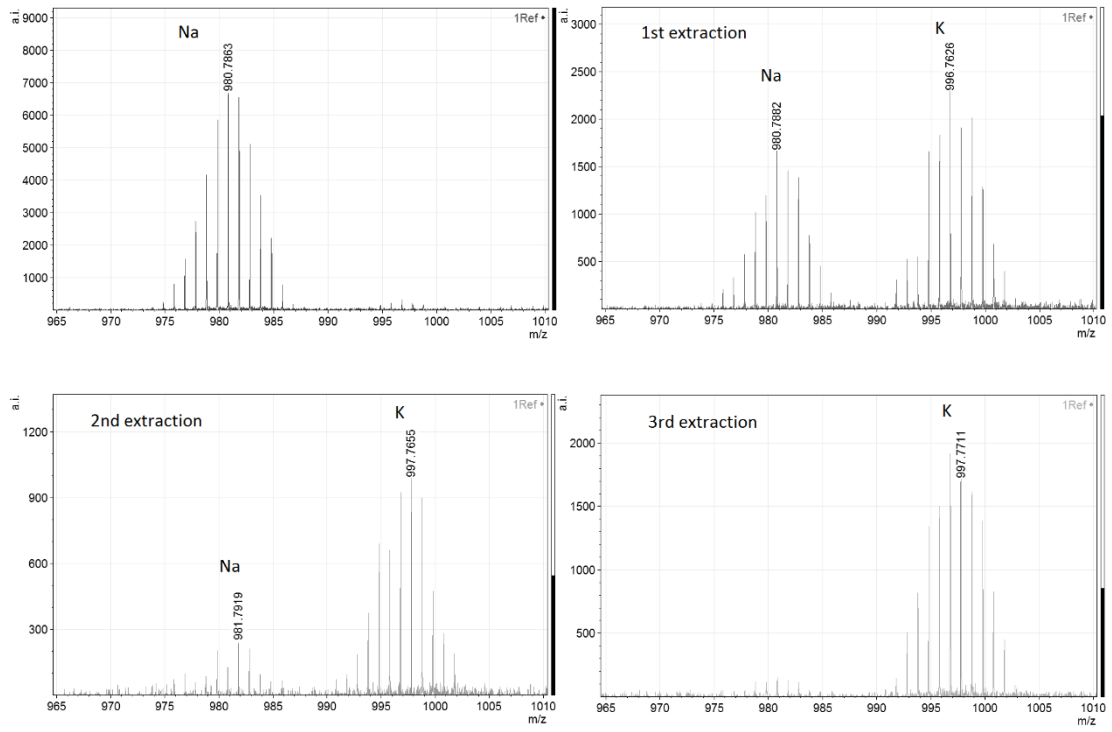

Figure III.S15. MALDI-TOF mass spectra of Na_2[**5**] with three consecutive extractions with 100 times excess of KCl.

ITC experiments

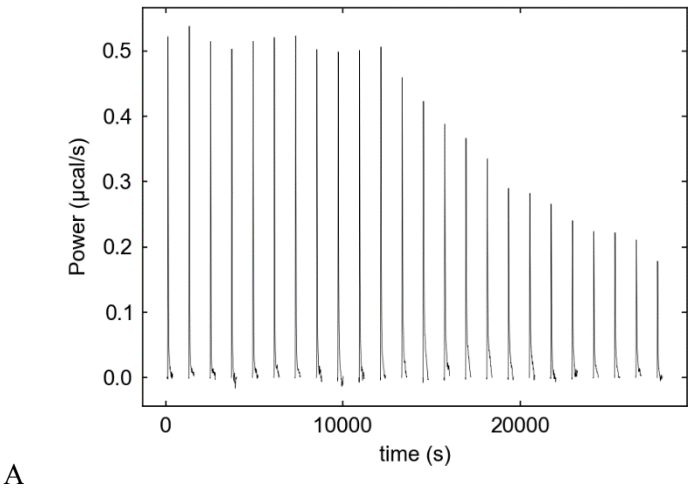

A

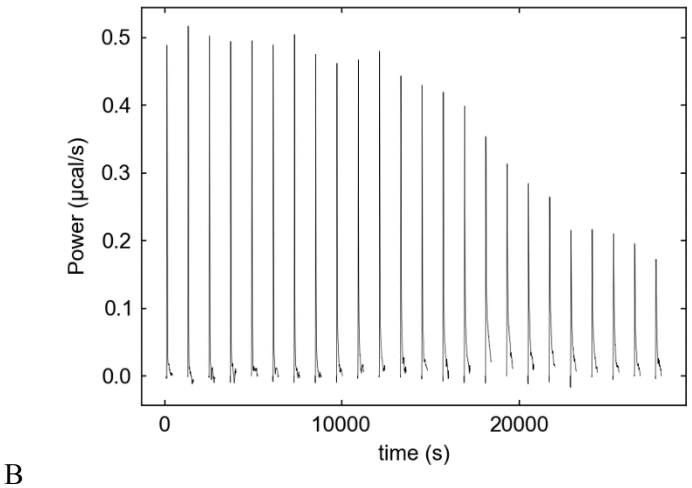

B

Figures III.S16. Raw measured heat changes processed by NITPIC software as a function of time for 16 mM KCl titrated into 1 mM (A) Li_2[**2**] and (B) Na_2[**2**].

Acknowledgements

This work was supported by MICINN (CTQ2010-16237), CSIC (I3P grant to P.G.), MICINN (FPU grant to M.T.) and the Generalitat de Catalunya (2009/SGR/00279). M.T. is enrolled in the PhD program of UAB. P.G. was also enrolled in it. Authors would like to acknowledge financial support of the Grant Agency of the Academy of Sciences of the Czech Republic (IAAX00320901), the Grant Agency of the Czech Republic (P208/12/P236), and long term Research Plans of the Ministry of Education of the Czech Republic (MSM 0021620857).

References

[1] a) M. F. Hawthorne, D. C. Young, T. D. Andrews, D. V. Howe, R. L. Pilling, A. D. Pitts, M. Reintjes, L. F. Warren, P. A. Wegner, *J. Am. Chem. Soc*. **1968**, *90*, 879; b) I. B. Sivaev, V. I.

Bregadze, *Collect. Czeck. Chem. Commun.* **1999**, *64,* 783; c) R. N. Grimes, in *Carboranes*, Academic Press, London, United Kingdom, **2011**.

[2] P. Bauduin, S. Prevost, P. Farràs, F. Teixidor, O. Diat, T. Zemb, *Angew. Chem. Int. Ed.* **2011**, *50*, 5298.

[3] J. Plesek, *Chem. Rev.* **1992**, *92,* 269.

[4] a) P. Rezacova, P. Cigler, P. Matejicek, M. Lepsik, J. Pokorna, B. Gruner, J. Konvalinka, In *Boron Science: New Technologies and Applications*; N. S. Hosmane, Ed., CRC Press, New York, pp. 41-70, **2012**; b) P. Farràs, E.J. Juárez-Pérez, M. Lepsik, F. Luque, R. Núñez, F. Teixidor, *Chem. Soc. Rev*. **2012**, *41*, 3445; c) C. Viñas, M. Tarrés, P. González-Cardoso, P. Farràs, P. Bauduin and F. Teixidor, *Dalton Trans.* **2014**, *43*, 5062.

[5] M. Corsini, F. Fabrizi de Biani, P. Zanello, *Coord. Chem. Rev.* **2006**, *250,* 1351.

[6] a) C. A. Reed, *Acc. Chem. Res.* **1998**, *31*, 133; b) C. A. Reed, K.-C. Kim, R. D. Bolskar, L. J. Mueller, *Science* **2000**, *289*, 101; c) I. Krossing, I. Raabe, *Angew. Chem. Int. Ed.* **2004**, *43*, 2066.

[7] C. Masalles, J. Llop, C. Viñas, F. Teixidor, *Adv. Mater.* **2002**, *14*, 826.

[8] G. Chevrot, R. Schurhammer, G. Wipff, *J. Phys. Chem. B* **2006**, *110*, 9488.

[9] a) P. Matejicek, P. Cigler, K. Prochazka, V. Kral, *Langmuir* **2006**, *22*, 575; b) P. Kubat, K. Lang, P. Cigler, M. Kozisek, P. Matejicek, P. Janda, Z. Zelinger, K. Prochazka, V. Kral, *J. Phys. Chem. B* **2007**, *111*, 4539; c) P. Matejicek, P. Cigler, A. B. Olejniczak, A. Andrysiak, B. Wojtczak, K. Prochazka, Z. Lesnikowski, *Langmuir* **2008**, *24*, 2625.

[10] D. Brusselle, P. Bauduin, L. Girard, A. Zaulet, C. Viñas, F. Teixidor, I. Ly, O. Diat, *Angew. Chem.* **2013**, *52*, 12114.

[11] J. W. Steed, J. L. Atwood, in *Supramolecular chemistry,* 2nd ed., Wiley, Chichester, **2009**.

[12] F. Teixidor, J. Pedrajas, I. Rojo, C. Viñas, R. Kivekäs, R. Sillanpää, I. Sivaev, V. Bregadze, S. Sjöberg, *Organometallics*, **2003**, *22* , 3414.

[13] a) P. Matejicek, J. Zednik, K. Uselova, J. Plestil, J. Fanfrlik, A. Nykanen, J. Ruokolainen, P. Hobza, K. Prochazka, *Macromolecules* **2009**, *42*, 4829; b) M. Uchman, P. Cigler, B. Grüner, K. Prochazka, P. Matejicek, *J. Colloid Interface Sci.* **2010**, *348*, 129; c) P. Matejicek, J. Brus, A. Jigounov, J. Plestil, M. Uchman, K. Prochazka, M. Gradzielski, *Macromolecules* **2011**, *44,* 3847.

[14] P. Farràs, F. Teixidor, R. Kivekäs, R. Sillanpää, C. Viñas, B. Grüner, I. Cisarova, *Inorg. Chem.* **2008**, 47, 9497.

[15] S. Keller, C. Vargas, H. Y. Zhao, G. Piszczek, C. A. Brautigam, P. Schuck, *Anal. Chem.* **2012**, *84*, 5066.

[16] CrysAlisPro, **2013**, Agilent Technologies Ltd, Yarnton, England.

[17] G. M. Sheldrick, *Acta Crystallogr. Sect. A* **2008**, *64*, 112.

[18] A. Altomare, M. C. Burla, M. Camalli, G. L. Cascarano, C. Giacovazzo, A. Guagliardi, A. G. G. Moliterni, G. Polidori, R. Spagna, *J. Appl. Cryst*. **1999**, *32*, 115.

[19] W. T. Pennington, *J. Appl. Crystallogr.***1999**, *32*, 1028.

[20] J. Plesek, K. Base, F. Mares, F. Hanousek, B. Stibr, S. Hermanek, *Collect. Czeck. Chem. Commun.* **1984**, *49,* 2776.

[21] M. Uchman, P. Jurkiewicz, P. Cigler, B. Grüner, M. Hof, K. Prochazka, P. Matejicek, *Langmuir* **2010**, *26*, 6268.

[22] J. Rak, B. Dejlova, H. Lampova, R. Kaplanek, P. Matejicek, P. Cigler, V. Kral, *Mol. Pharmaceutics* **2013**, *10,* 1751.

[23] J. Mendham, R. C. Denney, J. D. Barnes, M. J. K. Thomas, in *Vogel's Quantitative Chemical Analysis,* 6th ed., Prentice Hall, New York, **2000**.

[24] N. R. Dhumal, S. P. Gejji, *Chem. Phys.* **2006**, *323*, 595.

[25] J. Llop, C. Masalles, C. Viñas, F. Teixidor, R. Sillanpää, R. Kivekäs, *Dalton Trans.* **2003**, 556.

[26] P. González-Cardoso, A.-I. Stoica, P. Farras, A. Pepiol, C. Viñas, F. Teixidor, *Chem. Eur. J.* **2010**, *16*, 6660

[27] a) Y. Chao, D. Fu, *J. Biol. Chem.* **2004**, *279*, 17173; b) V. Dordovic, M. Uchman, K. Prochazka, A. Zhigunov, J. Plestil, A. Nykanen, J. Ruokolainen, P. Matejicek, *Macromolecules* **2013**, *46,* 6881; c) M. Uchman, M. Gradzielski, B. Angelov, Z. Tosner, J. Oh, T. Chang, M. Stepanek, K. Prochazka, *Macromolecules* **2013**, *46*, 2172.

[28] a) I. Herrera, M. A. Winnik, *J. Phys. Chem. B* **2013**, *117*, 8659; b) V. H. Le, R. Buscaglia, J. B. Chaires, E. A. Lewis, *Anal. Biochem.* **2013**, *434*, 233.

5.4 Paper IV

Compartmentalization in hybrid metallacarboranes nanoparticles formed by block copolymers with star-like architecture*

Abstract

One strategy to control the morphology of hybrid polymeric nanostructures is the proper selection of macromolecule architecture. We prepared metallacarborane-rich nanoparticles by interaction of doublehydrophilic block copolymers consisting of both poly(2-alkyl-2-oxazoline)s and poly(ethylene oxide) blocks with cobaltabisdicarbollide anion in physiological saline. The inner structure of the hybrid nanoparticles was studied by cryo-TEM, light scattering, SAXS, NMR, and ITC. Although the thermodynamics of diblock and star-like systems are almost identical, the macromolecular architecture has a great impact on the size and inner morphology of the nanoparticles. While hybrid nanoparticles formed by linear diblock copolymers are homogeneous, resembling gel-like nanospheres, the star-like shape of 4-arm block copolymers with PEO blocks in central parts of macromolecules leads to distinct compartmentalization. Because metallacarboranes are promising species in medicine, the studied nanoparticles are important for targeted drug delivery of boron cluster compounds.

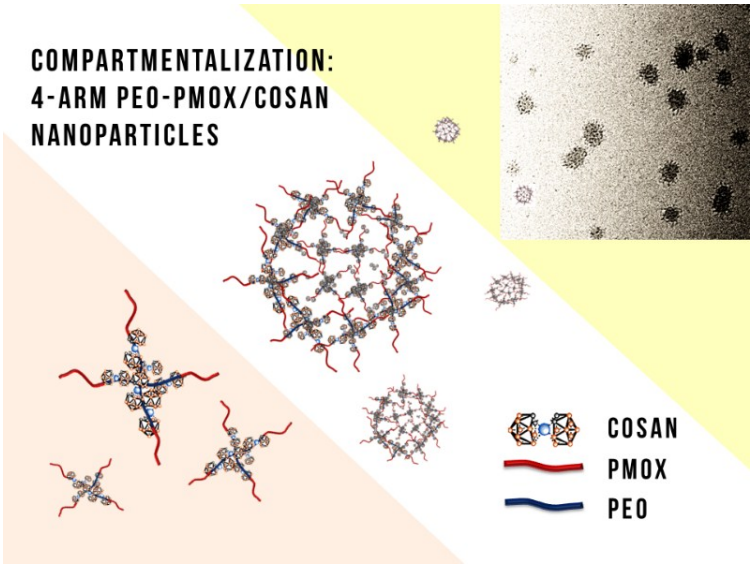

* In slightly modified version published as: Ďorďovič, V.; Uchman, M.; Zhigunov, A.; Nykanen, A.; Ruokolainen, J.; Matějíček, P.: Compartmentalization in Hybrid Metallacarborane Nanoparticles Formed by Block Copolymers with Star-Like Architecture, *ACS Macro Letters* **2014**, *3*, 1151–1155.

Introduction

The preparation of new types of hierarchically organized polymer nanoparticles with specific functions has attracted many researchers[1] because of the utilization of such nanoobjects in medicine and other applications.[2] Due to advanced synthetic techniques, various architectures of amphiphilic block copolymers are now available for the design of nanostructured particles based on direct self-assembly in solution.[1a,j] Another possibility for preparation is the use of nonchemical procedures because the character of complex nanosystems is often kinetically controlled and far from equilibrium.[3] Double-hydrophilic copolymers are particularly interesting, in which the formation of nanostructures is based on interaction with usually low-molecular-weight agents, such as ions with polyelectrolyte blocks (so-called coassembly).[4a−f] Furthermore, the use of coassembling compounds, such as hexacyanocobaltate and hexacyanoferrates, allows the introduction of less common thermodynamic (UCST), photosensitive, or electroactive properties to block copolymer nanostructures.[4g−i]

Recently, we began a systematic study of the coassembly of neutral hydrophilic polymers of poly(ethylene oxide), PEO, and poly(2-alkyl-2-oxazoline)s, POX, with the amphiphilic anion [3-cobalt(III) bis(1,2-dicarbollide)](–1), COSAN.[5] The interaction of COSAN with neutral polymers is unparalleled in macromolecular chemistry and is based on weak dihydrogen bonding between boron cluster compounds and CH_2CH_2 moieties in polymer backbones.[5,6] Metallacarboranes such as salts of COSAN are fully artificial boron-based inorganic compounds[7] that are intensively studied due to their unique properties and interactions, which open new opportunities in nanochemistry.[8]

The PEO homopolymer interacts with Na[COSAN] in NaCl aqueous solutions, and an insoluble nanocomposite with a uniquely organized structure forms as a result.[5b,c] Additionally, POX homopolymers form a complex with COSAN. Because Na^+ is not bound by POX, the complex retains solubility in water.[5e] Despite different solution behaviors, both PEO and PEtOx metallacarborane complexes exhibit very similar interaction energies (see ITC thermograms and further comments in Figure IV.S3 in the Supporting Information, SI). In other words, ITC data suggest that PEO/Na[COSAN] and PEtOx/Na[COSAN] interaction strengths are comparable, and determination of the type of polymer preferred in a mixture would be difficult.

In the case of linear block copolymer poly(ethylene oxide)-*block*-poly(2-ethyl-2-oxazoline), PEO−PEtOx (Figure 2.4), a core/shell structure is expected, with insoluble PEO-complex in the core and water-soluble PEtOx-complex in the micellar shell. Nevertheless, no core/shell micelles have been observed.[5e] Homogeneous gel-like nanospheres with high Na[COSAN] content forms instead. As no preferential complexation with any block occurs, both PEO and PEtOx blocks are intermixed within the nanospheres.

Due to the increasing interest in boron cluster compounds in medical applications (metallacarboranes act as potent inhibitors of HIV protease),[5a] hybrid nanocarriers for targeted drug delivery with well-designed properties are urgently needed. Since nanoparticles of block copolymers used in our previous studies[5] were of quite large dimensions (tens or few hundreds of nanometers), a new concept for the preparation of nanoparticles with controlled size would be very useful. In this paper, we examine nanostructures formed after the addition of Na[COSAN]

to physiological saline aqueous solutions (0.154 M NaCl) of the star-like block copolymer [poly(ethylene oxide)-*block*-poly(2-methyl-2-oxazoline)]$_4$, [PEO−PMeOx]$_4$, which has four arms (Figure 2.4). The results are compared with the previously studied linear PEO−PEtOx[5e] to demonstrate that the polymer architecture has a crucial role in the morphology of hybrid nanoparticles.[9]

Results and discussion

Both block copolymers were characterized by NMR and GPC to support the structures proposed in Figure 2.4 (details on copolymer structure are shown in chapter 2.2.3). Additional results of two other linear block copolymers, PEO−PEtOx(2) and PEtOx−PEO−PEtOx, are presented in chapter 2.2.3 and are fully consistent with all findings discussed in the main text (Figures IV.S3, IV.S4, and IV.S7).

We compare the behavior of block copolymers with PMeOx and PEtOx blocks, assuming that the pendant alkyl group length in POX segments (i.e., methyl and ethyl) has only a minor impact on the interaction with Na[COSAN]. To prove this assumption, we conducted isothermal titration calorimetry, ITC, experiments with PEO−PEtOx and [PEO−PMeOx]$_4$ (Figure IV.S5). Interaction of Na[COSAN] with each copolymer is exothermic and quite similar, indicating that the interaction of PEtOx and PMeOx segments with Na[COSAN] is nearly identical. The saturation point is located slightly above ξ = 0.1 in both cases (ξ is defined as COSAN-to-polymer segment molar ratio, where both PEO and POX segments are taken into account), and the overall "thermodynamics" is in fact the same. Additionally, ITC data for PEO and PEtOx homopolymers (Figure IV.S2) support our claims that the interaction of polymers with metallacarborane occurs mainly via ethylene units of the backbone.

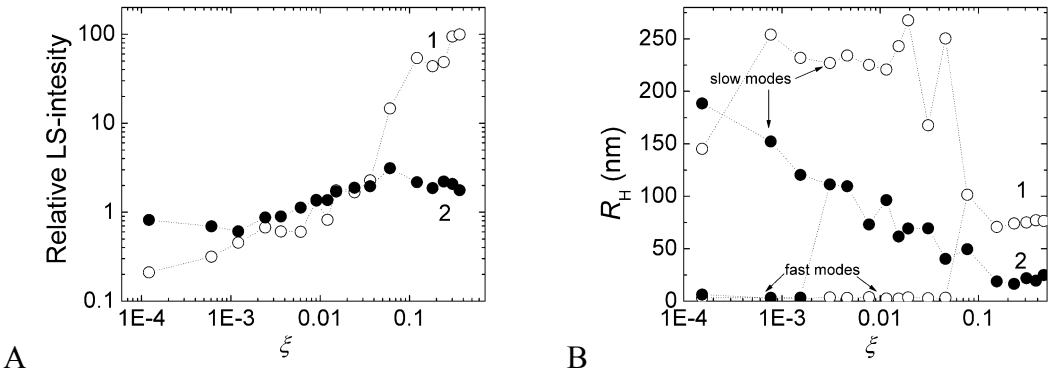

Figure IV.1. Dependence of (A) relative light scattering intensity (related to intensity of pure polymer solutions) and (B) hydrodynamic radius, R_H, on the addition of Na[COSAN] to PEO−PEtOx (hollow circles, curves 1) and [PEO−PMeOx]$_4$ (black circles, curves 2) solutions (2 g/L) in 0.154 M NaCl. In (B) there are slow and fast modes for both samples at low ξ that eventually merge into one. The values of R_H for pure polymer solutions are as follows: 3 and 161 nm for PEO−PEtOx, and 1 and 183 nm for [PEO−PMeOx]$_4$.

We monitored the formation of hybrid nanoparticles during consecutive titrations of [PEO−PMeOx]$_4$ and PEO−PEtOx with Na[COSAN] by means of static and dynamic light

scattering, SLS and DLS. The dependences of (A) relative light scattering intensity and (B) hydrodynamic radius, R_H, on ξ are shown in Figure IV.1. Nanoparticle formation is substantially influenced by copolymer architecture. A diblock copolymer suddenly self assembles into hybrid nanoparticles (R_H approximately 75 nm) at approximately $\xi = 0.1$ by the joining of large and loose preassociates. These large aggregates have also been observed for pure polymer solutions.[5e,10] The process is accompanied by a steep increase in LS intensity, reflecting the saturation of polymeric segments by COSAN and the formation of more compact nanostructures. In the case of star-like copolymers, the "transition" is not as obvious, even though the final step of nanoparticle formation is also observed at approximately $\xi = 0.1$. The resulting nanoparticles are surprisingly fairly small (R_H approximately 20 nm). Further LS results are shown in Figure IV.S3.

The process of immobilization of PEO and POX segments after interaction with COSAN clusters was directly monitored by the diminishing of corresponding signals in ^{1}H NMR spectra (fraction of frozen polymeric segments shown in Figure IV.S6 together with further comments).[5b,d,e] In the PEO-PEtOx system, POX segments are partially frozen, even at low metallacarborane concentration, and both types of segments are substantially immobilized after nanosphere creation at elevated Na[COSAN] concentration (PEO approximately 70%, PEtOx approximately 60%). In contrast, the incorporation of COSAN in the 4-arm system begins in the "central" area of the macromolecule in which PEO-blocks are located, and PEO segments are frozen to a larger extent than POX from early stages of hybrid nanoparticle formation. Clusters of COSAN are thus accumulated in fairly compact domains, surrounded by more flexible POX segments.

As shown above, NMR data at least partially reveal the degree of complexation of Na[COSAN] by both types of block copolymers. Both blocks in linear diblock copolymers are intermixed, as previously discussed.[5e] In the case of star-like block copolymers, the simultaneous interaction of both PEO and POX segments with one bulky metallacarborane cluster is partially restricted due to steric hindrance. Furthermore, the density of PEO segments is fairly high in the central parts of the star, increasing the probability of PEO/Na[COSAN] compartment formation.

Direct proof of our above assumptions is based on the visualization of corresponding nanostructures by cryo-TEM (Figure IV.2). AFM scans and further comments on AFM are included in SI for comparison (Figure IV.S7). While the linear architecture of copolymers leads to homogeneous nanospheres with intermixed PEO and POX segments (Figures IV.2B and IV.S4), the star-like shape manifests itself in the creation of compartments with dimensions of approximately 4 nm (Figure IV.2A). The number of compartments within each nanoparticle is in the range of several tens. In other words, COSAN clusters are not distributed evenly, as in linear diblocks, but are concentrated within the central areas of [PEO−PMeOx]$_4$ starlike macromolecules, glued together by less-compact POX parts, thus, resembling core/shell units. As shown in Figure IV.2, the size distribution of both types of nanoparticles is quite broad. As we have previously observed,[5b,d,e] nanoparticle formation is kinetically controlled. Size

distribution is thus affected by preparation protocol. The inner structure of the nanoparticles, however, remains unchanged.

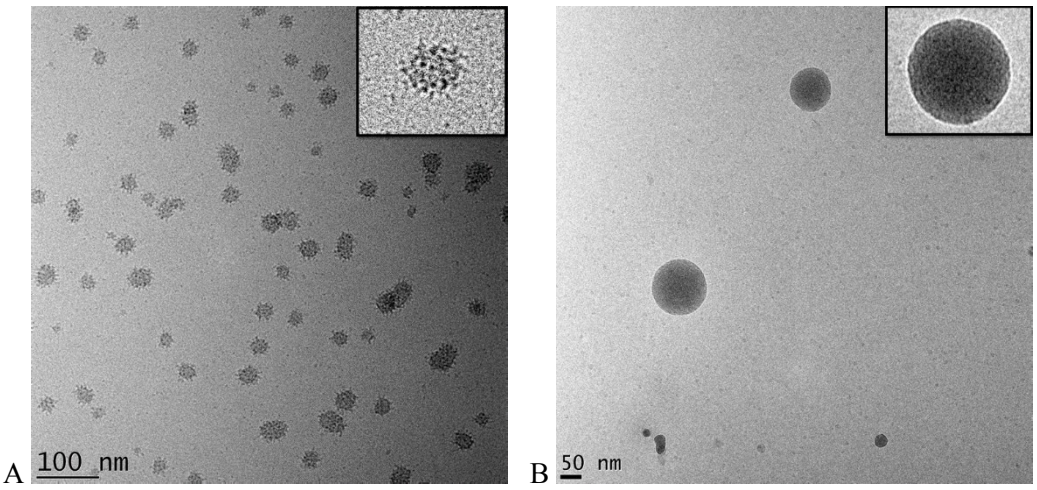

Figure IV.2. Typical cryo-TEM micrographs of (A) [PEO−PMeOx]$_4$/Na[COSAN], with a zoomed view of a compartmentalized nanoparticle, and (B) PEO−PEtOx/Na[COSAN], with a zoomed view of a homogeneous nanosphere, both in 0.154 M NaCl, $\xi = 0.4$.

Based on the proposed structures of both types of nanoparticles, we now seek to determine the types of interaction that keep such nanoparticles in solution. In addition to the role of the large fraction of segments, which are not affected by interactions with metallacarborane and remain mobile and hydrated,[5e] the nanoparticles are stabilized by their negative charge. We conducted electrophoretic light scattering experiments to determine the zeta-potential. In both cases, zeta-potential is approximately –30 mV, which indicates that there is a substantial number of negatively charged POX/COSAN segments in the outer parts of nanoparticles.

Final proof of our assumptions and qualitative characterization of [PEO−PMeOx]$_4$/Na[COSAN] nanoparticles with various ξ was obtained by SAXS and SANS experiments. Here, we will discuss only the selected SAXS results. In Figure IV.3 there are representative SAXS curves of hybrid nanoparticles for star-like (black points) and linear diblock (hollow points) systems. Further information for [PEO−PMeOx]$_4$/Na[COSAN] is given in SI and for PEO−PEtOx/Na[COSAN] in our previous paper.[5e] The most important feature is the presence of a correlation peak at 0.23 Å^{-1} (position not dependent on ξ) for multicompartmentalized nanoparticles that is not present in the case of all studied linear diblocks and triblock (see SAXS section in SI). The peak corresponds to distances between compartments of approximately 3 nm, which is close to the size of nanocompartments visualized by cryo-TEM in Figure IV.2A. The average number of COSAN clusters per polymer star was calculated from the saturation point of the ITC curve to be approximately 80. Assuming this value, we calculated the aggregation number of star-like macromolecules, $N^{agg} = 30$. Thus, metallacarborane clusters are compactly packed within the compartments that are most likely formed by one star-like macromolecule.

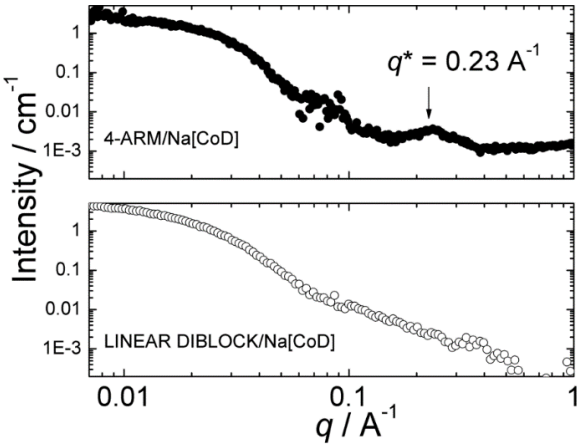

Figure IV.3. SAXS curves of (top) $[PEO{-}PMeOx]_4$/Na[COSAN] and (bottom) PEO−PEtOx/Na[COSAN] nanoparticles in 0.154 M NaCl at $\xi = 0.1$ and 0.15, respectively. The arrow indicates the position of a correlation peak for the star-like system.

Conclusions

In conclusion, we have prepared hybrid metallacarboranes-rich nanoparticles with distinct compartmentalization by the mixing of star-like double-hydrophilic polymer $[PEO{-}PMeOx]_4$ with Na[COSAN] in physiological saline. Each nanoparticle consists of approximately 30 compartments that are formed by one $[PEO{-}PMeOx]_4$ macromolecule with approximately 80 COSAN clusters densely packed within the central parts of the compartment in which PEO segments are located. From our study, we have clearly demonstrated the tuning of hybrid nanoparticle morphology and size by choice of block copolymer architecture, which could be useful in the design of drug delivery vessels. In a subsequent study, we will extend the set of copolymer structures from star-like with POX in the center of macromolecule to stars with higher number of arms and other types of branched copolymers. The influence of alkyl side groups in POX segments on bonding with COSAN should also be examined in detail.

Supporting Information

Interaction of PEO and PEtOx homopolymers with Na[COSAN]

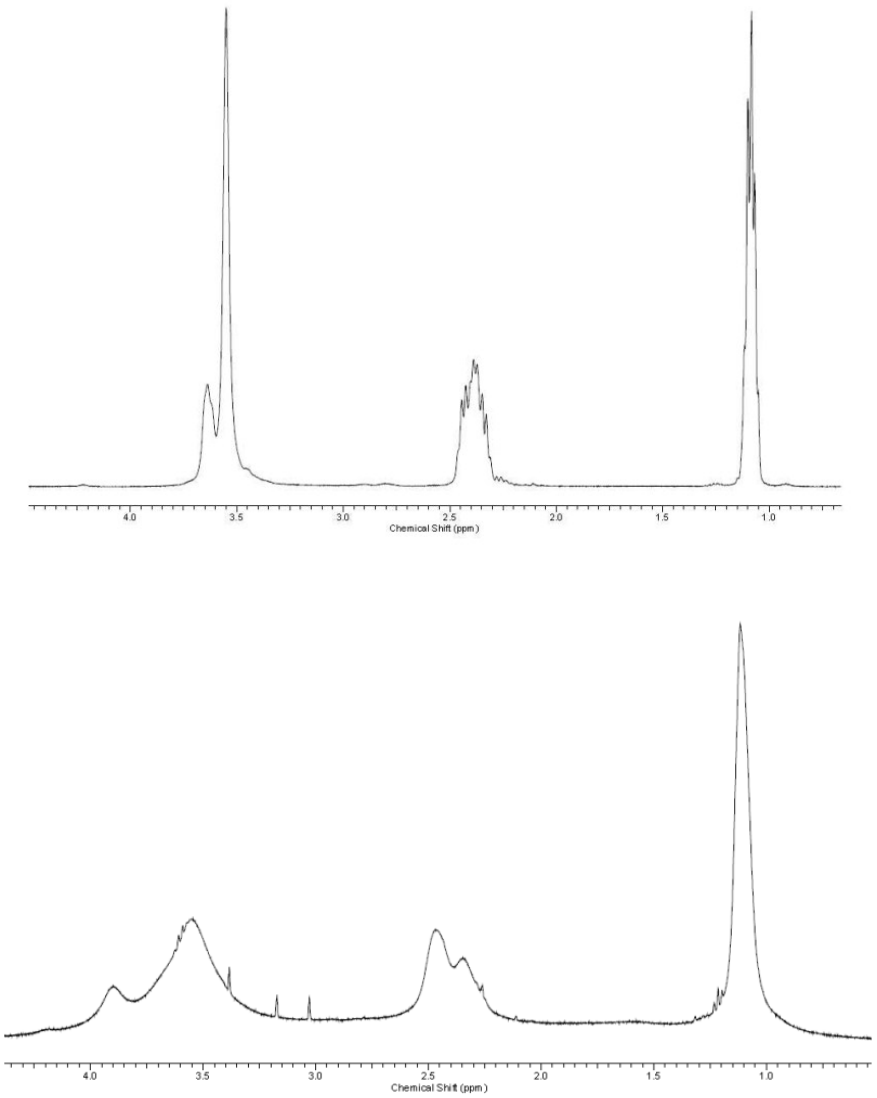

Figure IV.S1. Comparison of ^{1}H NMR spectra of (top) PEtOx homopolymer and (bottom) its metallacarborane complex PEtOx/Na[COSAN] (ξ = 0.11) in heavy water (ethylene backbone around 3.5 ppm; ethyl side group around 2.5 and 1 ppm). Interaction with metallacarboranes leads to distinct broadening mainly of ethylene signals of the backbone.

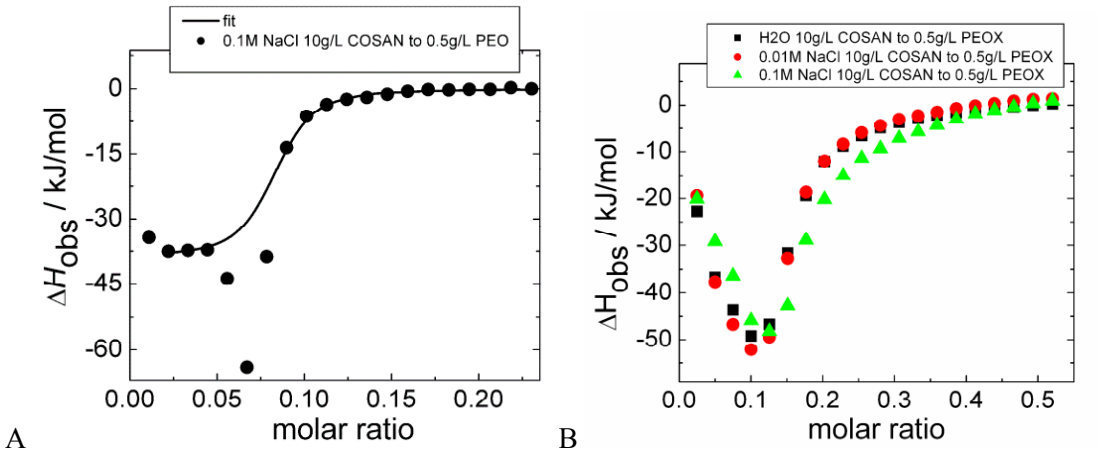

Figure IV.S2. ITC thermograms of (A) PEO homopolymer in water and (B) PEtOx homopolymer in water and NaCl solutions during titration by Na[COSAN] solution. In both cases, the complex formation is strongly exothermic with comparable interaction heats. In the case of PEO, strongly exothermic "aggregation" peak related to formation of highly organized insoluble nanocomposite is observed.

Additional SLS&DLS characterization of nanoparticles

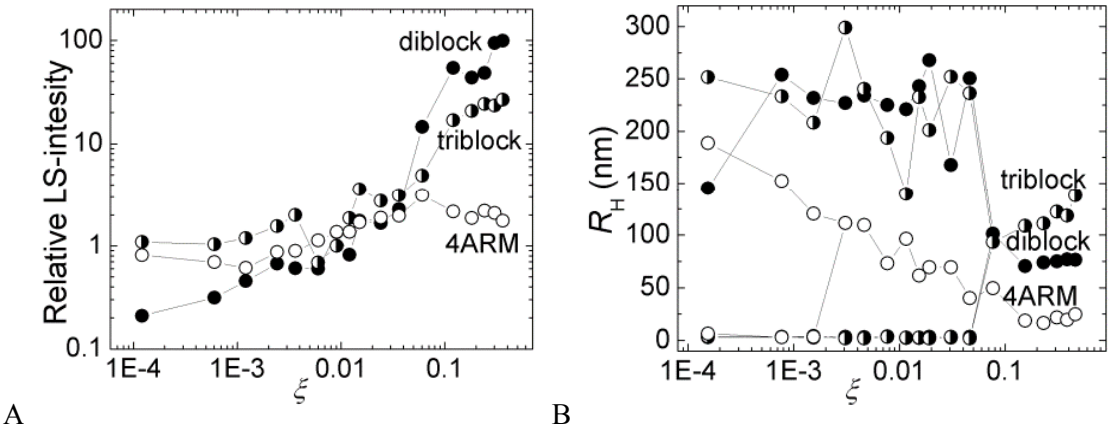

Figure IV.S3. Dependence of (A) relative light scattering intensity and (B) hydrodynamic radius, R_H, on the addition of Na[COSAN] to (diblock) PEO–PEtOx, (triblock) PEtOx–PEO–PEtOx, and (4-arm) $[PEO–PMeOx]_4$ solutions (2 g/L) in 0.154 M NaCl. It is evident that size and formation of nanoparticles formed by triblock copolymer are very similar to those of diblock copolymer, which confirms our assumption that linear architecture of block copolymers leads to similar type of nanoparticles. In both cases, we observed not only larger pre-associates (slow modes), but also very small object (fast modes) with radii 2–3 nm that can be attributed to single chains which can be both free or decorated by COSAN clusters. At certain ξ, the slow modes have been no longer detected for both samples by DLS. They could disappear or their light scattering contribution to the overall signal is too low to be detected.

Additional cryo-TEM characterization of nanoparticles

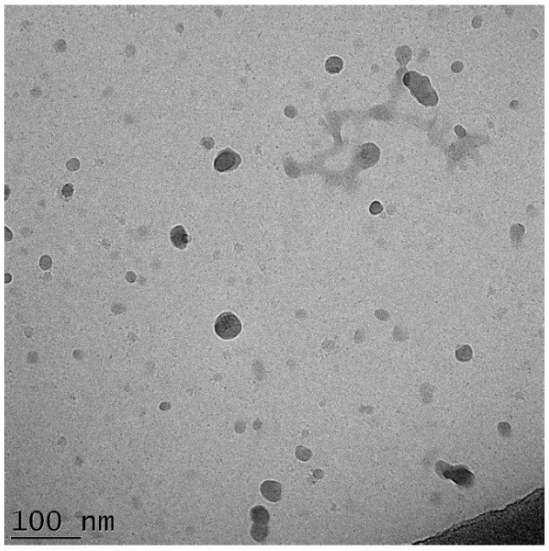

Figure IV.S4 Typical cryo-TEM micrographs of triblock PEtOx–PEO–PEtOx/Na[COSAN] in 0.154 M NaCl, ($\xi = 0.4$). Even though the nanoparticles are not such regular as in the case of PEO–PEtOx/Na[COSAN], they are also homogeneous with no sign of compartmentalization.

ITC characterization of nanoparticles

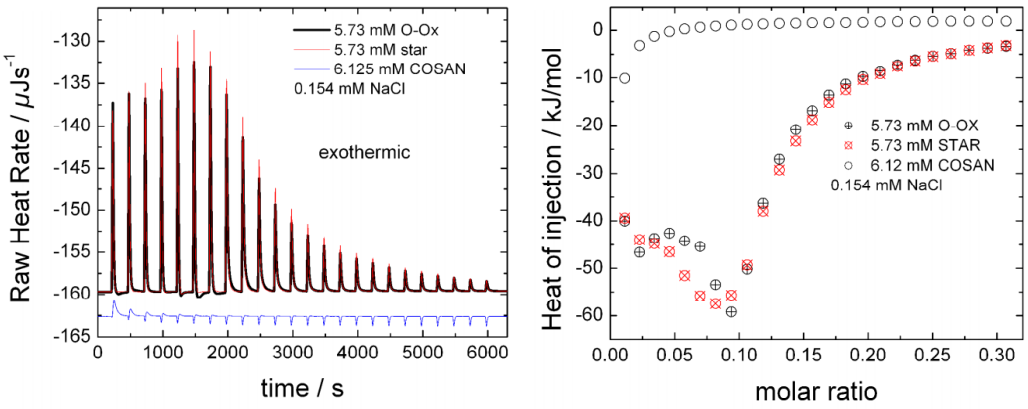

Figure IV.S5. (A) Raw ITC response for 6.125 mM Na[COSAN] titrated into (red) [PEO–PMeOx]$_4$, (black) PEO–PEtOx and (blue) blank solution in 0.154M NaCl. (B) ITC thermograms for 6.125 mM Na[COSAN] titrated into (red) [PEO–PMeOx]$_4$, (black) PEO–PEtOx and (hollow spheres) blank solution in 0.154M NaCl.

Additional information can be obtained from ITC curves (Figure IV.S5B). A slight difference is apparent from the fact that the "peak" at approximately 0.1 is sharper for the linear diblock than in the case of the 4-arm copolymer, resembling the so-called "aggregation peak" previously observed for PEO homopolymers (Figure IV.S2A).[5c,e] This result is consistent with the scenario in which hybrid nanospheres are created by the sudden attraction of originally loose, mobile and randomly intermixed polymeric segments of linear diblock. The formation of

[PEO−PMeOx]$_4$/Na[COSAN] nanoparticles is rather based on the consecutive addition of smaller building blocks, accompanied by an increase of their compactness; no thorough reorganization is necessary.

NMR characterization of nanoparticles

The fraction of frozen segments has been calculated from a diminishing of ^{1}H NMR signal of corresponding units after addition of Na[COSAN]. We took advantage from the well-known fact that the NMR signal decreases and the spectrum is broadened, if the mobility of corresponding moiety is restricted due to the formation of complex with metallacaborane. We added certain amount of an internal standard (*t*-BuOH) to solutions of pure copolymers and to their mixtures with Na[COSAN]. Then we compared ratios of all the copolymers signals to *t*-BuOH signal (1.25 ppm) in solutions with and without Na[COSAN]. From the obtained ratios we calculated fraction of "frozen segments", which are equal to number of segments involved in complexation with metallacarboranes. Further comments can be found in ref. 5e.

The following signals were examined in ^{1}H NMR spectra (Figure 2.5) of PEO–PEtOx and [PEO–PMeOx]$_4$: ethylene moieties in PEO (3.7 ppm) and POX backbones (3.65–3.4 ppm); methylene (2.4 ppm) and methyl (1.1 ppm) moieties of ethyl side group in PEtOx; methyl side group (2.1 ppm) in PMeOx. In general, we found that the mobility of backbone is the most restricted as compared to side groups. Both signals from ethyl side-group are almost equally restricted (the numbers shown in the graph are averages from both signals).

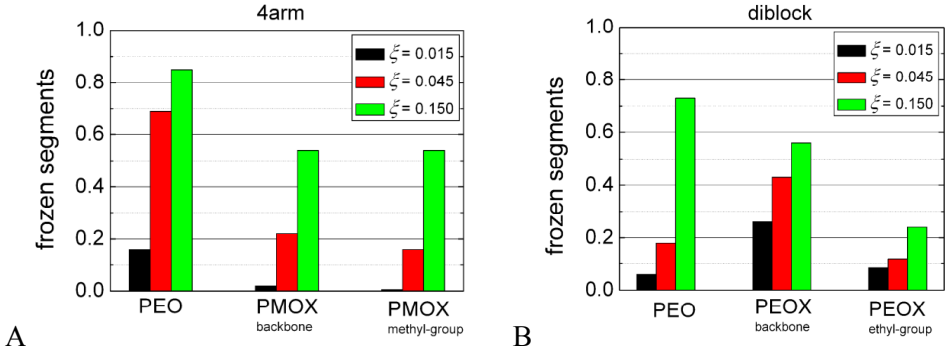

Figure IV.S6. Fraction of frozen polymeric segments in (A) [PEO–PMeOx]$_4$/Na[COSAN] and (B) PEO–PEtOx/Na[COSAN] (right) differing in Na[COSAN] content in 0.154 M NaCl calculated from a decrease of corresponding ^{1}H NMR signals related to pure PEO–PEtOx and *t*-BuOH (internal standard).

AFM imaging of nanoparticles

Samples for AFM were prepared by dip coating of very dilute (around 0.01 g/L) nanoparticle aqueous dispersions on freshly cleaved mica surface followed by evaporation of water in vacuum oven. [PEO–PMeOx]$_4$/Na[COSAN], PEO–PEtOx/Na[COSAN] and PEO–PEO–PEtOx/Na[COSAN] nanoparticles were visualized by AFM in tapping mode (Figures IV.S2A, B, and C respectively). They are of a round shape with no evidence of compartmentalization for [PEO–PMeOx]$_4$/Na[COSAN] (in topology as well as in phase image) due to a broadening effect

of AFM probe, a similar stiffness of PEO/Na[COSAN] and POX/Na[COSAN] domains and mainly the fact that the size of compartments revealed by other methods (cryo-TEM and SAXS) is far below the AFM resolution. However, the section analysis of the nanoparticles (Figure IV.S2C) reveals that [PEO–PMeOx]$_4$/Na[COSAN] nanoparticles adopt a more pronounced pancake shape on the mica surface as compared to both PEO–PEtOx/Na[COSAN] and PEO–PEO–PEtOx/Na[COSAN] nanoparticles, which are more round and compact.

We know from our previous research[13] that the size distribution of micelles in solution is strongly correlated with that one on a mica surface after the solvent evaporation. The shape of nanoparticles visualized by AFM is considerably deformed due to the broadening effect of AFM probe and drying on the mica surface. We assume that the extent of deformation is substantially influenced by the particle morphology and density. We therefore assume that homogeneous nanoparticles without compartmentalization suffer from a deformation on mica surface to a lesser extent than those with small compartments glued together by loose POX/Na[COSAN] segments. It indicates that PEO–PEtOx/Na[COSAN] forms homogeneous nanoparticles, while [PEO–PMeOx]$_4$/Na[COSAN] nanostructures are more loose and compartmentalized.

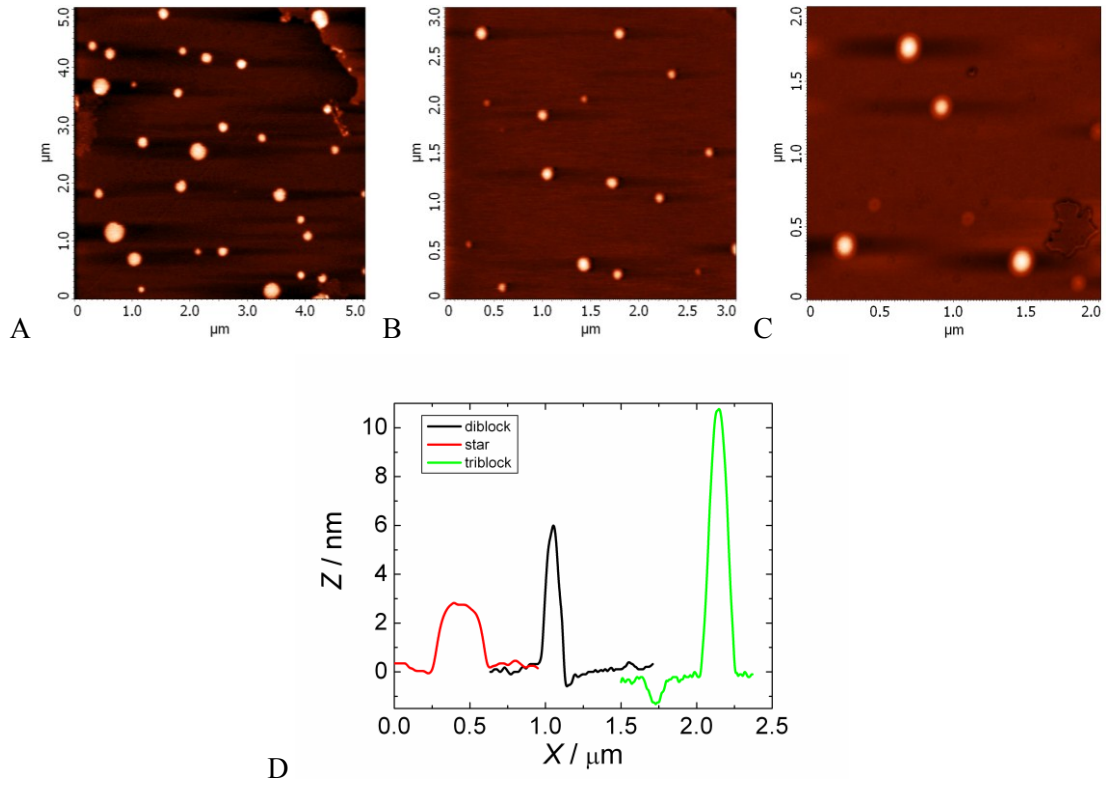

Figure IV.S7. Typical AFM scans of (A) star [PEO–PMeOx]$_4$/Na[COSAN]; (B) diblock PEO−PEtOx/Na[COSAN]; and (C) triblock PEtOx–PEO–PEtOx/Na[COSAN] nanoparticles in 0.154 M NaCl (ξ = ca. 0.2) deposited on a flat mica surface; (D) Cross-sectional analysis of micelles in (A), (B) and (C).

SAXS and SANS characterization of nanoparticles

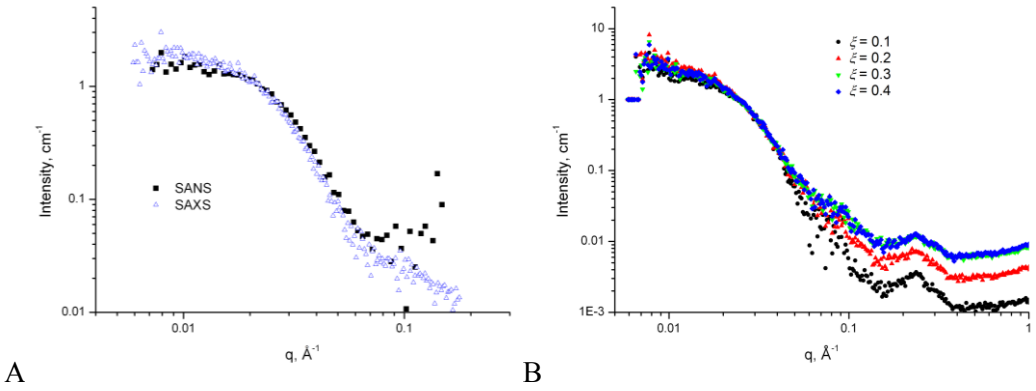

Figure IV.S8. (A) Comparison of SAXS and SANS curves for [PEO–PMeOx]$_4$/Na[COSAN] with concentration of polymer ca. 2 g/L and ξ = 0.4 in 0.154 M NaCl. (B) SAXS curves for [PEO−PMeOx]$_4$/Na[COSAN] in 0.154 M NaCl with concentration of polymer 10 g/L and ξ in the range 0.1–0.4.

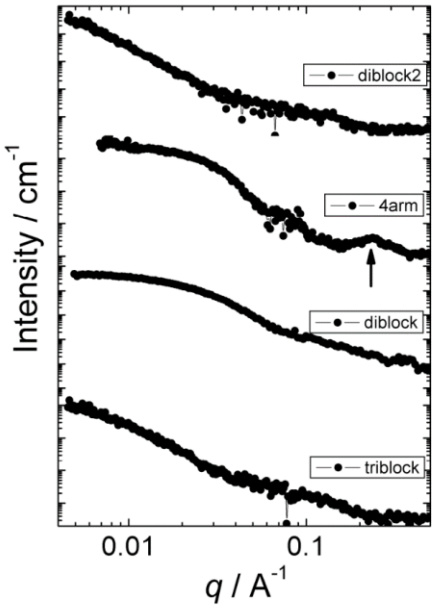

Figure IV.S9. Comparison of SAXS curves for (diblock2) PEO–PEtOx(2)/Na[COSAN], (4arm) [PEO−PMeOx]$_4$/Na[COSAN], (diblock) PEO–PEtOx/Na[COSAN], and (triblock) PEtOx−PEO−PEtOx/Na[COSAN] nanoparticles in 0.154 M NaCl with c ~ 10 g/L and ξ ~ 0.1. Only 4-arm nanoparticles show correlation peak assigned to compartments (indicated by arrow); all samples of linear copolymers have not any inner organized structure.

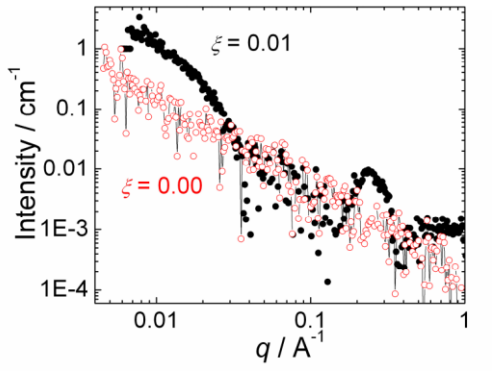

Figure IV.S10. SAXS curves for pure star-like copolymer [PEO–PMeOx]$_4$ and [PEO−PMeOx]$_4$/Na[COSAN] with very low ξ (0.01) in 0.154 M NaCl with concentration of polymer ca. 10 g/L. While pure copolymer is molecularly dissolved, appearance of correlation peak at q = 0.23 Å^{-1} indicates that the PEO/Na[COSAN] compartments form even at very low Na[COSAN] content (compare with NMR data in Figure IV.S6A).

Acknowledgments

The authors would like to acknowledge the financial support of the Grant Agency of the Czech Republic P205/14–14608S and P208/12/P236 and the Grant Agency of Charles University GAUK 512214. The authors thank Olga Trhlikova and Milos Netopilik from IMC Prague, as well as David Vrbata and Radoslava Sivkova from CU Prague, for the characterization of the block copolymers.

References

[1] (a) Zhang, L.; Eisenberg, A. *Science* **1995**, *268*, 1728. (b) Forster, S.; Zisenis, M.; Wenz, E.; Antonietti, M. *J. Chem. Phys.* **1996**, *104*, 9956. (c) Won, Y. Y.; Davis, H. T.; Bates, F. S. *Science* **1999**, *283*, 960. (d) Lodge, T. P.; Rasdal, A.; Li, Z.; Hillmyer, M. A. *J. Am. Chem. Soc.* **2005**, *127*, 17608. (e) Lutz, J. F.; Laschewsky, A. *Macromol. Chem. Phys.* **2005**, *206*, 813. (f) Laschewsky, A. *Curr. Opin. Colloid Interface Sci*. **2003**, *8*, 274. (g) Li, Z. B.; Hillmyer, M. A.; Lodge, T. P. *Macromolecules* **2006**, *39*, 765. (h) LoPresti, C.; Lomas, H.; Massignani, M.; Smart, T.; Battaglia, G. *J. Mater. Chem*. **2009**, *19*, 3576. (i) Li, Z. B.; Kesselman, E.; Talmon, Y.; Hillmyer, M. A.; Lodge, T. P. *Science* **2004**, *306*, 98. (j) Warren, N. J.; Armes, S. P. *J. Am. Chem. Soc*. **2014**, *136*, 10174. (k) Uchman, M.; Stepanek, M.; Prochazka, K.; Mountrichas, G.; Pispas, S.; Voets, I. K.; Walther, A. *Macromolecules* **2009**, *42*, 5605. (l) Matejicek, P.; Uchman, M.; Lokajova, J.; Stepanek, M.; Prochazka, K.; Spirkova, M. *J. Phys. Chem. B* **2007**, *111*, 8394.

[2] (a) MacKay, J. A.; Chen, M.; McDaniel, J. R.; Liu, W.; Simnick, A. J.; Chilkoti, A. *Nat. Mater.* **2009**, *8*, 993. (b) Cheng, R.; Feng, F.; Meng, F.; Deng, C.; Feijen, J.; Zhong, Z. Y. *J. Controlled Release* **2011**, *152*, 2. (c) Peters, R. J. R. W.; Marguet, M.; Marais, S.; Fraaije, M. W.; van Hest, J. C. M.; Lecommandoux, S. *Angew. Chem., Int. Ed.* **2014**, *53*, 146. (d) Hruby, M.; Filippov, S. K.; Panek, J.; Novakova, M.; Mackova, H.; Kucka, J.; Vetvicka, D.; Ulbrich, K. *Macromol. Biosci.* **2010**, *10*, 916. (e) Yih, T. C.; Al-Fandi, M. J. Cell. *Biochem*. **2006**, *97*, 1184.

[3] Hayward, R. C.; Pochan, D. J. *Macromolecules* **2010**, *43*, 3577.

[4] (a) Voets, I. K.; de Keizer, A.; Stuart, M. A. C. *Adv. Colloid Interface Sci*. **2009**, *147*, 300. (b) Zhong, S.; Cui, H. G.; Chen, Z. Y.; Wooley, K. L.; Pochan, D. *J. Soft Matter* **2008**, *4*, 90. (c)

Lindhoud, S.; de Vries, R.; Schweins, R.; Stuart, M. A. C.; Norde, W. *Soft Matter* **2009**, *5*, 242. (d) Uchman, M.; Prochazka, K.; Gatsouli, K.; Pispas, S.; Spirkova, M. *Colloid Polym. Sci*. **2011**, *289*, 1045. (e) Uchman, M.; Gradzielski, M.; Angelov, B.; Tosner, Z.; Oh, J.; Chang, T.; Stepanek, M.; Prochazka, K. *Macromolecules* **2013**, *46*, 2172. (f) Uchman, M.; Stepanek, M.; Prevost, S.; Angelov, B.; Bednar, J.; Appavou, M. S.; Gradzielski, M.; Prochazka, K. *Macromolecules* **2012**, *45*, 6471. (g) Zhang, Q.; Hong, J. D.; Hoogenboom, R. *Polym. Chem*. **2013**, *4*, 4322. (h) Plamper, F. A.; Murtomaki, L.; Walther, A.; Kontturi, K.; Tenhu, H. *Macromolecules* **2009**, *42*, 7254. (i) Plamper, F. A.; McKee, J. R.; Laukkanen, A.; Nykanen, A.; Walther, A.; Ruokolainen, J.; Aeyev, V.; Tenhu, H. *Soft Matter* **2009**, *5*, 1812.

[5] (a) Rezacova, P.; Cigler, P.; Matejicek, P.; Lepsik, M.; Pokorna, J.; Gruner, B.; Konvalinka, J. Medicinal Application of Carboranes: Inhibition of HIV Protease. In *Boron Science: New Technologies and Applications*; Hosmane, N. S., Ed.; CRC Press: New York, 2012; pp 41-70. (b) Matejicek, P.; Zednik, J.; Uselova, K.; Plestil, J.; Fanfrlik, J.; Nykanen, A.; Ruokolainen, J.; Hobza, P.; Prochazka, K. *Macromolecules* **2009**, *42*, 4829. (c) Matejicek, P.; Brus, J.; Jigounov, A.; Plestil, J.; Uchman, M.; Prochazka, K.; Gradzielski, M. *Macromolecules* **2011**, *44*, 3847. (d) Uchman, M.; Cigler, P.; Gruner, B.; Prochazka, K.; Matejicek, P. *J. Colloid Interface Sci.* **2010**, *348*, 129. (e) Dordovic, V.; Uchman, M.; Prochazka, K.; Zhigunov, A.; Plestil, J.; Nykanen, A.; Ruokolainen, J.; Matejicek, P. *Macromolecules* **2013**, *46*, 6881.

[6] Farras, P.; Juarez-Perez, E. J.; Lepsik, M.; Luque, F.; Nunez, R.; Teixidor, F. *Chem. Soc. Rev*. **2012**, *41*, 3445.

[7] (a) Hawthorne, M. F.; Young, D. C.; Wegner, P. A. *J. Am. Chem. Soc*. **1965**, *87*, 1818. (b) Plesek, *J. Chem. Rev*. **1992**, *92*, 269. (c) Grimes, R. N. *Coord. Chem. Rev*. **2000**, *200*, 773. (d) Sivaev, I. B.; Bregadze, V. I. *Collect. Czech. Chem. Commun*. **1999**, *64*, 783. (e) Sivaev, I. B.; Bregadze, V. V. *Eur. J. Inorg. Chem*. **2009**, *11*, 1433.

[8] (a) Planas, J. G.; Vinas, C.; Teixidor, F.; Comas-Vives, A.; Ujaque, G.; Lledos, A.; Light, M. E.; Hursthouse, M. B. *J. Am. Chem. Soc.* **2005**, *127*, 15976. (b) Grimes, R. N. *Mol. Cryst. Liq. Cryst*. **2000**, *342*, 7. (c) Khattar, R.; Knobler, C. B.; Hawthorne, M. F. *Inorg. Chem*. **1990**, *29*, 2191. (d) Malic, N.; Nichols, P. J.; Raston, C. L. *Chem. Commun*. **2002**, *1*, 16. (e) Farras, P.; Teixidor, F.; Kivekas, R.; Sillanpaa, R.; Vinas, C.; Gruner, B.; Cisarova, I. *Inorg. Chem*. **2008**, *47*, 9497. (f) Juarez-Perez, E. J.; Vinas, C.; Teixidor, F.; Santillan, R.; Farfan, N.; Abreu, A.; Yepez, R.; Nunez, R. *Macromolecules* **2010**, *43*, 150. (g) Dash, B. P.; Satapathy, R.; Maguire, J. A.; Hosmane, N. S. *Organometallics* **2010**, *29*, 5230. (h) Planas, J. G.; Teixidor, F.; Vinas, C.; Light, M. E.; Hursthouse, M. B. *Chem.–Eur. J.* **2007**, *13*, 2493. (i) Juarez-Perez, E. J.; Granier, M.; Vinas, C.; Mutin, H.; Nunez, R. *Chem.–Asian J*. **2012**, *7*, 277. (j) Tarres, M.; Vinas, C.; Gonzalez-Cardoso, P.; Hanninen, M. M.; Sillanpaa, R.; Dordovic, V.; Uchman, M.; Teixidor, F.; Matejicek, P. *Chem.–Eur. J*. **2014**, *20*, 6786. (k) Farras, P.; Escudero-Adan, E. C.; Vinas, C.; Teixidor, F. *Inorg. Chem*. **2014**, *53*, 8654. (l) Juarez-Perez, E. J.; Mutin, H.; Granier, M.; Teixidor, F.; Nunez, R. *Langmuir* **2010**, *26* (14), 12185. (m) Nunez, R.; Juarez Perez, E. J.; Teixidor, F.; Santillan, R.; Farfan, N.; Abreu, A.; Yepez, R.; Vinas, C. *Inorg. Chem.* **2010**, *49*, 9993.

[9] (a) Xu, J.; Zubarev, E. R. *Angew. Chem., Int. Ed*. **2004**, *43*, 5491. (b) Lin, Y. A.; Ou, Y. C.; Cheetham, A. G.; Cui, H. G. *ACS Macro Lett.* **2013**, *2*, 1088. (c) Pergushov, D. V.; Babin, I. A.; Zezin, A. B.; Muller, A. H. E. *Polym. Int*. **2013**, *62*, 13. (d) Steinschulte, A. A.; Schulte, B.; Erberich, M.; Borisov, O. V.; Plamper, F. A. *ACS Macro Lett.* **2012**, *1*, 504. (e) Li, Z. B.; Hillmyer, M. A.; Lodge, T. P. *Nano Lett.* **2006**, *6*, 1245. (f) Stepanek, M.; Uchman, M.; Prochazka, K. *Polymer* **2009**, *50*, 3638.

[10] Casse, O.; Shkilnyy, A.; Linders, J.; Mayer, C.; Haussinger, D.; Volkel, A.; Thunemann, A. F.; Dimova, R.; Colfen, H.; Meier, W.; Schlaad, H.; Taubert, A. *Macromolecules* **2012**, *45*, 4772.

[11] Plesek, J.; Base, K.; Mares, F.; Hanousek, F.; Stibr, B.; Hermanek, S. *Collect. Czech. Chem. Commun.* **1984**, *49*, 2776.

[12] Kuklin, A. I.; Islamov, A. Kh.; Gordeliy *Neutron News* **2005**, *16* (3), 16-18.

[13] Matejicek, P.; Stepanek, M.; Uchman, M.; Prochazka, K.; Spirkova, M. *Collect. Czech. Chem. Commun.* **2006**, *71*, 723.

5.5 Paper V

Cation-sensitive compartmentalization in metallacarborane containing polymer nanoparticles*

Abstract

Alkaline cations (Li^+, Na^+ and K^+) are introduced as agents suitable to control compartmentalization in metallacarborane-rich nanoparticles of double-hydrophilic block copolymer poly(ethylene oxide)-*block*-poly(2-alkyl-2-oxazoline), PEO–POX. Interaction of the metallacarborane (cobalt bis(dicarbollide) anion) with PEO–POX is based mainly on dihydrogen bonding between metallacarborane boron clusters and the polymer backbone resulting in compact nanoparticles. However, the cations are a crucial factor as to whether interaction with PEO or POX segments is preferred. Changes in the bulk concentration of alkaline cations can thus provoke changes in the inner structure of polymeric nanoparticles, which is accompanied by exchange of boron clusters and alkaline cations like Li^+. Because of the biomedical importance of metallacarboranes, their conjugates and also lithium salts, the hybrid nanoparticles can act as stimuli-responsive systems for drug delivery.

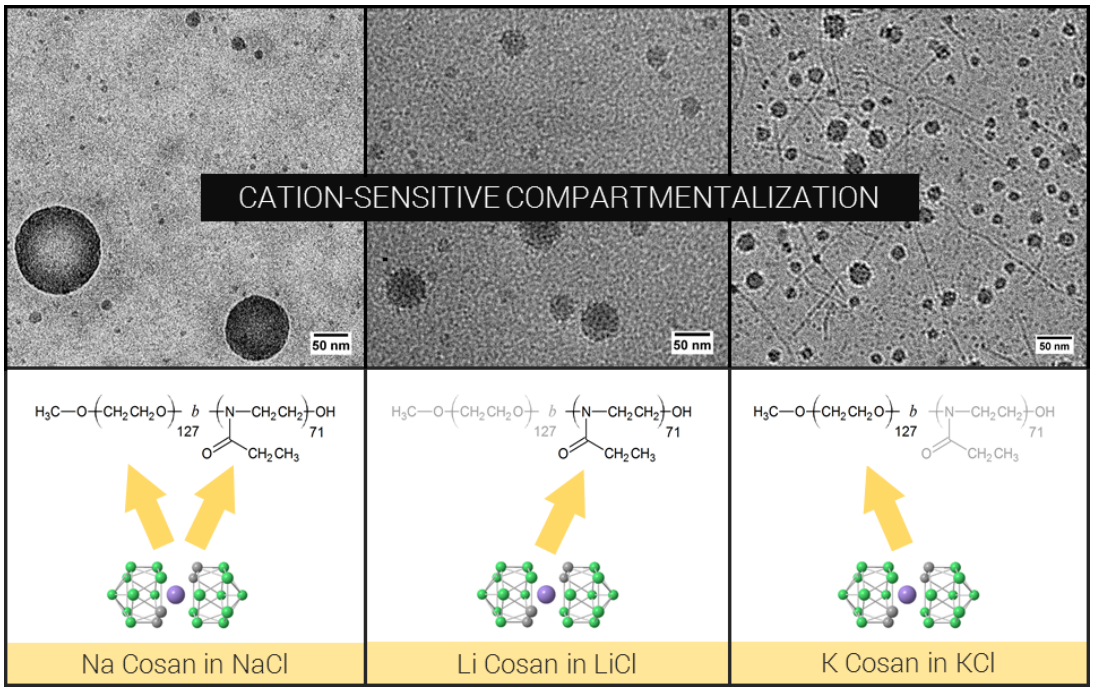

* In slightly modified version published as: Ďorďovič, V.; Uchman, M.; Reza, M.; Ruokolainen, J.; Zhigunov, A.; Ivankov, O.; Matějíček, P.: Cation-Sensitive Compartmentalization in Metallacarborane Containing Polymer Nanoparticles. *RSC Advances* **2016**, *6*, 9884–9892.

Introduction

Boron cluster compounds are boron-rich molecules of polyhedral geometry with the majority of vertices consisting of B–H units. Metallacarboranes, like cobalt bis(dicarbollide) anion, COSAN, (Figure 2.1) belong to this family, and they are extensively studied due to their stability and interesting properties.[1–4] They are considered as hydrophobic but water-soluble anions. It was demonstrated that they provide an unusual interaction potential resulting in self-assembly in solution[5,6] and complexation with various nanosystems.[7–25] They are utilized, for example, for ion extraction[26] and recently also in medicinal chemistry.[27–38] As regards medical applications, our interest is targeted to the preparation of stimuli-responsive hybrid nanosystems consisting of a nano-organized polymer matrix with embedded metallacarborane clusters,[39–42] which would lead to biocompatible vessels for drug-delivery purposes.[43–52] The importance of boron clusters is strengthened by the fact that some of their exoskeletal derivatives exhibit inhibition activity against enzymes like HIV protease and carbonic anhydrase.[31,38] After conjugation with biologically active molecules like nucleosides, DNA and cholesterol,[30,53–55] they can also act as their carriers.

Recently, we described the first type of unique nanostructures based on the complexation of hydrophilic poly(ethylene oxide), PEO, with water-soluble Na[COSAN] resulting in an insoluble nanocomposite.[39] This phenomenon can be used for the preparation of micelles with PEO block in the core.[39,40] The main driving force for COSAN complexation with polymers is dihydrogen bonding of the slightly hydridic B–H vertices with the ethylene subunits of the PEO chain and with polymers consisting of a similar motif such as poly(2-alkyl-2-oxazoline)s, POX. However, the POX/metallacarborane complex is water soluble while the PEO-complex is not.[41,42] The reason is that the Na^+ cation is not complexed by the amidic moiety in POX, but it interacts with oxy-groups in the case of PEO.[11,12] It was also reported that PEO/metallacarborane nanocomposite precipitation is significantly less pronounced in LiCl solution than it is in NaCl and KCl.[39] Further, we found that the short PEO linker spanning two metallacarborane clusters has an impact on their solution behavior because the cations can bind on the linker and other places of the molecule.[56] It is known that PEO chains form helical structures stabilized by the complexed cations, where K^+ has the highest affinity.[57] Furthermore, it was reported that interaction of cations with the amidic group is also selective.[58–60] This indicates that both POE and POX segments have a propensity to exhibit cation selectivity.

The above mentioned results initiated our deeper interest on the cation sensitivity of polymer/metallacarborane complexes. In this communication, our aim is to prepare polymeric nanostructures capable of exchanging bio-active metallacarboranes and cations. We used biocompatible and double-hydrophilic linear block copolymer poly(ethylene oxide)-*block*-poly(2-ethyl-2-oxazoline), PEO–PEtOx, and star-like block copolymer [poly(ethylene oxide)-*block*-poly(2-methyl-2-oxazoline)]$_4$, [PEO–PMeOx]$_4$ (Figure 2.4) as in our previous reports.[40,41] We used cryo-TEM imaging and NMR spectroscopy in order to reveal the impact of alkaline cations on the compartmentalization within the hybrid nanoparticles. Isothermal titration calorimetry, ITC, was found to be a suitable method for monitoring of cation and metallacarborane exchange after an external stimulus was applied (addition of cation).

Compartmentalization in polymeric nanosystems and the controlled formation of hierarchically organized nanostructures currently belongs to the extensively studied field of macromolecular nanochemistry.[61–76] The formation of distinct compartments is usually induced by a hydrophobic effect and a non-compatibility of the building blocks.[61] Temperature and electrochemical processes also act as stimuli leading to the formation of nanostructures.[75,76] Another possibility is the coassembly of polymers with low molecular mass compounds.[69,70]

Self- and co-assembly induced by inorganic salts have been studied mainly for the preparation of quantum dots (such as those formed by cadmium or lanthanides),[77,78] ferrofluids,[79] or for the delivery of metals like cisplatin for biomedical applications[80–82] and for the extraction of mercury.[83] Controlled drug release was described for hybrid polymer/silica nanoparticles after exchange of Zn^{2+} by H^{+} ions.[84] Ion-sensitive resins (both cationic and anionic) and other polymers sensitive to external stimuli (temperature, hydration, salting-out effect, etc.) are used for counterion-responsive drug release during digestion in the human body.[81]

As concerns the controlled release of physiologically active LiCl, there are two approaches in the literature: polyelectrolyte hydrogels (e.g., based on amino acid residues)[82] and current-controlled drug release from PEO-based electrolytes containing LiCl via iontophoresis.[85] Our system based on PEO–POX/metallacarborane nanoparticles can be thus considered as a third way for the delivery of alkaline cations with benefits such as the presence of bio-active boron cluster compounds.

Results and discussion

Structure of PEO–POX/metallacarborane nanoparticles in LiCl, NaCl and KCl

In our previous work, we already described several polymeric nanosystems based on mutual interaction of hydrophilic polymers with metallacarboranes like sodium cobalt bis(dicarbollide), Na[COSAN], all of them exhibiting a unique inner structure:[11,12,39–42] diblock copolymers with one block not interacting with COSAN but the second one (PEO-block) forming an insoluble complex with COSAN form micelles with PEO-block in the micellar core. The metallacarboranes and their bio-active conjugates are embedded within the PEO-matrix and can be released upon external stimulus (NaCl concentration).[39,40] A situation, where both blocks interact with boron clusters (PEO and POX block copolymers),[41,42] also leads to stable nanoparticles capable of accumulating fairly large portions of metallacarborane-based inhibitors of HIV protease.[41] Among the roles of the copolymer architecture,[42] there is however another possibility to control the particle nanostructure and the release of active species: a proper selection of salt medium, an interesting phenomenon that has never been explored in detail before. To reveal the cation sensitivity of the polymer/metallacarborane nanoparticles, we prepared hybrid metallacarborane-containing nanoparticles from doublehydrophilic diblock copolymer PEO–PEtOx and 4-arm diblock copolymer $[PEO–PMeOx]_4$ (Figure 2.4) by consecutive addition of Li[COSAN], Na[COSAN] or K[COSAN] in 0.154 M (physiological solution) LiCl, NaCl or KCl solutions, respectively.

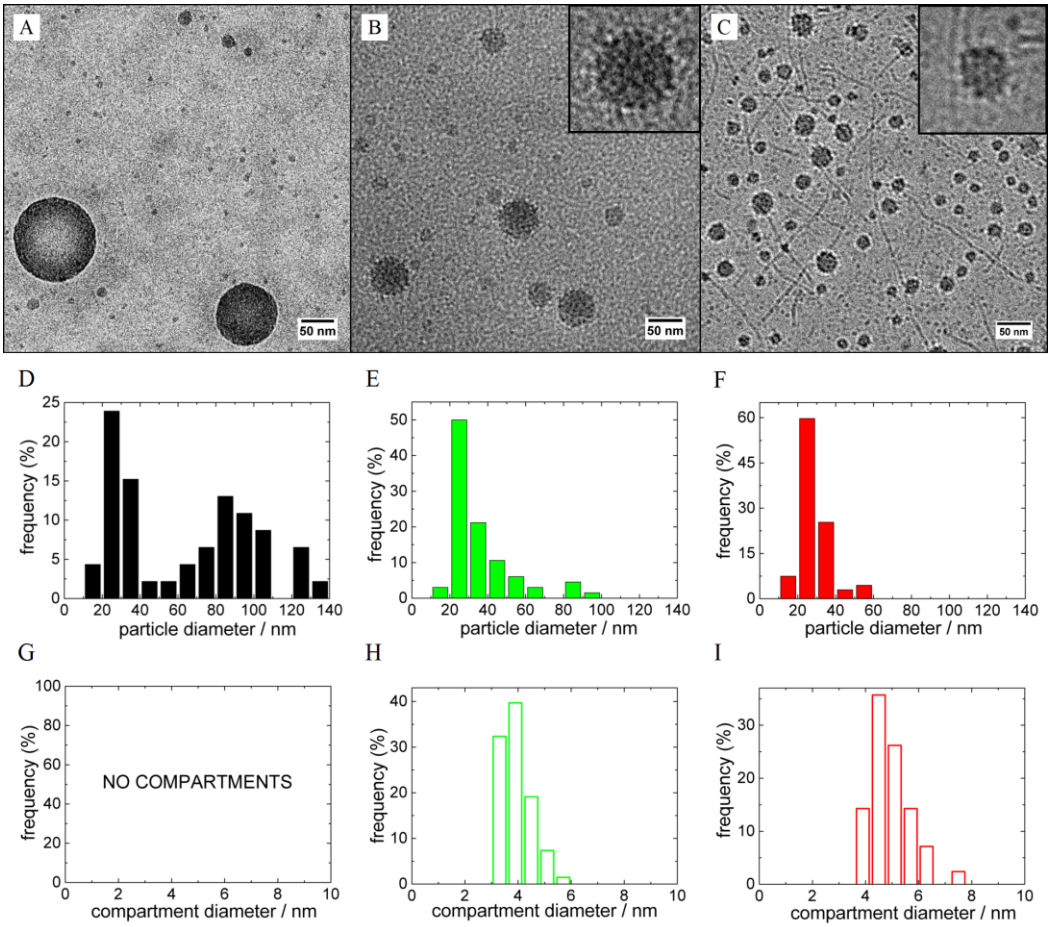

Figure V.1. Cryo-TEM micrographs of (A) PEO–PEtOx/Na[COSAN] in 0.154 M NaCl; (B) PEO−PEtOx/Li[COSAN] in 0.154 M LiCl; (C) PEO–PEtOx/K[COSAN] in 0.154 M KCl (polymer concentration 10 g L^{-1}). (D–I) Histograms based on the size analysis of nanostructures in different salt media (NaCl – black, LiCl – green, and KCl – red), where (D–F; filled columns) correspond to diameter distributions of "large" nanoparticles and (G–I; hollow columns) to diameter distributions of compartments within the "large" nanoparticles.

The morphology of PEO–PEtOx/M[COSAN] in MCl (M = Na, Li, and K) nanoparticles was visualized by cryo-TEM imaging (Figure V.1). Micrographs for the corresponding 4-arm systems, $[PEO–PMeOx]_4$/M[COSAN] in MCl (M = Na, Li, and K), are shown in Figure V.S1 in Supporting Information (SI). A distinct compartmentalization in the Li- and K-media, and a formation of homogeneous nanospheres in the Na-medium for the PEO–PEtOx linear diblock directly proves the impact of cations on the metallacarborane/polymer interaction. The particles are fairly polydisperse in general (kinetically controlled)[39] and there is a fraction of "small particles" that could be attributed to metallacarborane selfassemblies[5] and small pre-aggregates.[41] However, we will discuss the cation-selectivity on the structure of large particles exhibiting compartmentalization.

Long straight cylinders were detected in the K-system (see Figure V.1C). Such extended structures have never been observed for metallacarborane/polymer complexes before. The cylinders are longer than the contour length of single polymer chains, and their width is about 5

nm, which is close to dimensions of a single metallacarborane "micelle" (ca. 2.5 nm). Furthermore, some of them are shaped like a necklace of small spheres. The structure and origin of this shape is not clear yet, especially their straight shape. Our hypothesis is that it is closely related to the formation of extended helical structures of PEO–PEtOx that are stabilized by complexation with K^+.[57] The basic characterization of PEO–PEtOx/M[COSAN] in MCl nanoparticles was carried out by means of standard scattering techniques (light scattering and SANS). The results, which are in agreement with cryo-TEM and previously reported data,[41,42] are provided in SI (Figure V.S2 and 3 and Table V.S1).

Table V.1. Diameter of polymer/M[COSAN] (M = Na, Li, and K) nanoparticles and compartments within them from the analysis of corresponding cryo-TEM micrographs.

	Particle diameter/nm		
	Medium		
	Sodium	Lithium	Potassium
Linear diblock PEO-POX			
Large particles	93.5	12	18.5
Compartments	NO	3.8 ± 1.1	4.7 ± 1.3
Compartments after ITC [a]	3.1 ± 0.8	4.2 ± 1.0	3.5 ± 0.9
Star-like [PEO-POX]$_4$			
Large particles	26.3	17.6	12.4
Compartments	3.4 ± 0.8	3.7 ± 1.4	3.4 ± 1.4

[a] Originally PEO–POX/Li[COSAN] in 0.154 M LiCl sample, which was titrated by 0.154 M NaCl, LiCl and KCl solutions in the ITC experiment.

Size of the compartments

The cryo-TEM micrographs were analyzed by ImageJ software to obtain size distributions of the large compact nanoparticles and especially compartments within them (see histograms in Figure V.1; results are summarized in Table V.1). From the analysis, we found that compartments are slightly smaller in the Li-medium (diameter 3.8–1.1 nm) than in the K-one (diameter 4.7–1.3 nm). Further, the compartments are significantly larger than metallacarborane "micelles" (diameter 2.5–0.7 nm).[5] As concerns the star-like copolymer, the diameter of the compartments is independent of the nature of cation (it is around 3.5 nm in all three cases). However, the interpretation of cryo-TEM micrographs on a molecular level requires information on what kind of polymer segments (PEO or POX) are involved in the compartmentalization. This information would shed the light on the impact of cations on the metallacarborane polymer interaction. As shown below, NMR spectroscopy is a suitable tool for such a purpose.[39–42]

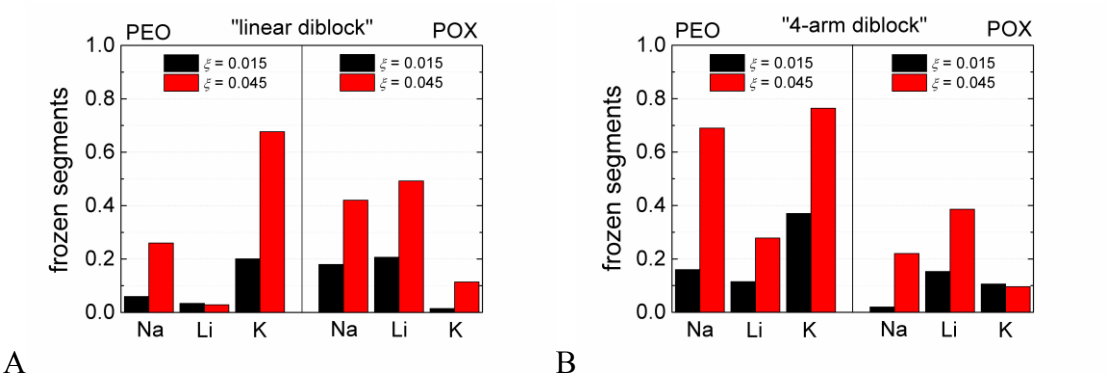

Figure V.2. Fraction of frozen polymeric segments in (A) PEO–PEtOx/M[COSAN] in MCl and (B) $[PEO–PMeOx]_4$/M[COSAN] in MCl (M = Na, Li, and K) differing in M[COSAN] content in 0.154 M MCl calculated from a decrease of corresponding ^{1}H NMR signals related to pure block copolymer and *t*-BuOH (internal standard).

Structure of the compartments and their origin

We used the ^{1}H NMR technique to estimate the fraction of polymer segments involved in the complexation with M[COSAN]. The fraction of frozen segments within the complex was calculated from the diminishing of the corresponding signals in NMR spectra as a function of ξ. The ratios of integrated intensities of ^{1}H signals of ethylene subunits in PEO and POX blocks to those in a molecularly dissolved polymer of the same concentration, which give the fractions of kinetically frozen monomer units, are shown in Figure V.2. In NaCl solution, the fraction of frozen POX is comparable to that of PEO, in the case of linear diblock (Figure V.2A). In LiCl solution, the fraction of frozen POX is much higher than that of PEO. An opposite effect occurs in the case of KCl solution, where PEO segments are substantially frozen as compared to POX. With respect to the cryo-TEM analysis, it indicates that there is no preference of COSAN in the Na-medium towards PEO and POX segments resulting in homogeneous nanoparticles.[41] Interaction of COSAN with POX segments is preferred in the Li-medium, and POX blocks thus form compartments. Finally, K^+ ions support interaction of COSAN with PEO segments, and PEO blocks are forming the compartments in this case. Since the PEO block is almost twice as long (127 segments) as the POX one (71 segments), we assume a different size of the PEO- and POX-compartments. This is in agreement with cryo-TEM analysis (Table V.1), where compartments have dimensions 3.8 nm and 4.7 in lithium and potassium solutions, respectively.

The cation selectivity of PEO and POX segments towards COSAN can be explained with the help of literature data on cation interaction with species consisting of an amidic moiety (as it is also in POX).[58,59] It is also related to salting in and salting out effects of ions on PEO-like polymers with connotations to the famous Hofmeister series.[60] It was reported that Li^+ ion has higher affinity towards O-group in amidic compounds than Na^+,[58] and K^+ has high affinity towards PEO-chains forming stable helical structures.[57] Further, the PEO/metallacarborane precipitation is more pronounced in the Na- and K-medium than in the Li-one.[39]

Based on the above mentioned results, we assume the following scenario for cation-sensitive compartmentalization on the molecular level. It is known from calorimetry

experiments that the COSAN cluster has roughly the same affinity towards PEO and POX segments in the Na-medium.[42] It should result in the formation of homogeneous nanostructures because none of the segments is preferred (Figure V.1A). Na^+ counterions are tightly complexed by PEO units[11,12] but only slightly by POX units. This stabilizes the nanospheres in the form of a nanogel because of the uncompensated charge on POX/metallacarborane segments.[42] In the Li-medium, Li^+ counterions have high affinity towards POX segments, and COSAN only weakly binds to PEO segments.[39] This shifts the equilibrium towards the complexation of metallacarborane with POX blocks. In the K-medium, the situation is just the opposite. K^+ counterions are strongly bound by PEO segments,[57] and PEO compartments are thus formed. In general, this confirms our general observations that the "solubility" of the otherwise hydrophobic COSAN anion is controlled by the mobility of counterions. If they are immobilized for any reason this leads to the formation of compact nanostructures like compartments. If the counterions remain free and the metallacarborane cluster is bound by the polymer, it results in gel-like structures.

Polymer architecture beats ion selectivity

Regarding the morphology of nanoparticles consisting of the star-like copolymer, the compartmentalization is observed in all three media (Na, Li, and K) (see micrographs in Figure V.S1, and their analysis in Table V.1), and the compartments are of similar dimensions in all three cases. It is evident from NMR results (Figure V.2B) that the star-like architecture with PEO blocks in the "core" of the star induced preferential compartmentalization of PEO segments[42] almost regardless of the cation type.

Cation selectivity of the nanoparticles: preferential sorption of Na^+ in Li-rich medium

In experiments dealing with the nanoparticles with a mix of alkaline cations, Na[COSAN] was used instead of Li(K)[COSAN] for the nanoparticle preparation in the Li(K)-medium. We noticed that the size of compartments in cryo-TEM micrographs as well as the fraction of frozen segments from the NMR spectra is different as compared with systems in the entirely Li(K)-medium. This suggests that Na^+ is preferentially adsorbed within the nanoparticles in the otherwise Li-rich solution and even a low portion of Na^+ is enough to provoke changes in the nanoparticle inner structure. In the case of Na[COSAN] in the K-medium, the effect of preferential Na^+ sorption is however fairly weak. For further details and experimental data see Figure V.S4 and the corresponding part of SI.

Cation exchange and its impact on the structure of nanoparticles

It encouraged us to study the ion-exchange issue in detail. We carried out isothermal titration calorimetry (ITC) experiments, where dispersion of PEO–PEtOx/Li[COSAN] nanoparticles in 0.154 M LiCl was titrated with 0.154 M LiCl, NaCl, and KCl solution. In Figure V.3A, there are raw heat rates. Since all the solutions have the same salt concentration (0.154 M), additional heats of dilution are negligible and do not interfere with cation exchange/sorption reactions. An almost zero heat flow is seen in the "Li to Li" experiment (green curves in Figure V.3A and B).

However, the addition of NaCl and KCl (black and red curves, respectively) provokes two processes. They can be clearly distinguished in the zooms of the raw heat flow curves.[86–89] In the beginning of the titration, there is only one strongly exothermic process, which is related to the cation exchange or sorption. Close to the saturation, the endotherm of simple salt mixing appears which eventually prevails. The endothermic peak is sharp and occurs immediately after the injection. On the contrary, the ion exchange/sorption (related to the exotherm) is a relatively slow process, because it is accompanied by a mass flow (bulky metallacarborane clusters) and changes in the polymer chain conformation.

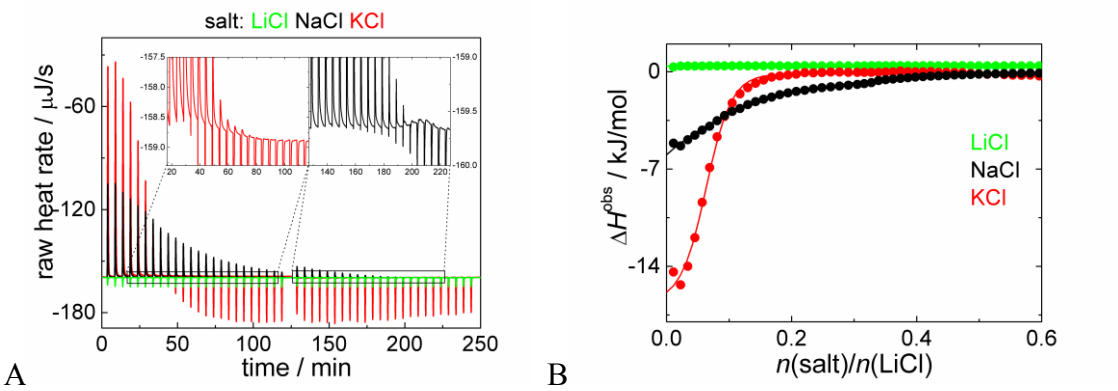

Figure V.3. (A) ITC raw heat flows with zooms and (B) corresponding thermograms with subtracted heats of mixing (dilution) for 0.154 M NaCl, LiCl and KCl titrated into 0.154 M LiCl solution of PEO−POX/Li[COSAN] particles with $\xi = 0.301$ (the polymer segment-to-Li^+ ratio is around 1:1).

The heats of the ionic exchange ($\Delta H^{exchange}$) estimated as the intercept of the ITC curve with the *y*-axis (Figure V.3B) for "Na to Li" and "K to Li" processes are 6 kJ mol^{-1} and 16 kJ mol^{-1}, respectively. The heats are smaller than for the overall interaction of Na[COSAN] with PEO/POX-polymers (around 40 kJ mol^{-1}),[11,41,42] but much larger than for the cation exchange of the relatively small "dumbbell" molecules (sub 1 kJ mol^{-1}).[56]

The shape of the ITC curves (Figure V.3B) is hardly comparable with a simple one-site binding model with a sigmoidal shape.[11,12] The shape without a plateau in the early stages of the titration indicates that there is not a single set of identical binding sites and that the inner structure of the nanoparticles is changing continually with increasing concentration of the guest cation.[86] This is why the value of ΔH^{obs} has to be estimated from the intercept with the *y*-axes rather than with fitting by a sigmoidal curve, which has no physical meaning in this case. However, the ITC curves are comparable with a partition model employed for example for distribution of small molecules in systems exhibiting a microphase separation.[87–89]

The saturation of the Li-based nanoparticles by K^+ and Na^+ occurred at molar ratios of 0.23 and 0.51, respectively (see leveling off of the red and black curves in Figure V.3B). To interpret this, we analyzed the structure changes during the titration also by cryo-TEM and NMR (shown as Figure V.S5 with further comments in SI). It is evident that the addition of K^+ leads to the "melting" of POX compartments and formation of PEO ones. K-ions bind only to a limited portion of polymer segments (ca. 25%) most likely to PEO blocks. Saturation of the nanoparticles by Na^+ requires a higher portion of the cation (ca. 50% of both POE and POX

segments) accompanied by diminishing of the compartments. The overall fraction of the frozen segments remains however roughly the same. From the above-mentioned results, it seems that metallacarborane clusters are rapidly released from POX-domains and migrate towards PEO-rich areas after addition of KCl to the Li-medium. The changes after addition of NaCl are milder and slower than the previous ones, and the compartments partly homogenize within the nanoparticles.

Conclusions

Mono-anionic metallacarboranes like cobalt bis(dicarbollides), COSAN, which are fully artificial boron cluster compounds with unusual binding capacity and interesting bio-activity, interact with water soluble polymers like poly(ethylene oxide), PEO, and poly(2-alkyl-2-oxazoline), POX, via dihydrogen bonding between B–H vertices and C–H groups of the polymeric backbone. The affinity of the anionic cluster to both PEO and POX segments is roughly the same, but the key-factor affecting the compact complex formation is the selectivity of alkaline cations towards PEO and POX segments. This is a phenomenon that has never been studied in detail before.

In the Na-medium, there is no preference and homogeneous nanospheres with COSAN bound to both types of segments are formed. In the Li-medium, interaction of both Li^+ and COSAN with POX segments is preferred resulting in distinct compartmentalization of POX segments within the hybrid nanoparticles. In the K-medium, the situation is just the opposite and PEO-compartments are formed instead. The PEO–PEtOx/M[COSAN] in MCl (M = Li, Na, and K) nanoparticles and compartments within them were studied by means of cryo-TEM imaging, NMR spectroscopy and ITC calorimetry.

An exchange of cations of different affinity was demonstrated by titrations with NaCl, KCl and LiCl solutions monitored by ITC, cryo-TEM and NMR. It is clear that even a small amount of K^+ and Na^+ ions provokes substantial changes in the inner structure of the nanoparticles accompanied by the flux of metallacarborane clusters and alkaline cations. This is the first example, where compartmentalization in polymeric nanoparticles is controlled by the selectivity of alkaline cations. With respect to bio-activity of metallacarborane clusters and also alkaline cations like Li^+, the nanoparticles can be utilized for stimuli-responsive drug delivery.

Supporting Information

Cryo-TEM micrographs of star-like copolymers

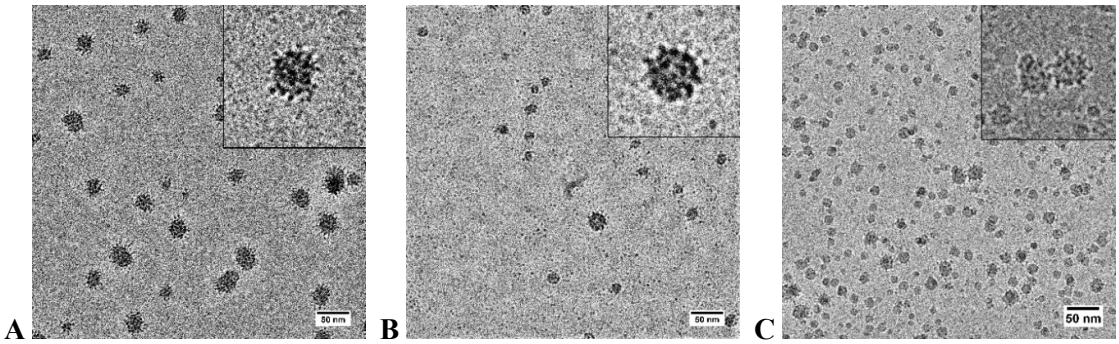

Figure V.S1. Cryo-TEM micrographs of (A) [PEO–PMeOx]$_4$/Na[COSAN] in 0.154 M NaCl, (B) [PEO–PMeOx]$_4$/Li[COSAN] in 0.154 M LiCl, and (C) [PEO–PMeOx]$_4$/K[COSAN] in 0.154 M KCl (polymer concentration 10 g/L).

Light scattering and SANS analysis

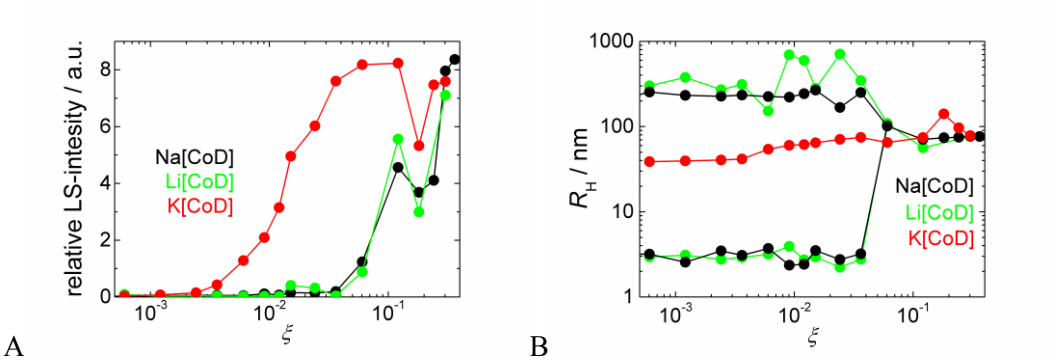

Figure V.S2. (A) Light scattering intensity and (B) hydrodynamic radius after addition of M[COSAN] (c = 0.019 M) in 0.154 M MCl to PEO–PEtOx (2g/L) in 0.154 M MCl solution, where M is Na (black), Li (blue), and K (red).

In Figure V.S2, there is a comparison of the relative LS-intensity and hydrodynamic radius, R_H, for Li- and K-systems with previously studied Na-one as functions of ξ, which is defined as COSAN-to-number of polymer segments ratio. In all three cases, the formation of compact hybrid nanoparticle is accompanied by a substantial increase of LS-intensity. However, the nanoparticles in the K-medium appeared in earlier stages of titration than for the Na- and Li-systems. The R_H *vs.* ξ dependence (Figure V.S2B) in the K-medium has a different shape but the same mean size after saturation as compared to the Li- and Na-systems. Two modes in the unstable region merge into one close to the saturation point in the Na-medium and stable compact nanoparticles form as a result. Thus, LS-study indicates that counterions play a role in

the process of nanoparticle formation. In this case, the presence of K^+ accelerates a formation of the compact nanoparticles.

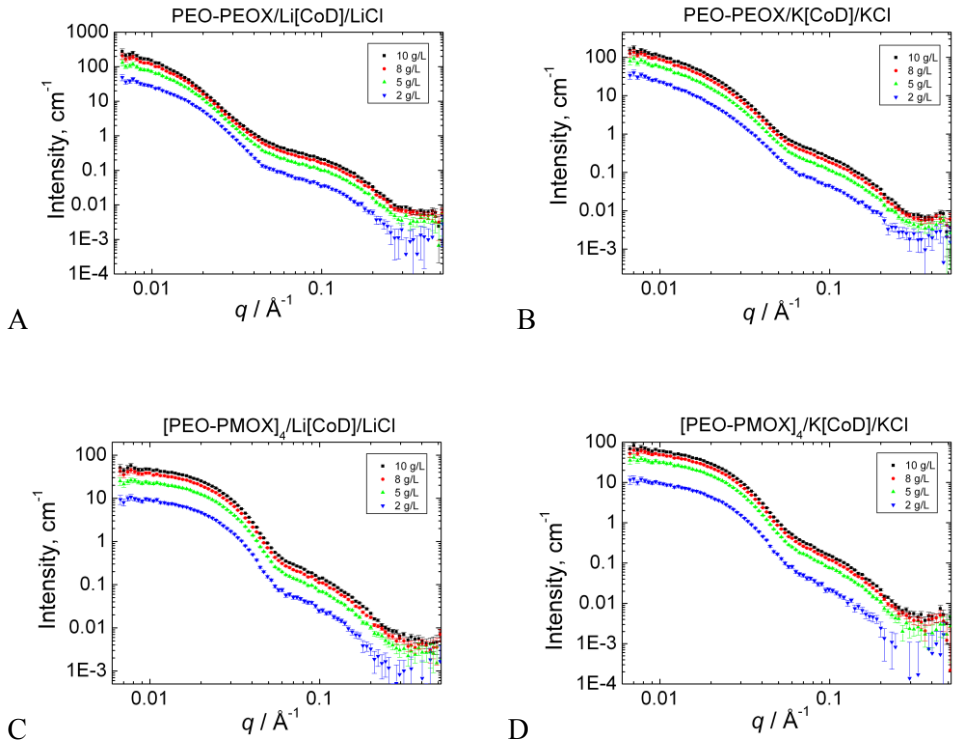

Figure V.S3 SANS curves of (A) PEO–PEtOx/Li[COSAN] in 0.154 M LiCl, (B) PEO–PEtOx/K[COSAN] in 0.154 M KCl, (C) [PEO–PMeOx]$_4$/Li[COSAN] in 0.154 M LiCl, and (D) [PEO–PMeOx]$_4$/K[COSAN] in 0.154 M KCl. Polymer concentration was 10 g/L.

Table V.S1 Results of SANS fitting of curves in Figure V.S3 extrapolated to zero angle, where $R_{g,1}$ and $R_{g,2}$ are radii of gyration of particle 1 and 2 in the "two particle" model; and R_{sph} is radius of sphere, R_c and l_c are radius and length of cylinder in the "spheres and cylinders" model.

	Fitting Model				
	Two particles		Spheres with attached cylinders		
	$R_{g,1}$/nm	$R_{g,2}$/nm	R_{sph}/nm	l_c/nm	R_c/nm
PEO–PEtOx/Li[COSAN]	14.86	2.80	-	-	-
PEO–PEtOx/K[COSAN]	14.26	1.59	-	-	-
[PEO–PMeOx]$_4$/Li[COSAN]	-	-	7.49	2.60	1.47
[PEO–PMeOx]$_4$/K[COSAN]	-	-	5.14	2.23	1.47

The SANS curves for the Li- and K-systems are shown in Figure V.S3 and the results of the fitting procedure in Table V.S1. A presence of two types of particles is evident, where the large ones correspond to compact particles, and the small ones can be assigned to a mixture of compartments, M[COSAN] micelles and small pre-aggregates. An absence of correlation peaks in SANS curves for nanoparticles with otherwise distinct compartmentalization indicates a low level of ordering of the compartments within the nanoparticles.

Nanoparticles with the mix of cations

We also studied different combinations of counterions of PEO–PEtOx/M[COSAN] in MCl (M = Na, K or Li). The same amounts of Na[COSAN] as in the standard experiments were added to 10 g/L polymer solutions in 0.154 M LiCl or KCl. Analytical concentration of Na^+ was thus 2.45 mM and 7.35 mM (respectively for increasing ξ). A comparison of the fraction of frozen polymer segments from NMR experiments for the Li-systems with added Na[COSAN] or Li[COSAN], and for the K-systems with added Na[COSAN] or K[COSAN], together with cryo-TEM micrographs are shown in Figure V.S4.

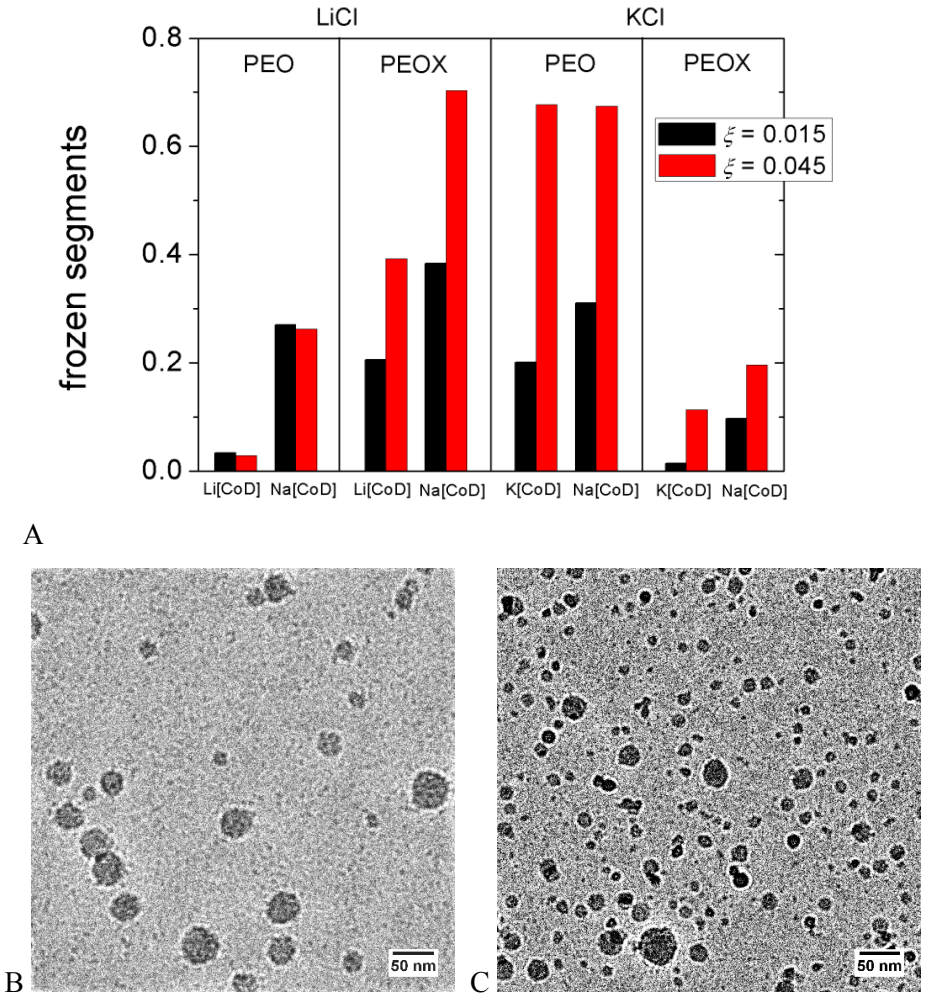

Figure V.S4. (A) The fraction of frozen PEO–PEtOx polymeric segments in 0.154 M LiCl and KCl differing in amount of M[COSAN] (M = Na, K, or Li) as indicated with the graph calculated from a decrease of corresponding ^{1}H NMR signals related to pure PEO–PEtOx and *t*-BuOH (internal standard). Cryo-TEM micrographs of (B) PEO–PEtOx/Na[COSAN] in 0.154 M LiCl, and (C) PEO−PEtOx/Na[COSAN] in 0.154 M KCl.

In Figure V.S4B, C, cryo-TEM micrographs of PEO–PEtOx/Na[COSAN] in 0.154 M LiCl and PEO–PEtOx/Na[COSAN] in 0.154 M KCl are shown, respectively. Both large and small particles are slightly larger than in solution with only one type of cation, compartments in

lithium salt are less visible and even disappeared in KCl. Average diameter of small particles and compartments of Na[COSAN] in LiCl was 6 nm (while for Li[COSAN] in LiCl it is only 3.8 nm) and size of small particles of Na[COSAN] in KCl was 7.8 nm (while for K[COSAN] in KCl it is 4.9 nm).

Titration of KCl, NaCl and LiCl to PEO-POX/Li[COSAN] in LiCl nanoparticles

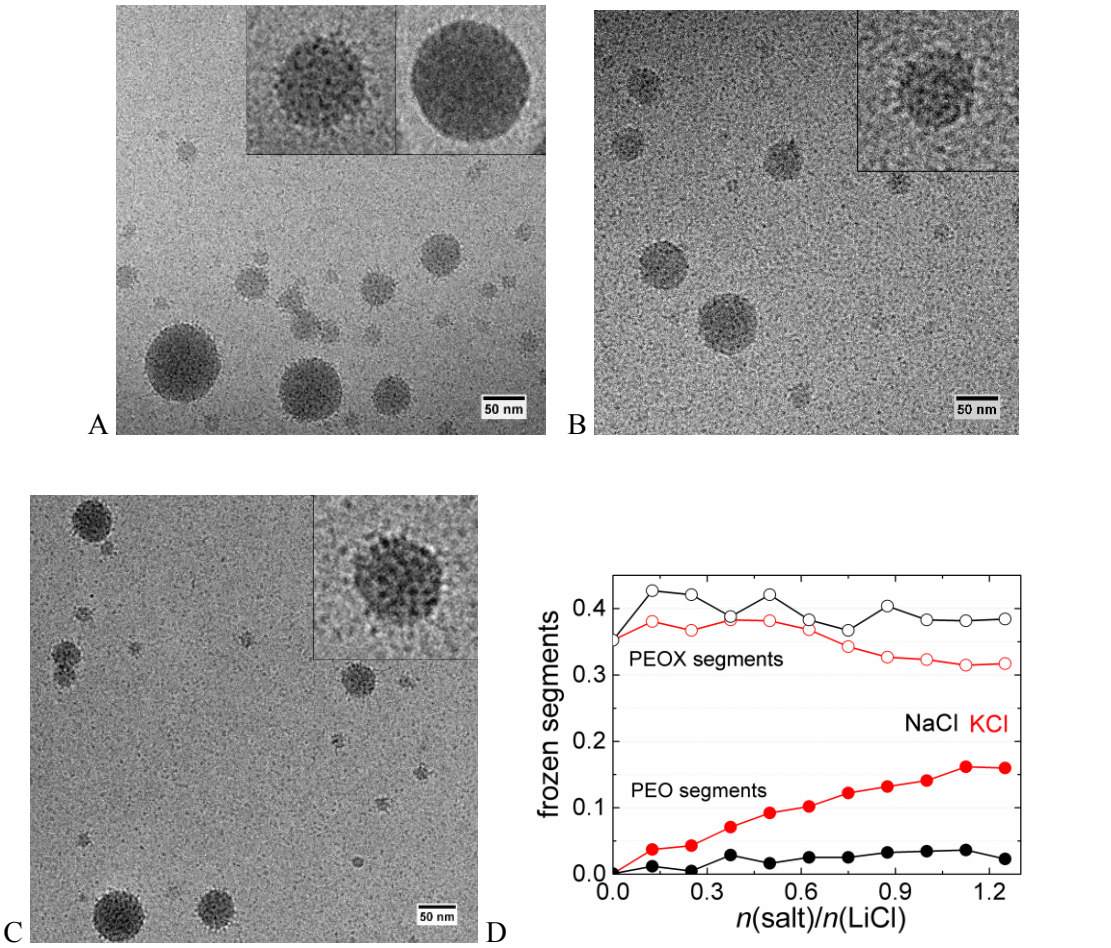

Figure V.S5. Cryo-TEM micrographs of PEO–PEtOx/Li[COSAN] in 0.154 M LiCl after titration with 0.154 M (A) NaCl; (B) LiCl and (C) KCl. (D) Fraction of frozen polymeric segments in PEO−PEtOx/Li[COSAN] in 0.154 M LiCl ($\xi = 0.045$) during the titration by 0.154 M NaCl (black curves) and 0.154 M KCl (red curves), calculated from a decrease of corresponding ^{1}H NMR signals related to pure PEO–PEtOx and *t*-BuOH (internal standard).

The samples from the ITC experiment were analyzed also by means of cryo-TEM (Figure V.S5A–C). The nanoparticles after the "K to Li" process are compartmentalized in a similar way as original nanoparticles in Li-medium, and it is quite difficult to distinguish any differences. However, in the sample after the "Na to Li" addition, a fraction of nanoparticles without compartments was observed. They are very similar to those of PEO–PEtOx/Na[COSAN] in NaCl and they coexist with the multicompartmentalized ones. In order to understand what processes take place during the titration, ^{1}H NMR technique was employed. We choose

PEO−PEtOx/Li[COSAN] in LiCl with lower value of ξ (0.045) to better detect changes in ^{1}H NMR spectra. The changes in fractions of frozen segments during the "Na(K) to Li" additions are shown in Figure V.S5D. We can see that "K to Li" leads to the situation similar to that in pure K-medium. Ratio of frozen PEO segments is increasing (up to 16 %) in opposite to POX, which has slightly decreasing tendency (from 35 to 31 %). This is in agreement with our assumption that potassium supports interaction with PEO and suppresses interaction with POX. In the case of "Na to Li", the changes are however almost insignificant.

Acknowledgements

The authors would like to acknowledge financial support of Czech Science Foundation P205/14–14608S and P106/12/0143, and The Charles University Grant Agency GAUK 512214. The authors thank Adnana Zaulet, Clara Vinas and Francesc Teixidor (ICMAB, Barcelona) for the preparation of potassium and lithium salts of cobalt bis(dicarbollide).

References

[1] R. N. Grimes, *Coord. Chem. Rev.*, 2000, **200**, 773.
[2] J. Plesek, *Chem. Rev.*, 1992, **92**, 269.
[3] I. B. Sivaev and V. I. Bregadze, *Collect. Czech. Chem. Commun.*, 1999, **64**, 783.
[4] P. Farras, E. J. Juarez-Perez, M. Lepsik, R. Luque, R. Nunez and F. Teixidor, *Chem. Soc. Rev.*, 2012, **41**, 3445.
[5] M. Uchman, V. Dordovic, Z. Tosner, and P. Matejicek, *Angew. Chem., Int. Ed.*, 2015, **54**, 14113.
[6] P. Bauduin, S. Prevost, P. Farras, F. Teixidor, O. Diat and T. Zemb, *Angew. Chem., Int. Ed.*, 2011, **50**, 5298.
[7] R. N. Grimes, *Dalton Trans.*, 2015, **44**, 5939.
[8] M. Uchman, P. Jurkiewicz, P. Cigler, B. Gruner, M. Hof, K. Prochazka and P. Matejicek, *Langmuir*, 2010, **26**, 6268.
[9] K. Kowalski, T. Goszczynski, Z. J. Lesnikowski and J. Boratynski, *ChemBioChem*, 2015, **16**, 424.
[10] M. Tarres, E. Canetta, E. Paul, J. Forbes, K. Azzouni, C. Vinas, F. Teixidor and A. J. Harwood, *Sci Rep.*, 2015, **5**, 7804.
[11] P. Matejicek, J. Brus, A. Jigounov, J. Plestil, M. Uchman, K. Prochazka and M. Gradzielski, *Macromolecules*, 2011**, 44**, 3847.
[12] J. Brus, A. Zhigunov, J. Czernek, L. Kobera, M. Uchman and P. Matejicek, *Macromolecules*, 2014, **47**, 6343.
[13] J. Rak, M. Jakubek, R. Kaplanek, P. Matejicek and V. Kral, *Eur. J. Med. Chem.*, 2011**, 46**, 1140.
[14] C. Masalles, J. Llop, C. Vinas and F. Teixidor, *Adv. Mater.*, 2002, **14**, 826.
[15] S. Gentil, E. Crespo, I. Rojo, A. Friang, C. Vinas, F. Teixidor, B. Gruner and D. Gabel, *Polymer*, 2005, **46**, 12218.
[16] C. Masalles, S. Borros, C. Vinas and F. Teixidor, *Adv. Mater.*, 2000, **12**, 1199.
[17] J. G. Planas, C. Vinas, F. Teixidor, A. Comas-Vives, G. Ujaque, A. Lledos, M. E. Light and M. B. Hursthouse, *J. Am. Chem. Soc.*, 2005, **127**, 15976.
[18] R. N. Grimes, *Molecular Crystals and Liquid Crystals*, 2000, **342**, 7.

[19] P. Farras, F. Teixidor, R. Kivekas, R. Sillanpaa, C. Vinas, B. Gruner and I. Cisarova, *Inorg. Chem.*, 2008, **47**, 9497.

[20] E. J. Juarez-Perez, C. Vinas, F. Teixidor, R. Santillan, N. Farfan, A. Abreu, R. Yepez and R. Nunez, *Macromolecules*, 2010, **43**, 150.

[21] B. P. Dash, R. Satapathy, J. A. Maguire and N. S. Hosmane, *Organometallics*, 2010, **29**, 5230.

[22] J. G. Planas, F. Teixidor, C. Vinas, M. E. Light and M. B. Hursthouse, *Chem. Eur. J.*, 2007, **13**, 2493.

[23] E. J. Juarez-Perez, M. Granier, C. Vinas, H. Mutin and R. Nunez, *Chem. Asian J.*, 2012, **7**, 277.

[24] E. J. Juarez-Perez, H. Mutin, M. Granier, F. Teixidor and R. Nunez, *Langmuir*, 2010, **26**, 12185.

[25] R. Nunez, E. J. Juarez Perez, F. Teixidor, R. Santillan, N. Farfan, A. Abreu, R. Yepez and C. Vinas, *Inorg. Chem.*, 2010, **49**, 9993.

[26] B. Gruner, J. Plesek, J. Baca, I. Cisarova, J. F. Dozol, H. Rouquette, C. Vinas, P. Selucky and J. Rais, *New J. Chem.*, 2002, **26**, 1519.

[27] I. B. Sivaev and V. V. Bregadze, *Eur. J. Inorg. Chem.*, 2009, **11**, 1433.

[28] D. Gabel, *Pure Appl. Chem.*, 2015, **87**, 173.

[29] M. Scholz and E. Hey-Hawkins, *Chem. Rev.*, 2011, **111**, 7035.

[30] Z. J. Lesnikowski, *Collect. Czech. Chem. Commun.*, 2007, **72**, 1646.

[31] P. Rezacova, P. Cigler, P. Matejicek, M. Lepsik, J. Pokorna, B. Gruner and J. Konvalinka, *Medicinal Application of Carboranes: Inhibition of HIV Protease*. In *Boron Science: New Technologies and Applications*, ed. N. S. Hosmane, CRC Press, New York, 2012, pp. 41-70.

[32] R. F. Barth, A. H. Soloway, J. H. Goodman, R. A. Gahbauer, N. Gupta, T. E. Blue, W. L. Yang, and W. Tjarks, *Neurosurgery*, 1999, **44**, 433.

[33] A. H. Soloway, W. Tjarks, B. A. Barnum, F. G. Rong, R. F. Barth, I. M. Codogni and J. G. Wilson, *Chem. Rev.*, 1998, **98**, 1515.

[34] M. F. Hawthorne, *Angew. Chem. Int. Ed.*, 1993, **32**, 950.

[35] M. F. Hawthorne and A. Maderna, *Chem. Rev.*, 1999, **99**, 3421.

[36] R. Satapathy, B. P. Dash, J. A. Maguire and N. S. Hosmane, *Collect. Czech. Chem. Commun.*, 2010, **75**, 995.

[37] F. Issa, M. Kassiou and L. M. Rendina, *Chem. Rev.*, 2011**, 111**, 5701.

[38] J. Brynda, P. Mader, V. SIcha, M. Fabry, K. Poncova, M. Bakardiev, B. Gruner, P. Cigler and P. Rezacova, *Angew. Chem. Int. Ed.*, 2013, **52**, 13760.

[39] P. Matejicek, J. Zednik, K. Uselova, J. Plestil, J. Fanfrlik, A. Nykanen, J. Ruokolainen, P. Hobza and K. Prochazka, *Macromolecules*, 2009, **42**, 4829.

[40] M. Uchman, P. Cigler, B. Gruner, K. Prochazka and P. Matejicek, *J. Colloid Interface Sci.*, 2010*,* **348**, 129.

[41] V. Dordovic, M. Uchman, K. Prochazka, A. Zhigunov, J. Plestil, A. Nykanen, J. Ruokolainen and P. Matejicek, *Macromolecules*, 2013, **46**, 6881.

[42] V. Dordovic, M. Uchman, A. Zhigunov, A. Nykanen, J. Ruokolainen and P. Matejicek, *ACS Macro Lett.*, 2014*,* **3**, 1151.

[43] A. Wicki, D. Witzigmann, V. Balasubramanian and J. Huwyler, *J. Control. Release*, 2015, **200**, 138.

[44] J. A. MacKay, M. Chen, J. R. McDaniel, W. Liu, A. J. Simnick and A. Chilkoti, *Nature Materials*, 2009, **8**, 993.

[45] R. Cheng, F. Feng, F. Meng, C. Deng, J. Feijen and Z. Y. Zhong, *J. Control. Release*, 2011, **152**, 2.

[46] R. J. R. Peters, M. Marguet, S. Marais, M. W. Fraaije, J. C. M. van Hest and S. Lecommandoux, *Angew. Chem. Int. Ed.*, 2014, **53**, 146.
[47] T. C. Yih and M. Al-Fandi, *J. Cell. Biochem.*, 2006, **97**, 1184.
[48] A. Harada and K. Kataoka, *Prog. Polym. Sci.*, 2006, **31**, 949.
[49] Q. Zhao and P. H. Ni, *Prog. Chem.*, 2006, **18**, 768.
[50] J. Rodriguez-Hernandez, F. Checot, Y. Gnanou and S. Lecommandoux, *Prog. Polym. Sci.*, 2005, **30**, 691.
[51] E. S. Gil and S. A. Hudson, *Prog. Polym. Sci.*, 2004, **29**, 1173.
[52] A. Lavasanifar, J. Samuel and G. S. Kwon, *Adv. Drug Delivery Rev.*, 2002, **54**, 169.
[53] M. Matuszewski, A. Kiliszek, W. Rypniewski, Z. J. Lesnikowski and A. B. Olejniczak, *New J. Chem.*, 2015, **39**, 1202.
[54] A. B. Olejniczak, J. Plesek, O. Kriz and Z. J. Lesnikowski, *Angew. Chem. Int. Ed.*, 2003, **42**, 5740.
[55] M. Bialek-Pietras, A. B. Olejniczak, S. Tachikawa, H. Nakamura and Z. J. Lesnikowski, *Bioorg. Med. Chem.*, 2013, **21**, 1136.
[56] M. Tarres, C. Vinas, P. Gonzalez-Cardoso, M. M. Hanninen, R. Sillanpaa, V. Dordovic, M. Uchman, F. Teixidor and P. Matejicek, *Chem.-Eur. J.*, 2014, **20**, 6786.
[57] Y. Yokoyama, R. Hirajima, K. Morigaki, Y. yamaguchi and K. Ueda, *J. A. Soc. Mass Spectrom.*, 2007, **18**, 1914.
[58] H. I. Okur, J. Kherb and P. S. Cremer, *J. Am. Chem. Soc.*, 2013, **135**, 5062.
[59] C. Yan and T. Mu, *Phys. Chem. Chem. Phys.*, 2015, **17**, 3241.
[60] J. C. Lutter, T. Y. Wu, Y. Zhang, *J. Phys. Chem. B*, 2013, **117**, 10132.
[61] L. Zhang and A. Eisenberg, *Science*, 1995, **268**, 1728.
[62] T. P. Lodge, A. Rasdal, Z. Li and M. A. Hillmyer, *J. Am. Chem. Soc.*, 2005, **127**, 17608.
[63] J. F. Lutz and A. Laschewsky, *Macromol. Chem. Phys.*, 2005, **206**, 813.
[64] Z. B. Li, M. A. Hillmyer and T. P. Lodge, *Macromolecules*, 2006, **39**, 765.
[65] C. LoPresti, H. Lomas, M. Massignani, T. Smart and G. Battaglia, *J. Mater. Chem.*, 2009, **19**, 3576.
[66] Z. B. Li, E. Kesselman, Y. Talmon, M. A. Hillmyer and T. P. Lodge, *Science*, 2004, **306**, 98.
[67] R. C. Hayward and D. J. Pochan, *Macromolecules*, 2010, **43**, 3577.
[68] S. Zhong, H. G. Cui, Z. Y. Chen, K. L. Wooley and D. J. Pochan, *Soft Matter*, 2008, **4**, 90.
[69] M. Uchman, M. Gradzielski, B. Angelov, Z. Tosner, J. Oh, T. Chang, M. Stepanek and K. Prochazka, *Macromolecules*, 2013, **46**, 2172.
[70] M. Uchman, S. Pispas, L. Kovacik and M. Stepanek, *Macromolecules*, 2014, **47**, 7081.
[71] P. Matejicek, F. Uhlik, Z. Limpouchova, K. Prochazka, Z. Tuzar and S. E. Webber, *Macromolecules*, 2002, **35**, 9487.
[72] F. Uhlik, Z. Limpouchova, P. Matejicek, K. Prochazka, Z. Tuzar and S. E. Webber, *Macromolecules*, 2002, **35**, 9497.
[73] Y. A. Lin, Y. C. Ou, A. G. Cheetham, H. G. Cui, *ACS Macro Lett.*, 2013, **2**, 1088.
[74] Z. B. Li, M. A. Hillmyer and T. P. Lodge, T. P. *Nano Lett.*, 2006, **6**, 1245.
[75] F. A. Plamper, L. Murtomaki, A. Walther, K. Kontturi and H. Tenhu, *Macromolecules*, 2009, **42**, 7254.
[76] F. Plamper, J. R. McKee, A. Laukkanen, A. Nykanen, A. Walther, J. Ruokolainen, V. Aeyev and H. Tenhu, *Soft Matter*, 2009, **5**, 1812.
[77] M. Uchman, K. Prochazka, K. Gatsouli, S. Pispas and M. Spirkova, *Colloid Polym. Sci.*, 2011, **289**, 1045.

[78] A. Sedlmeier and H H. Gorris, *Chem. Soc. Rev.*, 2015, **44**, 1526.

[79] R. Ladj, A. Bitar, M. M. Eissa, H. Fessi, Y Mugnier, R. Le Dantec and A. Elaissari, *Int. J. Pharm.*, 2013, **458**, 230.

[80] B. Surnar, K. Sharma and M. Jayakannan, *Nanoscale*, 2015, **7**, 17964.

[81] T. Yoshida, T. C. Lai, G. S. Kwon and K. Sako, *Expert Opin. Drug Delivery*, 2013, **10**, 1497.

[82] M. Casolaro and I. Casolaro, *Polymers*, 2012, **4**, 964.

[83] B. Hashemi, M. Shamsipur, A. Javadi, M. K. Rofouei, A. Shockravi, N. Tajarrod and N. Mandumy, *Anal. Methods*, 2015, **7**, 9641.

[84] L. Xing, H. Zheng, Y. Cao and S. Che, *Adv. Mater.*, 2012*,* **24**, 6433.

[85] T. S. Sahota, R. J. Latham, R. G. Linford and P. M. Taylor, *Drug Dev. Ind. Pharm.*, 2000, **26**, 1039.

[86] O. Mertins and R. Dimova, *Langmuir*, 2011, **27**, 5506.

[87] F. M. Coreta-Gomes, P. A. T. Martins, A. Velazquez-Campoy, W. L. C. Vaz, C. F. G. Geraldes and M. J. Moreno, *Langmuir*, 2015, **31**, 9097.

[88] M. J. Moreno, M. Bastos and A. Velazquez-Campoy, *Anal. Biochem.*, 2010, **399**, 44.

[89] H. Osanai, T. Ikehara, S. Miyauchi, K. Shimono, J. Tamogami, T. Nara and N. Kamo, *J. Biophys. Chem.*, 2013, **4**, 11.

5.6 Paper VI

Tuning of thermoresponsivity of poly(2-alkyl-2-oxazoline) block copolymer by interaction with surface active and chaotropic metallacarborane anion*

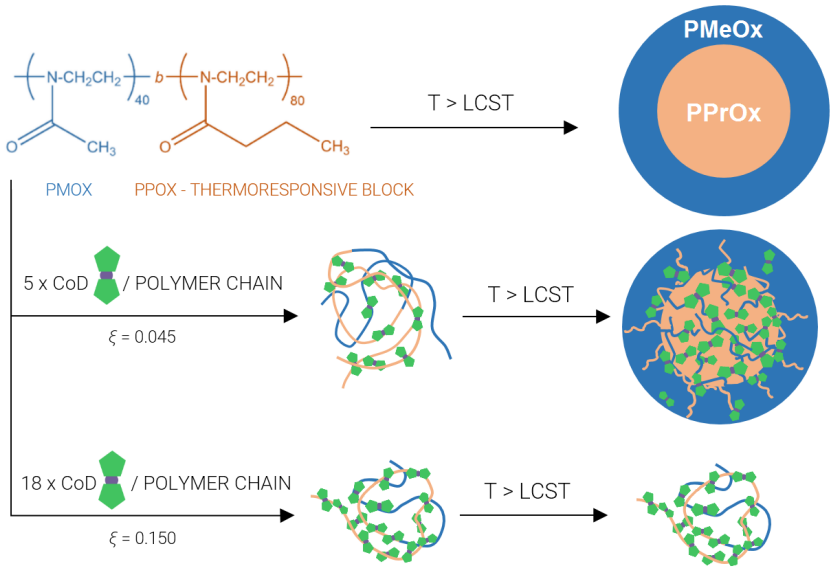

Abstract

In this study, we prepared thermoresponsive nanoparticles based on interaction of metallacarboranes, bulky chaotropic and surface active anions, with poly(2-alkyl-2-oxazoline) block copolymers. Recently, metallacarboranes gained a great potential in biomedicine and many delivery nanosystems have been proposed. However, none of them have thermoresponsive character. Therefore, we synthesized a thermoresponsive block copolymer poly(2-methyl-2-oxazoline)-*block*-poly(2-*n*-propyl-2-oxazoline), PMeOx–PPrOx. Light scattering, NMR spectroscopy, ITC and cryo-TEM were used to characterize all the solutions of the formed nanoparticles. The cloud point temperature of the block copolymer was observed at 30°C and above this temperature polymeric micelles were formed. Sodium cobalt bis(dicarbollide), COSAN, was found to interact with both polymeric segments. Depending on COSAN concentration, this affinity influenced the phase transition of thermoresponsive PPrOx block. LCST was shifted to lower values at mild COSAN content. At elevated concentrations of COSAN, the hybrid nanoparticles are fragmented into relatively small pieces. This system is also thermoresponsible, but the increase in temperature leads to higher polymer mobility and COSAN release.

* Submitted as: Ďorďovič, V.; Verbraeken, B.; Hogenboom, R.; Kereiche, S.; Matějíček, S.; Uchman, M. Tuning of thermoresponsivity of poly(2-alkyl-2-oxazoline) block copolymer by interaction with surface active and chaotropic metallacarborane anion.

Introduction

Cobalt bis(1,2-dicarbollide) anion, also called COSAN (Figure 2.1), is the most studied member of an interesting group of metallacarboranes, which attracts attention thanks to its unique properties and potential applications.[1-5] COSAN anion with a peanut shape is composed of two *nido*-carborane clusters sandwiching a cobalt(III) ion. A negative charge is fully delocalized over the cluster that results in its weakly coordinating character. It contains not only slightly positively charged C–H but also B–H units bearing negative partial charges on hydrogens, which are able to form dihydrogen bonds.[6] Due to its unique structure, COSAN has amphiphilic character despite a lack of a classical head-tail structure, and therefore COSAN has an ability to self-assemble and shows surface activity.[7,8] Some of these properties probably provide specific interactions between COSAN and some other compounds like surfactants, cyclodextrins, biomolecules and polymers.[9,10]

Recent studies show that COSAN interacts with poly(ethylene oxide), PEO, which is widely used in various biomedical applications and drug delivery systems. This interaction leads to insoluble nanocomposite with uniquely organized structure.[11,12] Only limited number of polymeric nanoparticles with COSAN have been prepared so far. For example, interaction of COSAN with poly(ethylene oxide)-*block*-poly(methacrylic acid) leads to the nanoparticles with the PEO/COSAN complex in the core and the shell of polyanionic PMA, which provides a pH-responsive behavior.[13]

Our initial reason to study such nanoparticles was focused on drug delivery of metallacaboranes to extend potential use of already known biomedical applications – inhibition of HIV protease[14] and BNCT for cancer treatment.[15] Instead of PMA in alkaline buffers, we therefore chose poly(2-alkyl-2-oxazoline)s, POXs, which have become a highly promising alternative for PEO in biomedical applications, because of their biocompatibility, possibility of various modifications, hydrophilicity and thermoresponsive behavior depending on type of side chains.[16,17] Further studies showed that the interaction between COSAN and poly(2-alkyl-2-oxazoline)s is strong enough for a formation of nanoparticles, leading however to fairly soluble complexes. As a result, the block copolymer of PEO and poly(2-ethyl-2-oxazoline), PEO−PEtOx, created gel-like nanoparticles without core-shell structure with COSAN.[18] On the other hand, star-like copolymer of PEO and poly(2-methyl-2-oxazoline), PMeOx, formed multicompartmentalized particles with COSAN.[19] It is worth noting that the compartmentalization in the PEO–POX/COSAN nanoparticles is cation sensitive.[20]

The most popular thermoresponsive POX is poly(2-isopropyl-2-oxazoline) which has a cloud point temperature in the range 36–39°C,[21] which is in the range of body temperature and very similar to the most studied thermoresponsive polymer poly(*N*-isopropylacrylamide), PNIPAM, with LCST = 32°C.[22-24] However, poly(2-isopropyl-2-oxazoline) suffers from irreversible crystallization when heating for longer times above the cloud point temperature.[25] Thus, in this study we used poly(2-*n*-propyl-2-oxazoline) PPrOx, which has a cloud point temperature of 24°C.[26]

Herein, we propose the preparation of the first example of thermoresponsive metallacarborane containing nanoparticles. For this purpose we synthesized PMeOx–PPrOx

block copolymer, in which the length of the thermoresponsive block PPrOx is twice as long as PMeOx (Figure 2.4E).[27-29] Nanoparticles were characterized by means of light scattering DLS/SLS, microscopy cryo-TEM, calorimetry (ITC) and NMR spectroscopy. All the experiments related to this work were carried out in physiological solution (0.154 M NaCl) and with sodium salt of COSAN.

Results and discussion

Influence of alkyl pendant groups on interaction of POX with COSAN: Homopolymers PMeOx, PEtOx and PPrOx

Albeit the interaction of COSAN with PEO, PEtOx and PMeOx copolymers was already discussed in our previous papers,[18-20] we decided to explore an influence of the alkyl group of POX in detail. Therefore, we studied interaction of $PMeOx_{100}$, $PEtOx_{500}$ and $PPrOx_{100}$ (number denote for degree of polymerization) with COSAN by means of light scattering (SLS&DLS), NMR spectroscopy and calorimetry ITC. It is a well-known fact that PPrOx has a cloud point temperature around 24°C and for the sample of $PPrOx_{100}$ it was observed at 25°C by DLS and NMR. Hence, we added COSAN to PMeOx, PEtOx and PPrOx solutions below this temperature (at 20°C). PMeOx/COSAN and PEtOx/COSAN complexes remained soluble, whereas PPrOx/COSAN partly precipitated at higher COSAN concentrations and elevated temperatures.

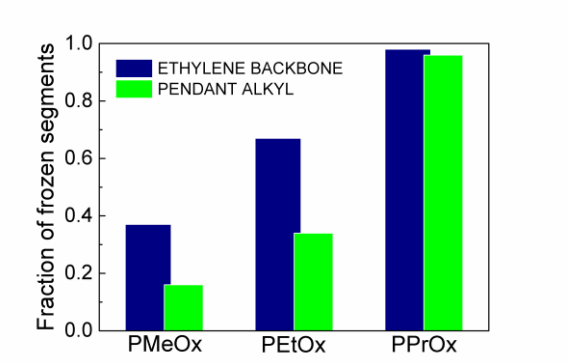

Figure VI.1. Influence of side alkyl groups in PMeOx, PEtOx and PPrOx on immobilization of polymeric segments (fraction of frozen segments) in the presence of COSAN (the COSAN-to-polymer segment ratio $\xi = 0.15$) calculated from the decrease of ^{1}H NMR signals related to pure copolymer at 20°C: (blue columns) ethylene signals in the polymer backbone, and (green columns) signals from protons on the first carbon atoms of side alkyl groups adjacent to the backbone.

Useful tool for clarifying inner structure of the complexes is NMR spectroscopy. We compared a decrease of ^{1}H signals of ethylene backbone and alkyl side groups of polymer after addition of COSAN (expressed as the COSAN-to-polymer segment ratio, ξ) to molecularly dissolved pure homopolymers at 20°C (Figure VI.1). It allows a calculation of the fraction of "frozen" POX-segments. Results showed a substantial influence of alkyl pendant groups on the mobility of the segments after the binding of COSAN. For PPrOx sample, the mobility of the hydrogens of ethylene backbone decreased by 94% and in PMeOx only by 20%. Further, the difference for alkyl groups is even more distinctive (green columns in Figure VI.1).

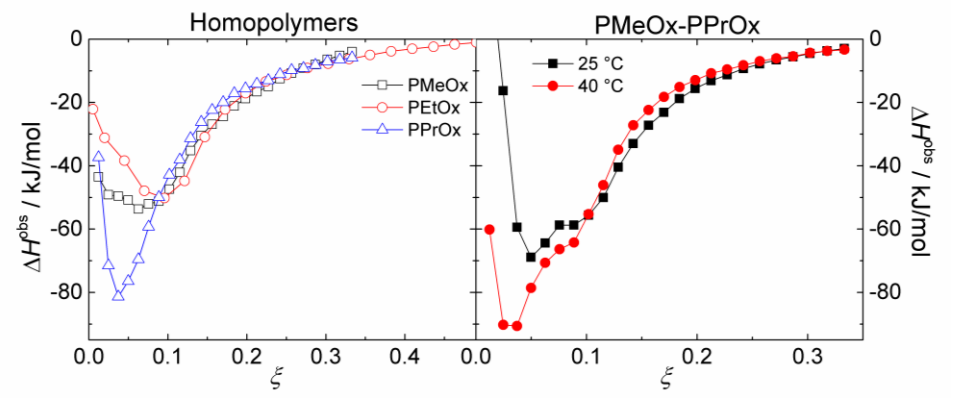

Figure VI.2. ITC curves for a titration of (left) PMeOx, PEtOx, and PPrOx homopolymers at 20°C, and (right) PMeOx–PPrOx block copolymer by COSAN at temperatures below and above the cloud point temperature. Amount of added COSAN is expressed as the COSAN-to-polymer segment ratio, ξ. All experiments were carried out in 0.154 M NaCl.

To decide if it is caused by the different affinity of COSAN or if it is related to the different solubility (i.e. mobility) of various POX/COSAN complexes, we employed isothermal titration calorimetry, ITC, (Figure VI.2). It is quite clear, that stoichiometry of COSAN interaction with the homopolymers (expressed as the COSAN-to-polymer segment ratio ξ) is almost the same or at least comparable to each other and also very similar to the thermogram for interaction between poly(ethylene oxide), PEO, and COSAN.[11,12] Nevertheless, the curves differ in shape and in the value of interaction heats. For example, the formation of PPrOx/COSAN is more exothermic (–80 kJ/mol) than PMeOx/COSAN (–50 kJ/mol). Furthermore, the shape of the thermograms is not sigmoidal. Therefore, the COSAN–POX interaction does not obey the simple one side binding model. A cooperative complexation and other accompanying processes should be expected.

Thermoresponsive block copolymer PMeOx–PPrOx

In the newly synthesized PMeOx–PPrOx block copolymer (Figure 2.4E), we decided to combine the mobile (soluble) character of PMeOx/COSAN complex with the rigid and thermoresponsive character of PPrOx, and we expected nanoparticles (micelles) with the core/shell structure.[17] The block copolymer was dissolved in 0.154 M NaCl in water and its cloud point temperature was observed approximately at 30°C by means of NMR and light scattering. The DLS results (Figure VI.3A) showed that below the cloud point temperature polymer was molecularly soluble, containing a fraction of particles with hydrodynamic radius, R_H, of 3 nm corresponding to the polymer coils and a negligible fraction of the large aggregates (size above 100 nm – see black curves in Figure VI.3). Above the cloud point temperature, a fraction of small nanoparticles with R_H of 12–15 nm appeared (Figure VI.3).

NMR spectroscopy supported the idea of temperature induced micellization. ^{1}H NMR spectrum of molecularly dissolve diblock copolymer PMeOx–PPrOx in water is shown in Figure 2.6. Figures 4 and 5 shows that above the cloud point temperature 55% of ethylene backbone is kinetically frozen (ca. 66 segments out of 120), which is close to the fraction of PPrOx (80

segments out of 120). Methyl groups of PMeOx blocks stayed mobile whereas propyl groups of PPrOx were affected in different extent depending on the distance from ethylene. Parts closer to the backbone (propyl 1) are more frozen (60%) than propyl 2 and 3 (45% and 40%). Evidently, PPrOx block was immobilized in the micellar core whereas PMeOx segments stayed mobile and formed the shell.

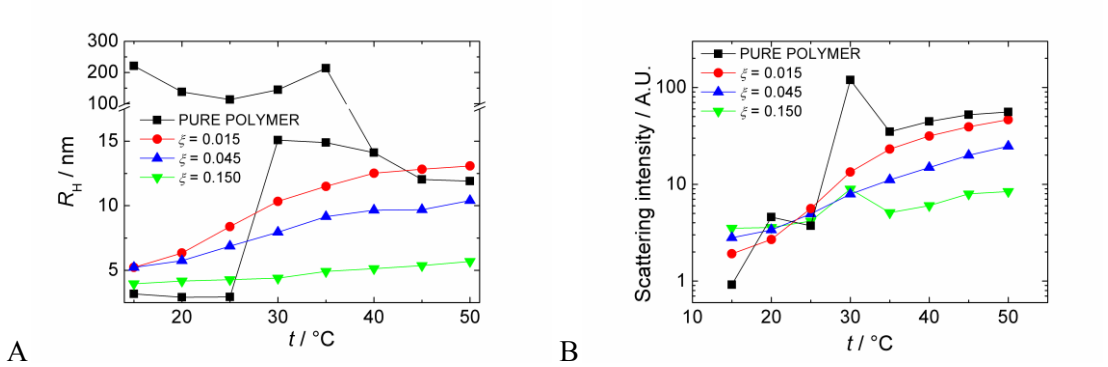

Figure VI.3. Temperature dependence of (A) hydrodynamic radius, R_H, and light scattering intensity of PMeOx–PPrOx nanoparticles with different amount of COSAN (indicated as the COSAN-to-polymer segment ratio, ξ).

We aimed to prepare the first thermoresponsive COSAN-containing nanoparticles by combining the specific interactions between COSAN and POXs with the PPrOx thermoresponsiveness. For this purpose, we added three different quantities of COSAN to the block copolymer solution with the values of ξ (COSAN-to-polymer segment ratio) 0.015, 0.045 and 0.150. Figure VI.3 shows that for COSAN containing samples the scattering intensity and R_H gradually increase with temperature, albeit decreasing after every addition of COSAN (from 5 to 13 nm for $\xi = 0.015$ and from 5 to 10 nm for $\xi = 0.045$). However, at the highest COSAN concentration, we did not observe any significant changes in scattering intensity and R_H with increasing temperature (small size increase from 4 nm to 5 nm).

The influence of temperature on the samples of PMeOx–PPrOx with the fraction of COSAN was studied in detail by NMR (Figures VI.4 and VI.5). After the first COSAN addition ($\xi = 0.015$), we observed a shift of the cloud point temperature in the curves for ethylene backbone and propyl- side chains (from 32°C to 25°C) and the curves became shallower than in the pure polymer. After the second addition ($\xi = 0.045$), segments immobilized even more and the cloud point became almost undetectable. After the third COSAN addition ($\xi = 0.150$), no cloud point could be recognized and the immobilization of polymer segments was unexpectedly decreasing with the temperature. While ethylene and propyl parts of the polymer were strongly affected and they showed the temperature controlled changes, methyl part remains almost unaffected with minimal temperature dependence. Nevertheless, it is worth noting that methyl segments became much more immobilized at $\xi = 0.150$ (jump from 10% to 52%). At the same concentration, Propyl 1 is almost fully immobilized, which means that PPrOx is probably saturated by COSAN. We can also see that at 50°C immobilization of all segments, except methyl group, slightly decreased at the highest COSAN concentration.

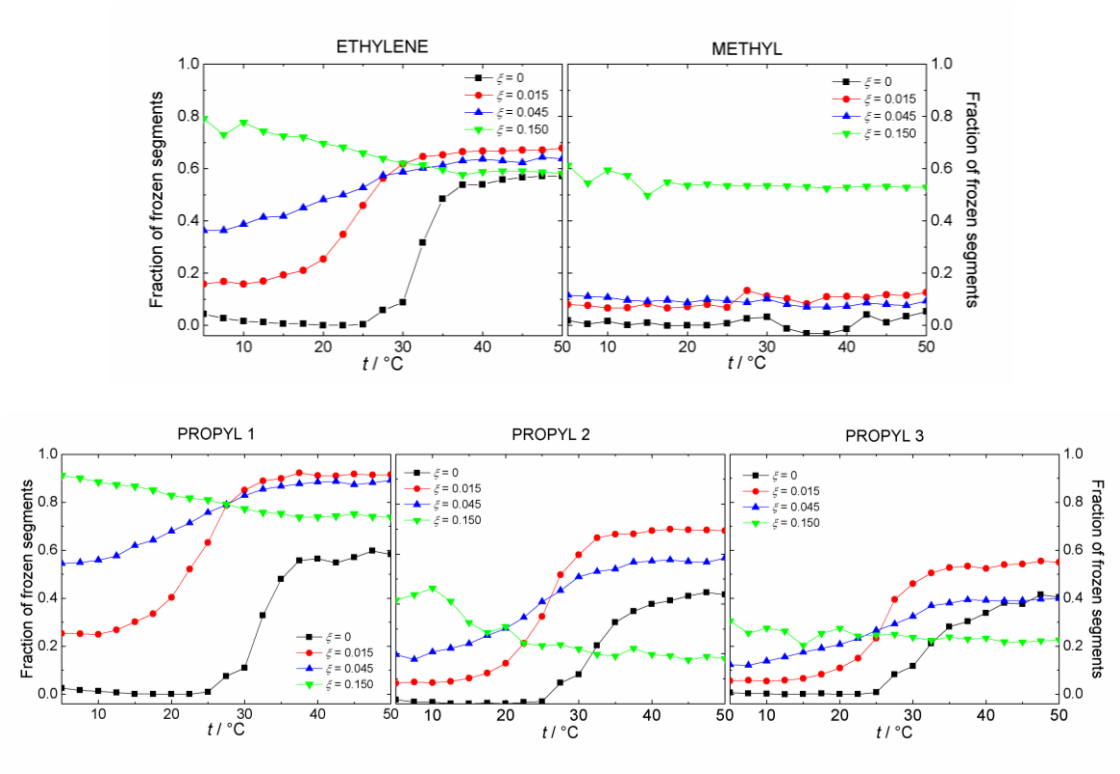

Figure VI.4. Temperature dependent fraction of frozen PMeOx–PPrOx segments calculated from the decrease of the corresponding ^{1}H NMR signals relating to pure copolymer at 20°C and *t*-BuOH as internal standard (description of signals in Figure VI.S1) for the various part of the copolymer chain and various content of COSAN as marked within the graphs).

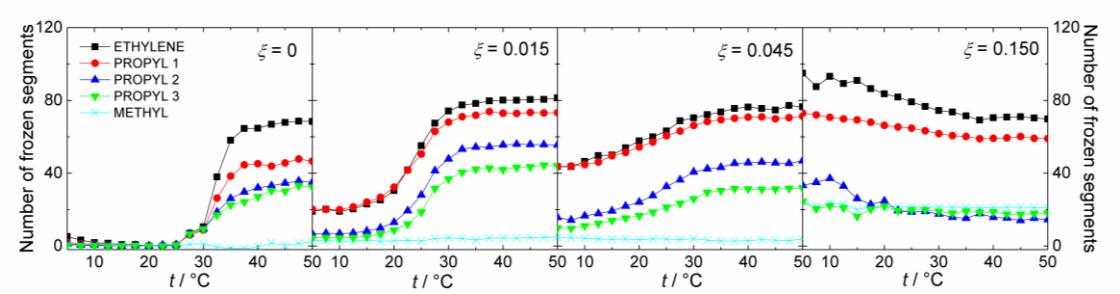

Figure VI.5. Temperature dependent number of frozen PMeOx–PPrOx segments for pure polymer and three different COSAN fraction (calculated from the fraction of frozen segments in Figure VI.4 and molecular structure of the block copolymer).

To investigate internal thermochemistry, we carried out ITC measurements (Figure VI.2). Above the cloud point temperature (40°C), addition of COSAN was more exothermic (–96 kJ/mol) than at 25°C (–73 kJ/mol). Positions of the minimums were similar (even to homopolymers) thus stoichiometry did not change significantly, was also independent on side groups and the interaction occurred even above the cloud point. However, the studied samples differed in the shape of the thermograms below the saturation. ITC curves of the copolymer visually reminded the combination of a deeper minimum of PPrOx with a flat shape of PMeOx.

Cryo-TEM micrographs (Figures VI.6) showed that the pure copolymer solution at 50°C contained nanoparticles with average diameter of 15 nm (Figure VI.6A). Smaller size comparing with DLS (R_H = 11 nm) could be explained by low visibility of the shell because of lower electron density of chains swelled by water molecules. Below the cloud point temperature (20°C) no particles were detected. In the polymer solution with COSAN (ξ = 0.150) at 50°C we could observe two fractions of particles: the first with an average diameter of 4 nm and the second of 10 nm (Figure VI.6B). System was obviously saturated by COSAN, which formed small aggregates[8] (4 nm) and the larger nanoparticles corresponded to COSAN/PMeOx–PPrOx nanoparticles. Because of unfeasibility of DLS CONTIN method to distinguish sizes of similar diffusion, obtained value of R_H (5 nm) was an average value of these fractions.

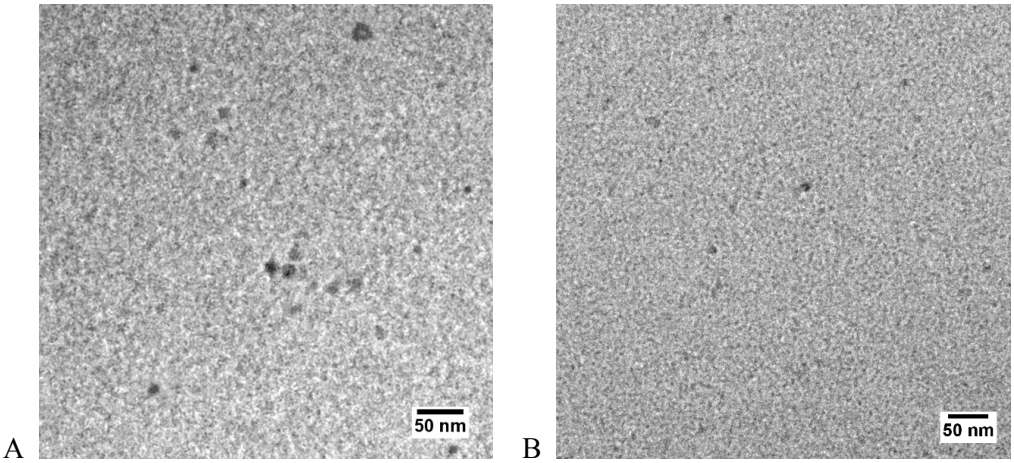

Figure VI.6. Cryo-TEM micrographs of (A) PMeOx–PPrOx nanoparticles at 50°C, and (B) PMeOx−PPrOx/COSAN (ξ = 0.150) nanoparticles at 50°C together with small COSAN aggregates. All nanoparticles visualized as spherical dark stains.

Apparently, two driving forces towards the nanoparticle formation occurred – strong interaction of COSAN with both PMeOx and PPrOx at any temperature (effect A), and phase separation of thermoresponsive block PPrOx only above the cloud point temperature or LCST (effect B). At lower temperatures, dissolved copolymer interacts with COSAN via dihydrogen bonding with ethylene backbone segments as evidenced by ITC experiments (Figure VI.2). However, only the binding to PPrOx segments is "visible" in NMR spectra as manifested by signal diminishing (Figures VI.4 and VI.5), because COSAN/PMeOX segments are fully mobile and almost undistinguishable with free POX segments. The presence of hydrophobic propyl group provokes the microphase separation. It is accompanied by release of extra heat in ITC, so-called aggregation peak, at early stages of COSAN binding (ξ < 0.1).

In the case of pure block copolymer, spherical micelles with the core consisting of almost all available PPrOX segments are assumed above the cloud point (Figure VI.7, top). However, every COSAN cluster attached to both PMeOX and PPrOX segments should change a local distribution of water molecules and charge densities. Since the LCST phenomenon is closely related with the chain hydration,[30] the presence of COSAN that is considered as

hydrophobic or chaotropic anion,[31] should have a substantial impact on the cloud point. In other words, the effect A should influence the effect B, and therefore also the nanoparticle morphology (Figure VI.7).

The mechanism how ions can change LCST of poly(N-isopropylacrylamide), PNIPAM, has been recently clarified in literature by Cremer et al., and trends that are in line with the famous Hofmeister series were observed.[32,33] There are three proposed mechanisms of action: (i) Ion interacts with the hydration shell of hydrophilic amid unit in PNIPAM chain; (ii) Ion can change the interfacial tension of hydrophobic ethylene units and pendant alkyl groups; (iii) Ion can directly bind to the amid unit and change the electron density there. The mechanisms (i) and (ii) should lead to the destabilization of polymer in solution and hence to the lowering of LCST, while the mechanism (iii) should lead to the opposite effect in PNIPAM aqueous solutions with various kosmotropic or chaotropic salts. The presence of kosmotropic anion results in the LCST decrease by means of the mechanism (i). The impact of chaotropic anions is not monotoneous and it is relatively weak. It is mostly related to the effect (ii) – change of the surface tension of hydrophobic parts of the macromolecule, and partly also by the direct adsorption on the amidic group – the effect (iii). To apply these rules to our system of COSAN-anion and POXs, we should keep in mind that bulky metallacarboranes are known to bind to ethylene backbone[11-13,18-20] and that the interaction with amidic moieties is arguable. Therefore, the impact of COSAN on LCST of the studied PMeOx–PPrOx should be explained most likely by the mechanism (ii – "surface tension mechanism") and LCST should decrease with the increase of COSAN concentration.

Even though the shift of the cloud point to lower temperatures is actually observed at low COSAN concentrations (ξ = 0.015), the effect A (the complex formation accompanied by microphase separation) prevails and gradually eliminates the effect B. In other words, the immobilized segments of COSAN/PPrOx are de-solvated at all and are incorporated within the compact parts of the nanoparticles at any temperature – almost no LCST effect is possible in the totally collapsed system.

However, at low COSAN concentration (ξ = 0.015) some PPrOx segments are covered by COSAN (effect A) but many segments are still available to undergo the phase separation above the cloud point temperature (effect B) and they shrink to the micellar PPrOx core (Figure VI.7, middle). Figures VI.4 and VI.5 show that at 50°C immobilization increased after the first COSAN addition (effect A + B), but at higher COSAN concentrations the tendency was opposite because effect A prevails and gradually eliminates effect B.

At ξ = 0.015, 1.8 COSAN molecules can interact with one polymer chain (120 segments, 80 PPrOx). Analyzing the NMR results we know that 25% of 'propyl 1' was frozen below the cloud point temperature which theoretically means that single COSAN molecule could affect 11 PPrOx segments. Although we can only estimate the actual number of segments involved in the process, the single COSAN molecule can affect at least 11 PPrOx segments (for ξ = 0.045 it was 8.1 and for ξ = 0.150 3.6 segments). Thus, COSAN/PPrOx complex can have an impact also on other parts of the chain and also other different chains.

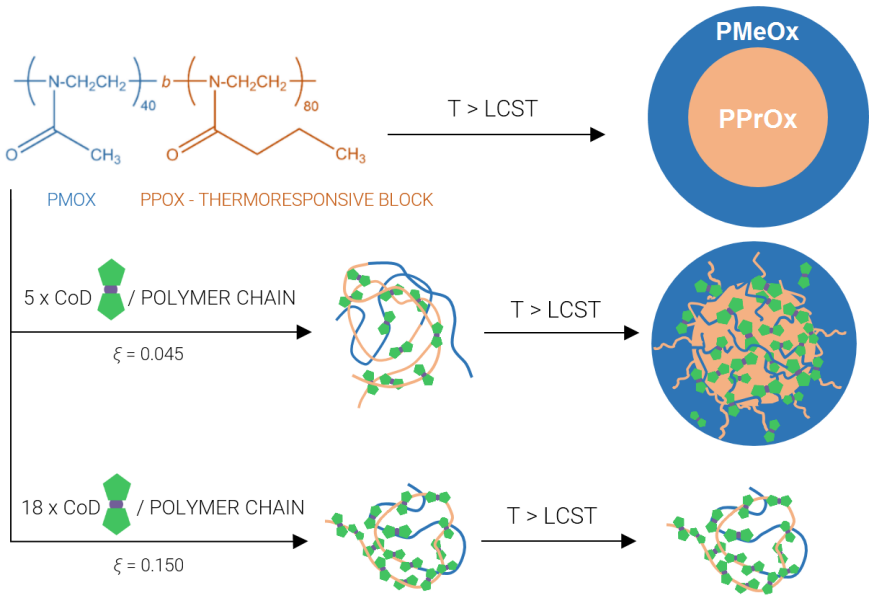

Figure VI.7. Different temperature response of PMeOx–PPrOx/COSAN nanoparticles after addition of COSAN

At high COSAN concentration ($\xi = 0.150$) every PPrOx segment (even half of PMeOx) was affected by COSAN and thus virtually unable to undergo LCST. System was even oversaturated by COSAN as evidenced by a detection of COSAN aggregates in cryo-TEM micrographs (Figure VI.6B) and by the appearance of the COSAN signal in ^{1}H NMR spectra (Figure VI.S1). At lower temperatures, these particles are smaller than those at $\xi = 0.045$, (Figure VI.7, middle and bottom). Distributions of relaxation times for COSAN/PMeOx–PPrOx ($\xi = 0.15$) revealed that R_H of these particles is only slightly larger (4–5 nm) than free polymer coils in the absence of COSAN (3 nm). We can imagine that at the highest COSAN concentrations, both PPrOx and PMeOx segments are intermixed and oversaturated by COSAN clusters, and thus the negative charge of attached COSAN causes the fragmentation of the polymeric nanoparticles into the system with much smaller dimensions.

Another effect observable at the highest COSAN content ($\xi = 0.15$) is an increase of the chain dynamic at high temperatures (see green curves in Figure VI.4). This effect is just an opposite as compared to the LCST of pure copolymer, and surprisingly the position of the break overlaps with the value of LCST for vanishing COSAN concentration can be observed. It is interesting that the effect is pronounced for ethylene units and "propyl 1" unit (the corresponding curves in Figure VI.4 intersect at approximately 30°C), and vanishes for the ends of propyl groups and methyl segments of PMeOx.

It can be explained by a certain redistribution of COSAN within the nanoparticles, because the clusters are bound to the ethylene segments and immobilization of the ends of propyl groups is controlled by hydrophobicity. It leads to the formation of domains of pure PPrOx segments that obviously had similar properties as the pure PPrOx block above the cloud point.

However, it immediately raises the question about the position of COSAN in the nanoparticles with high ξ at elevated temperatures. It is probable thet they are released from the nanoparticles. The above described process is accompanied by the destruction of COSAN aggregates incorporated within the polymer matrix, where the overall COSAN concentration should be higher than critical aggregation concentration in solution. Similar effects, e.g. de-aggregation upon increasing of temperature, were observed also in aqueous solutions of sodium COSAN.

Conclusions

To prepare the first thermoresponsive metallacarborane nanoparticles we studied aqueous solutions of the homopolymers poly(2-methyl-2-oxazoline), PMeOx, poly(2-ethyl-2-oxazoline), PEtOx, and poly(2-*n*-propyl-2-oxazoline), PPrOx, and the block copolymer PMeOx–PPrOx, where PPrOX block exhibits LCST around 30°C. The polymers were mixed with sodium cobalt bis(dicarbollide), COSAN, the most studied representant of metallacarboranes. Both PMeOx and PPrOx blocks forms complex with COSAN. Therefore, we assume the combined effect of thermoresponsivity of PPrOx and affinity of COSAN. We carried out experimental study on COSAN/PMeOx–PPrOx mixtures differing in metallacarborane content and temperature by light scattering, ^{1}H NMR spectroscopy, calorimetry and cryo-TEM microscopy. The pure copolymer solution shows the cloud point temperature at 30°C and above this temperature, micelles with radius of 11 nm appears. Phase separation of PPrOx provides the core and PMeOx forms the shell of micelles.

The structure and size of COSAN/PMeOx–PPrOx particles depends on COSAN concentration and temperature. Depending on COSAN concentration, the COSAN affinity influenced the phase transition of thermoresponsive PPrOx block. LCST is shifted to lower values at mild COSAN content. At elevated concentrations of COSAN, the hybrid nanoparticles are fragmented into relatively small piecies. This system is also thermoresponsible, but in the opposite sense as compared to LCST. The temperature increase leads to higher polymer mobility and COSAN release.

The studied system opens new possibilities to control and trigger the COSAN release by temperature. Further investigation of COSAN complexes with other poly(2-oxazoline)s and other thermoresponsive polymers are planned to bring interesting findings in the field of the drug delivery of metallacarboranes.

Supporting Information

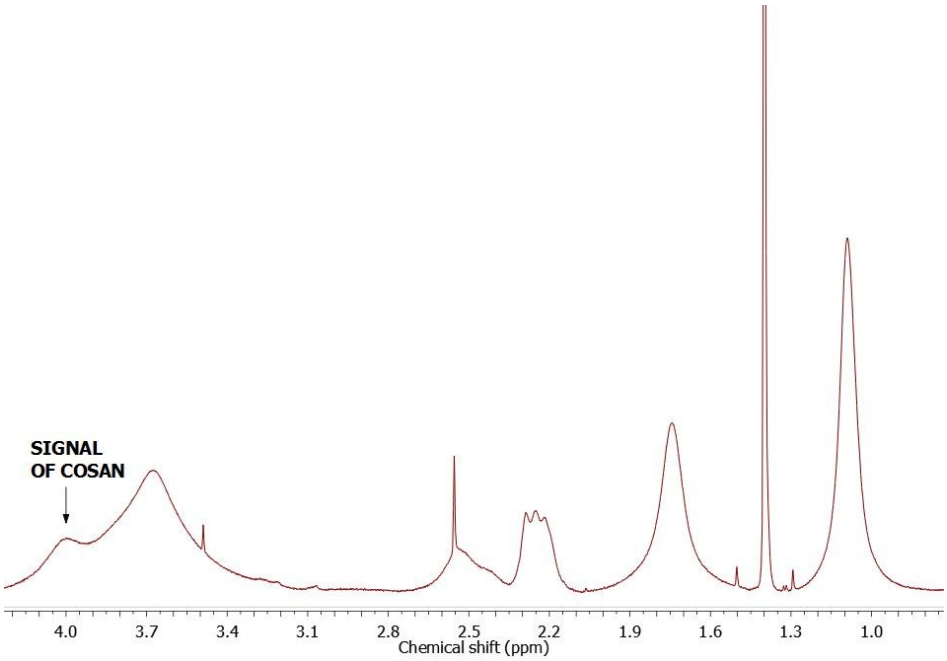

Figure VI.S1. ^{1}H NMR spectrum of COSAN/PMeOx–PPrOx solution at 50°C. The system is saturated by COSAN and the signal of COSAN is visible at 4 ppm.

Acknowledgements

VD acknowledges the financial support of the Charles University Grant Agency GAUK 512214. PM, MU and SK would like to acknowledge the financial support of the Czech Science Foundation 17–00648S and 17–00289Y. The authors thank Dr. Simona Hybelbauerová (CU) for NMR measurements and Alexander Zhigunov (IMC CAS, Prague) for SAXS analysis.

References

[1] Grimes, R. N. *Coord. Chem. Rev.* **2000**, *200*, 773.

[2] Plesek, J. *Chem. Rev.*, 1992, **92**, 269.

[3] Sivaev, I. B.; Bregadze, V. I. *Collect. Czech. Chem. Commun.* **1999**, *64*, 783.

[4] Farras, P.; Juarez-Perez, E. J.; Lepsik, M.; Luque, R.; Nunez, R.; Teixidor, F. *Chem. Soc. Rev.* **2012**, *41*, 3445.

[5] Grimes, R. N. *Dalton Trans.* **2015**, *44*, 5939.

[6] Fanfrlik, J.; Lepsik, M.; Horinek, D.; Havlas, Z.; Hobza, P. *Chem. Phys. Chem.* **2006**, *7*, 1100.

[7] Popov, A.; Borisova, T. *J. Colloid Interface Sci.* **2001**, *236*, 20.

[8] Uchman, M.; Dordovic, V.; Tosner, Z.; Matejicek, P. *Angew. Chem., Int. Ed.* **2015**, *54*, 14113.

[9] Uchman, M.; Jurkiewicz, P.; Cigler, P.; Gruner, B.; Hof, M.; Prochazka, K.; Matejicek, P. *Langmuir* **2010***, 26*, 6268.

[10] Rak, J.; Jakubek, M.; Kaplanek, R.; Matejicek, P.; Kral, V. *Eur. J. Med. Chem.* **2011**, *46*, 1140.

[11] Matejicek, P.; Brus, J.; Jigounov, A.; Plestil, J.; Uchman, M.; Prochazka, K.; Gradzielski, M. *Macromolecules* **2011**, *44*, 3847.

[12] Brus, J.; Zhigunov, A.; Czernek, J.; Kobera, L.; Uchman, M.; Matejicek, P. *Macromolecules*, **2014**, *47*, 6343.

[13] Matejicek, P.; Zednik, J.; Uselova, K.; Plestil, J.; Fanfrlik, J.; Nykanen, A.; Ruokolainen, J.; Hobza, P.; Prochazka, K. *Macromolecules* **2009**, *42*, 4829.

[14] Rezacova, P.; Cigler, P.; Matejicek, P.; Lepsik, M.; Pokorna, J.; Gruner, B.; Konvalinka, J. Medicinal Application of Carboranes: Inhibition of HIV Protease. In *Boron Science: New Technologies and Applications*, ed. N. S. Hosmane, CRC Press, New York, 2012, pp. 41-70.

[15] Lesnikowski, Z. J.; Paradowska, E.; Olejniczak, A. B.; Studzinska, M.; Seekamp, P.; Schussler, U.; Gabel, D.; Schinazi, R. F.; Plesek, J. *Bioorg. Med. Chem.* **2005**, *13*, 4168.

[16] Kaberov, L. I.; Verbraeken, B.; Hruby, M.; Riabtseva, A.; Kovacik, L.; Kereïche, S.; Brus, J.; Stepanek, P.; Hoogenboom, R.; Filippov, S. K. *Europ. Polym. J.* **2017**, *88*, 645.

[17] Takahashi, R.; Sato, T.; Terao, K.; Qiu, X.-P.; Winnik, F. M. *Macromolecules* **2012**, *45*, 6111.

[18] Dordovic, V.; Uchman, M.; Prochazka, K.; Zhigunov, A.; Plestil, J.; Nykanen, A.; Ruokolainen, J.; Matejicek, P. *Macromolecules* **2013**, *46*, 6881.

[19] Dordovic, V.; Uchman, M.; Zhigunov, A.; Nykanen, A.; Ruokolainen, J.; Matejicek, P. *ACS Macro Lett.* **2014***, 3*, 1151.

[20] Dordovic, V.; Uchman, M.; Reza, M.; Ruokolainen, J.; Zhigunov, A.; Ivankov, O. I.; Matejicek, P. *RSC Advances* **2016**, *6*, 9684.

[21] Uyama, H.; Kobayashi, S. *Chem. Lett*. **1992**, *21*, 1643.

[22] Schild, H. G. *Prog. Polym. Sci*. **1992**, *17*, 163.

[23] Aoshima, S.; Kanaoka, S. *Adv. Polym. Sci*. **2008**, *210*, 169.

[24] Rzaev, Z. M. O.; Dincer, S.; Piskin, E. *Prog. Polym. Sci*. **2007**, *32*, 534.

[25] Demirel, A. L.; Meyer, M.; Schlaad, H. *Angew. Chem. Int. Ed*. **2007**, 46, 8622.

[26] Park, J.-S.; Kataoka, K. *Macromolecules* **2007**, *40*, 3599.

[27] Hoogenboom, R.; Thijs, H. M.; Jochems, M. J.; van Lankvelt, B. M.; Fijten, M. W.; Schubert, U. S. *Chem. Commun.* **2008**, *44*, 5758.

[28] Wiesbrock, F.; Hoogenboom, R.; Leenen, M.; van Nispen, S. F.; van der Loop, M.; Abeln, C. H.; van den Berg, A. M. J.; Schubert, U. S. *Macromolecules* **2005**, *38*, 7957.

[29] Verbraeken, B.; Monnery, B. D.; Lava, K.; Hoogenboom, R. *Eur. Polym. J.* **2017**, *88*, 451.

[30] Heyda; J.; Dzubiella, J. *J. Phys. Chem. B* **2014**, *118*, 10979.

[31] Dordovic, V.; Tosner, Z.; Uchman, M.; Zhigunov, A.; Reza, M.; Ruokolainen, J.; Pramanik, G.; Cigler, P.; Kalikova, K.; Gradzielski, M.; Matejicek, P. *Langmuir* **2016**, *32*, 6713.

[32] Zhang, Y.; Furyk, S.; Bergbreiter, D. E.; Cremer, P. S. *J. Am. Chem. Soc*. **2005**, *127*, 14505.

[33] Zhang, Y.; Furyk, S.; Sagle, L. B.; Cho, Y.; Bergbreiter, D. E.; Cremer, P. S. *J. Phys. Chem. C* **2007**, *111,* 8916.

Summary

This work contains the results of the six research papers. The first two[I,II] are focused on amphiphilicity and self-assembly of boron cluster compounds. The third paper[III] deals with the self-assembly of carborane conjugates and their cation selectivity. The last three papers[IV–VI] contain the studies on the coassembly of cobalt bis(dicarbollide), COSAN, with the hydrophilic block copolymers based on poly(2-alkyl-2-oxazoline), POX.

Among the studied boron cluster compounds were sodium COSAN, Na[3,3'-Co($C_2B_9H_{11}$)$_2$], sodium decaborate, $Na_2[B_{10}H_{10}]$, sodium dodecaborate, $Na_2[B_{12}H_{12}]$, potassium 1-carbadodecaborate, $K[CB_{11}H_{12}]$, and sodium mercaptododecaborate, $Na_2[B_{12}H_{11}SH]$. We described their behavior in water and all the studied compounds were found to behave as amphiphiles, which was demonstrated by their surface activity and aggregation.

The most hydrophobic and the largest among the studied compound is COSAN. Its behavior showed evident similarities with the classical surfactant, such as SDS, despite the absence of amphiphilic head-tail topology.[I] The aggregation obeyed closed association model resulting in the CAC and the formation of aggregates, which size did not depend on concentration. These aggregates could not grow beyond a certain limit because of electrostatic restrictions, as almost all the counterions were not condensed in the aggregates. However, thermodynamics of SDS micellization was driven by entropy, whereas the self-assembly of COSAN is enthalpy-driven.

On the other hand, anions $[B_{10}H_{10}]^{2-}$, $[B_{12}H_{12}]^{2-}$, $[CB_{11}H_{12}]^{-}$ and $[B_{12}H_{11}SH]^{2-}$ are less hydrophobic, their size is smaller and the charge density is higher comparing to COSAN. Their aggregates grew with an increasing concentration without a limit and with the aggregation number higher than that of COSAN, and without an electrostatic restriction because of the effective counterion condensation.[II] Their behavior resembled hydrotropes or chaotropes. Interestingly, the presence of the exoskeletal substitution (–SH group) or the C–H unit within the cluster did not influence the aggregation process. Thus, the most probable reason of this "stealth" amphiphilicity is nonclassical hydrophobic effect related to the unusual borane hydration. The boron cluster compounds as a family of stealth amphipiles open new possibilities for the rational design of self-organized structures.

In the study of COSAN conjugates,[III] two COSAN anions were connected by a linker to achieve a function of cations complexation. The four synthesized conjugates, dumbbells, differed in length and nature of the oligo(ethylene oxide) linker. All the dumbbells aggregated in water and the morphology of aggregates depended on salt concentration. The linker was found to bound to the alkaline metal ions with different affinities, resembling crown ether effect. From a mixture containing Li^+, Na^+, K^+, Rb^+ and Cs^+, the highest affinity was shown towards K^+. ITC study of K^+ complexation provided evidence for three binding sites on the dumbbell molecules.

Further research focused on coassembly of COSAN with block copolymers[IV-VI] and was based on the earlier findings that COSAN interacts with poly(ethylene oxide), PEO, and

poly(2-ethyl-2-oxazoline), PEtOx, via dihydrogen bonding between B–H vertices and C–H groups of the polymeric backbone.

In the first study on the COSAN coassembly[IV], we prepared COSAN multicompartment nanoparticles by the mixing of COSAN with star-like double-hydrophilic polymer, [poly(ethylene oxide)-*block*-poly(2-methyl-2-oxazoline)]$_4$, [PEO−PMeOx]$_4$ in physiological saline. The nanoparticles consisted of approximately 30 compartments that were formed by one [PEO−PMeOx]$_4$ molecule with COSAN clusters densely packed within the central parts of the compartment in which PEO segments are located. Comparing to the previously studied linear block copolymer, PEO−PEtOx, we demonstrated that the polymer architecture has a crucial role in the morphology of nanoparticles.

The further study[V] deals with the selectivity of alkaline cations towards PEO and POX segments. Nanoparticles formed by the interaction of COSAN with POX were studied in three media: NaCl, KCl and LiCl. In the Na-medium, there was no preference and homogeneous nanospheres with COSAN bound to both types of segments were formed. In the Li-medium, interaction of both Li^+ and COSAN with POX segments was preferred resulting in distinct compartmentalization of POX segments within the hybrid nanoparticles. In the K-medium, the situation is just the opposite and PEO-compartments are formed instead. We also demonstrated an exchange of cations of different affinity, when even a small amount of K^+ and Na^+ ions to Li-medium changed the inner structure of the nanoparticles accompanied by the flux of COSAN clusters and alkaline cations.

In the last study,[VI] we prepared the first thermoresponsive metallacarborane nanoparticles by the interaction between COSAN and the block copolymer poly(2-methyl-2-oxazoline)-*block*-poly(2-*n*-propyl-2-oxazoline), PMeOx–PPrOx, which aqueous solution showed a cloud point at 30°C. Since both blocks formed complex with COSAN, we assumed the combined effect of thermoresponsivity of PPrOx and affinity of COSAN. The structure and size of the formed hybrid nanoparticles depended on COSAN concentration and temperature. We demonstrated that COSAN affinity influenced the phase transition of thermoresponsive PPrOx block and we observed the shift of LCST to lower values after the COSAN addition. At high COSAN concentrations, the hybrid nanoparticles are fragmented into smaller species, and the increase in temperature led to the higher polymer mobility and the release of COSAN.

The COSAN/POX systems presented herein show excellent combination of three parameters, by which we can tune the nanoparticles formation: side alkyl groups of POX, type of present salt and COSAN counterion, and temperature. With respect to bio-activity of metallacarborane clusters, these findings can be utilized for stimuli-responsive drug delivery, as well as for the design of new materials for nanotechnology.